COMPUTER AIDED RELIABILITY BASED DESIGN OF RING-STIFFENED CYLINDRICAL SHELLS UNDER EXTERNAL PRESSURE

by

Alberto Ceravolo Morandi M.Sc.

Thesis submitted for the Degree of Doctor of Philosophy

Department of Naval Architecture and Ocean Engineering

Faculty of Engineering

University of Glasgow

September 1994

ABSTRACT

A Level I code format is proposed for the buckling design of ring-stiffened cylindrical shells under external pressure. Depth independent partial safety factors to be applied to the resistance (collapse pressures), are proposed for the four relevant collapse modes (Interframe Shell Collapse, Frame Yield, Plate Yield and Frame Tripping), covering design and fabrication factors. A partial safety factor to be applied to the load (external pressure), and varying with the design pressure and the maximum expected overdiving, is proposed to cover operational factors. For deep diving vessels or in cases in which the risk of overdiving is not relevant, it is proposed that the overall safety factors used in design may be smaller than those presently recommended.

In order to obtain such partial safety factors, different aspects of strength modelling and Structural Reliability had to be addressed. On the strength modelling side, the work was focused on the frame collapse modes.

Seventy two experimental results were compiled, corresponding to machined models failing by elastic General Instability. Finite Element (FE) meshes were validated in view of mesh studies and experimental results and further used in parametric studies. The effect of boundary conditions on the elastic General Instability pressure p_n was investigated in view of both experiments and results of the FE models. Statistical properties were obtained for the model uncertainty associated with p_n.

Thirty five experimental results were compiled corresponding to welded models failing by General Instability. FE models were validated in view of the most relevant of these experiments as well as in view of other numerical results found in the literature.

A closed form solution for the elastic Frame Tripping pressure, based on energy methods and showing good agreement with FE and other numerical results, was introduced. FE parametric studies showed the effects of initial tilting angles of up to 4° to be considerably less harmful than an initial o-o-c of 0.5%R, supporting the use of a modified Tangent Modulus approach for inelastic Tripping.

On the Structural Reliability side, different reliability methods were reviewed, implemented and compared and the possibility of obtaining the failure probability in case of overdiving (or as a function of the external pressure in general) was verified, using any of the above methods.

Notional safety levels of various types of existing structures were reviewed and target safety levels were proposed for externally pressurised, internally ring-stiffened cylinders in the four modes under consideration. Finally, partial safety factor optimisation was carried out to obtain the partial safety factors.

To my wife, Nadine

DECLARATION

Except where reference is made to the work of others, this thesis is believed to be original

ACKNOWLEDGEMENTS

The work presented in this thesis was made possible by the Grant 200686/91-7 from the CNPq - Conselho Nacional de Desenvolvimento Científico e Tecnológico, Brasília, Brasil (National Research Council of Brazil) whose support is gratefully acknowledged.

The work was carried out under the joint supervision of Professor Douglas Faulkner, Head of Department, and Dr. Purnendu K. Das, Lecturer, of the Department of Naval Architecture and Ocean Engineering, to whom I wish to express my gratitude. Their advice, encouragement and technical excellency made possible the successful completion of the present work.

I also wish to acknowledge the encouragement and support given to my attendance in conferences and other activities by the Department of Naval Architecture and Ocean Engineering as well as the friendly and efficient help given by the departmental staff whenever necessary: Mrs. I. Faulkner, Mrs. M. McGrady, Mrs. A. Byrnes, Mrs. J. Zhu and Mr. D. Percival.

I also would like to thank Dr. S.B. Kendrick, Dr. D. Creswell (DRA Dunfermline), Prof. V. Zanic (Zagreb University), Mr. I.E. Winkle (NAOE Dept.) and my friend and collaborator Mr. Costas Tolikas for useful discussions during the course of this work.

I wish to thank my wife for being so supportive, even when my mind seemed to be floating somewhere else while she was trying to talk to me !

Last but not least, I thank my family and friends for their vital moral support.

CONTENTS

	Page
Abstract	i
Acknowledgements	v
Contents	vi
List of Figures	viii
List of Tables	xi
Notation	xiii

CHAPTER 1 - INTRODUCTION

1.1) Aims and Scope	1
1.2) Outline of the Thesis	8
1.3) Literature Review	
1.3.1) Overview	9
1.3.2) Basic Concepts of Column and Shell Buckling	11
1.4) Present Deterministic Design Criteria	
1.4.1) Submarine Design Thinking	16
1.4.2) Codes of Practice	17

CHAPTER 2 - ELASTIC BUCKLING

2.1) General Instability	
2.1.1) Analytical Modelling	28
2.1.2) Finite Element Modelling	30
2.1.3) Experimental Results	34
2.1.4) Comparison between Test and Theory	35
2.1.5) Parametric Studies	41
2.1.6) Modelling Uncertainty	42
2.2) Interframe Shell Buckling and Frame Tripping	
2.2.1) Analytical Modelling	43
2.2.2) Finite Element Modelling	45
2.2.3) Parametric Studies	46

CHAPTER 3 - COLLAPSE PREDICTION

3.1) Factors Affecting Collapse Prediction
- 3.1.1) Shape-Perfect Shell - Stress Analysis in the Elastic Range 48
- 3.1.2) Shape-Perfect Shell - Stress Analysis beyond the Elastic Limit 50
- 3.1.3) Classical Buckling Estimates 50
- 3.1.4) The Effect of Boundary Conditions 51
- 3.1.5) The Effect of Shape Imperfections 51
- 3.1.6) Residual Stresses 53
- 3.1.7) Mode Interaction 57

3.2) Finite Element Modelling 58

3.3) Modelling Uncertainty
- 3.3.1) Interframe Shell Collapse 62
- 3.3.2) General Instability 62
- 3.3.3) Frame Tripping 66
- 3.3.4) Summary of Proposed Values 68

CHAPTER 4 - ASPECTS OF CODE DEVELOPMENT

4.1) Brief Introduction to Structural Reliability 69
4.2) Statistical Properties of the Basic Variables 72
4.3) Reliability Methods 73
4.4) Sensitivity Studies 82
4.5) Code Format 83
4.6) Design Space 84
4.7) Target Reliability 85
4.8) Partial Safety Factor Optimisation 89

CHAPTER 5 - CONCLUSIONS AND FUTURE WORK

5.1 Conclusions 92
5.2 Future Work 95

REFERENCES 103

LIST OF FIGURES

Figure 1 - Inner Space Exploration and Exploitation - Brief History 130
Figure 2 - Possible Concepts of Submersible Vehicles 131
Figure 3 - Distribution of Ocean Depth, [76] 132
Figure 4 - Collapse Depth vs. W/Δ for Stiffened Cylinders, [11] 132
Figure 5 - Bifurcation Buckling, [234] 133
Figure 6 - Post Buckling Behaviour in the Elastic Range, [234] 133
Figure 7 - Structural Proportional Limit, [61] 133
Figure 8 - ECCS Column Curves, [40] 134
Figure 9 - Column Test Results 135
Figure 10 - Comparison between Test and Theory, Cylinders under Axial Comp., [150] 135
Figure 11 - Comparison between Test and Theory, Cylinders under External Pressure, [150] 135
Figure 12 - Comparison between Test and Theory, Cylinders under Torsion, [150] 136
Figure 13 - Comparison between Test and Theory, Clamped Spherical Caps, Ext. Pres., [150] 136
Figure 14 - Post-Buckling Behaviour of Cylinders, External Pressure 136
Figure 15 - Relevant Buckling Modes 137
Figure 16 - Plot of Interframe Shell Collapse Results [18] with Bias and COV of the Model Uncertainty (Mean Curve) 138
Figure 17 - Buckling Coefficient for eq. (10), [42] 139
Figure 18 - Empirical Curve for Interframe Shell Collapse, [97] 139
Figure 19 - Critical Buckling Mode for Long Cylinders, [51] 140
Figure 20 - FE Models for Elastic General Instability 141
Figure 21 - Experimental Postbuckling Behaviour, Elastic General Instability, [137] 140
Figure 22 - Buckling Modes from FE Eigenvalue Analysis, Model 3 of [136], Boundary Conditions of Fig. 20 142
Figure 23 - Buckling Modes from FE Eigenvalue Analysis, Model 3 of [136], Detail 143
Figure 24 - Postbuckling Behaviour from FE Riks Analysis, Radial Displacement at Mid-Compartment, Model 3 of [136] with Different Initial o-o-c 144
Figure 25 - Deformed Shapes from FE Riks Analysis, Model 3 of [136] with o-o-c = 0.001 mm 145

Figure 26 - Postbuckling Behaviour from FE Riks Analysis, Radial Displacement at Mid-Compartment 146
Figure 27 - Experimental Data - Elastic General Instability 148
Figure 28 - Comparison Experimental vs. FE Results, Elastic General Instability 149
Figure 29 - Comparison Experimental vs. FE Results, Models of [74] 150
Figure 30 - Comparison Experiments of [74] vs. Experiments of [85] 151
Figure 31 - X_{m1} vs. χ, 72 Experimental Results 151
Figure 32 - Group A Model, [79] 152
Figure 33 - Group B Model, [148] 152
Figure 34 - Redefinition of X_{m1} for Group B Models 152
Figure 35 - X_{m1} vs. L_c/R_i, Group B Models 153
Figure 36 - Effect of end Restraint, FE Eigenvalue Analysis 153
Figure 37 - General Instability Buckling Mode from FE Eigenvalue Analysis, Case 3 of Table 6, L_c=11543 mm, n=3, Axial Restrained, p_n = 26.42 N/mm^2 154
Figure 38 - FE Models for Frame Tripping 155
Figure 39 - Elastic Buckling Pressures, Case 3 of Table 6 156
Figure 40 - Basic Geometry 157
Figure 41 - Relevant Imperfections 157
Figure 42 - Geometry of Ref. [18], pp. 409 158
Figure 43 - Typical Cold Rolling Residual Stress Distribution, [18] 158
Figure 44 - Measured Cold Rolling Residual Stress Distribution, [150] 158
Figure 45 - Apparent Stress-Strain Curves, [82] 159
Figure 46 - Welding Shrinkage Actions, [61] 159
Figure 47 - Example of Mode Interactive Collapse, [73] 159
Figure 48 - Collapse Prediction eqs. (62,63) (Lines) vs. STAGS, Thick Shell, [73] 160
Figure 49 - Collapse Prediction eqs. (62,63) (Lines) vs. STAGS, Moder. Thick Shell, [73] 161
Figure 50 - Collapse Prediction eqs. (62,63) (Lines) vs. STAGS, Thin Shell, [73] 161
Figure 51 - Effect of Stiffener Size on Load-Carrying Capacity, [122] 162
Figure 52 - FE models - Infinite Compartments 163
Figure 53 - FE models - Finite Compartments 164
Figure 54 - Modelling of Residual Stresses by means of a Modified Stress-Strain Curve 162
Figure 55 - Experiments of Bosman et al. [149] 165
Figure 56 - Experiments of Morihana et al. [142] 165
Figure 57 - Numerical Analysis of Esslinger [140] 165

Figure 58 - Numerical Analysis of Smith and Kirkwood [72] 166
Figure 59 - $X_{m_{fy}}$ vs. p_y/p_{c5}, 35 Fabricated Models Failing by General Instability 167
Figure 60 - $X_{m_{fy}}$ vs. e/R, 35 Fabricated Models Failing by General Instability 167
Figure 61 - $X_{m_{fy}}'$ vs. p_y/p_{c5} 168
Figure 62 - $X_{m_{fy}}''$ vs. p_y/p_{c5} 168
Figure 63 - $X_{m_{fy}}'''$ vs. p_y/p_{c5} 169
Figure 64 - Idealisations of Loading, Strength and Safety Margin Distributions, [25] 169
Figure 65 - Reliability Methods 170
Figure 66 - Comparison of Reliability Methods, Case 3, Tripping 171
Figure 67 - Comparison of Reliability Methods, Case 3, Total Failure Probability 172
Figure 68 - Results of Optimisation Studies [12] 173
Figure 69 - ALARP Principle [205] 174
Figure 70 - Risk Experiences [206] 174
Figure 71 - Risk Levels due to Natural Uncertainties Only [207] 175
Figure 72 - Safety Levels for Various Structures [208] 175
Figure 73 - Safety Index, Flange Yield 176
Figure 74 - Safety Index, Plate Yield 177
Figure 75 - Safety Index, Interframe Shell Collapse 178
Figure 76 - Safety Index, Frame Tripping 179
Figure 77 - Total Failure Probability 180
Figure 78 - Safety Index, Flange Yield, Designs with $p_m/p_{c5} < 8$ 181
Figure 79 - Safety Index, Plate Yield, Designs with $p_m/p_{c5} < 8$ 182
Figure 80 - Safety Index, Interframe Shell Collapse, Designs with $p_m/p_{c5} < 8$ 183
Figure 81 - Safety Index, Frame Tripping, Designs with $p_m/p_{c5} < 8$ 184
Figure 82 - Total Failure Probability, Designs with $p_m/p_{c5} < 8$ 185
Figure 83 - Target β vs. F, eq. (68) for o-o-c, F_{max}= 1.15 186
Figure 84 - Target β vs. F, o-o-c = 0.5% R, F_{max}= 1.15 187
Figure 85 - Target β vs. F, eq. (68) for o-o-c, F_{max}= 1.30 188
Figure 86 - Target β vs. F, o-o-c = 0.5% R, F_{max}= 1.30 189

Figure 87 - $\gamma_{xm_j}\gamma_f$ vs. F, eq. (68) for o-o-c, F_{max}= 1.15 190
Figure 88 - $\gamma_{xm_j}\gamma_f$ vs. F, o-o-c = 0.5% R, F_{max}= 1.15 191
Figure 89 - $\gamma_{xm_j}\gamma_f$ vs. F, eq. (68) for o-o-c, F_{max}= 1.30 192
Figure 90 - $\gamma_{xm_j}\gamma_f$ vs. F, o-o-c = 0.5% R, F_{max}= 1.30 193
Figure 91 - Effect of using $\gamma_{xm_j}\gamma_f$ =1.4 for $p_m/p_{c5} > 2.5$ 194
Figure 92 - Procedure to Include Imperfections and Residual Stresses in FE Models, [243] 194

LIST OF TABLES

Table 1 - Limiting Slenderness Ratios for Webs and Flanges [38] 195
Table 2 - p_n (N/mm^2), Models 3 and 10 [136] 195
Table 3 - Mesh Study for the Frames, Models 3 and 10 [136], Case III Bound. Cond., Ext. Frames, Lateral Pressure 195
Table 4 - Comparison Experiments [136] vs. FE Eigenvalue Analysis 196
Table 5 - Brief Description of the Experimental Data 196
Table 6 - Sample Design Cases 197
Table 7 - p_n (N/mm^2), Case 3 of Table 6, t Increased to 46 mm 198
Table 8 - p_n (N/mm^2), Other Cases of Table 6 198
Table 9 - Elastic Buckling Pressure (N/mm^2), Case 1 of Table 6 199
Table 10 - Elastic Buckling Pressure (N/mm^2), Case 2 of Table 6 200
Table 11 - Elastic Buckling Pressure (N/mm^2), Case 3 of Table 6 201
Table 12 - Elastic Buckling Pressure (N/mm^2), Case 4 of Table 6 202
Table 13 - Elastic Buckling Pressure (N/mm^2), Case 4b of Table 6 203
Table 14 - Elastic Buckling Pressure (N/mm^2), Case 5 of Table 6 204
Table 15 - Elastic Buckling Pressure (N/mm^2), Case 6 of Table 6 205
Table 16 - Elastic Buckling Pressure (N/mm^2), Case 7 of Table 6 206
Table 17 - Bending Stresses due to Initial Tilt for the 207 Geometry of Fig. 42 [18] 207
Table 18 - Summary of Khaw's Results [241] 208
Table 19 - Collapse Pressure (N/mm^2), ABAQUS vs. Refs. [23,140,142,149] 210
Table 20 - Collapse Pressure (N/mm^2), ABAQUS vs. Smith & Kirkwood [72], No Residual Stresses 210
Table 21 - Collapse Pressure (N/mm^2), ABAQUS vs. Smith & Kirkwood [72], Welding Residual Stresses 210
Table 22 - Interframe Shell Collapse - Empirical Design Curve 211

Table 23 - ABAQUS Collapse Pressures (N/mm^2) for Sample Cases, General Instability, No Residual Stresses and Shell Cold Bending Residual Stresses 212
Table 24 - ABAQUS Collapse Pressures (N/mm^2) for Sample Cases, General Instability, Welding Residual Stresses 213
Table 25 - ABAQUS Collapse Pressures (N/mm^2) for Sample Cases, Tripping, No Residual Stresses 214
Table 26 - Statistical Properties of the Basic Variables 215
Table 27 - Sensitivity Studies, Flange Yield 215
Table 28 - Sensitivity Studies, Plate Yield 216
Table 29 - Sensitivity Studies, Interframe Shell Collapse 216
Table 30 - Sensitivity Studies, Tripping 217
Table 31 - Material Properties 217
Table 32 - Risk of Death [172] 217
Table 33 - Average Reliability, No Overdiving 218
Table 34 - Average Reliability, 15% Overdiving 218
Table 35 - Average Reliability, 30% Overdiving 218
Table 36 - f for Format I, No Overdiving 219
Table 37 - f for Format I, 15% Overdiving 219
Table 38 - f for Format I, 30% Overdiving 219
Table 39: Comparison with Present Practice 219

APPENDIX 1: Experimental Results, Machined Models failing by Elastic General Instability 220
APPENDIX 2: Analytical Solution for the Elastic Tripping Pressure 235
APPENDIX 3: Experimental Results, Welded Models failing by General Instability 244
APPENDIX 4: ABAQUS Post-Processing Results 249
APPENDIX 5: Design Solutions for Partial Safety Factor Optimisation 268
APPENDIX 6: BS5500 [24] Method for Effective Breadth Calculation 272

NOTATION

(valid unless a different local specification is found)

a,b,c	Coefficients of eq. (46), given in Appendix 2
A1,B1,B2,C1,C2	Arbitrary Constants, eq. (38)
A_f	Cross Sectional Area of Frame Flange
A_{pl}	Cross Sectional Area of Plating, $A_{pl} = L_s t$
A_s	Cross Sectional Area of Frame
A_w	Cross Sectional Area of Frame Web
b	Koiter's Imperfection Sensitivity Parameter
b_f	Flange Breadth
C	Rotational Constraint, $C = C_{0n}\,(1 - p_t/p_m)$
C_{0n}	Stable Rotational Constraint, $C_{0n} = \frac{Et^3}{3(1-\nu^2)L}\left[1+\left(\frac{n\,L}{\pi R_m}\right)^2\right]^2$
C_θ	Buckling Coefficient used in eq. (10), given in Fig. 17
d	Distance of Frame Flange from Neutral Axis (with Effective Length of Shell), Fig. 40
d_1	Distance of Outer Shell Fibre from Neutral Axis (with Effective Length of Shell), Fig. 40
d_c	Distance of Shear Centre from the Shell Plating, $d_c \sim d_w + t_f/2$
D	Diameter (General)
D1,D2,E1,E2	Arbitrary Constants, Appendix 2
D_s	Flexural Rigidity of Shell Plating, $D_s = Et^3/12(1-\nu^2)$
D_w	Flexural Rigidity of Frame Web, $D_w = Et_w^3/12(1-\nu^2)$
d_w	Web Depth
e	Maximum Deviation from the Mean Circle
E( )	Expected Value of a Random Variable
e_r	Ring Eccentricity, Fig. 40
E	Young's Modulus
E_s	Secant Modulus
E_t	Tangent Modulus
f	Scalar Safety Factor, eq. (67)
F	Overdiving Factor, $F = (p_d+\Delta p)/p_d$

F_{max}	Maximum Overdiving Factor
F_{min}	Minimum Overdiving Factor
G	Transcendental Function, eq. (52)
G′	Shear Modulus, $G' = E/2(1+\nu)$
H	Rise of the Apex of a Spherical Cap above its Base Plane
I_c	Second Moment of Area of Frame Cross Section (with Effective Length of Shell)
I_{pl}	Second Moment of Area of Shell Plating, $I_{pl} = L_s t^3/12$
I_s	Polar Second Moment of Area of Frame Cross Section in relation to its Shear Centre, $I_s = t_w d_c^3/3 + t_f b_f^3/12$
I_z	Second Moment of Area of Frame Cross Section in relation to its Axis of Symmetry, $I_z = (d_w t_w^3 + t_f b_f^3)/12$
I_0	Polar Moment of Inertia of the Frame Cross Section (without Effective Length of Shell) in relation to the Toe of the Web
k_a	Axial Buckling Coefficient, Fig. 10, $k_a = (l^2 t/\pi^2 D)\,\sigma_{cr}$
k_l	Compartment Length Reduction Coefficient
k_t	Shear Buckling Coefficient, Fig. 12, $k_t = (l^2 t/\pi^2 D)\,\tau_{cr}$
k_1-k_6	Coefficients of eq. (45), given in Appendix 2
J	St. Venant Torsional Constant, $J = (b_f t_f^3 + d_w t_w^3)/3$
l	Cylinder Length (General)
L_c	Compartment Length
L_e	Effective Length of Shell, eq. (37)
$\overline{L_e}$	Modified Effective Length of Shell, eq. (64)
L_s	Frame Spacing
L	Unsupported Length of Shell, $L = L_s - t_w$
m	Number of Waves in the Axial Direction
n	Number of Waves in the Circumferential Direction
N	Transcendental Function, eq. (51)
N_{0f}	Hoop Force in the Stiffener just prior to Buckling, eq. (39)
N_{0x}, N_{0y}	Membrane Forces per Unit Length of Shell just prior to Buckling, eq. (39)
n_c	Number of Circumferential Parts (FE Models)
n_f	Number of Axial Parts in the Flange (FE Models)
n_{fr}	Number of Frames in the Compartment
n_l	Number of Axial Parts in the Shell (FE Models)

n_w	Number of Radial Parts in the Web (FE Models)
P	Load (General)
p	External Pressure (General)
$\bar{p}$	Normalised Pressure, Fig. 11, $\bar{p} = (l^2R/\pi^2D)\, p_{cr}$
p_{ax}	Pressure at which the Shell fails Elasto-Plastically with Meridional Hinges forming at Mid-Bay and Frame Positions (o-o-c = 0), Fig. 49
p_c	Interframe Shell Collapse Pressure
p_{cI}	Buckling Pressure, FE without Axial End Restraint, Fig. 36
p_{cIII}	Buckling Pressure, FE with Axial End Restraint, Fig. 36
p_{c5}	Shell Circumferential Membrane Yield Pressure, eq. (9)
p_{cr}	Elastic Critical Pressure (General)
p_{cr_i}	Inelastic Critical Pressure (General)
p_d	Design Pressure (Safe Operation)
p_{exp}	Experimental Collapse Pressure
p_f	Probability of Failure (General)
p_m	Interframe Shell Elastic Buckling Pressure, eq. (8)
p_n	General Instability Elastic Buckling Pressure, eq. (28)
p_s	Structural Proportional Limit Ratio, $p_s = \sigma_{ps} / \sigma_y$
p_{sb}	Shell Biaxial Membrane Yield Pressure, Figs. 48-50
$\overline{p_{s\theta}}$	Pressure at which the Average Circumferential Stress in the Shell reaches Yield (o-o-c = 0), Figs. 48-50
$\overline{p_{sB}}$	Pressure at which the Average Biaxial Stress in the Shell reaches Yield (o-o-c = 0), Figs. 48-50
p_t	Frame Tripping Elastic Buckling Pressure, eq. (46)
p_{ti}	Frame Tripping Inelastic Buckling Pressure, eq. (66)
P_y	Yield Load, Fig. 9
p_y	Frame Yield Pressure, considering o-o-c, eqs. (54) and (56)
p_{yp}	Plate Yield Pressure, considering o-o-c, eqs. (55) and (57)
p_{yf}	Frame Membrane Yield Pressure, eq. (53)
R	Radius (General)
R_c	Radius to the Frame Centroid (with Effective Length of Shell), Fig. 40
R_f	Radius to the Frame Flange, Fig. 40
R_i	Internal Radius, Fig. 40
R_m	Mean Radius, Fig. 40
R_s	Radius to the Frame Centroid (without Effective Length of Shell), Fig. 40

t	Shell Thickness
t_w	Web Thickness
t_f	Flange Thickness
u,v,w	Displacement Components, Fig. 20
uu,vv,ww	Rotation Components, Fig. 20
x,y,z	Rectangular Coordinates, Fig. 20
X_m	Model Uncertainty Factor: $\frac{\text{observed data (test, FE, etc.)}}{\text{predicted value (design equations)}}$:
$X_{m_{fy}}$	Model Uncertainty Factor, Frame Yield
$X_{m_{fy}}'$	Same, but: observed data from FE models excluding residual stresses, predicted value according to eq. (56)
$X_{m_{fy}}''$	Same, but: observed data from FE models excluding residual stresses, predicted value according to eq. (56)
$X_{m_{fy}}'''$	Same, but: observed data from FE models including residual stresses, predicted value according to eq. (65)
$X_{m_{ft}}$	Model Uncertainty Factor, Frame Tripping
$X_{m_{ic}}$	Model Uncertainty Factor, Interframe Shell Collapse
$X_{m_{py}}$	Model Uncertainty Factor, Plate Yield
X_{m_l}	Model Uncertainty Factor, Elastic General Instability
Z	Batdorf Parameter, $Z = \frac{l^2}{Rt}\sqrt{1-\nu^2}$
z_s	Distance of Frame Centroid from Shell (without Effective Length of Shell), Fig. 40
W	Weight
α_i	Sensitivity Factor of Variable i, eq. (77)
β	Safety Index
χ	Bodily Factor, eq. (42)
δ_n	Out-of-Circularity Amplitude in Mode n
δ_p	Shell Distortion due to Welding
Δ	Displacement
$\Phi( )$	Standard Normal Distribution
$\varphi( )$	Probability Density Function for a Normally Distributed Random Variable with Zero Mean and Unit Variance
η	Tension Block Coefficient
η_{pl}	Usage Factor for Shell Plating, eq. (13)
γ	Factor given by eq. (48)

γ_{xm_j}	Modelling Partial Safety Factor for Collapse Mode j
γ_f	Load Partial Safety Factor
Γ	Frame Warping Constant, $\Gamma = \Gamma_1 + \Gamma_2$
Γ_1	Primary (Longitudinal) Warping, $\Gamma_1 = I_z\,(d_w+t_f/2)^2$
Γ_2	Secondary (Transverse) Warping, $\Gamma_2 = (b_f^3 t_f^3/4+d_w^3 t_w^3)/36$
κ_i	Curvatures of Paraboloid, Second Order Reliability Analysis
λ	Slenderness Parameter (General), $\lambda = \sqrt{\sigma_y / \sigma_{cr}}$
λ_s	Shallowness Parameter, Fig. 13, $\lambda_s = 2\sqrt[4]{3(1-\nu^2)}\,\sqrt{H/t}$
μ_i	Mean of Variable i
ν	Poisson's Ratio
θ	Cylindrical Coordinate, Fig. 20
ρ	Material Density, Table 31
σ	Uniaxial Stress (General)
σ_b	Modified Bending Stress at the Frame, eq. (63)
σ_c	Collapse Stress (General)
σ_{cl}	Critical Stress of a Spherical Cap Clamped at its Edge, Fig. 13, $\sigma_{cl} = \dfrac{Et}{R\sqrt{3(1-\nu^2)}}$
σ_{cr}	Elastic Critical Stress (General)
σ_{cr_i}	Inelastic Critical Stress (General)
σ_i	Standard Deviation of Variable i
σ_{ps}	Structural Proportional Limit, $\sigma_{ps} = \sigma_y - \sigma_{rc}$
σ_{rc}	Midbay Residual Compression Stress
σ_{rc1}	Along-the-Weld component of σ_{rc}
σ_{rc2}	Across-the-Weld component of σ_{rc}
σ_{rf}	Residual Tension Stress in Frame
σ_t	Elastic Tripping Stress
σ_{t_i}	Inelastic Tripping Stress
σ_u	Structural Average Ultimate Stress, Fig. 7
σ_y	Material Yield Stress (General)
σ_{yf}	Yield Stress of Frame Material
σ_{yp}	Yield Stress of Shell Plating Material
σ_1, σ_2	Shell Cold Rolling Residual Stresses, Fig. 43
τ_{cr}	Critical Shear Stress, Fig. 12
ξ	Ratio σ_t/p_t, $\xi = \dfrac{\sigma_{yf}R_f}{p_{yf}R_s}$

Chapter 1 - INTRODUCTION

1.1) AIMS AND SCOPE

Oceans correspond to about 70% of the earth's surface. Such a vast hydrospace contains natural resources which may become vital as the world's population increases in number and, hopefully, in living standards. Some of these resources, notably oil, have already been exploited by the offshore industry for a number of years. As offshore activities move deeper, externally pressurised vessels, presently used as primary structural members in offshore platforms, buoyancy elements and submersible vehicles, tend to become even more important. Onshore, externally pressurised vessels are also important structural components of vacuum chambers. These structures have their structural design based, to a large extent, on submarine pressure hull (PH) design criteria.

Submarines and submersibles have been traditionally used for military purposes such as mining and mine countermeasures, rescue vehicles and submarine and antisubmarine warfare. Well established design criteria exist for their pressure hulls, based on deterministic safety factors covering many uncertainties arising from operational as well as design and construction factors. Such criteria were developed in the 1950's and 60's and successfully employed by the major navies of the world for the design of relatively shallow water vessels, with pressure hulls made usually of quenched and tempered steels such as Q1N (HY80) and Q2N (HY100).

Important changes have happened, though, as far as underwater operations are concerned. Offshore oil exploration and production has been moving steadily to deeper waters; drilling at 1000m below the sea level is not an unrealistic scenario for the near future. Submersibles can also be employed in a number of other commercial applications: inspection and repair of cables, pipelines and other underwater installations, transport to and from subsea completions, inspection and recovery of sunken vessels and objects,

recreation and tourism. Furthermore, environmental and scientific concerns tend to require extensive oceanographic surveying. Small Remotely Operated Vehicles are popular for shallow waters, but for deep waters manned submersibles may be preferred. The latter offer a direct viewing for its occupants in a dry one-atmosphere pressure hull, without relying on long guide wires and umbilicals and without having its operations limited by adverse weather conditions at the sea surface.

As far as submersible design and operation in general are concerned, the reader may refer to [1-8]. Fig. 1 gives a brief history of inner space exploration and exploitation, with emphasis on manned submersibles. Fig. 2 shows some possible concepts:

The Trieste I, with a spherical pressure hull 180mm thick, made of Ni-Cr-Mo steel, which achieved a record depth of 10900m in 1960. The pressure hull was relatively small, but so heavy that an array of gasoline-filled tanks was necessary to provide neutral buoyancy

Offshore Service Submarines aiming to operate at the North Sea, Gulf of Mexico and Offshore Brazil [9]

The Nomad 1000 [10], which is also a motor yacht capable of 12 knots at the surface. As a curiosity, a price of US $ 4.5 million is given with the following comment [10]: 'clearly, a vessel of this capability is not going to be cheap, on the other hand it opens up to the private owner huge tracts of the world where few have ventured before'

Fig. 3 gives the distribution of ocean depth in which two values are highlighted: 1500m, which would possibly cover most commercial applications, and 6000m, which would cover almost 100% of the ocean. Fig. 4 shows, for some candidate pressure hull materials, the collapse depth plotted against the estimated W/Δ ratio, for ring-stiffened cylinders, from [11]. Recent optimisation studies [12], limited to steel, aluminium and titanium, showed

similar trends but with somewhat larger W/Δ ratios, when actual code formulations and fabrication constraints are considered. It seems that for depths less than about 1500m, steel and other metals can provide feasible solutions and may probably be cheaper to use; for deeper operations composite materials tend to be necessary.

The unstiffened sphere may be structurally the most efficient hull form for high external pressure but can lead to difficult interior arrangement and incurs large hydrodynamic drag, dynamic stability and draft problems. Pressure hulls, whenever possible, consist of a stiffened cylinder closed by domed ends, with a shallow stiffened truncated cone sometimes being used as a transition element. Their structural design is dominated by ultimate strength considerations (buckling), serviceability ones (fatigue and fracture) being less important and less influential on weight.

Important technical improvements are occurring in areas such as propulsion, materials and control. Air-independent nuclear propulsion has been employed for a number of years, although it is suitable only for large military vessels. A lot of attention is being given to other air-independent forms such as fuel cells or Stirling Engine, suitable for smaller and cheaper boats. Alternative materials such as titanium and aluminium alloys are now easily available. Intensive research is under way on composite materials [11,13,14] and it is hoped that enough information will be disclosed for it to be considered in the future. Future designers will be in a much better position to tackle the two major technical problems involved in the design and operation of such vessels: obtaining an air-independent propulsion and a pressure hull light enough for neutral buoyancy to be achieved at even very large depths. The impact on both commercial and military applications is likely to be high.

Traditional safety factors used in the design of other marine structures pay high regard to the uncertainties in wave induced loading and in material properties and structural behaviour. In submersibles, however, the operational loading is known very precisely, being the hydrostatic sea

pressure for the required design diving depth. Moreover, because of the dominance of compression loading in the pressure hull of submersibles, the need for high standards of notch ductility and for fatigue inspections is much less than those required for internally pressurised vessels and for marine structures generally. The quality of material selection and construction is in any case much higher than for most other marine structures.

It would therefore seem that the reasons for having a safety factor in pressure hull (PH) design are:

(a) possible accidental or intentional excursions below the design diving depth

(b) the sensitivity of collapse of compression structures to the effects of shape imperfections and residual welding stresses

(c) the uncertainty over the magnitude and distribution of welding residual stresses in real structures

(d) the modelling uncertainty associated with collapse prediction, particularly in those modes associated with frame collapse

(e) the sudden and explosive nature of collapse with no reserve strength whatever (in contrast to most other structures)

(f) the importance of the pressure hull for the overall safety of the vessel, given the absence of any structural redundancy (in contrast to other structures)

Other factors, not explicitly allowed for in PH design, are also expected to be sufficiently covered by the safety factors. These are all quite complex phenomena, some of them dynamic in nature:

(g) the effects of damage, due to collision, grounding and docking, on the pressure hull collapse strength

(h) the effect of high local stresses in the vicinity of PH penetrations and PH connections with the internal structure

(i) in naval submarines, possible adverse local pressure effects arising from nearby underwater explosions

These factors can be grouped in three categories:

Operational: in naval submarines accidental depth overshoots can and do occur, and arise from a systems failure or from jamming of the sternplanes. There are therefore depth dependent limitations placed on speed. To evade weapons or reduce the risk of sonar detection, the captain may also, in extreme war conditions, decide to overdive, for example by 30% or more. Thus (a) is a very real risk and the notional structural collapse probabilities associated with depth overshoot and overdiving have been assessed recently [15] and previously [16,17]

Design and Fabrication: (b) to (f) show the importance and the difficulties involved in predicting the pressure at which the PH is expected to collapse. Designers have had to resort to semi-empirical prediction methods, and a deterministic design procedure evolved for the design of Royal Navy (RN) submarines [17-19] in which Interframe Shell Collapse is accurately predicted and arranged to have adequate but not excessive safety, while General Instability and Tripping are avoided rather than predicted

Other factors: factors (g) to (i) cannot, at present, be explicitly included in PH design although new research [20-22] has been reported in some of these areas. These can be tackled, in general, by a careful design of structural details, with the aid of Finite Element (FE) analyses

Factors (e) and (f), coupled with the difficulty in predicting collapse from strain gauge or other measurements (for example, taken during deep diving trials), suggests that proof testing of the completed structure would be appropriate for external pressure applications [15,17,23]. Unfortunately, practical difficulties seem to preclude this and the requirement does not appear in design codes. This places a premium on the use of well validated design and assessment methods as well as on their constant improvement.

The present constant safety factor approach could be improved, particularly when designing for deep diving and for commercial applications, in the following grounds:

1) in naval submarines, operational as well as design and fabrication factors have to be allowed for in the safety factors used in PH design. The former suggest a safety factor depending on the diving depth: an overshooting of 50m, say, would be more harmful to a PH designed to operate at 300m than to one designed to operate at 1500m. Design and fabrication factors alone, on the other hand, suggest a safety factor independent of the diving depth

2) in commercial submersibles and other externally pressurised vessels in which overshooting may not be a real risk, it appears that, in order to have the same notional safety as in naval submarines, only design and fabrication factors would need to be considered. It is interesting to note that the same safety factors are often used in their design as for the design of naval submarines [24]

3) in extreme conditions, the captain of a submarine may be faced with a choice between overdiving and risking a structural collapse or not overdiving and risking detection and/or weapon effects. The present methods do not give a rational basis for such a decision

4) if the maximum value allowed for a shape imperfection (o-o-c, e.g.) is exceeded, large penalties have to be imposed, like reducing the operational

depth of the vessel. It may well happen that, although the maximum value is exceeded, the spatial distribution of the imperfection is favourable: the predominant mode of the imperfection may not coincide with the critical mode of the structure or the maximum stress under external pressure may occur in a region where the yield stress of the material is higher than assumed in design, e.g.

To address such limitations, a pilot study on the application of reliability methods to naval submarine PH design, was initially undertaken for the MoD [25-27]. The potential for using such methods was demonstrated but, because of the geometry supplied for the study (not representative of RN designs at all), rather paradoxical results were obtained: the failure probabilities associated with the frame collapse modes were higher than those associated with Interframe Shell Collapse. Such a result attracted a lot of criticism because it contradicted a well established design philosophy and, indeed, previous collapse tests in decomissioned vessels which have shown Interframe Shell Collapse occurring first. This highlighted the need for more representative designs to be considered as well as the need for improved modelling of the frame collapse modes. The present work deals with these aspects, incorporating recent advances such as:

the introduction of semi-probabilistic code formats (Level I) derived from reliability based methods in which a more rational, statistical approach is given to the uncertainties involved

new model tests allowing a more accurate prediction of the effect of initial imperfections on the collapse load

the use of general purpose FE programs, able to solve complex non-linear structural problems

It aims at proposing a Level I reliability based design method for the ultimate strength of ring-stiffened cylinders under external pressure. It will be

focused at tee ring stiffeners, but some attention will also be given to other forms of stiffening, such as flat bar ring frames.

The work here described involved many different aspects. Frame design formulations were reviewed and compared with experimental data and FE analyses [28-34]. Improvements to these formulations were implemented when necessary. FE models for both Elastic Eigenvalue Analysis and Non-Linear Analysis (Riks method) were validated in view of experimental results and mesh studies. The later type of analysis can handle material behaviour beyond the elastic limit, shape imperfections and residual stresses. The program ABAQUS [35] was used. Both FE and experimental results were used in the selection of adequate values for the mean and coefficient of variation (cov) of the modelling uncertainty associated with collapse prediction in the various modes [34]. Different reliability methods were implemented and compared [36,37]. Suitable code formats and target reliabilities were investigated [37]. Multi Criteria Optimisation techniques were used to find solutions, according to the BS 5500 [24] design criteria, for different operational pressures, radii, compartment lengths and materials, which were further used in partial safety factor optimisation [12,37].

Although the present work is mostly aimed at naval submarines and commercial submersibles, its implications may well be relevant to the external pressure design and assessment of, for example, buoyancy chambers, columns, pontoons, seabed structures, habitats, etc., used in offshore and subsea engineering. The work related to the modelling of the frame collapse modes, Frame Tripping in particular, may also be relevant for other types of ring-stiffened shells under buckling conditions [38,39].

1.2) OUTLINE OF THE THESIS

The remainder of Chapter 1 is concerned with the literature review and present design criteria. The main sources of information as well as some basic concepts in column and shell buckling design are outlined. A review of some

of the major codes of practice for externally pressurised cylinders, in Western Europe and the USA, is given, showing the relevant buckling modes and how they are dealt with in the codes.

Chapter 2 is concerned with elastic buckling, with emphasis given to the buckling modes more directly affecting frame collapse. Comparisons between experiments, FE results and theory are given.

Chapter 3 deals with collapse prediction with emphasis given to the frame collapse modes. The main factors affecting collapse prediction are reviewed and the modelling uncertainty associated with the formulations used in design is investigated.

In Chapter 4, a brief introduction to Structural Reliability theory is given, the different aspects involved in the development of a Level I code format are reviewed (statistical properties of the basic variables, reliability methods, sensitivity studies, code format, design space, target reliability) and a partial safety factor optimisation is carried out. Chapter 5 gives conclusions and future work.

1.3) LITERATURE REVIEW

1.3.1) Overview

Externally pressurised ring-stiffened cylinders have been the subject of intense research due to their extensive range of practical applications and are treated in many codes, such as:

the external pressure section of the ECCS [40] which evolved from the British Standard BS 5500 [24] which itself evolved from the RN pressure hull design practice [17-19]

the Det norske Veritas (DnV) classification notes for mobile offshore units [41], largely based on research programmes undertaken in Norway [42]

the recently issued Germanischer Lloyd (GL) [43] rules for underwater technology

the American Petroleum Institute (API) bulletin on stability design of cylindrical shells [44] which is part of API's Tension Leg Platform code development and follows earlier RCC work [45]. API has also recently issued a Level I reliability based design code for fixed offshore platforms [46]. Shape tolerances are given in [44, 47]

A major source of information on the subject is the extensive research on externally pressurised cylinders, combining theoretical and experimental work, carried out in the UK and in the USA in the development of pressure hulls for naval submarines and rescue submersibles, between the mid-50s and the mid-70s. Such a work was carried out mainly in the DRA, Dunfermline, UK (formerly NCRE - Naval Construction Research Establishment) and the DTNRC, Washington, USA (formerly DTMB - David Taylor Model Basin). The DRA work has been partly released to the public by authors such as Kendrick [18,19,23,48-60], Faulkner [17,61-63], Creswell [64-67], Wilson [68-70] and others [11,13,71-73]. The DTNRC work has also been partly released by a number of authors [74-105]. The subject also attracted, at that time, the attention of other researchers in different areas [106-118].

Intense research on stiffened cylinders has been carried out in recent years [119-141] for the offshore industry. There has also been renewed interest on submarines and submersibles, with recent experiments been reported in Japan [142-148], Canada and The Nethelands [21,149]. As far as the numerical modelling of shell buckling in general is concerned, the work of Bushnell [150-161] provides the best reference. More recently, improved methods have been developed to calculate snap-through loads in shells [162-164] and particular attention has been given to the numerical calculation of collapse in a General Instability mode [165-170].

Reliability based design methods have been implemented in some codes of practice [171-175] and are the subject of intense research worldwide [46,176-230].

1.3.2) Basic Concepts of Column and Shell Buckling

Some of the basic concepts involved in column buckling will be summarised, since they are often also important in stiffened cylinder design. The stiffeners in ring-stiffened cylinders under external pressure may be viewed as columns under compression, since the state of stress is similar. The major difference is that radial stresses are present in cylindrical stiffeners, but these are typically small in comparison with the hoop or 'axial' stresses.

The classical approach to buckling is that in which the structure is considered as initially 'perfect', that is, free of initial shape imperfections, residual stresses and with the material within its elastic range. By including second order terms in the differential equations of equilibrium it is possible to arrive at a characteristic value problem. Its solution will give the loads (eigenvalues) and mode shapes (eigenmodes) in which neutral equilibrium positions exist. Physically, it means that for certain critical values of the compressive load, it is possible for the structure to be in equilibrium in deformed positions which may be considerably different from its fundamental one. This phenomenon is generally referred to as *Bifurcation Buckling*, after the behaviour of straight columns under a uniform compressive load: upon reaching Euler's critical load, there are two positions in which equilibrium is possible, the straight form and a bent form, Fig. 5.

Engesser extended the classical approach for columns in the inelastic range by introducing the Tangent Modulus approach:

$$\sigma_{cr} = F_1 \sigma_{cr_e}, \text{ where: } F_1 = \frac{E_t}{E} \qquad (1)$$

For other types of structure, the factor F_1 is often generalised by combining the tangent modulus, the secant modulus and even the elasto-plastic

Poisson's ratio. For instance [42]:

$$F_1 = \sqrt{\frac{1-\nu^2}{1-\nu_p^2}} \frac{\sqrt{E_s E_t}}{E} \tag{2}$$

Another extension of the classical buckling approach to the inelastic region, for stocky sections, is the Merchant-Rankine type formula:

$$\sigma_{cri} = F_2 \sigma_y, \text{ where: } F_2 = \sqrt[k]{\frac{1}{1+\lambda^{2k}}} \tag{3}$$

The Tangent Modulus approach was further modified by Shanley [232], who showed that a straight column buckling in the elasto-plastic range has a initially stable post buckling behaviour and therefore could theoretically withstand loads above the bifurcation load given by the tangent modulus approach. The concept of postbuckling behaviour is important because the load deflection curve of a structure with shape imperfections tends to resemble that of an imperfection-free one. Therefore, the sensitivity of the limit load to imperfections is linked to the post-buckling behaviour, as illustrated in Fig. 6 for some compressed members, in the elastic range. The heavy lines indicate the behaviour of the shape-imperfect member while light lines indicate the behaviour of the shape-perfect one.

The main importance of the Tangent Modulus approach, from a design point of view, is that it can be generalised to include the effect of residual stresses. A structural proportional limit can be assumed:

$$\sigma_{ps} = \sigma_y - \sigma_{rc} \tag{4}$$

and a structural stress-strain curve can be obtained for columns depending, basically, on their section and residual stresses distribution. If the later is of a 'block' shape, the structural stress-strain curve tends to be discontinuous, Fig. 7b, while for a 'spikey' distribution it tends to be rounded, Fig. 7a. For materials with a yield plateau, Ostenfeld and Bleich [233] proposed a set of

quadratic parabolae to represent the modified tangent modulus:

$$\frac{E_t}{E} = \frac{\sigma(\sigma_y - \sigma)}{\sigma_{ps}(\sigma_y - \sigma_{ps})} \tag{5}$$

So far, none of these theories considered the effect of shape imperfections. The simplest way is using the Perry-Robertson approach in which an initial deflection is considered to be magnified by the factor:

$$\Phi = \frac{\sigma_\sigma}{\sigma_\sigma - \sigma} \tag{6}$$

and collapse is assumed to correspond to a condition of initial yield, leading to the following expression for the collapse stress:

$$\frac{\sigma_c}{\sigma_y} = \frac{1+\lambda^2+\mu-\sqrt{(1+\lambda^2+\mu)^2-4\lambda^2}}{2\lambda^2} \tag{7}$$

These rather 'historical' solutions for columns (Tangent Modulus and Perry-Robertson) cannot be regarded as complete, since none of them takes into account all relevant factors. They are nevertheless universally used as code formats for columns, after proper adjustment in view of experimental and numerical results. Some prefer the Tangent Modulus approach on the grounds that buckling depends fundamentally on the average stress acting over the cross section.Others, like the ECCS [40], use different families of column curves defined by eq. (7), with the factor μ being adjusted to fit experimental and numerical results, depending on the shape of the cross section and the manufacturing procedures (residual stresses), Fig. 8.

In the end, the most adequate method is of course the one which best approximates experimental results. Fig. 9 illustrates the conservative nature of the ECCS curves in comparison with test results. A Tangent Modulus approach would tend to be more adequate as a mean curve. Fig. 9 also shows the scattering, in terms of a coefficient of variation (cov), of the test data as a

function of column slenderness. A value of 15% is representative of the peak, occurring at the transition between elastic and inelastic buckling. Such a value is often found to be associated with the modelling uncertainty for column buckling, in various reliability based codes of practice.

Buckling may also be a critical mode of failure in thin shell structures, which have their membrane stiffness much in excess of their bending stiffness. This type of structure is often used due to its structural efficiency in the fundamental equilibrium position: because of its curvature, shells resist loads such as external pressure predominantly by membrane deformations. Unfortunately, their bifurcation buckling often involves other positions of neutral equilibrium (buckling modes) in which bending is relevant. If these are triggered, by unavoidable shape imperfections, large deflections may arise and as a consequence the structure may fail quite catastrophically. These other equilibrium positions may be dramatically different from the fundamental one: for instance, thin, shallow domes convex to a pressure loading may buckle in a shape which is concave to the pressure. Or cylinders under external pressure may buckle in a wavy pattern quite different from the fundamental axisymmetric equilibrium. Such a gross change in geometry is often called *Snap-Through*.

The structural stability of shells is a complex problem to be dealt with. The apparently simple case of an unstiffened cylinder under axial load puzzled engineers for many years, because of the drastic discrepancies between test results and predictions of the classical approach even for very carefully made specimens. Figs. 10 to 13, from Bushnell's compilation of [150], show the discrepancy between test and classical theory for axially compressed cylinders, externally pressurised cylinders, cylinders under torsion and spherical shells under external pressure.

Koiter [236] formally showed that these discrepancies are due to the effect of unavoidable shape imperfections. He employed an asymptotic expansion of the structural response around the bifurcation buckling load of the corresponding shape-perfect structure. It resulted in simple formulae for the

pre-buckling and the post-buckling response of the structure and for the effect of unimodal shape imperfections on the buckling strength. Classical bifurcation buckling analysis searches for the loads at which neutral equilibrium positions other than the fundamental one exist. Koiter's theory aims to investigate the stability of the equilibrium in these other positions, in the vicinity of the bifurcation point. As hinted in Fig. 6, if the post-buckling behaviour is unstable, the limit load that the structure can attain will be reduced by imperfections. This fact tends to be confirmed in practice: Fig. 14a shows that experimental results tend to disagree from the classical buckling theory when Koiter's imperfection sensitivity parameter b is negative.

The discrepancy for external pressure is less dramatic than for axial load, but cannot be ignored. Fig. 14 shows results for external pressure due to Budianski and Amazigo [117], Hutchinson and Amazigo [118] and Gonçalves and Batista [138]. Stiffeners tend to reduce imperfection sensitivity but introduce different forms of buckling. Fig. 14a shows results for unstiffened cylinders and Interframe Shell buckling in ring-stiffened cylinders (stiffeners modelled as radial supports). Fig. 14b shows results for General Instability (closely spaced, light stiffeners) and Fig. 14c again for Interframe Shell buckling (sparsely spaced stiffeners). There are no results for Frame Tripping.

It is important to stress that post-buckling behaviour may depend on a number of factors, such as geometry, buckling mode, whether or not the structure has some of its parts loaded beyond the limit point, etc.. Care has to be taken when interpreting general statements often found in the literature regarding post buckling behaviour of a given type of structure, without clearly specifying whether all of these factors were taken into account.

Although important in a theoretical sense, Koiter's theory does not account for many important factors affecting collapse prediction in marine structures (treated in Chapter 3), such as multi-modal imperfections and residual stresses. To account for such factors, designers have had to rely on empirical evidence and engineering judgement.

The term 'buckling' will be used, from now on, to refer to bifurcation buckling of an initially shape-perfect shell while the term 'collapse' will refer to an initially shape-imperfect one.

1.4) PRESENT DETERMINISTIC DESIGN CRITERIA

1.4.1) Submarine Design Thinking

The design requirements given by most of the codes of practice for externally pressurised structures have, to a great extent, evolved from previous practice with naval submarine pressure hull design. They naturally follow the submarine design thinking in which representative modes of failure are selected and the corresponding collapse pressures are estimated with fairly simple analytical methods, assuming no mode dependency effects. Deterministic safety factors are imposed to keep these collapse pressures sufficiently above the operational pressure, thus providing adequate safety, and also to keep them apart from each other, minimising mode interaction. The relevant modes of buckling normally considered are:

a) Interframe Shell Collapse: the shell deforms between the frames, either axisymmetrically or with n circumferential waves , Fig. 15b. Its critical form is usually associated with short wavelengths in both the circumferential and axial directions ($n > 10$, $m=L_c/2L_s$).

b) General Instability: shell and frame deform together between bulkheads, Fig. 15a. Its critical form is usually associated with long wavelengths in both the circumferential and axial directions ($n \sim 2,3$, $m=1/2$).

c) Frame Tripping: the frame twists about its point of attachment to the shell, Fig. 15c. Its critical form is usually associated with n~4-8, say, and a quarter of wave along the frame depth.

d) Local Buckling of the Web: the frame web deforms like a plate under compression supported by the shell and the frame flange, Fig. 15d. Its critical form is usually associated with $n > 10$, say, and a half wave along the frame depth.

As the reader may observe from Fig. 15, the distinction between them is purely artificial. The buckling modes calculated with a FE model, for instance, tend to be a combination of these idealised forms. Furthermore, design has to be based on collapse rather than on elastic buckling so that material plasticity, shape imperfections and residual stresses have to be accounted for, further complicating the problem.

Submarine designers, however, realised that Interframe Shell Collapse is the mode which most directly governs the pressure hull weight and can usually be empirically predicted with good accuracy. So a reasonably simple design method was devised retaining this artificial distinction [17-19]. Interframe Shell Collapse is arranged to have an adequate but not excessive safety margin. The other buckling modes require less material for them to be prevented in traditional submarine hulls and received far less attention. They are conservatively estimated, and the additional safety is supposed to cover uncertainties in post-buckling behaviour and possible effects of residual stresses and mode interaction. This is the rationale behind the design method developed at DRA-Dunfermline (formerly NCRE) for designing RN submarines. This was partially released to the public in the early 70's and formed the basis for the external pressure section of the BS 5500 [24] which in turn forms the basis for the relevant European regulations, ECCS [40].

1.4.2) Codes of Practice

This section reviews the recommendations for design, in case of external pressure, given by some of the major codes of practice in North America and Western Europe, such as BS 5500 [24], ECCS [40] (external pressure section), DnV [41] (mobile offshore units), GL [43] (underwater technology), API RP 2A [46,47] (fixed platforms, $R_m/t < 150$) and API Bul 2U [44] (floating platforms,

$R_m/t \geq 150$). Their requirements may be substantially different, since these are derived from different databases and tend to be influenced by local specialists. Comparisons between them can be found in the literature [119,235] so this section will simply summarise the major aspects. The common point between them is the submarine design thinking explained before in which Interframe Shell Collapse is empirically predicted and arranged to have adequate but not excessive safety and the other modes are avoided rather than predicted.

Interframe Shell Collapse

BS 5500 [24] and ECCS [40] use a lower bound of collapse tests of 700 cylinders in the range:

$$5.9 < R_m/t < 250$$
$$0.04 < L_s/R_m < 50$$

These are plotted against p_m/p_{c5} in Fig. 16. p_m is given by the von Mises formula:

$$p_m = \frac{Et/R_m}{n^2 - 1 + 0.5\left(\frac{\pi R_m}{L}\right)^2}\left\{\frac{1}{\left[n^2\left(\frac{L}{\pi R_m}\right)^2 + 1\right]^2} + \frac{t^2}{12R_m^2(1-\upsilon)^2}\left[n^2 - 1 + \left(\frac{\pi R_m}{L}\right)^2\right]^2\right\} \quad (8)$$

p_{c5} is the pressure causing membrane yield in the shell midway between stiffeners:

$$p_{c5} = \frac{\sigma_{yp} t}{R_m(1+\gamma G)} \quad (9)$$

The advantages of such a plot are given in [18]:

The stiffener area is taken into account by p_{c5}

p_{c5} is based on the maximum membrane stress, which seems to be physically reasonable

It can be generalised to other forms of shell, like cones, remote from end effects

Collapse at very low mean stress values usually occurs close to p_m

When p_m is much greater than p_{c5} , collapse usually occurs at a slightly higher pressure than p_{c5}

Fig. 16 also shows a mean curve which tends to approximate the experimental data by about 20%, for $p_m/p_{c5} > 1.5$. For $p_m/p_{c5} < 1.5$, elastic buckling is dominant and shape imperfections lead to a greater scatter of results. According to [18], experimental data for fabricated cylinders show that collapse pressures can be little greater than $p_m/2$. That is why the lower bound curve is arranged to have a slope corresponding to $p_c=p_m/2$ at the origin. On the other hand, extruded tubes with a high degree of circularity show that pressures very close to p_m can be achieved. These curves are applicable to a wide range of geometries, the exception being cylinders with closely spaced heavy stiffeners, as discussed in [18]. The collapse pressure calculated with the lower bound is required to be at least $1.5p_d$. The shell out-of-circularity is limited to 0.5% of the radius.

The technical basis for the DnV [41] recommendations is given by Odland [42]. The framework is the classical buckling stress based on Donnell's equations [237]:

$$\sigma_E = C_\theta \frac{\pi^2 E}{12(1-\nu^2)}\left(\frac{t}{L_s}\right)^2 \qquad (10)$$

where C_θ is a buckling coefficient given in Fig. 17. It can be seen that using C_θ'(hydrostatic pressure), the von Mises solution (non-deflecting simple

supports at the frames) is obtained. The code recommends, however, a reduced buckling coefficient which takes into account the effect of shape imperfections on the elastic buckling:

$$C_p = 4\sqrt{1+0.025Z} \qquad \text{for lateral pressure}$$
$$C'_p = 2\sqrt{1+0.1Z} \qquad \text{for hydrostatic pressure} \qquad (11)$$

Although it is not clear in [42] how such a reduction is obtained, it seems to be based on Koiter's postbuckling theory.

A Merchant-Rankine type formula is used in the inelastic range:

$$\frac{\sigma_{cr_i}}{\sigma_y} = \sqrt{\frac{1}{1+\lambda^4}} \qquad (12)$$

Finally usage factors η relating σ_{cr_i} to the maximum acting hoop membrane stress σ_θ are imposed. These are dependent on the type of structure and loading condition. For shells of single curvature and functional loads:

$$\eta_{pl} = 0.6\alpha' \qquad (13)$$

where:
$$\alpha' = 1.0 \qquad \text{if } \lambda \le 0.2$$
$$\alpha' = 1.05 - 0.25\lambda \qquad \text{if } 0.2 < \lambda \le 1.0$$
$$\alpha' = 0.8 \qquad \text{if } \lambda > 1.0$$

The o-o-c is again limited to 0.5% of the radius.

The Germanischer Lloyd [43] bases its predictions on a modified Tangent Modulus approach, given by Reynolds [75], for periodic buckling and Lunchick [81], for axisymmetric buckling. Deterministic safety factors are used to cater for shape imperfections and residual stresses. The shell out-of-circularity is limited to 0.5% of the radius.

Other German submarine designers [238] use similar procedures, but with the empirical curve of Fig. 18, given by Pulos and Krenzke [97] to account for

the effect of shape imperfections and residual stresses. The curve compares results of machined models with results of fabricated models and shows a reduction factor between 0.75 and 1.0 which is a function of the ratio elastic/inelastic buckling pressure. Maximum reduction corresponds to the transition between elastic and elastic-plastic buckling, similarly to columns under compression, Fig. 9.

API RP2A [46] has a reliability based Level I - also referred as Load and Resistance Factor Design (LRFD) - code format and covers cylinders with $R_m/t < 150$. The recommended design pressure p_d is given by:

$$p_d = \gamma_d \rho_{sw} H_z \tag{14}$$

where γ_d is a loading partial safety factor (1.3 for normal operation or 1.1 for extreme environmental conditions), ρ_{sw} is the sea water density and H_z is the design diving depth.

The following requirements are given for Interframe Shell Collapse:

$$f_h \le \phi_h F_{hc} \tag{15}$$

where $f_h = p_d D/2t$, ϕ_h is a partial safety factor for the resistance (0.8 is recommended) and F_{hc} is the nominal hoop buckling stress given by:

$$F_{hc} = F_{he} \qquad \text{for } F_{he} \le 0.55\sigma_{ys} \quad \text{(elastic buckling)} \tag{16}$$

$$F_{hc} = 0.7\sigma_{ys}\left(\frac{F_{he}}{\sigma_{ys}}\right)^{0.4} \le \sigma_{ys} \qquad \text{for } F_{he} > 0.55\sigma_{ys} \quad \text{(inelastic buckling)}$$

F_{he} is the elastic buckling stress, taking into account the effect of imperfections, given by:

$$F_{he} = 2C_h Et/D \tag{17}$$

C_h is a coefficient implying a constant 20% reduction over the classical buckling stress due to imperfections:

$$\begin{aligned} C_h &= 0.44t/D + \frac{0.21(D/t)^3}{M^4} && 0.825D/t \le M < 1.6D/t \\ C_h &= 0.737/(M-0.579) && 1.5 \le M < 0.825D/t \\ C_h &= 0.80 && M < 1.5 \end{aligned} \qquad (18)$$

$$C_h = 0.44t/D \qquad M \ge 1.6D/t$$

where $M = \frac{L_s}{D}\sqrt{\frac{2D}{t}}$

The o-o-c is defined in [47] as the difference between the major and minor outside diameters and shall not exceed 1% of the nominal diameter or 1/8 of the shell thickness, whichever is the most critical, if the shell thickness is greater than 2 in. If the shell thickness is smaller than 2 in, the maximum o-o-c is limited to 1/4 in.

API Bul 2U [44] covers cylinders with $R_m/t \ge 150$. In the case of hydrostatic pressure, it is imposed that:

$$F_\theta \le \frac{F_{hcL}}{FS} \qquad (19)$$

where FS is the safety factor given by:

$$FS = 1.67\psi, \text{ for normal design conditions} \qquad (20)$$

where

$$\begin{aligned} \psi &= 1.2 && \text{if } F_{hcL} \le 0.55F_y \\ \psi &= 1.444 - 0.444F_{hcL}/F_y && \text{if } 0.55F_y < F_{hcL} < F_y \\ \psi &= 1.0 && \text{if } F_{hcL} = F_y \end{aligned} \qquad (21)$$

F_y is the yield stress and F_{hcL} is the inelastic buckling stress given by:

$$F_{hcL} = \eta F_{heL} \qquad (22)$$

where η is the plasticity reduction factor given by:

$$\begin{aligned} \eta &= 1 && \text{if } 1/\lambda^2 \le 0.55 \\ \eta &= 0.45\lambda^2 + 0.18 && \text{if } 0.55 < 1/\lambda^2 \le 1.6 \\ \eta &= \frac{1.31}{1 + 1.15/\lambda^2} && \text{if } 1.6 < 1/\lambda^2 < 6.25 \\ \eta &= \lambda^2 && \text{if } 1/\lambda^2 \ge 6.25 \end{aligned} \tag{23}$$

and F_{heL} is the elastic buckling stress given by:

$$F_{heL} = \frac{\alpha_{\theta L} p_{eL} R_0}{t} K_{\theta L} \tag{24}$$

where p_{eL} is the elastic buckling pressure (same as p_m) calculated with eq. (8), R_0 is the radius of the outside shell, $\alpha_{\theta L}$ is an imperfection factor assumed as 0.8 and $K_{\theta L}$ is given by:

$$\begin{aligned} K_{\theta L} &= 1.0 && \text{if } M_x \ge 3.42 \\ K_{\theta L} &= 1 - \varepsilon\psi && \text{if } M_x < 3.42 \end{aligned} \tag{25}$$

where $\varepsilon = \dfrac{0.85}{1 + L_e t / A}$, $A = A_s (R/R_s)^2$, $L_e = 1.56\sqrt{R_m t} + t_w \le L_s$, $M_x = L_s / \sqrt{R_m t}$

and

$$\begin{aligned} \psi &= 1.0 && \text{if } M_x \le 1.26 \\ \psi &= 1.58 - 0.46 M_x && \text{if } 1.26 < M_x < 3.42 \\ \psi &= 0 && \text{if } M_x \ge 3.42 \end{aligned} \tag{26}$$

F_θ in eq. (19) is the hoop stress in the shell midbay between ring stiffeners, given by $F_\theta = \dfrac{p_d R_0}{t} k_{\theta L}$.

The shell out-of-circularity is limited to 0.5% of the radius.

General Instability

The European codes, BS 5500 [24], ECCS [40], DnV [41], GL [43] use the same

method, which is similar to the Perry-Robertson approach to column buckling. It requires that, with the maximum permissible out-of-roundness occurring in the worst possible mode and which is at the same time distributed as a half-sine wave over the compartment length, the frame flange stress is less than the yield stress at a pressure well above the design pressure. The different requirements can be summarised as:

$$\sigma_{fl} = S_1 \frac{p_d \sigma_{yf}}{p_{yf}} + S_2 \frac{Ed\delta_n (n^2 - 1) p_d}{R_m^{\,2}(p_n - S_3 p_d)} \leq S_4 \sigma_{yf} \qquad (27)$$

where:

BS 5500 [24] and ECCS [40]: $S_1=S_2=S_3=1.8$ for hot formed or fabricated frames
$S_1=S_2=S_3=2.0$ for cold bent frames
$S_4=1.0$

GL[43]: $S_1= 1.7$
$S_2= 3.0$
$S_3=S_4=1.0$

DnV[41]: $S_1=S_2=S_3=2.0$
$S_4=0.9$ for cold formed frames

All of them assume a maximum out-of-roundness of the structural compartment with an amplitude of 0.5% of the radius and calculate p_n using the Bryant formula [71] for elastic buckling :

$$p_n = \frac{\left(\frac{Et}{R_m}\right)\left(\frac{\pi R_m}{L_c}\right)^4}{\left(n^2 - 1 + \frac{\left(\frac{\pi R_m}{L_c}\right)^2}{2}\right)\left(n^2 + \left(\frac{\pi R_m}{L_c}\right)^2\right)^2} + \frac{(n^2 - 1) EI_c}{R_m^3 L_s} \qquad (28)$$

The BS 5500 [24] and the ECCS [40] recommend also $p_n > S_1\, p_d$

The API RP 2A [46] requires that the stress corresponding to the elastic General Instability pressure p_n has to be at least 20% above the Interframe Shell elastic buckling stress (given by $1.25F_{he}$). p_n is calculated for n=2 with the second term of eq. (28) only, assuming that the shell does not offer any additional support to the frame. The following requirement is derived [46]:

$$I_c = F_{he}\frac{tL_sD^2}{8E} \tag{29}$$

The API Bul 2U [44] similarly requires the General Instability stress F_{heG}:

$$F_{heG} = \frac{\alpha_{\theta G}p_{eG}R_0}{t}K_{\theta G} \tag{30}$$

to be at least 20% above the Interframe Shell elastic buckling stress, now given by F_{heL}. p_{eG} is equal to p_n, eq. (28). $\alpha_{\theta G}$ is an imperfection factor assumed as 0.8 and $K_{\theta G}$ is given by:

$$K_{\theta G} = \frac{0.85L_et}{A_s + L_et} \tag{31}$$

where $L_e = 1.56\sqrt{R_mt} + t_w \le L_s$

Frame Tripping

As far as Frame Tripping is concerned, the BS 5500 [24] used to have a very conservative requirement, in which the elastic buckling stress for the ring, calculated ignoring the rotational constraint provided by the shell, had to be higher than the yield stress of the frame:

$$\sigma_t = \frac{EI_z}{A_sR_tz_s} > \sigma_{yf} \tag{32}$$

It was assumed that such a procedure would guarantee that the actual elastic buckling stress (including such a constraint) would be at least 3 times the yield stress. The present version of such a code allows a relaxation by requiring that, for flanged stiffeners, the Tripping stress has to be higher than the axisymmetric component of the stress acting at the stiffener considered as perfectly circular at the design pressure p_d:

$$\sigma_t = \frac{EI_z}{A_s R_t z_s} > \sigma_{ax} = \frac{p_d \sigma_{yf}}{p_{yf}} \tag{33}$$

For flat bar stiffeners, it is required that σ_t shall be 4 times such an axisymmetric component, for the n that minimizes eq. (8). σ_t is then given by Tables 3.6(4) and 3.6(5) of the BS 5500 [24], based on Kendrick's theory of Ref. [57]. The ECCS, in the future, may allow a further relaxation, by requiring that σ_t, calculated now including the rotational constraint given by the shell with a numerical program such as BOSOR 4, has to be 3 times the mentioned axisymmetric component [49].

The GL [43] requirements seem to be extreme: σ_t calculated according to eq. (32) has still to be 3 times the yield stress, for tee stiffeners ! For flat bar stiffeners, Figs. 9 and 10 of [23] (Tables 3.6(4) and 3.6(5) of BS 5500 [24] in graphical form) are used for σ_t and the associated pressure has to be 3 times the design pressure.

DnV [41] gives, for the elastic Tripping stress of flanged stiffeners, the same equations for both stiffened cylinders and stiffened panels. They have a first term with the contributions from the shell and from the St. Venant pure torsion and a second term with the contribution from warping:

$$\sigma_t = \beta \frac{A_w + (t_f / t_w)^2 A_f}{A_w + 3A_f} G' \left(\frac{t_w}{d_w}\right)^2 + \frac{EI_z}{\left(\frac{A_w}{3} + A_f\right) R_m d_w} \tag{34}$$

where: $\beta = \dfrac{3C+0.2}{C+0.2}$ and $C = \dfrac{d_w}{1.56\sqrt{R_m t}}\left(\dfrac{t}{t_w}\right)^3\sqrt{1-\eta_{pl}}$

For flat bars:

$$\sigma_t = \left(\beta + 0.2\frac{d_w}{R_m}\right)G'\left(\frac{t_w}{d_w}\right)^2 \tag{35}$$

These are intended to be used with a Perry-Robertson type column curve for lateral-torsional buckling:

$$\sigma_{ti}/\sigma_{yf} = 1.0 \qquad \text{if } \lambda \le 0.6$$

$$\sigma_{ti}/\sigma_{yf} = \frac{1+\mu+\lambda^2-\sqrt{(1+\mu+\lambda^2)^2-4\lambda^2}}{2\lambda^2} \qquad \text{if } \lambda > 0.6 \tag{36}$$

where $\mu = 0.35(\lambda - 0.6)$. A usage factor is recommended, defined similarly to the plating case, eq. (13).

Local Buckling of Webs and Flanges

The slenderness of the webs and flanges has to be restricted to avoid local buckling. This is usually achieved by imposing that the local elastic buckling stress exceeds the yield stress by a certain margin. In this way, it is possible to derive upper limits to the slenderness ratios of webs and flanges. These limits are shown in Table 1 for some of the various codes.

Tripping is sometimes regarded as local buckling, despite the fact that wavelengths in tripping buckling modes seldom are comparable with the cross section proportions. DnV [41] and API [44,46] do not require tripping checking if the slenderness requirements are fulfilled.

Chapter 2 - ELASTIC BUCKLING

2.1 GENERAL INSTABILITY

2.1.1 Analytical Modelling

As shown in the previous chapter, p_n is calculated in all codes surveyed with the Bryant formula, eq. (28). Other simple formulae combining shell and frame contributions were early on proposed by other authors, but eq. (28) has persisted to the present days because it tended to agree, for usual cases, with the more accurate theory proposed by Kendrick [54]. Originally an effective breadth L_e equal to a full frame spacing was assumed in the calculation of the frame moment of inertia to be used in the second term of eq. (28). It has been realized, however, that a reduced effective breadth is necessary. The present work uses the Bijlaard expression:

$$L_e = \frac{1.556\sqrt{RtN}}{\left[\sqrt{1+0.5n^4\left(\frac{t}{R}\right)^2}+0.577n^2\left(\frac{t}{R}\right)\right]^{0.5}} \qquad (37)$$

The BS5500 [24] method given in Appendix 6 can also be used. Very small differences were found when comparing the failure probabilities calculated with these two alternatives of effective breadth [28].

Kendrick's solution [54] is based on energy methods and assumes a mode shape corresponding to simply supported compartment boundaries, in the form:

$$\begin{aligned} u &= A1\cos(n\theta)\cos(\pi x/L_c) \\ v &= B1\sin(n\theta)\sin(\pi x/L_c) + B2\sin(n\theta)\,[1-\cos(2\pi x/L_s)] \\ w &= C1\cos(n\theta)\sin(\pi x/L_c) + C2\cos(n\theta)\,[1-\cos(2\pi x/L_s)] \end{aligned} \qquad (38)$$

so that mode interaction with Interframe Shell buckling is considered. The pre-buckling components were approximated by:

$$\begin{aligned} N_{0x} &= -pR_m/2 \\ N_{0y} &= -pR_m tL_s/(A_s+tL_s) \\ N_{0f} &= -ptA_sL_s/(A_s+tL_s) \end{aligned} \tag{39}$$

Torsion, warping and out-of-plane bending were ignored as they were assumed to be small for practical cases. This solution seems to be the most accurate available, but leads to a 5 x 5 eigenvalue problem which probably was considered too cumbersome to be included in the codes, where eq. (28) is normally adopted, since the mentioned mode interaction effects become important, in typical cases, for short compartments ($L_c/R_i < 2.0$, usually) or larger values of n ($n > 4$, usually) only. Creswell [65-67] extended both solutions to more general cases such as non-uniform frame spacing.

It is pointed out in [51] that there could be modes associated with smaller buckling loads, flatter at mid-compartment as in Fig. 19, but the corresponding reduction in the buckling pressure, again for usual geometries, would be too small to compensate the additional calculation difficulties involved. Kaminsky [93] and Ross [110] have proposed similar theories, based also on energy methods, to calculate the buckling pressure for fixed or partially fixed boundary conditions, but their solutions seemed to be unconservative because, in order to fulfil the desired boundary conditions with reasonably workable equations, they assumed buckled shapes that overestimated the displacements away from the boundaries, thus overestimating the collapse pressures [51,85,110].

Eq. (28) and Kendrick's method, on the other hand, always seemed to be on the safe side in relation to the experimental results available. But in these tests there was always some degree of end restraint, since it is difficult to

obtain experimentally a simply supported boundary condition and at the same time ensure proper sealing of the model. Such an end restraint may considerably raise the buckling pressure and Singer [116] pointed out that the restraint of the in-plane displacements tends to be a lot more important than the restraint of the rotational displacements. Such an effect may be particularly important for n=2, as discussed in [74] and in Chapter 6 of [150]. So there would be an uncertainty on how conservative such equations actually are. Nevertheless, this uncertainty has not been considered important in the past, given the overall conservative nature of the design methods and the fact that some end restraint will also be present in the compartments of a real submersible. In a reliability based approach such an uncertainty could be properly quantified by a modelling parameter (X_{m1}) based on experimental and FE results.

2.1.2 Finite Element Modelling

FE models can give a very accurate theoretical prediction of the buckling pressure, provided that adequate elements, mesh sizes and boundary conditions are used. Once the models are validated in view of experimental results and mesh studies they can be used in parametric studies improving our understanding of the problem. The program ABAQUS [35], available at the University of Glasgow, was used for the F.E. calculations and the modelling used is summarised in Fig. 20.

Type of Analysis

Two types of analysis were carried out:

Eigenvalue analysis: a 'dead' load and a small 'live' load are applied, and the elastic bifurcation buckling is estimated, based on the differential stiffness of the structure:

$$(K + \lambda \Delta K)v = 0 \tag{40}$$

where: K =Stiffness under dead loads ΔK =Differential stiffness
λ =Eigenvalue v =Eigenmode

The buckling load corresponds to the live load multiplied by the eigenvalue. The 'dead' load was taken as zero so that non-linear pre-buckling effects were neglected, since they were not found relevant.

Riks analysis: a reference 'live' load is applied on the structure by means of small increments, and the load magnitude corresponding to equilibrium is calculated for each of these increments, defining the load-displacement curve of the structure. The increment size is controlled by the program, according to the path length along the load-displacement curve. The total load magnitude for each increment is given by:

$$P = P_0 + \lambda_p (P_{ref} - P_0) \tag{41}$$

where: P_0 = loads other than the reference, taken as 'dead' loads
P_{ref} = reference load
λ_p = load factor given by the program

This type of analysis allows for the calculation of limit points and of the postbuckling behaviour of the structure.

Type of Element

Quadrilateral curved shell elements were considered: S4R, S8R (4 and 8 nodes respectively, thick shell, 6 degrees of freedom per node). Previous mesh studies [28,29] have shown that elements S4R5, S8R5 and S9R5 (4,8 and 9 nodes, thin shell, 5 degrees of freedom per node) although leading to a

smaller total number of d.o.f. in the model, have generated many spurious modes, and were therefore discarded. For the same number of d.o.f. in the model, element S8R leads to a much faster convergence than S4R and was therefore preferred. Plating, frame webs and frame flanges were all modelled by shell elements in order to allow for mode interaction effects. The shell elements were located at the mean radius, for the plating, and at the mean flange radius, for the frame flange.

Mesh Size and Boundary Conditions

Models 1, 3 ,5, 8 and 10 of Ref. [136] were chosen initially for mesh studies, since both the buckling and the postbuckling behaviour was reported. Since they had a rather large compartment (L_c/R_i=7), Model 6 of Ref. [110] was also included, having L_c/R_i=3.9. The relevant information regarding the models can be found in Appendix 1, and Fig. 21 shows the experimental postbuckling results for models 1, 3, 5, 8, 10.

Eigenvalue analysis: an important aspect in elastic buckling is the effect of boundary conditions. Table 2 shows the influence of the boundary conditions on the elastic bifurcation buckling of Models 3 and 10 (same dimensions) of Ref. [136], considering additionally external and internal framing, and both lateral and hydrostatic pressure. The F.E. models consisted of 7 bays, each bay being described by a grid of four S4R shell elements in the axial direction by 12 in the circumferential direction, to model an angle of $\pi/2n$. The frames were modelled by a grid of 2 such elements in the radial direction by 16 in the circumferential direction and 4 eigenmodes were extracted per model. Figs. 22 and 23 show the buckling modes for some of the different boundary conditions. Table 2 confirms that the restriction of the axial displacement considerably raises the buckling pressure and that this effect is particularly important for n=2.

A mesh study was then undertaken, with several mesh alternatives being tested under the restriction that no element should have an aspect ratio exceeding 2.0. First only the discretization of the hull plating was refined, being each bay modelled by a grid of 10 by 10 S4R elements and results agreed with those of Table 2 within 1%. This is attributed to the fact that, for the critical General Instability modes the shell contribution to the buckling pressure (given by the first term in eq. (28), e.g.) is quite small in comparison with the frame contribution (second term in eq.(28)). As a consequence it is the modelling of the frames that is critical; Table 3 shows results for different alternatives of mesh and element used in the frames. Element S4R needed less nodes and apparently underestimated the stiffness of the structure*, but element S8R converged much faster and was therefore preferred.

The results of the FE models were then compared with the six experimental results. Element S8R was used, modelling each bay by a grid of 4 such elements in the axial direction by 5 in the circumferential direction, each frame with one such element in the radial direction and using boundary conditions of the axially restrained case. Table 4 shows that the experimental results were approximated within a margin of 3%-10%, which was considered satisfactory since the axial displacements in the experiments were probably not fully restrained and the experimental results do not agree much better than that between themselves. This is shown by models 3 and 10, which although having the same nominal dimensions, had experimental buckling pressures 7% different.

Riks Analysis : the analysis was then extended to the post-buckling behaviour, Riks analysis being carried out still using S8R elements and axially restrained boundary conditions. The meshes were similar to the previous ones but with twice as much elements in the circumferential direction, since now an angle of π/n was considered to model the imperfection growth. Different values for the out-of-roundness amplitude, ranging from 0.002% to

* this is unusual since the stiffness usually decreases with increasing mesh refinement

2% of the radius, were used, in the critical circumferential mode n and according to a quarter of a sine wave (given the model symmetry) in the longitudinal direction.

For the small imperfections the structure closely followed the bifurcation model, with axisymmetric deformations that 'snap-through' into predominantly wavy ones, as the bifurcation load is exceeded, Figs. 24a and 25. For larger imperfections there is no clear bifurcation, Figs. 24b, and the bending deformations, in the form of Fig. 25b, are predominant even for small loads. In all models a slightly stable, quasi-neutral postbuckling behaviour was verified with the structure being able to withstand loads slightly higher than the elastic bifurcation limit in the expense of large deformations, in agreement with results reported in [136] and [110]. Fig. 11 shows the postbuckling behaviour given by the F.E. models, for a qualitative comparison with the experimental ones given in Fig. 21.

2.1.3. EXPERIMENTAL RESULTS

A compilation of 76 test results corresponding to machined ring-stiffened cylinders failing by elastic General Instability was made and is summarised in Table 5; details are given in Appendix 1. The models were in the range: $1.57< Z\,(l=L_s) < 29.213$, $33.3< R/t < 264$, $1.17< L_c/R_i < 10.41$ and $1.18< \chi < 8.53$.

From all these parameters, the only one to which the experimental data has showed some correlation was the 'Bodily Factor' χ proposed by Yokota et al. [147], Fig. 27. Such a factor is actually a clever combination of geometrical and material properties:

$$\chi = \frac{\sigma_{yf}}{E}\frac{L_c}{2R}\left(\frac{2R}{t}\right)^{1.5}\left(\frac{I_{pl}}{I_c}\right)^{0.75}\frac{A_{pl}+A_s}{A_{pl}} \qquad (42)$$

It is possible to fit a mean curve in this group of data:

$$p_{cr}/p_{yf} = 1.0/\chi \qquad \text{if } 1.0 < \chi < 9.0 \tag{43}$$

The model uncertainty associated with eq. (43), for this group of data, would have the following statistical properties: bias= 1.03, cov = 16.5%. The scattering of the experimental data is mainly due to the already mentioned effect of end restraint in the model boundaries; increasing the degree of restraint may not only raise the buckling pressure, but also raise the critical value of n. Reynolds and Blumenberg [74] explained this effect as being equivalent to a shortening of the compartment length. A graph of buckling pressure versus compartment length tends to reveal a series of intersecting 'sky-jump' curves, one for each mode (n=2,3,...). On a flat portion of such curves a change of the length would lead to a small change of the pressure, but for a steep slope such a change may be large. It is proposed in [74] that a simple reduction coefficient, to be applied to the compartment length, could be derived from the experiments, so that the minimum theoretical buckling pressure could approximate the experiments more closely. This proposal was tried but such a reduction was in the range of 0-30%, again with a large scattering. These simple curve fittings and reduction factors were not considered further. The experimental data was then compared with the more accurate predictions of eq. (28) and Kendrick's method and of the F.E. models.

2.1.4. COMPARISON BETWEEN TEST AND THEORY

Milligan et. al. [109]: the 4 experimental results were much above the corresponding theoretical ones, possibly due to the shallow stiffeners used, and were therefore not included further in the analysis. They suggested however that an externally framed vessel may be weaker than an internally framed one, as far as the elastic General Instability is concerned. This possible weakening effect is not predicted by the BS 5500 [24], since in

the second term of eq. (28) the mean shell radius R_m is used. It was found more appropriate to use R_c instead of R_m in the second term of eq. (28), for externally framed models.

Galletly et. al. [85], Reynolds and Blumenberg [74]: in these two references 34 experimental results obtained non-destructively are reported, in which the models had always the same nominal dimensions, except for the compartment length, but different boundary conditions. First, 24 results are given, corresponding to different compartment lengths and 5 different types of boundary conditions. Fig. 28 shows some of the results obtained in comparison with F.E. results for the axially restrained and for the axially non-restrained boundary conditions and it can be seen how difficult it is to obtain experimentally anything close to a non-restrained condition. It is perhaps worth noting that, in a model with L_c/R_i~14, the effect of end restraint virtually had vanished and both eq. (28) and Kendrink's method had converged closely to the experimental value obtained.

One of the longest cylinders, with 37 frame spacings, was used to generate new experimental results, now using machined disc inserts to simulate bulkheads. Varying the spacing between the discs, 10 results were obtained. The disks had sharpened edges and were in contact with but not physically attached to the shell. It was intended to minimize the end restraint, but surprisingly the experimental results were still considerably above the theoretical predictions. This was attributed to a possible partial end restraint due to friction forces between the disks and the shell. In our opinion there was another important factor : the compartments defined by the discs were bounded by smaller compartments which probably also acted as an 'end restraint'. Fig. 29 shows these experimental results compared with F.E. results for idealised boundary conditions and Fig. 30 shows them compared to the most extreme boundary conditions obtained previously in the experiments. It can be seen that the discs were able to raise the buckling pressure to be closer to the axially restrained case. It also

shows how such a restraint greatly affects the results for n=2, even for large compartments, while for n=3, it is relevant only for smaller compartments. That is, the curve buckling pressure versus length had still a steep slope for n=2 even for very large compartments, while it tended to become flat faster for n=3.

Blumenberg [80] and Reynolds and Blumenberg [79]: in these two reports the authors investigated the effect of intermediate deep frames of different stiffness. Only those results in which the deep frames were effectively limiting the structural compartments were used in the present analysis. Since the authors were careful in producing models divided in compartments with similar length and the deep frames had relatively small torsional stiffness, these results were probably the closest possible to a simply supported boundary condition. They were still about 15% above the F.E. results, about 5-10% above predictions of Kendrick's solution and about 5-20% above predictions of eq. (28).

Boichot and Reynolds [94]: the authors tested a great number of small models, intended to fail by plastic Interframe Shell buckling. Many of them, however, failed by plastic General Instability and 3 of them by elastic general instability which could be included in the present analysis. They had quite small compartment lengths.

Ross [110]: the author tested 7 models, 3 of them failing by elastic general instability. Since the tests were intended to verify the author's theory for partially fixed edges, there was a relatively large degree of end restraint in all of them.

Midgley and Johnson [113]: the authors tested many thin shells, 8 of them failing by elastic General Instability. These were internally stiffened and had relatively short compartments failing with n> 3.

Seleim and Roorda [136]: in these more recent tests, 10 models were tested, 5 of which failed by elastic General Instability. The degree of end restraint was again relatively high.

Yokota et al [147], Yamamoto et al [148], Morihana et al [142]: these papers present results of an extensive experimental program, reflecting the interest in submersible structures shown in Japan in recent years. Although most of them were intended to verify the effect of imperfections or plasticity, 7 of them failed by elastic General Instability and could be used here.

Fig. 31 shows the overall results for the modelling parameter X_{m1}, initially defined as the experimental buckling load divided by the minimum theoretical buckling load calculated with either Kendrick's method or eq. (28), again plotted against χ. The statistical properties of X_{m1} were:

bias = 1.25, cov = 15.5%, Kendrick's method
bias = 1.25, cov = 15.2%, eq. (28)

A previous analysis [30], limited to 24 experiments, gave a bias, using eq. (28), of 1.303 and a cov of 5.5%. The bias has not changed significantly, but the cov is considerably bigger, indicating that the small cov obtained in [30] was due to the small sample size.

Since the cov's remained quite large a more detailed study was carried out. The tests were divided in two groups:

Group A: 20 models, from Refs. [74,79,80], with small axial end restraint, like deep frames, Fig. 32. In this group, the boundary conditions are expected to be closer to simple support and the experimental buckling mode coincided with the minimum theoretical one

Group B: remaining 52 models, with larger end restraint, like bolted end rings, Fig. 33. In this group, the boundary conditions are expected to be closer to axially restrained and in most cases, experimental buckling occurred with n immediately after the minimum theoretical one

For the models of group A, both theories gave quite accurate results:

bias = 1.05, cov. = 4.4%, Kendrick's method
bias = 1.09, cov = 10.5%, eq. (28)
(sample size = 20 models)

For Group B models, it is important to redefine the modelling parameter, as in Fig. 34, so those models in which buckling occurred with n different from the minimum theoretical would actually yield information for two different values of n. Some of them would be conservatively estimated to be lower than 1.0 and would lead to overall safe results. Fig. 35 shows the results obtained. The following statistical properties were found for the modelling parameter:

- For n=2
  bias = 1.40, cov = 14.8 %, Kendrick's method
  bias = 1.34, cov = 15.2 %, eq. (28)
  (sample size = 27 models)

- For n=3
  bias = 1.07, cov = 17.5 % , Kendrick's method
  bias = 1.06, cov = 14.0 %, eq. (28)
  (sample size = 28 models)

- For n=4
  bias 1.10, cov 17.4 % , Kendrick's method
  bias 1.14, cov 23.3 %, eq. (28)
  (sample size = 17 models)

The sample sizes are relatively small but are probably sufficient to give an estimate for the bias. These values are thought to be on the safe side and it is

clear that the end restraint is quite important for n=2. It can be seen that, if the end restraint is not relevant, the scattering of the modelling parameter is reduced and therefore a cov of somewhat smaller than 15% can be used. For n=4 and L_c/R_i>4.0 or n>4, however, there was no experimental information available.

For each of the experiments, F.E. results were obtained using both simply supported and axially restrained boundary conditions, for the minimum theoretical and for the experimental n, when these were different. F.E. models without axial restraint were used to approximate group A, while F.E. models with axial restraint were used to approximate group B, with the meshes and elements recommended in 2.1.2. By doing so, most of the experiments could be approximated within a margin of 15%. The exception were models in which the end restraint raised the buckling pressure to a value approximately halfway between the two idealised conditions. Using the F.E. results as the predicted values and the experiments as the observed values for the buckling pressure, the model uncertainty would have the following properties: bias 1.020 and cov 11.8%.

Using eq. (28) for prediction and the FE results without end restraint as observed values for the buckling pressure, the model uncertainty would have the following properties: bias = 0.95, cov = 12.6%

Singer [116] proposed that a correlation exists between the boundary conditions in vibration and in buckling, provided that the modes are similar. By determining the natural frequencies of vibration of the loaded model and comparing them with appropriate theoretical predictions it would be possible to estimate equivalent elastic restraints representing the boundary conditions. If such information was available, the boundary conditions could be approximated by springs in the F.E. models, probably minimising data scattering due to end effects and providing an even smaller cov.

Fig. 36 shows the ratio between the buckling pressures obtained with the non-axially restrained F.E. models and those obtained with the axially restrained ones, for 70 of the models. The general trend would be for the bias and the cov to decrease with increasing n and increasing compartment length, as the end effect progressively vanishes. This trend is apparent in Fig. 36 for n=3; it is not so evident for n=2 because this mode is important for long compartments and was not present in the smaller ones; a similar situation happens for n= 4, 5 which were not present in long compartments.

2.1.5. PARAMETRIC STUDIES

Since none of the experimental models had tee frames, F.E. models were then applied to six realistic design cases (given in Table 6). In some cases the thickness had to be increased to avoid an excessive number of Interframe Shell buckling modes. For Case 3 different compartment lengths and n=2,3,4 were considered and results are shown in Table 7. The main observations were:

even using t=46 mm, modes corresponding to pressures above 38 N/mm^2 could not be obtained within the computer budget available, due to the excessive number of Interframe Shell modes before the General Instability ones. Therefore no results were obtained for smaller compartments and n=2 and n=4

predictions of eq. (28) and Kendrick's method were quite similar, except for the smaller compartment in n=2, for which the latter was about 8% lower, possibly because it incorporates mode interaction effects with Interframe Shell Buckling

both analytical methods seemed to lose accuracy with increasing n, due to mode interaction effects with Frame Tripping, which become apparent in n=4

the axial restraint increased the buckling pressure, according to ABAQUS [35] results, from 18% in a 8.8 m length compartment to 9% in a 14 m compartment, for n=3. For n=2 and n=4 it was not possible to obtain results for the axially restrained case even with the overthick shell

some General Instability modes, affected by the axisymmetric stress concentration in the models ends, were found with buckling pressures of 21.5 N/mm^2, for n = 2, and 20.3 N/mm^2, for n = 3, and almost insensitive to the compartment length, indicating their local nature. Table 7 shows only results corresponding to modes without such effects, as in Fig. 37

The other design cases were analysed only on their critical n and results are summarised in Table 8. The most important observations are:

the analytical methods, for n =2,3, approximate well the more refined F.E. models. For external frames, though, eq. (28) may be somewhat unconservative because of the mean shell radius been used in the second term

the effect of end restraint is much more pronounced for n=2

for n> 4, the buckling modes are mostly associated with Frame Tripping and Interframe Shell buckling

2.1.6. MODELLING UNCERTAINTY

The following statistical properties of X_{m1} are proposed for reliability calculations using eq. (28):

a.) ignoring the end restraint: bias = 1.10, cov = 12.5% (n=2,3,4)

b.) considering the end restraint: bias = 1.35, cov = 15% (n=2)
bias = 1.10, cov = 12.5% (n=3,4)

Very little experimental and no numerical information was obtained for General Instability in $n > 4$, as in this range Frame Tripping and Interframe Shell Collapse become much more critical even for overthick shells. A more conservative modelling is proposed in this range: bias = 1.0 and cov = 15%.

2.2) INTERFRAME SHELL BUCKLING AND FRAME TRIPPING

The elastic buckling in the Interframe Shell and Frame Tripping modes will be treated in the same section, since they are highly similar and related, as shown in Figs. 15b and 15c: the only difference is that, in the former, the shell radial displacement w predominates over the frame axial displacement u, while in the latter the opposite happens.

2.2.1) Analytical Modelling

Eq. (8) gives a analytical solution for Interframe Shell Buckling which is widely used, as shown in the code review of Chapter 1, and is known to be reasonably accurate (if the frames are not closely spaced) and slightly conservative. It assumes a unstiffened cylinder pinned at non-deflecting cylindrical supports at the frame positions, therefore ignoring both the radial displacement and the rotational stiffness of the frames.

A similar approach is often used for Frame Tripping, assuming the frames pinned at non-deflecting cylindrical supports and ignoring the shell radial displacement and rotational stiffness, and leading to the solution of eq. (32). The problem is that by ignoring the rotational constraint provided by the shell, the buckling pressure is underestimated by a factor of at least three in many cases.

Kennard [92] early on proposed a solution for the elastic Tripping stress as well as for the stresses due to an initial tilting, but considering the frame clamped at the shell. Kendrick has developed an accurate analytical solution, based on energy methods, which properly takes into account the rotational constraint [23] provided by the shell. Such a solution involves, for practical cases, the solution of a 6 x 6 determinant and is implemented in the N9E code. It is somewhat time consuming for hand calculation and for reliability analysis.

A simpler solution was proposed by Faulkner et al. [239], working on flat stiffened panels: the plating is modelled by a rotational spring (allowing for interaction with plate buckling) and the cross section is assumed to rotate uniformly around the connection to the plating. An energy approach is used including terms associated with St. Venant pure torsion, warping of the cross section around an enforced axis and the spring itself. Faulkner [25] has recently adapted such a solution for cylinders, neglecting the radial stresses at the frame and using a spring constant which takes into account the possible interaction between Tripping and Interframe Shell buckling. The Tripping stress is given by:

$$\sigma_t = \frac{G'J + E\Gamma\left(\frac{n}{R_m}\right)^2 + C_{0n}\left(\frac{R_m}{n}\right)^2}{I_0 + \frac{C_{0n}}{\xi p_m}\left(\frac{R_m}{n}\right)^2} \qquad (44)$$

Comparisons were carried out with ABAQUS [35] results for tee frames [28,29] and it was verified that this solution gave accurate predictions for $n \sim$ 2 - 4. For $n \sim$ 5 - 10, buckling no longer occurred with the section rotating uniformly around the connection with the shell and web deformation effects should be taken into account. For $n >$ ~10, the buckling modes were associated mostly with Interframe Shell and local web deformations and Frame Tripping was no longer relevant. Still working on flat stiffened panels,

Adamchack [104] proposed a solution including the web deformation effect, again using energy methods. Such a solution was, in a similar way, adapted to cylinders [12]:

$$\sigma_t^2\left(k_2k_4 - k_6^2\right) + \sigma_t\left(k_1k_4 + k_2k_3 - 2k_5k_6\right) + \left(k_1k_3 - k_5^2\right) = 0 \qquad (45)$$

Since the coefficients k_1-k_6 are dependent on the Tripping stress itself, a numerical solution is needed. A closed form solution was pursued, more suitable for hand calculation and reliability analysis. The Tripping stress in this solution is given by :

$$\sigma_t = \frac{b - \sqrt{b^2 - 4ac}}{2a} \qquad (46)$$

The derivation of eq. (46) and the coefficients of eqs. (45,46) are given in Appendix 2.

2.2.2) Finite Element Modelling

The program ABAQUS [35] was used for the FE calculations and the modelling used is summarised in Fig. 38.

Type of Analysis

Eigenvalue Analysis, see 2.1.2.

Type of Element

Quadrilateral curved shell elements S8R were used for the shell and the frames. The shell elements were located at the mean radius, for the plating and at the mean flange radius, for the frame flange.

Mesh Size and Boundary Conditions

Two bay models were used, with symmetry conditions in the axial borders, simulating an infinite compartment. Each case was split into several models, where only part of the circumference was modelled and tangential symmetry and anti-symmetry conditions were imposed for the eigenvalue extraction. The hydrostatic axial load component pR/2, was applied in the middle surface of the shell, in one axial border, while axial displacements were restrained in the opposite border. Four S8R elements were used for the shell between frames in the axial direction; two for the web in the radial direction and two for the flange in the axial direction. In the circumferential direction, the number of elements was always chosen to avoid the aspect ratio of the shell elements exceeding 2.0. Finer meshes did not lead to appreciably different results than those obtained with the above arrangement.

2.2.3 Parametric Studies

Comparisons between analytical and numerical results were carried out for Cases 1, 2, 3, 4, 4b, 5, 6 and 7 of Table 6 . Most of them had internal tee frames, the most usual configuration for submarine pressure hulls, but an externally tee framed and a flat bar framed vessel (buoyancy chamber) were also considered. Fig. 39 shows typical results for the elastic buckling pressures, as a function of n, for Interframe Shell Buckling , eq. (8) and Frame Tripping, eq. (46). This figure corresponds to Case 3, a design solution fairly typical of the BS 5500 [24] criteria, and ABAQUS [35] results are also given for comparison. It can be seen that for $n \geq 8$, the hull is buckling in an Interframe Shell mode. For $n < 5$, however, Frame Tripping is more critical. But this pressure hull was designed according to eq. (32) and its elastic Tripping pressures are a lot more than 3 times the axisymmetric component acting at the frame (~ 3.0 N/mm^2). The web was designed to have quite a large safety margin against local buckling: the elastic buckling pressure, calculated for a plate under compression simply supported at the shell and at the flange is 83.64 N/mm^2.

Tables 9 to 16 show comparisons between the various theories outlined and ABAQUS [35] results for the design cases. For some of them, BOSOR 4 [153] and N9E results were also found in the literature. The tables also show, from the amplitudes in the buckling modes obtained with ABAQUS [35], whether Tripping or Interframe Shell buckling was dominant. Cases 3,4,5,6, in particular, are representative of BS 5500 [24] design using eq. (32). Cases 1 and 4b have narrow, stocky flanges and therefore violate such a criteria, but can be seen to have an elastic buckling pressure which is still a lot higher than 3 times the axisymmetric component at the frame.

Results of eq. (46) agree well with F.E. results where Tripping is dominant. For n=2,3, however, the stiffener is effectively clamped at the shell and the buckling mode assumed in eq.(46) may not be critical; this can be simply checked comparing such a solution with Kendrick's N9B [23] or with Kennard's theory [92]. An example of such a situation is given by Kendrick in [48], where buckling modes were accurately calculated with BOSOR 4 [153] for Case 6b of Table 6. This is not important, however, because the minimum Tripping pressure tends to be associated with n>3, where the frame is no longer clamped at the shell and the mode assumed in eq. (46) is critical.

Chapter 3 - COLLAPSE PREDICTION

3.1) FACTORS AFFECTING COLLAPSE PREDICTION

3.1.1) Shape-Perfect Shell - Stress Analysis in the Elastic Range

If a shell is assumed initially stress-free and of a perfectly cylindrical shape, the differential equation governing its deformations (purely axisymmetric) under external hydrostatic pressure , assuming small deflections, is given by:

$$\frac{d^4w}{dx^4}+\left(\frac{pR_m}{2EI}+\frac{\nu}{R_m^2}\right)\frac{d^2w}{dx^2}+\frac{t}{IR_m^2}w=\frac{p\left(1-\nu/2\right)}{EI} \qquad (47)$$

where $I = t^3 / 12\left(1-\nu^2\right)$

The second term reflects the effect of the axial pressure on the bending deformations and produces 'beam-column' type non-linearity. By neglecting it, the analysis is greatly simplified. Eq. (47), without the second term, was early on solved for uniform ring-stiffened cylinders by von Sanden and Gunther [98]. Wilson improved their solution by using a more rigorous modelling of the frame rigidity [68]. Referring to Fig. 40, the more important results obtained were:

Pressure at which the elastic mean circumferential stress midbay between stiffeners equals the yield stress of the plate material:

$$p_{c5}=\frac{\sigma_{yp}t}{R_m(1+\gamma G)} \qquad (9 \text{ repeated})$$

where:

$$\gamma=\frac{A(1-\nu/2)}{A+t_w t+2Nt/\alpha} \qquad (48)$$

$$A = A_s\left(R_m / R_s\right)^2 \tag{49}$$

$$\alpha = \sqrt[4]{\frac{3\left(1-\nu^2\right)}{R_m^2 t^2}} = \frac{1.285}{\sqrt{R_m t}} \text{ for } \nu = 0.3 \tag{50}$$

$$N = \frac{\cosh(\alpha L) - \cos(\alpha L)}{\sinh(\alpha L) + \sin(\alpha L)} \tag{51}$$

$$G = -2\frac{\sinh(\alpha L/2)\cos(\alpha L/2) + \cosh(\alpha L/2)\sin(\alpha L/2)}{\sinh(\alpha L) + \sin(\alpha L)} \tag{52}$$

Pressure at which the elastic mean circumferential stress in the stiffener flange equals the yield stress of the frame material:

$$p_{yf} = \left[\frac{\sigma_{yf} t R_f}{R_m^2\left(1-\nu/2\right)}\right]\left[1 + \frac{A}{t_w t + 2Nt/\alpha}\right] \tag{53}$$

Solutions of eq. (47) for uniform ring-stiffened cylinders, including the second term, were later proposed by Pulos and Salerno [91] and Wilson [70] using different methods and the resulting formulae for the deflections and stresses are no longer linear in the pressure. The error incurred when neglecting the second term of eq. (47) tends to be larger the closer the operational pressure gets to the elastic buckling pressure. Since in practice the elastic buckling pressure is usually much greater than the operational pressure, the above simpler equations are more often used in practice.

Stress analysis in the elastic range, for initially stress-free, perfectly axisymmetric shells, can now be performed with reasonably inexpensive and simple models even for complex geometries such as non-uniform ring-stiffened shells and combinations of cylinders, cones and domes, with the use of general purpose Finite Difference or Finite Element programs, like BOSOR 4 [153] or ABAQUS [35].

3.1.2) Shape-Perfect Shell - Stress Analysis beyond the Elastic Limit

The stress analysis of an initially stress-free, perfectly circular shell has also been extended beyond the elastic limit for bays far from end disturbances such as bulkheads, deep frames, cylinder-cone intersections, etc.. Such disturbances usually induce a region of axisymmetric stress concentration, basically because different forms of shell, having different radial stiffness, usually deform quite differently when subjected to external pressure. Compatibility forces may then appear at the juncture, leading to the formation of a premature plastic hinge and to premature collapse of the adjacent bay.

Sufficiently far from these, however, yielding usually starts in one of the following positions, depending on the frame size: at the outside surface of the shell midway between frames in the circumferential direction or at the inside surface of the shell adjacent to the frames in the longitudinal direction. In the latter case, the pressure at which a subsequent yield condition is then reached at midbay can be calculated similarly to the previous section, provided that the boundary condition at the frame is changed [99]. For the former case approximations were proposed by Lunchick [100] and Wilson [69]. Again, this type of stress analysis can be performed with FD or FE programs such as BOSOR 5 [154] and ABAQUS [35].

These solutions did not become popular for direct use in design because buckling tends to be more critical than axisymmetric shell yielding. As Faulkner points out in the discussion of [69], their merit would be to give an improved value for p_{c5} that could perhaps reduce the scattering of the experimental results of Fig. 16 when plotted against p_m/p_{c5}.

3.1.3) Classical Buckling Estimates

As shown in Chapter 2, elastic buckling is often estimated by simple analytical solutions such as eqs. (8,28,46). These usually agree reasonably well, in the critical modes and within certain limits, with more accurate energy

methods and Finite Difference or Finite Element codes as BOSOR 4 [153] and ABAQUS [35].

The BOSOR 5 [154] program can be used to estimate the elasto-plastic buckling load of initially shape-perfect axisymmetric shells. Approximate analytical solutions for the plastic Interframe Shell buckling pressure, using a modified Tangent Modulus approach [75,81], have been proposed and are used in some codes of practice as shown in Chapter 1. A modified Tangent Modulus approach was used for the plastic General Instability pressure in [76]. A modified Tangent Modulus approach was used for the plastic Frame Tripping pressure by Faulkner in [25].

3.1.4) The Effect of Boundary Conditions

Boundary conditions may have a significant effect on the buckling pressure of shells, particularly in the elastic range as verified for General Instability in Chapter 2 (see Table 2).

As also verified in chapter 2, it is not easy to obtain experimentally simply supported or clamped boundary conditions, nor is it easy to determine the real boundary conditions in a given experiment. This tends to complicate the comparison between theoretical and experimental results.

Determining boundary conditions is a difficult task in laboratory conditions and can be expected to be even more difficult in a real structure. So it is usual to assume simply supported boundary conditions in design and ignore the effect of restraints present in the structure which then provide an additional safety margin.

3.1.5) The Effect of Shape Imperfections

In Chapter 1 the concept of imperfection sensitivity and postbuckling behaviour was introduced and the work of Koiter and its followers summarised. This has however been restricted in its application to unimodal

imperfections, which are seldom found in practice. As far as ring-stiffened cylinders are concerned, the most relevant imperfections are the out-of-circularity and the stiffener tilting, Fig. 41*. Out-of-circularity may considerably increase the stress at the frame flange and precipitate yielding and collapse. For an unimodal out-of-circularity, the pressure first causing yield in the flange can be calculated from:

$$\sigma_{yf} = \frac{p\sigma_{yf}}{p_{yf}} + \frac{Ed\delta_n(n^2-1)p}{R_m^2(p_n-p)} \tag{54}$$

Similarly, the pressure causing first yield in the shell plating can be calculated from:

$$\sigma_{yp} = \frac{p\left(R_m L_s - \frac{\sigma_{yf}}{p_{yf}}\frac{R_f}{R_s}A_s\right)}{L_s t} + \frac{Ed_1\delta_n(n^2-1)p}{R_m^2(p_n-p)} \tag{55}$$

An imperfection of general shape can be decomposed in a combination of buckling modes, with the corresponding amplitudes obtained by a Fourier analysis, and the above equations can be generalised as:

$$\sigma_{yf} = \frac{p\sigma_{yf}}{p_{yf}} + \sum_{n=2}^{=} \frac{Ed\delta_n(n^2-1)p}{R_m^2(p_n-p)} \tag{56}$$

$$\sigma_{yp} = \frac{p\left(R_m L_s - \frac{\sigma_{yf}}{p_{yf}}\frac{R_f}{R_s}A_s\right)}{L_s t} + \sum_{2}^{=} \frac{Ed_1\delta_n(n^2-1)p}{R_m^2(p_n-p)} \tag{57}$$

For tee frames, it is usually sufficient to consider the first six values of n.

Kendrick proposed a simplified method to calculate frame collapse due to out-of-circularity which compared well with more accurate incremental methods [23]. Results of such a theory showed that the overall collapse pressure can be close to the pressure first causing yield in the flange or considerably more than this value [23]. For very small imperfections, yielding

* the 'hungry horse' deformation: 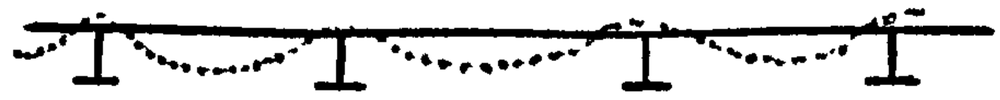
is also important and may reduce the interframe shell collapse pressure by up to 10%

occurs first in the shell plating so that collapse actually tends to occur at a pressure smaller than that causing first yield of the flange. Tsang and Harding [127] proposed a rigid-plastic mechanism approach to General Instability, but applicable only for $n>5$.

As far as tilting is concerned, the bending stresses for the geometry of Frame 5 of Fig. 42, caused by an initial angle of tilt of about 5º (bigger than usually found in practice) are shown in Table 17, from Ref. [18]. For a tilt of one web thickness (2.5º) the maximum stress is quoted in [18] to be 51400 psi, not more than 25% larger than in a perfect cylinder. Louca and Harding [141] very recently carried out parametric numerical investigations in which the effect of tilt on the stiffener collapse pressure did not seem to be relevant, even for slender rings. To calculate collapse loads taking shape imperfections into account, 3-D models and a program such as ABAQUS [35] is necessary.

3.1.6) Residual Stresses

Residual stresses will be present in a real structure, basically due to forming and welding of the shell plating and stiffeners. Faulkner [61] gives a review on the subject, that can be summarised as follows:

Forming Actions

Cold bending of the shell plating: when a plate is rolled to a radius R, the residual stress distribution can be easily calculated if the material is assumed to be ideal elastic-plastic and the Bauschinger effect is ignored [61]. There is a characteristic zig-zag distribution as shown in Fig. 43 for a particular structure, from [18]. Fig. 44 shows measurements in aluminium cylinders given in [150]. Lunchick [82] proposed apparent stress-strain curves, Fig. 45, for such a prestressed condition by averaging effective stresses and strains at 12 stations through the thickness of the shell wall. It can be seen that the greatest weakening effect of residual stresses occurs in the transition elastic/inelastic buckling.

Cold bending of the stiffeners: in the same way, when the stiffener is cold bent to form a ring frame, the distribution of residual stresses again has a zig-zag distribution through the depth. Shama [240] gives a method for predicting cold bending stresses in frames.

Weld shrinkage actions

Welding temperatures are about twelve times greater than the range to cause yield in resisted thermal expansion of structural steels. It is therefore not surprising that, despite small weld cross-sections, contraction forces amounting to many kiloNewtons per weld arise on cooling. These:

(a) leave a system of self-equilibrating locked-in stresses, with tensile yield stress close to the weld

(b) distort the cross section

The balancing compressions away from the welds and the distortions both increase the tendency to buckle and reduce compressive stiffness and strength. These compression stresses are generally much more serious than the distortions in this respect, and yet are less amenable to treatment in the form of fabrication tolerances because they cannot be easily measured. Thermal stress relieving is an expensive remedy*, and over-load stress relief is not always possible, nor is it usually very effective [62].

As far as T-fillet welds of essentially circular ring frames to cylindrical plating are concerned, the two main actions associated with welding shrinkage are:

Along the weld or hoop shrinkage, which gives rise to the well known region of tensile yield extending over a width $2\eta t$ of the plating and a depth ηt_w of the stiffener web adjacent to the weld, balanced by approximately uniform compressive residual stresses σ_{rc1} distributed over the remainder of the cross section. From equilibrium considerations:

*It may actually be no remedy at all as it may reduce the yield stress of steels like HY80(Q1N)

$$\frac{\sigma_{rc1}}{\sigma_{yp}} = \frac{\left[2+\left(\frac{t_w}{t}\right)^2\right]\eta}{\frac{L_s}{t}\left(1+\frac{A_s}{L_s t}\right)-\left[2+\left(\frac{t_w}{t}\right)^2\right]\eta} \tag{58}$$

Single-pass welding may lead to values of η up to 6. It is difficult to expect something less than η=3, even for multi-pass welding. Values of η=4 [72] and η=3 [150] were used in numerical studies found in the literature.

Across-the-weld or axial shrinkage. In ring-stiffened cylinders, the distortion of the shell plating radially toward the stiffener induces hoop stresses in the shell σ_{rc2} which must be balanced by hoop stresses σ_{rf} of opposite sign in the stiffener and adjoining shell which therefore move radially in the opposite direction, Fig. 46. Again from equilibrium:

$$\sigma_{rf} = \frac{2E\delta_p}{\pi R_m\left(1+\frac{A_s}{L_s t}\right)} \tag{59}$$

$$\sigma_{rc2} = \sigma_{rf} - E\delta_p / R_m, \quad \delta_p \sim 0.1t \tag{60}$$

and

$$\sigma_{rc} = \sigma_{rc1} + \sigma_{rc2} \tag{61}$$

The effect of residual stresses on the collapse load of stiffened cylinders has been of concern to many authors. Some of their conclusions can be summarised as:

Cold rolling of the shell seems not to greatly affect Interframe Shell Collapse. This was verified experimentally [18] by testing a pair of models of equal dimensions, one of them stress relieved. It was verified that the stress relieving actually lowered the yield stress of the material. After allowing for that, the cold rolling stresses did not appear to change the collapse pressure significantly. Khaw [241] obtained similar results in parametric studies using energy methods

Kendrick [23,48] investigated analytically the effect of residual stresses on the collapse pressure in a General Instability mode. He considered a combination of cold bending stresses at the shell and at the frame, unmodified by welding the two together. It was found that, for a particular geometry, the collapse pressure is reduced, due to such residual stresses, by about 13% for 0.25%R_m o-o-c, but only by about 4% for 1%R_m o-o-c. Therefore, the effects of shape imperfections and cold bending residual stresses seemed not to be additive

Smith and Kirkwood [72] carried out similar studies, using beam elements to model the frame and attached plating. Attention was again focused on cold bending effects. The main conclusions can be summarised as :

residual stresses caused by cold bending of ring frames may cause reductions of up to about 30% in overall buckling strength. Further inclusion of cold bending of the shell did not change the results appreciably

again, these residual stresses had most effect where initial imperfections were small and the effects of imperfections and cold bending tended not to be additive

welding residual stresses with η=4 may cause loss of strength in the frames approaching 50%. Further inclusion of stiffener cold bending residual stresses did not change the results appreciably. Unfortunately, calculations with welding residual stresses were carried out only for a very small shape imperfection

cold bending of the shell alone caused only small reduction in the overall collapse strength (about 7%)

Kirsten and Slankard [102,103] tested two nominally identical ring-stiffened cylinders, one machined and the other fabricated by cold rolling the shell and welding flat bar stiffeners to it. Collapse pressures were 540 psi and 390

psi respectively, indicating a reduction of 28%. Although the imperfection level was not given, this reduction compares reasonably well with the empirical curve of Fig. 18

Khaw [241] carried out parametric studies on the effect of welding residual stresses on the Interframe Shell Collapse loads, summarised in Table 18. Differently from cold bending, welding residual stresses became more detrimental with increasing out-of-circularity. A maximum reduction in the collapse pressure of 18% was found for η=6

3.1.7) Mode Interaction

It is a natural first reaction to think that, if our knowledge of the buckling process was complete enough to accurately predict collapse in all modes individually, an optimised solution would be achieved by designing the structure to fail at the same given load in all of these modes. This has been referred to in the literature as the 'naive approach' because such a structure would tend to collapse prematurely due to mode interaction effects. For instance, an Interframe Shell o-o-c may lead to a premature yielding of the shell that, combined with an overall o-o-c, would lead to a collapse pressure smaller than the one achieved if only one of these imperfections was present.

Ref. [73] gives Fig. 47 as a classical example of such a General Instability/Interframe Shell interaction, showing a quasi central Interframe Shell pleat superimposed on an n=2 overall inelastic buckling mode. The collapse pressure is quoted in [73] as being 14% lower than both the empirical Interframe Shell Collapse pressure and the overall n=2 frame bending collapse pressure. Since the DRA database allows Interframe Shell Collapse to be predicted within a 5% margin, such a larger reduction was explained in [73] as being due to the interaction effect between the two modes of failure.

Two approximate solutions for the Interframe Shell Collapse accounting for mode interaction with General Instability are proposed in [73]:

$$\text{a)}\ \frac{p\sigma_{yp}}{p_{c5}} + \frac{Ed_1\delta_n(n^2-1)p}{R_m^2(p_n-p)} \le \sigma_{yp} \tag{62}$$

$$\text{b)}\ \frac{p}{p_{yf}}\frac{R_{fl}}{R_m}\sigma_{yp} + \sigma_b \le \sigma_{yp} \tag{63}$$

in which the following equation is used to recalculate the effective length of plating which bends circumferentially with the frame, taking shell destabilising effects into account:

$$\left(\frac{\bar{L}_e}{L_e}\right)^2 + \left(\frac{p}{p_c}\right)^2 = 1 \tag{64}$$

A reduced moment of inertia and modified neutral axis are then used to calculate the modified bending stress σ_b. These solutions can be seen to be modifications of eq. (35) for the calculation of the plate yield pressure accounting for the o-o-c of the frames. Figs. 48 to 50 show comparisons between eqs. (62,63) and numerical results from STAGS [73].

Fig. 51 shows the effect of stiffener size on the load carrying capacity of stiffened shells according to Tsang [122]. FE models considering mode interaction effects were used in the parametric studies but residual stresses seemed not to be included. Perhaps more important, for the geometries considered, axisymmetric buckling was dominant and therefore the stiffener area was the most important parameter. In submersible pressure hulls, the design of the stiffeners will be dominated by buckling in a periodic General Instability mode in which the frame moment of inertia is the important parameter.

3.2) FINITE ELEMENT MODELLING

The modelling uncertainty is estimated usually in view of experimental results. But, since tests are often costly, sometimes there is little information available for a particular mode of failure or geometry range. Additionally,

experimental results often contain uncertainties on boundary conditions, shape imperfections, etc.

F E models, validated against experimental and theoretical results, can be used to complement the experimental information and address the mentioned problems. This section describes the models used and show comparisons with other experimental and numerical results.

Type of Analysis

Riks analysis: see 2.1.2.

Type of Element, Mesh Size, Boundary Conditions and Load Increments

TABLE 3

As shown in Chapter 2, S8R elements lead to a fast convergence and that, for General Instability modes, the modelling of the shell is less relevant than the modelling of the frames. In the present studies, the total number of nodes in the models had to be restricted to a maximum of about 2100, due to memory limitations. S8R elements could be used for infinite compartments, which were simulated by single bay models with axial symmetry conditions in the midbay positions, see Fig. 52. For the finite compartments, Fig. 53, S4R elements had to be used to limit the number of nodes. Simply supported boundary conditions were used at the axial extremities. An angle of π/n was considered to model the imperfection growth. The load increments were chosen automatically by ABAQUS [35].

Material Behaviour

The material non-linearity was handled by using the SHELL SECTION option in ABAQUS [35] that allows for numerical integration over a number of points across the thickness of the shell elements. The default option of 5 points was used as more points seemed not to change the results appreciably. The options chosen for the material behaviour were those recommended for metals at low temperature (below half the melting point temperature on an

absolute scale according to the ABAQUS manual [35]) and low strain rates. The material was considered to be isotropic before yield and therefore with a von Mises yield surface. Kinematic hardening was adopted, as it takes into account, in a simplified form, the Bauschinger effect: the basic concept is that the yield surface shifts in stress space so that straining in one direction reduces the yield stress in the opposite direction. Rate dependency effects were ignored.

Shape Imperfections

Unimodal imperfections were considered in order to use symmetry in the axial and circumferential directions. For the comparisons with experimental results, an equivalent unimodal imperfection in the critical overall buckling mode (with minimum p_n) was used. The amplitude was chosen so that the frame yield pressure with the equivalent imperfection, calculated with eq. (54) would be the same as the frame yield pressure calculated with eq. (56) considering the measured imperfections.

Residual Stresses

Shell cold bending residual stresses were modelled by the Lunchick's effective stress x strain material curve of Fig. 45. The modelling of welding residual stresses is a more difficult task, though. These can be modelled as an initial stress field, but the residual stresses given by eqs. (58)-(61) tend to deform the structure even without external load. This effect could be minimised in ABAQUS [35] by using an initial step without external load and with constrained displacements, although some unbalanced component is probably carried to the subsequent loading steps. An alternative simple modelling that was used to cross-check results consisted in altering the material curve on the initially tensile and compressive regions in the models, Fig. 54.

Comparison with other Results

The FE models were verified in view of the following results:

two experimental results given by Bosman et al. [149] corresponding to machined aluminium 6061-T6 cylinders with rather stocky external flat bar frames, Fig. 55. An n=3 General Instability o-o-c was induced mechanically on them by a heavy circular frame with three screws spaced at 120 degrees. This device applied the imperfection in three ring frames at a time. The o-o-c amplitudes in the various modes as well as numerical results with ADINA are reported. The residual stresses are not reported

two experimental results given by Morihana et al. [142] corresponding to welded cylinders reinforced by external flat bar frames, Fig. 56. The main components of the o-o-c are given as well as results from the author's FE code. The residual stresses are not reported

theoretical results of Kendrick (geometry A, Table 9 of [23]), considering a $0.25\%R_m$ and a $0.5\%R_m$ unimodal o-o-c in an n=2 General Instability mode

numerical results of Esslinger and Geier [140] considering an initial imperfection in the form of a critical buckling mode. Geometry D92 was chosen because its critical buckling mode was of an interactive Tripping-Interframe Shell form, Fig. 57

numerical results of Smith and Kirkwood [72] considering a range of shape imperfections and residual stress distributions, Fig. 58

A summary is given in Tables 19 to 21. Both the numerical and experimental results given by Bosman et al. [149] and Morihana et al. [142] were approximated reasonably well, despite the unknown level of residual stresses and the need to reduce the imperfections to an equivalent unimodal one. The results of Kendrick [23] and Esslinger and Geier [140] were approximated quite well.

Table 20 compares ABAQUS [35] results with results of Smith and Kirkwood [72], without considering residual stresses. The agreement is good, in general, but the collapse pressures calculated with ABAQUS [35] are somewhat limited by p_{c5}, the shell membrane yielding pressure. The beam model of [72] is not sensitive to such an effect and therefore, for the smaller imperfections, ABAQUS [35] results were in general below those given in [72]. Table 21 gives the same comparison including residual stresses and agreement was again good, in general, except for Calculation 17. The same Table 21 also gives some new calculations with residual stresses and larger imperfections and reductions of 21%-35%, attributable to residual stresses, were found.

Overall, ABAQUS [35] results tended to agree reasonably well (within a 15% margin) with those different theoretical, experimental and numerical results.

3.3) MODELLING UNCERTAINTY

3.3.1) Interframe Shell Collapse

The bias and cov of the modelling uncertainty factor $X_{m_{ic}}$ for Interframe Shell Collapse, using the mean curve for collapse prediction (given in detail in Table 22), were calculated in the pilot study [26], based on the 700 experimental results of Fig. 16. They are shown for various ranges of p_m/p_{c5} in Fig. 16 itself.

3.3.2) General Instability

Experimental Results

Figs. 59 and 60 show the modelling uncertainty factor $X_{m_{fy}}$ based on results from 35 fabricated models, failing by General Instability. These correspond to references [124,126,139,142,143,147-149] and are detailed in Appendix 3. Eq. (56) was used for collapse prediction. Only [142,149], which were also used for

comparison with F.E. results (see 3.2), gave somewhat detailed information on the o-o-c. The others gave only information on the maximum deviation from the mean radius, which was used in eq. (56) as the amplitude of an unimodal o-o-c. Even without such detailed information in many cases, Figs. 59 and 60 show that the wide scattering normally associated with this failure mode depends on p_y/p_{c5} and therefore on the frame o-o-c.

Appendix 4 illustrates such a collapse behaviour: in a very imperfect model, frame yielding may occur prematurely, when the shell plating is under relatively small stresses. Such a yielding may then spread considerably before final collapse. In a slightly imperfect model, yielding in the frames may coincide or even be preceded by membrane yielding in the shell. Collapse may occur with little or even no yielding in the frames. One of the models in Figs. 59 and 60 had actually $p_{c5} < p_y$ (which is unusual) and $X_{m_{fy}} < 1.0$.

Using eq. (56) for collapse prediction, the statistical properties of the modelling uncertainty would be:

all models: bias = 2.48, cov = 62%

models with $0.3 \leq e/R \leq 1$ only: bias = 1.80, cov = 16.7%

An accurate definition of the modelling uncertainty requires models fabricated with an o-o-c similar to that recommended by the codes, $0.5\%R_m$. Also the fabrication process must be similar to that used in real structures. Therefore just the 4 models indicated in Fig. 60 would be useful for this purpose. But these models had ring stiffeners with flat bar sections which tend to have a higher shape factor than tee sections. Therefore parametric studies with FE models were used to complement the experimental information.

Results of the Finite Element Models

Ten geometries were considered, Table 6: seven representative of current designs, collected from the literature, and three with improved materials and

slender frames, taken from optimisation studies [12]. Table 23 gives the collapse pressures obtained for the seven geometries considering finite compartments (with S4R elements), for a residual stresses free condition and for shell cold rolling residual stresses only. For the smaller imperfections, p_{c5} tended to be smaller than p_y and the results were therefore heavily influenced by shell membrane yielding. For an o-o-c of $0.5\%R_m$, the shell cold rolling residual stresses seemed to have only a small influence, in agreement with the previous results surveyed in 3.1.6.

Table 24 shows results for the ten geometries, considering the same finite compartments (with S4R elements) as well as infinite compartments (with S8R elements). A constant value of the o-o-c of $0.5\%R_m$ was considered in the worst possible General Instability mode. Fig. 61 shows the results obtained when residual stresses are ignored and the variability of the modelling uncertainty factor was found to be relatively small:

using eq. (56), bias = 1.09, cov = 7%

Fig. 62 shows results for the seven geometries, when welding residual stresses are considered in the FE models and the collapse pressure is predicted with eq. (56). The residual stresses in the FE models were according to eqs. (58-61), with $\eta = 4$ and $\delta_p = 0.1t$. Eqs. (58-61) originate from similar expressions, well accepted for flat plates. There is far more uncertainty over their applicability to frames, though. In the present study, the total residual stress at the frame was taken as the compressive σ_{rc1}, eq. (58) (due to longitudinal shrinkage) added to the tensile σ_{rf}, eq. (59) (due to transverse shrinkage). Such a composition is rather similar to that of eq. (61), used for the shell plating. It may give compressive residual stresses at the frame, which can be large for closely spaced frames. Results from the only measurement known to the author [63] contradict it, since tensile residual stresses were found at the flange.

Such a modelling is thought to lead to results which are conservative but more accurate than those of previous similar numerical investigations

[72,242] which did not even considered σ_{rf}. For closely spaced frames, such as in Cases 1 and 2, the compressive residual stresses are quite large, while for more widely spaced frames, they are relatively small. It is not surprising that, when using eq. (56) for collapse prediction, quite a large variability is found:

bias = 0.823, cov = 20%

The flange yield pressure, however, remains a good estimator for the collapse pressure if the absolute stress at the flange is considered instead of the incremental stress. Fig. 63 shows results when the collapse pressure is estimated by altering eq. (56) to:

$$\sigma_{yf} = \frac{p\sigma_{yf}}{p_{yf}} + \sum_{n=2}^{\infty} \frac{Ed\delta_n(n^2-1)p}{R_m^2(p_n-p)} + \sigma_{rf} \qquad (65)$$

The resulting variability is again small:

bias = 1.006, cov = 7.5%

Another reason to consider the F E results as being conservative is the fact that the residual stresses were always bigger in the shell plating than in the frames. As a consequence, the results of the F E models including residual stresses showed some influence of premature yield at the shell midbay which tended to lower the collapse pressure.

It is suggested, for further reliability analyses of internally tee framed vessels with frame yielding predicted by eq. (56), to use, for the statistical properties of the model uncertainty, bias = 1.1 (similar to Fig. 61 and smaller than that found from the experimental results) and a cov = 10% (higher than that suggested by Fig. 61 to account for residual stresses). Such a value for the bias is probably conservative, since eq. (56) assumes the amplitudes of all modes 'in phase' at the same section of the frame, while in practice they tend to be phased out. The FE had to use unimodal imperfections, due to memory limitation, and did not reflect this particular factor.

3.3.3) Frame Tripping

Prediction of Frame Tripping is a much more difficult task: present solutions are not accurate even in the elastic range and there is virtually no relevant experimental information available. As mentioned in Chapter 2, a closed form solution is proposed for predicting Tripping in the elastic range, Appendix 2. For inelastic Tripping, Faulkner [25] proposed a modified Tangent Modulus approach in which fabrication effects of welding or cold bending of the frames are approximately allowed for. For shorter wave lengths, $\sqrt{E_t E}$ is considered to govern collapse, mainly because secondary local bending effects and hence uneven compression stress distributions are more marked with Tripping than with columns. For longer wave lengths the Tangent Modulus is used. This can be summarised as follows:

$$\sigma_{ti} = \sigma_{yf}[1-p_s(1-p_s)\lambda^2] \qquad \text{if } n \le \pi R_m/3(d_w+t_f) \text{ and } \lambda \le p_s^{-0.5}$$

$$\sigma_{ti} = \sigma_{yf}[1+p_s(1-p_s)\lambda^4]^{-1} \qquad \text{if } n > \pi R_m/3(d_w+t_f) \text{ and } \lambda \le p_s^{-0.5} \qquad (66)$$

$$\sigma_{ti} = \sigma_t \qquad \text{if } \lambda > p_s^{-0.5}$$

where $\lambda = \sqrt{\sigma_{yf} / \sigma_t}$

$p_s = 0.8$ is recommended if the ring frame webs and flanges are fabricated to the required radius or if they are stress relieved after cold bending to the required radius; $p_s = 0.5$ is recommended if the rings are cold bent to the required radius.

Table 25 shows results from the F E models (with S8R elements) in which different initial tilting angles were considered. Two variations of Case 4 were considered with narrower flanges and even in these cases, the initial tilt did not affect the collapse appreciably. The main reason for such a small influence is that, perhaps because the present Tripping design criteria are overconservative, even the critical p_{ti} is still greater than p_{c5}. Therefore, the

FE models tend to show a collapse mode that is mostly associated with shell membrane yielding, at a pressure between p_{c5} and p_{ti}, even if the shell is perfectly circular and the frame has an initial tilt. This is a situation similar to that experienced previously in the General Instability modes, for small imperfections. It follows that the present results suggest that a 4º initial tilt angle is considerably less harmful than a $0.5\%R_m$ o-o-c; this can also be verified by comparing results of Table 25 with those of Table 23.

For Cases 1-7, the maximum reduction attributed to a 4º tilt, in relation to the predictions of eq. (66) with $p_s = 0.8$, was 8% for Case 7. Such a smaller sensitivity to shape imperfections favours a Tangent modulus approach as used in eq. (66).

Table 25 also gives results for two Titanium hulls obtained from previous optimisation studies [12], chosen for having $p_{c5} < p_{ti}$. In this case a more harmful effect of the initial tilt is observed. Care must be taken when using such improved materials: slender frames may be obtained, which fulfil the present deterministic design criteria, but are more sensitive to initial tilting.

Other numerical results appeared in the literature at the same time as the present study was been carried out: Louca and Harding [141] used LUSAS and found initial tilting also not to be very influential on the collapse pressure, for geometries typical of offshore platforms, even for slender frames.

When introducing residual stresses in the F E models, the fact that those are usually greater in the shell plating than in the frames, according to eqs. (58-61), led to the shell membrane yielding being even more dominant over any premature yielding at the frame due to the initial tilt. Therefore it was not possible to find results in which Tripping had clearly had any relevant influence.

Given the relatively small influence of an initial tilting angle on the collapse pressure, the Tangent Modulus approach of eq. (66) is believed to work reasonably well to predict mean values. It could be used in further

reliability studies in connection with a modelling uncertainty factor with bias 1.0 and a conservative value for the cov. A value of 15%, similar to that usually assumed as a peak for columns under compression is suggested.

3.3.4) Summary of Proposed Values

The following statistical properties are recommended for the modelling uncertainty factors associated with the collapse modes treated in this Chapter, for internally tee stiffened cylinders, to be used in further reliability analyses:

X_{m_i}- Interframe Shell Collapse: predicted with the mean curve of Fig. 16 (Table 22). Bias and cov: Fig. 16.

$X_{m_{fy}}$- Frame Yielding (General Instability): predicted with eq. (56). Bias=1.1 and cov =10%

$X_{m_{py}}$- Plate Yielding (Approximately allowing for the interaction between General Instability and Interframe Shell Collapse): predicted with eq. (57). Bias=1.0 and cov =13%

X_{m_t}- Frame Tripping: predicted with eq. (66). Bias=1.0 and cov=15%

Chapter 4 - ASPECTS OF CODE DEVELOPMENT

4.1) BRIEF INTRODUCTION TO STRUCTURAL RELIABILITY

Structural Reliability theory is concerned with the rational, probabilistic treatment of uncertainties in structural engineering and with the methods for assessing the safety and serviceability of structures. It is a subject which has grown rapidly in recent years and has evolved from being a topic for academic research to a set of well-developed or developing methodologies with a wide range of practical applications [175,176]. The recent ICOSSAR'93 (Intl. Conf. Structural Safety and Reliability), for instance, had numerous papers in which a probabilistic approach was used in different areas such as buckling, vibrations, earthquake, human error, offshore structures, materials, wind and geotechnical engineering.

The simplest code format for any design check can be expressed as follows:

$$\frac{R}{f} \geq Q \tag{67}$$

Q and R are the load and the resistance, respectively. The deterministic approach to design has been to impose that the structure has a certain safety margin (expressed by the scalar safety factor f) against a given set of pessimistic combinations of such parameters, however likely (or unlikely) such combinations may be. The safety factor f is supposed to 'sufficiently' separate Q from R in order to cover the uncertainties involved in their calculation. It is often a constant, as in the case of tension members, or may vary with a particular parameter as, for example, in column design where sensitivity to eccentricities, initial imperfections and variations in support conditions has led to safety factors which vary with the slenderness ratio.

'Sufficient' safety factors have seldom been derived from an understanding of all the uncertainties that affect the loading and the resistance, but rather by

codifying practice that was known by experience to be satisfactory. This is the basis of most present day codes of practice for structures, which are deterministic in nature.

In structural reliability, it is recognised that the major parameters affecting the response of a given structure, such as load, material properties, shape imperfections, etc., have an essentially random nature. In its general sense, Structural Reliability is the ability of the structure to fulfil its design purpose for some specified time. In a more narrow, mathematical sense, it is the probability that a structure will not attain each specified limit state (ultimate or serviceability) during a reference period.

Ideally, a design-for-reliability approach would consist in designing the structure to a certain maximum value of the failure probability $p_f = p(R-Q<0)$, where R and Q are now random variables representing the resistance and the loading respectively, Fig. 64. Such an approach would have several advantages, as far as decision making is concerned:

as opposed to a safety factor, cost or some other measure of the consequences of failure can be assigned to the failure probability

a failure probability can be understood by people other than structural designers. This may allow a better integration with other members of a design team. More important, it does give a framework in which risk levels may be adequately understood and perhaps established by society

cross check between risk levels of different types of structures may be facilitated

new information on R and Q may be readily translated into weight savings, which has the desirable effect of reducing costs

design procedures may be obtained which can be applied with more confidence to new forms of design and construction

Reliability based methods were initially criticised for being cumbersome; furthermore, few data were available, certainly not enough to define the important 'tails' of the distributions of R and Q. The mentioned advantages seemed difficult to materialise, as they require the failure probabilities calculated to be as close to reality as possible. According to Madsen et. al. [176]: 'it seemed difficult to justify replacing a design "rationale" that is irrational but works, with another one, more complicated but also irrational'.

Since the mid-70's, however, theoretical developments, new data and a drive to achieve safety with minimised cost helped Structural Reliability to become quite popular in the design of civil and marine structures, particularly in the offshore industry where structural failure may lead to the loss of human lives, serious environmental hazards and often huge costs. Safety is very important, but has to be achieved with acceptably low cost and weight.

The essence of applying reliability analysis to structural safety, in its present form, is twofold:

(a) to reduce the element of judgement by introducing a formal consideration of the nature of the main uncertainties

(b) then to formally calculate a suitable combination of partial safety factors for a chosen target notional probability of failure and design code format

The design-for-reliability approach may not yet be at hand; the failure probabilities presently obtained have a notional value (as with any other engineering parameter). But the partial safety factors derived from this probabilistic approach are considered to provide better measures of uncertainty than the deterministic safety factors.

The deterministic codes are slowly being superseded by semi-probabilistic codes of the Level I type (or LRFD - Load and Resistance Factor Design) which introduce separate partial factors for load and resistance variables, [40,46,171-

174]. These cover a wider range of structural elements, load combinations and failure modes and incorporate the results of much experimental and theoretical research [175]. Their use is expected to have a number of potential benefits:

the same or more consistent levels of safety can be obtained with reduced costs

the different uncertainties involved in design and their influence in the safety margins are more clearly recognised

more information is taken into account. A mean curve from experimental results, for instance, considers all the available information, while a lower bound, typical of deterministic design, may ignore most of it

4.2) STATISTICAL PROPERTIES OF THE BASIC VARIABLES

The basic variables and their statistical properties are shown in Table 26. They can be grouped as follows:

Loading : the design pressure, considered as deterministic

Dimensions : Fig. 40: R, t, L_s, d_w, t_w, b_f, t_f, L_c. The assumption of normal distribution is the usual practice in reliability assessment

Material Properties : σ_{yp}, σ_{yf}, E. The values on the table for the cov of the yield stresses correspond to results from 219 two-test sets of 0.2% proof stress values for Q1N hull plating and 448 0.2% proof stress results from Q1N frame material tests, all of them provided by the MoD and meeting their acceptance criteria [26]. The log-normal distribution for the yield stresses and the properties for the Young's modulus E is the usual practice in reliability assessment. The Poisson's ratio was assumed to be deterministic at 0.3.

Shape Imperfections : the MoD empirically derived equation was used for the frame out-of-circularity:

$$\delta(n) = \frac{a + bn}{n^2 - 1} \tag{68}$$

where, with a and b in mm and R in m, the following mode independent constants are given:

$$\bar{a} = 3.51R \,,\; a_k = 8.38R$$
$$\bar{b} = 1.20R \,,\; b_k = 3.31R \tag{69}$$

the bar denotes mean values and subscripts k denote the upper three standard deviation values. The above equation usually leads to quite large values for the cov, in the order of 50%. The shape imperfections were assumed as normally distributed. Eq. (68) may reflect the RN practice of giving the shipbuilder only half of the tolerance used in design to work with. In cases when eq. (68) may not be relevant, the usual unimodal o-o-c can be assumed, distributed in the worst possible mode, with a mean amplitude of 0.5% of the radius. If such a conservative modelling is used, a somewhat smaller cov, of 20% say, can be assumed.

Modelling Parameters: see 2.1.6 and 3.3.4 for bias and cov. All modelling parameters were assumed as normally distributed as usual in reliability assessment. For General Instability, the effect of end restraint was ignored as it had negligible effect on the failure probabilities.

4.3) RELIABILITY METHODS

The different methods for safety checking (Reliability Methods) are broadly grouped as follows [175]:

Level I Methods

Design methods in which appropriate levels of structural safety are provided by the use of partial safety factors, related to the nominal values of the main structural and loading variables:

$$\gamma_c\left[\frac{P_c\Psi}{\gamma_{xm}\gamma_m}\right] \geq [\gamma_f Q_i] \qquad (70)$$

where P_c and Q_i are the design values of the structural strength and of the load effects, respectively. The partial safety factors (PSF) as identified in this equation include:

(i) Strength reduction factor Ψ
(ii) Material PSF γ_m
(iii) Load factors γ_f
(iv) Consequence factor γ_c
(v) Modelling PSF γ_{xm}

Level I design methods are particularly attractive for codes of practice. By properly choosing the PSF, it is possible to obtain structures with a failure probability reasonably close to a given target, without departing radically from the traditional safety factor approach which most of the structural designers are used to.

Level II Methods

Approximate methods in which the probability of failure is evaluated from the means and standard deviations of the design variables. An idealization of the failure region as well as a simplified representation of the joint probability density function of R and Q are normally required.

For the one dimensional case, the safety margin can be simply expressed by Z=R-Q, Fig. 64. If both R and Q are normally distributed with mean R_m and

Q_m respectively and standard deviation s_r, s_q respectively, the probability of failure p_f, can be calculated as [177]:

$$p_f = \Phi (-\beta) \tag{71}$$

where Φ is the standard normal distribution and β is the safety index, defined as [177]:

$$\beta = \frac{\mu_R - \mu_Q}{\sqrt{s_R^2 + s_Q^2}} \tag{72}$$

This can be generalised to a multi variate problem by using the Advanced First Order Second Moment Method (AFOSM) [178,179], in the following way:

If $x_1, x_2, ..., x_n$ are the n independent basic variables involved in a structural design problem, a general expression for any limit state equation for the structure is:

$$Z = g (x_1, x_2, ..., x_n) > 0 \tag{73}$$

where the nature of g depends on the structural type and limit state under consideration. A failure surface may be defined as Z=0 and a linear approximation to this can be found by using the Taylor series expansion:

$$Z = g(x^*) + \sum_1^n (x_i - x_i^*) g_i'(x^*) \tag{74}$$

where $g_i'(x^*) = \frac{\partial g}{\partial x_i}$ is evaluated at the design point $x^* = (x_1^*, x_2^*, ..., x_n^*)$ which is the point of maximum probability of failure density when all the variables are normally distributed. If the variables are transformed to a standard normalised space $u_i = \frac{x_i - \mu_i}{\sigma_i}$, the design point is the point in the failure surface closest to the origin, Fig. 65. The safety index β is now defined as Z_m / s_z (Z_m, s_z are the mean and standard deviation of the safety margin Z) and

obtained from:

$$\beta = \frac{\sum_{1}^{n}(\mu_i - x_i^*)g_i'(x^*)}{\sum_{1}^{n}\alpha_i g_i'(x^*)\sigma_i} \tag{75}$$

from which it follows :

$$x_i^* = \mu_i - \alpha_i \beta \sigma_i \tag{76}$$

where α_i are the sensitivity factors reflecting the relative influence each of the design variables has on the strength model:

$$\alpha_i = \frac{g_i'(x^*)\sigma_i}{\left[\sum_{1}^{n}\left\{g_i'(x^*)\sigma_i\right\}^2\right]} \tag{77}$$

In the standard normalised space, the sensitivity factors give the direction cosines of the vector defined by the origin and the design point. For given values of μ_i and σ_i and an initial value of β, an iterative procedure can be used to solve eqs. (75-77). The failure probability is given by eq. (71) using the final β obtained. If any of the design variables have non-normal distribution, the following transformation is adopted:

$$\mu_i^N = x_i^* - \Phi^{-1}\left\{F(x_i^*)\right\}\sigma_i^N \tag{78}$$

$$\sigma_i^N = \frac{f^N\left[\Phi^{-1}\left\{F(x_i^*)\right\}\right]}{f(x^*)} \tag{79}$$

where μ_i^N, σ_i^N are the mean and standard deviation of the equivalent normal distribution, F(x) is the cumulative distribution function of x_i, f(x) is the probability density function of x_i, and $f^N(x)$ is the normal probability density function which has the effect of equating the cumulative probabilities and the probability densities of the actual and approximating normal distributions at the design point x_i^*.

AFOSM gives partial safety factors for each variable as the ratio between its value at the design point and its mean value:

$$\gamma_i = \frac{x_i^*}{\mu_i} = 1 - \frac{\alpha_i \beta \sigma_i}{\mu_i} \tag{80}$$

By applying the appropriate PSF to each of the variables, it would be possible, in principle, to obtain structures exactly with the same reliability. The PSF, however, would have one value for each variable in each different structure in each different load case, making it impossible to codify them. These are usually grouped in Level I design codes, forming a code format (as in eq. 70) which may consist of several equations and will lead to designs with approximately (but not exactly) the same reliability.

AFOSM assumes the failure surface as being linear, that is, a hyperplane in the standard normalised space. It may lose accuracy in the case of highly curved failure surfaces. In order to remedy this problem, the linear expansion can be substituted by a quadratic expansion: the failure surface is approximated by a quadratic curve at the design point instead of by a hyperplane. This is the basis of the Second Order Reliability Methods (SORM) [180-184]. If, for instance, a hyperparaboloid is fitted at the design point [180], the failure probability can be approximated by [185]:

$$p_f \sim \Phi(-\beta) \prod_{i=1}^{n-1} (1 - \beta \kappa_i)^{-1/2} \tag{81}$$

where κ_i are the n-1 curvatures of the failure surface which are assumed as the curvatures of the paraboloid fitted [180]. This approximation is valid for $\beta\kappa_i < 1$.

The curvatures can be found, for instance, as the eigenvalues of the Hessian which is the matrix of the second derivatives of the failure surface (g=0), at the design point [180]. An alternative method is proposed in [183,184].

For small values of β, eq. (81) may lose accuracy and may be replaced by the three term approximation [186]:

$$p_f \sim A_1 + A_2 + A_3 \tag{82}$$

where:

$$A_1 = \Phi(-\beta)\prod_{i=1}^{n-1}(1-\beta\kappa_i)^{-1/2}$$

$$A_2 = [\beta\Phi(-\beta) - \varphi(\beta)]\left\{\prod_{i=1}^{n-1}(1-\beta\kappa_i)^{-1/2} - \prod_{i=1}^{n-1}(1-(\beta+1)\kappa_i)^{-1/2}\right\}$$

$$A_3 = (\beta+1)[\beta\Phi(-\beta) - \varphi(\beta)]\left\{\prod_{i=1}^{n-1}(1-\beta\kappa_i)^{-1/2} - \mathrm{Re}\left[\prod_{i=1}^{n-1}(1-(\beta+i)\kappa_i)^{-1/2}\right]\right\}$$

It is often the case that a structural design problem is defined not by one but by a number of limit state equations and therefore a number of design points and safety indexes. This problem can be tackled by using the concept of systems reliability, assuming each mode as part of a series system. Bounds to the total failure probability are given by [187]:

$$p_f \le \sum_{j=1}^{m} p_{f_j} - \sum_{j=2}^{m} \max_{k<j}\left(p_{f_k} \cap p_{f_j}\right) \tag{83}$$

$$p_f \ge p_{f_1} + \sum_{j=2}^{m} \max\left[\left(p_{f_j} - \sum_{k=1}^{j-1} p_{f_k} \cap p_{f_j}\right), 0\right] \tag{84}$$

where m is the number of failure modes and p_{f_j} is the failure probability for mode j. The numbering of the modes may influence the bounds and therefore one has to investigate the different possible numberings. These bounds become very narrow for the small values of p_f usually of interest.

Level III Methods

The probability of failure is directly calculated by :

$$p_f = \int_{w_f} f_{r,q}(r,q)\, dr\, dq \tag{85}$$

where $f_{r,q}$ (r,q) is the joint probability density function in R and Q and w_f is the failure domain where Z=R-Q < 0. The above integral cannot, in general, be solved analytically. Numerical integration techniques can be used but, as the number of variables increases, computations become very time consuming. Furthermore, explicitly defining the failure domain w_f is usually difficult. These techniques are often useful only for problems with a small number of variables - generally less than six - and with w_f in a special form such as a hypercube, hyperparaboloid, etc. [188].

Simulation methods offer an alternative [188-200]. The basic one is Monte Carlo Simulation (MCS) [188-190] in which combinations of the basic variables are sampled, by random generation, and the failure probability is estimated as the ratio between the number of failures and the number of non-failures. More formally, eq. (85) is rewritten as:

$$p_f = \int_{w_f} I\,[g(x)]\, f(x)\, dx \tag{86}$$

where f(x) is the probability density function of x (the vector of the basic variables) and I [g(x)] is a function with value 1 in the case of failure ($g(x) \leq 0$) or zero in the case of non-failure ($g(x) > 0$). Eq. (86) represents the first moment of I [g(x)] so that an unbiased estimator of p_f is given by:

$$p_f = E\big(I\,[g(x_i)]\big) = \frac{1}{N}\sum_{i=1}^{N} I\,[g(x_i)] \tag{87}$$

where N is the sample size and x_i (i=1,2,...,N) are the samples generated from f(x). The name Monte Carlo derived from the fact that the complex problem of solving eq. (85) is reduced to a gamble-like hit-and-miss evaluation problem. MCS has become a quite popular method for approximating complex multi-dimensional integrals since its application in Nuclear Physics some 50 years ago and has received considerable help from the fast

development of powerful computers. It is straightforward to implement and is the only method that unconditionally converges to an accurate solution, provided the sample size is large enough. The failure domain does not need to be explicitly defined and the computational effort does not increase much with the number of variables, provided that the sampling process is not time consuming. It can also tackle the problem of multiple modes of failure without resorting to bounds. Finally, it works equally well with discrete variables for which FORM and SORM are often difficult to use. The error in MCS can be estimated with the formula [201]:

$$\varepsilon\% = 200\left[\frac{(1-p_f)}{Np_f}\right]^{1/2} \tag{88}$$

which states that there is a 95% confidence level that the actual error in the estimated p_f is less than ε if N samples are used. It follows that for small p_f and ε=20%, $N = 100/p_f$ samples are necessary. For $p_f = 10^{-4}$, for instance, a million samples would be necessary.

In order to improve the efficiency of MCS, various variance reduction techniques have been proposed. The most used one is Importance Sampling [191-196] in which the sampling is biased towards the region with most likelihood of failure. More formally, eq. (86) is rewritten as:

$$p_f = \int_{w_f} I\,[g(x)]\,\frac{f(x)}{h(x)}\,h(x)\,dx \tag{89}$$

which can be estimated by:

$$p_f = E\left(I\,[g(x)]\frac{f(x)}{h(x)}\right) = \frac{1}{N}\sum_{i=1}^{N} I\,[g(x_i)]\frac{f(x_i)}{h(x_i)} \tag{90}$$

which is similar to eq. (87), but with the samples now generated according to a sampling density function h(x) located in the region of maximum likelihood of failure and giving more failure points. Eq. (88) can be used for error

estimation but with p_f now being the 'success rate' which is the probability of obtaining a failure point. For a 'success rate' of about 50% and ε = 20%, only 100 samples would be necessary, for instance. The choice of h(x) tends, however, to influence the results quite heavily and a poorly chosen one can lead to inaccurate estimates even for large samples.

It is common to use information from a previous Level II analysis to improve the efficiency of simulation methods. For instance, in Importance Sampling Using Design Point (ISPUD), h(x) is centred at the design point obtained from a previous AFOSM analysis [188]. Another possibility is to use information from AFOSM and SORM to limit the sampling region as in [202-204]. These methods are important to improve AFOSM and SORM results in the case of a highly curved failure surface, but lead to the same restrictions associated with Level II methods, regarding discrete variables and multiple modes of failure. To overcome these problems, in Adaptative Sampling [197] and Directional Simulation [198-200] the region of maximum likelihood of failure is located as the simulation process advances, without resorting to a previous Level II analysis.

In most of the practical cases, the failure surface is relatively smooth and AFOSM gives accurate results with relatively small computing time, but it is always useful to have one or some of the other methods implemented for checking purposes, particularly MCS, when feasible.

Results from AFOSM, SORM, ISPUD (500 and 5000 simulations) and MCS (10000 and 3 million simulations) were compared for Cases 1,2 and 3 of Table 6. The four collapse modes were considered; for the total failure probability, Ditlevsen bounds, eqs. (83,84) were used in connection with AFOSM, SORM and ISPUD. In SORM, the curvatures were found as the eigenvalues of the Hessian and eq. (81) was used to estimate the failure probability. Figs. 66 and 67 show typical results for Tripping and for the total failure probability. The main conclusions were [36]:

For the design cases considered, the four methods gave somewhat similar results, as far as the failure probabilities of the individual modes were concerned. The only exception was MCS with 10000 simulations, for values of p_f lower than 1%, as should be expected from such a number of simulations. ISPUD gave reasonable results with only 500 simulations even for very small failure probabilities

As far as the total failure probability is concerned, the use of Ditlevsen bounds in connection with AFOSM, SORM and ISPUD also gave good results in comparison with the more accurate results from MCS with 3 million simulations

AFOSM is the most convenient method for use in design in this case, giving accurate results with smaller computing time

4.4) SENSITIVITY STUDIES

In order to investigate the relative importance of the different basic variables on the failure probability, reliability analyses using AFOSM were carried out for Cases 1-5. Case 2 corresponds to the pilot study [26] and was not considered; a redesign (Case 2b) was used in its place. Tables 27 to 30 show the sensitivity factors α_i, the mean and design points, the partial safety factors of the modelling uncertainty and the safety index β for the four collapse modes. Table 30 also gives the upper Ditlevsen bound values.

The dominance of the modelling uncertainty is quite clear from the values of α_i. It can be seen that α_i^2 for the modelling parameter is usually in the range of 0.88-0.98 in all modes. For other variables, α_i^2 seldom reaches a value of 0.10.

The values of the modelling uncertainty factor, at the design point, can be seen to be, in most of the cases, in the range of 0.45 - 0.55. This happens due to assuming a continuous normal distribution for such a variable and due to its

impact on the failure probability (as shown above). Such a drastic reduction may be possible in real structures, for the frame collapse modes, if a very adverse residual stress distribution is present, as indicated by FE analyses in Chapter 3. For Interframe Shell Collapse, on the other hand, there is a well established lower bound curve to the experiments, as shown in Fig. 16. Such a lower bound has been confidently called 'guaranteed collapse pressure', and is only about 15% below the mean curve defined in Table 22. Therefore, the failure probabilities associated with this mode (which are the minimum ones) are essentially conservative since truncation effects were not included.

4.5) CODE FORMAT

In the present case there is no reserve strength, the design equations already account for the different strength reduction factors and the failure probability shows small sensitivity to the yield stress (see 4.4). Therefore, referring to eq. (70), it is reasonable to assume γ_c, Ψ, γ_m as equal to the unity. Two formats will be studied:

Format I:

$$\frac{p_{c_j}}{f_j} \geq p_d \tag{91}$$

where f_j and p_{c_j} are the safety factors and collapse pressures for the four collapse modes. This is essentially the present deterministic format, in which the same notional safety is used irrespectively of the design pressure and of whether overshooting is a real possibility or not, and will be calibrated for the new design equations proposed.

Format II:

$$\frac{p_{c_j}}{\gamma_{xm_j}} \geq \gamma_f p_d \tag{92}$$

where γ_{xm_1} is a modelling PSF covering design and fabrication uncertainties and γ_f is a load PSF covering accidental depth overshoots. For commercial submersibles in which there is no possibility of overshooting, $\gamma_f = 1$. For naval submarines, γ_f would increase with the overdiving factor $F = \frac{p_d + \Delta p}{p_d}$ (Δp being a 'design overshoot'): for deep diving vessels ($F \rightarrow 1$), γ_f would also approach the unity. As F increases, γ_f would approach the higher values corresponding to shallow water vessels.

For Interframe Shell Collapse, values depending on p_m / p_{c5} (a form of slenderness measure) will be introduced owing to the large difference of scattering between data in the region of $1.0 < p_m / p_{c5} \leq 2.5$ and data in the region of $p_m / p_{c5} > 2.5$. Internally tee framed vessels will be considered. The study included Flange Yielding and Plate Yielding pressures calculated with the o-o-c given by the MoD formula, eq. (68) as well as in the more usual way: 0.5% of the radius and distributed as a half-sine wave over the axial direction of the compartment.

4.6) DESIGN SPACE

For the choice of a target reliability as well as for the partial safety factor optimisation, it is important to have a number of designs carried out according to the present practice (design space). An investigation on the application of alternative materials to externally pressurised vessels was recently carried out [12], using the BS 5500 [24] design criteria. Different steels, aluminium alloy and titanium alloy were considered and the mechanical properties assumed are given in Table 31. Three geometries were considered: a small research vessel with R_i=1m and L_c=5m, a large research vessel with R_i=4m and L_c=12m similar to that assumed in [17], and an offshore service submarine with R_i=2.5m and L_c=15m similar to that proposed in [9]. Four alternatives of design depth were considered: 300m, 600m, 1500 and 6000m. The following internal space and fabrication constraints were imposed:

Maximum Frame Depth: $d_w+t_f \leq 305$ mm, for $R_i = 2.5$ m, 4 m

≤ 200 mm, for $R_i = 1$m

Maximum Thickness: $t, t_w, t_f \leq 200$ mm

Minimum Free Space Between Flanges: $L_s - b_f \geq 450$ mm

Minimum Free Space Between Flange and Compartment End:

$0.5 [L_c - (n_{fr} - 1)L_s] - 0.5b_f \geq 450$ mm

Maximum Relative Thickness: $t/t_w, t_f/t_w \leq 2.5$

Maximum Flange Length: $b_f \leq 0.7 (d_w+t_f)$

Weight optimised solutions were found and typical results are shown in Fig. 68. From the various cases considered, 32 solutions were used to form the design space, together with Cases 1,2b,3,4 and 5 of Table 6, for the selection of target reliabilities and partial safety factor optimisation. These 32 solutions, given in Appendix 5, used steel, had $p_m/p_{c5} > 1$ and corresponded to pressures of 300m, 600m, 1500m. For a pressure of 6000m, only Titanium offered some solutions, although with negative buoyancy.

4.7) TARGET RELIABILITY

The selection of a target reliability should, in principle, be based on a combination of social considerations (risks to life and environment) and economic considerations (costs of loss, repair or non-utilisation of the structure). This is often difficult since structures are supposed not to fail. Table 32 illustrates how little the risk of death due to a structural failure is in comparison with other risks taken in our everyday life: death as a consequence of a car accident is much more 'acceptable' than due to structural failure.

Sometimes the selection of a hard limit is avoided: for offshore platforms in the UK sector of the North Sea, for instance, the Health and Safety Executive (HSE) introduced the ALARP (As Low As Reasonably Possible) principle [205], Fig. 69: in the upper very high risk region of the diagram the activity cannot be justified as the risk of failure is too high and cannot be tolerated; in the lowest risk region of the diagram the risks are broadly acceptable so that it is unnecessary to apply further substantial effort to reduce them further provided that they will remain at that level. In the central zone (the ALARP zone) the risks are tolerable only if further risk reduction is not reasonably practical.

Fig. 70, from [206] shows the yearly accident rate experience for various types of industries including the offshore industry, based on information gathered at the World Offshore Accident Database (WOAD) including accidents from 1990 to 20 years back. The risk for floating structures can be seen to be higher than for fixed systems, since in the former case a number of accidents are related to temporary phases during transit and installation. Consistently with the ALARP principle, two curves are given: 'accepted' and 'marginally accepted'. The same concept is apparent in Fig. 71 from [207] in which only natural uncertainties are considered (modelling uncertainties excluded).

Fig. 72, from [208] shows the range of lifetime reliability indices found in various forms of construction in both Europe and the United States. Some of these indices are notional in that they have been determined from comparative studies. β in the range of 3 to 4 can be seen to cover land-based and some offshore structures. The RCC [209] selected β=3.72 corresponding to p_f of 10^{-4} as the TLP lifetime target reliability. Assuming a lifetime of 20 years this would correspond to a yearly value of 5.10^{-6}. The Eurocodes on steel and concrete structures [40,173] assume yearly target reliabilities in the range of 10^{-4} - 10^{-6}.

It is often impractical to be specific about a target reliability based on such social and economic considerations, since the failure probabilities, as we now

calculate them, are essentially notional and their target values vary widely in different structures and codes, as shown above. A reasonable way to overcome this problem is by investigating the average reliability of designs carried out according to the present practice. Such an average tends to reflect the implicit levels of risk so far tolerated for the particular type of structure under consideration and may therefore be a good choice for the target reliability. Mansour et. al. [210], for instance, proposed a lifetime target reliability of $\beta = 3.2$ ($p_f = 7. 10^{-4}$) for the ship's hull girder longitudinal strength, based on the average reliability of 300 ships designed according to the ABS rules. This would correspond to a yearly target of $p_f = 3.5. 10^{-5}$, again assuming a lifetime of 20 years.

For the pressure hulls under consideration*, Figs. 73 to 82 show the reliability levels found for the various design cases considered. Overshooting is not included. The geometry of the pilot study [26] is included in the figures to explain the paradoxical results previously obtained. Its frames have inadequate dimensions and it can be seen, from Figs. 78 to 82 that the safety indices for Flange Yield and Plate Yield fall below the average values. These safety indices were even lower in the pilot study due to the conservative modelling assumed for these two modes. The conservative modelling of Frame Tripping also reduced the safety index for this mode of failure in the pilot study. For Interframe Shell Collapse, on the other hand, the geometry used fell on the region of $p_m/p_{c5} > 2.5$, where there is considerably less scatter of the experimental results and therefore a smaller cov. It is natural therefore that, for this particular geometry, the notional safety calculated for Interframe Shell Collapse is much higher than for the frame collapse modes.

It can be observed that present day designs (indicated by black squares in the figures), tend to fall in the region $1 < p_m/p_{c5} < 2.5$ and to have in general a higher notional safety for the frame collapse modes than for Interframe Shell Collapse, as expected from the usual submarine design thinking. But for designs falling in the region of $p_m/p_{c5} > 2.5$, the opposite result can be expected.

* For the design cases of Table 6, L_c was adjusted to just meet the BS5500 criteria for frame yield

Finally, the figures show results for two designs failing by elastic Interframe Shell buckling $p_m/p_{c5} < 1$. These have a much smaller notional safety than the others due to the large scattering normally associated with elastic buckling. These points are not included in the calibration.

Tables 33 to 35 show the average values for β and p_f as well as the range of β for the 37 geometries and the 4 collapse modes, considering no overshooting as well as overshootings of 15% and 30% of the design pressure p_d. The average total failure probabilities are in the order of 0.05%, 0.5%, and 2%, for zero, 15% and 30% overshooting respectively.

These could be understood as lifetime risks, since collapse by buckling will occur once a critical load is exceeded. In terms of failure consequences, a PH collapse would probably lead to the loss of the vessel and part or all of its crew. Assuming, for comparison purposes, 100 lives lost, from Fig. 70, an 'acceptable' value for offshore platforms would be 0.1% annual failure probability or a 2% failure probability over a 20 year lifetime. Fig. 72 gives similar values. The 'acceptable' curve of Fig. 71 would tolerate even higher risks for quite costly accidents. Therefore, the results obtained for the above PHs are reasonably within the risk levels accepted by the offshore industry, even when a quite severe overshooting is considered. One has to remember, though, that the above numbers are essentially notional and no great confidence can be placed in such comparisons. It is sometimes argued that ignoring human errors, as in all of these cases, leads to an underestimation of the failure probability by a factor of 10 or more [211].

The failure probabilities calculated for Interframe Shell Collapse, which determine to a large extent the total failure probability, are conservative since truncation effects are not considered. Furthermore, the modelling of the frame collapse modes was improved as far as the mean values are concerned, but conservative values for the cov were still assumed. Finally, the high standards which are characteristic of design, fabrication and operation of submarines tend to minimise to some extent the possibility of human error. Therefore, the values found above are probably a conservative estimation for the risk of a PH failure. Overshootings of the magnitude considered do occur

in practice and, so far, there are no known submarine loss attributable to a PH collapse.

The average reliabilities shown in Tables 33 to 35 were used as target reliabilities in the derivation of the safety factors for Format I. For Format II the target reliability varied with the 'design overshooting' factor F. For a given value of F, the target values β_{t_i} were taken as the average reliability found for the 37 models, calculated for an overdiving of F_{max} - (F - 1). F_{max} is a 'maximum overdiving factor', representing the maximum acceptable overdiving of present day designs, for which two values were considered: 1.15 (15%) and 1.30 (30%). If F_{max} is assumed as 1.15, a submarine expected not to overdive would have a target reliability equal to the average reliability obtained from the 37 models considered as overdiving to 15 % above their operational pressure (minimum reliability β_{min}). A submarine expected to overdive to the maximum value of F = 1.15 would have a target reliability equal to the average reliability obtained from the 37 models without overdiving (maximum reliability β_{max}). In this way, Figs. 83 to 86 were obtained giving the target reliabilities for the various modes as a function of the factor F.

For Interframe Shell Collapse, the target reliabilities used in the partial safety factor optimisation always corresponded to the average values obtained from the designs with $1 < p_m/p_{c5} < 2.5$, as the typical present day designs tend to fall in this range.

4.8) PARTIAL SAFETY FACTOR OPTIMISATION

The process of partial factor optimisation is one of constrained minimisation. Thus the probabilities of failure of designs performed in accordance with a chosen code format are compared with the target reliability and the code format partial safety factors altered until the spread of reliabilities for a range of designs is minimised. This can be expressed by the following set of equations:

$$s = \sum_{i=1}^{M} w_i \left[\log(p_{f_i}) - \log(p_{f_t}) \right] \tag{93}$$

where p_{f_i} is the failure probability of the ith design according to the code format using the trial values of the partial factors, p_{f_t} is the target reliability, w_i is the weight given to design i and M is the total number of models in the design space. The constraints are:

$$\sum_{i=1}^{M} w_i p_{f_i} = p_{f_t} \tag{94}$$

and

$$\sum_{i=1}^{M} w_i = 1 \tag{95}$$

p_{f_i} is evaluated with AFOSM, defining the failure function as:

$$g(x) = X_{m_j} p_{c_j} - \frac{\overline{p_{c_j}}}{\gamma_j} \tag{96}$$

where X_{m_j}, p_{c_j}, and $\overline{p_{c_j}}$ are the modelling uncertainty factor, the collapse pressure and the mean collapse pressure for mode j respectively and γ_j is the partial safety factor for the collapse mode j. w_i =5 was assumed for the designs of Table 6* and w_i=1 was used for the remaining designs.

Partial safety factors were derived for Format I, using the values given in Tables 33 to 35 as target reliabilities, and results are shown in Tables 36 to 38.

Partial safety factors were then derived for Format II in the following way: for each mode a single safety factor f_j was obtained for various values of $F = \frac{p_d + \Delta p}{p_d}$, according to the target reliabilities of Figs. 83 to 86.

It was then verified that f_j tended to increase linearly with F, Figs. 87 to 90, and f_j could be decomposed in a constant component γ_{xm_j} (design and fabrication PSF) and a component γ_f linearly varying with F (operational PSF). Table 39 compares the values obtained with the present practice.

* For the design cases of Table 6, L_c was adjusted to just meet the BS5500 criteria for frame yield

To summarise, the following average notional values of β were found for designs carried out according to the present practice:

Flange Yield with eqs. (56)+(68): 5.08, 4.37, 3.68, for F=1, 1.15, 1.3 respectively
Flange Yield with eq. (56)+0.5%R: 4.04, 3.36, 2.71
Plate Yield with eqs. (56)+(68): 3.88, 3.32, 2.77
Plate Yield with eq. (56)+0.5%R: 3.68, 3.10, 2.53
Frame Tripping with eq. (66): 3.93, 3.52, 3.11
Interframe Shell Collapse (mean curve): 3.20, 2.65, 2.12

Based on the present practice and on the partial safety factor optimisation (F_{max}=1.15), provisional values are recommended for the safety factor $\gamma_{xm_j}\gamma_f$:

(i) For vessels with small or no overdiving requirement ($F \rightarrow 1$), γ_f=1 can be used leading to the safety factors:

Flange Yield: 1.75 with eqs. (56)+(68) or 1.55 with eq. (56)+0.5%R
Plate Yield: 1.80 with eqs. (56)+(68) or 1.75 with eq. (56)+0.5%R
Frame Tripping: 2.0 with eq. (66)
Interf. Shell Col. (mean curve): 1.55 for $1<p_m/p_{c5}\leq 2.5$ or 1.3 for $p_m/p_{c5}>2.5$

(ii) For vessels with overdiving requirement in the range ($1.15 \leq F \leq 1.30$), γ_f=1.15 can be used leading to safety factors similar to the present practice:

Flange Yield: 2.0 with eqs. (56)+(68) or 1.8 with eq. (56)+0.5%R
Plate Yield: 2.1 with eqs. (56)+(68) or 2.0 with eq. (56)+0.5%R
Frame Tripping: 2.3 with eq. (66) (see also [32,33])
Interf. Shell Col. (mean curve): 1.75 for $1<p_m/p_{c5}\leq 2.5$ or 1.5 for $p_m/p_{c5}>2.5$

(iii) For vessels with overdiving requirement in the range ($1.0 \leq F \leq 1.15$) linear interpolation in F should be used.

Chapter 5 - CONCLUSIONS AND FUTURE WORK

5.1) CONCLUSIONS

A Level I code format is proposed for the buckling design of ring-stiffened cylindrical shells under external pressure. Depth independent partial safety factors γ_{xm_j}, to be applied to the resistance (collapse pressures), are proposed for the four modes considered (Interframe Shell Collapse, Frame Yield, Plate Yield and Frame Tripping), covering design and fabrication factors. A partial safety factor γ_f, to be applied to the load (external pressure), and varying with the design pressure and the maximum expected overdiving, is proposed to cover operational factors.

The values for γ_{xm_j} and γ_f proposed in Chapter 4 were obtained assuming as a target the same safety levels of designs carried out according to the present practice (BS5500 [24]) in overdiving conditions. For deep diving vessels or in cases in which the risk of overdiving is not relevant, it is proposed that the safety factors $\gamma_{xm_j}\gamma_f$ used in design could be smaller than those presently recommended. This would imply allowing the pressure hull to operate at stress levels higher than those presently accepted. The implications on other failure modes such as fatigue and fracture should be assessed before fully accepting such smaller safety factors.

It is also proposed that smaller safety factors can be used for Interframe Shell Collapse in the range of $p_m/p_{c5} > 2.5$. The values proposed in Figs. 87-90 and Table 39 are largely a consequence of the statistical properties of the modelling uncertainty (Fig. 16), obtained in the pilot study [26]. It would be important to check them in view of the raw data and perhaps some new data, as will be discussed in the next section.

Both the depth and the slenderness dependency of $\gamma_{xm_j}\gamma_f$ would not affect present day designs such as Cases 1 to 5 of Table 6. These tend to have p_m/p_{c5}

< 2.5: to increase such ratio it is necessary, for a given material, to increase t or decrease L_s or a combination of both. But this inevitably leads to an increase in structural weight. Therefore, solutions in the range of $p_m/p_{c5} < 2.5$ will remain the minimum weight ones for these traditional designs. On the other hand, for deep diving vessels (with stockier geometries), the smaller safety factors could extend the range of application of some materials as illustrated in Fig. 91.

In order to obtain such partial safety factors, different aspects of strength modelling and Structural Reliability had to be addressed. On the strength modelling side, the work was focused on the frame collapse modes.

Seventy two experimental results were compiled, corresponding to machined models failing by elastic General Instability. FE meshes were validated in view of mesh studies and experimental results and further used in parametric studies. The FE results showed a small sensitivity to variations on the mesh describing the plating, but a large sensitivity to the modelling of the frames, when using Eigenvalue Analysis. The effect of boundary conditions on the elastic General Instability pressure p_n was investigated in view of both experiments and results of the FE models. Statistical properties were obtained for the model uncertainty associated with p_n.

The development of limit point calculation algorithms like the modified Riks method allows for the effect of initial shape imperfections on the collapse pressure to be successfully estimated. Thirty five experimental results were compiled corresponding to welded models failing by General Instability. Unfortunately, detailed information on shape imperfections was found only for a few of these experimental results. No detailed information was found regarding residual stresses. FE models were validated in view of the most relevant of these experiments as well as in view of other numerical results found in the literature. It would be important in future tests that the shape imperfections, residual stresses and elastic restraints in the boundaries are measured and reported to provide all the information necessary for a more accurate validation of FE models.

Potentially harmful effects of compressive welding residual stresses on the collapse pressure in a General Instability mode were identified in the FE parametric studies. It has to be said, though, that little is known about welding residual stresses at the stiffeners of ring-stiffened shells. The only measurement known to the author actually showed tensile residual stresses at the frame flange.

The margin between initial yield on the frame and final collapse was found to depend on the ratio p_y/p_{c5} and therefore on the level of imperfection (affecting the frame yield pressure p_y) of the frame. For typical values of o-o-c (0.5%R), such a margin was of about 10% for tee frames (from the FE results without residual stresses) and of about 25% for flat bar frames (from the experimental results). Statistical properties were proposed for the model uncertainty associated with collapse prediction using p_y in view of the experimental and FE results.

A closed form solution for the elastic Frame Tripping pressure, based on energy methods and showing good agreement with FE and other numerical results, was introduced. FE parametric studies showed the effect, on the collapse pressure, of initial tilting angles of up to 4º to be considerably less harmful than the effect of an initial o-o-c of 0.5%R, supporting the use of a modified Tangent Modulus approach for inelastic Tripping.

On the Structural Reliability side, different reliability methods (AFOSM, SORM, ISPUD and MCS) were reviewed, implemented and compared. AFOSM was the most suitable for design as it gave accurate results with smaller computing times.

The possibility of obtaining the failure probability in case of overdiving (or as a function of the external pressure in general) was verified, using any of the above methods. The paradoxical results obtained in the pilot study [26] were found to be a consequence of the geometry supplied for the study and of the conservative modelling that had to be used for the frame collapse modes.

Notional safety levels of various types of existing structures were reviewed and target safety levels were proposed for externally pressurised, internally ring-stiffened cylinders in the four buckling modes under consideration. Finally, partial safety factor optimisation was carried out to obtain the partial safety factors mentioned in the beginning of this section.

5.2) FUTURE WORK

Measurements in Real Structures

All engineering models involve idealisations which are only meaningful if reflecting the actual behaviour of the real systems they wish to represent. Both FE models and Structural Reliability theory are powerful tools which allow great generality on the description of the structural behaviour both deterministically and stochastically. Their proper use may be limited, though, by a relative lack of information on real structures.

Some important areas needing more information were identified, like boundary conditions and the spatial variation of material properties and shape imperfections, although some attention has been given recently to the measurement of out-of-circularity. Perhaps the most important, as far as marine structures are concerned, is the distribution of welding residual stresses and combinations of residual stresses, which may have severe implications on frame collapse. The appropriate modelling of fabrication procedures for further collapse analysis is therefore a major area for future work.

Strength Modelling

The modelling uncertainty factor dominated quite strongly the failure probabilities obtained, at the expense of more 'physical' variables such as dimensions, imperfections and material properties. This was a consequence of the simplified formulae used for collapse prediction.

Design methods more accurate than the present simplified formulae may be considered in the future. In deterministic design, simple formulae are often preferred even when somewhat inaccurate: since the overall procedure is in general conservative, improvements in the calculation of individual parameters often prove of little use. On the other hand, in reliability based design, improved methods (in the sense of leading to a smaller scattering of their modelling uncertainty) may be readily translated into weight savings, as the failure probability usually depends heavily on the cov of the modelling uncertainty factor, and into improved code formats, as the influence of the 'physical' variables is made clearer.

Several of these design methods were reviewed: Chapter 2 showed Kendrick's accurate energy methods which are suitable for the elastic buckling in all modes and simply involve the solution of eigenvalue problems. These could be used to a more accurate estimation of p_m, p_n and p_t. Chapter 3 also reviewed theories which allow a better estimation of p_{c5}, by correctly including the 'beam-column' effect. Also in Chapter 3, several modified Tangent Modulus approaches for inelastic buckling were reviewed and Kendrick's method for predicting frame collapse, including the effect of shape imperfections and residual stresses was mentioned.

Further work is still needed as far as mode interaction effects are concerned. Frame design should, in the future, concentrate on obtaining minimum scantlings to keep mode interaction with Interframe Shell Collapse at an acceptable value, when residual stresses and shape imperfections are taken into account.

For more specialised design, the pilot study [26] gave many suggestions for future work, like the use of FE models representing discrete frames, sections of the pressure hull between bulkheads as well as transition regions (cylinder-cone, e.g.) which could be validated by experimental results and then used to define the failure surface for reliability analysis or to investigate both material and geometric imperfection spatial variations. These models could have the

advantage of considering all buckling modes as well as the interaction between them. FE models were validated in the present work, but the accurate inclusion of welding residual stresses in the FE models is an area which needs further work. A clever method was recently proposed in [242,243], where ADINA was used to estimate the effect of residual stresses on the collapse loads of stiffened plates [242] and tubulars under axial compression [243]. The procedure can be summarised as follows, Fig. 92:

Step 1: Create an initial geometry including measured shape imperfections resulting from all fabrication processes, including welding. Assign a coefficient of thermal expansion to the elements adjacent to the weld

Step 2: Increase the temperature in these elements to produce reversed residual stresses. The updated nodal geometry is stored in a file

Step 3: This updated geometry is now the initial geometry. The imperfections in the model now include measured geometric imperfections as well as displacements due to the thermal loading. The shell is free of residual stresses

Step 4: The temperature is decreased and the shell is strained back to the original initial geometry with the measured shape imperfections only, as well as with the desired residual stresses

FE models were not directly used in the reliability analyses carried out in the present work due to the computational effort involved, but must be mentioned as an important area for future work. Initial applications may consist of connecting a FE code directly to a reliability method such as AFOSM, SORM, etc. as in [212-214]. The amount of computation necessary, however, is often excessive. Different techniques have been investigated to improve the interaction between a general purpose FE code and a reliability method [215,216]. Response Surface methods have also been proposed [217-219]: the FE model is only used to evaluate a limited number of points which will define an approximating surface (polynomial, e.g.); this more

Note: Cyclic loading effects, such as the Bauschinger effect, must also be considered in the future

computationally inexpensive surface will then be used as a failure function.

The most advanced approach deals with the inclusion of probabilistic concepts in the formulation of the finite elements. This has opened a new area of research, Stochastic Finite Elements [220-223], in which the basic random parameters are recognised as having a spatial distribution which depends on their location in the structure, therefore forming random fields rather than random variables. These random fields are discretised so that the random input will consist of a vector of random variables (i.e. local averages of the underlying random field across each element) whose covariance matrix depends on the finite element mesh [221].

Finally, future research is also needed to make it feasible to account for factors (g) to (i) of Section 1 (explosions, collision, docking, etc.), explicitly in PH design.

Probabilistic Modelling

Future work should include the effects of truncations in the probability density functions of some of the basic variables. The possible effect of truncation was clear in the present study for the Interframe Shell Collapse mode (see Chapter 4). The yield stress or the out-of-circularity may also, at the design point, assume values which would be rejected in the quality control and therefore are not realistic, although this was not verified in the present study. The clarification of the effect of residual stresses may allow for a rational truncation in the case of the frame collapse modes, in the same way as the lower bound curve of Fig. 16 may be used for truncation in the case of Interframe Shell Collapse.

The reduction in the factor $\gamma_{xm_i}\gamma_f$, for Interframe Shell Collapse in designs with $p_m/p_{c5} > 2.5$, is highly dependent on the values adopted for the cov for the modelling uncertainty associated with this mode, Fig. 16. The values used were given in the pilot study and were derived there from the points in the figure, rather than from the raw data. If such data is made available, in addition to new experiments [122,136,144-146] and perhaps numerical results

(cheaper single-bay FE models could be used) and if truncation is taken into account, the code calibration procedure used in Chapter 4 can be repeated to refine these partial safety factors.

The present study assumed normally distributed, uncorrelated variables (except for the yield stresses, assumed as log-normal). Such assumptions are usual in the reliability assessment of marine structures, but should be investigated in more detail in the future, if relevant information is available. There has been particular concern with the form of the probability density functions assumed for the basic variables [224-226], which is a major area for future research. Another aspect that could not be explored in the present work, because of time and computing limitations, is the use of well validated FE models to generate large samples of results which could then be used for a better choice of probability density functions.

Another area identified as of primary concern [206] is the statistical modelling of human error which involves various possible inadequacies, from gross errors and misinterpretations in design to inadequate operation or inspection.

Closure: Putting in Perspective...

The present work was aimed at steel structures for operation at depths below 300m where design solutions usually involve relatively stocky cylindrical shells ($R/t<120$) in which yielding and elastic-plastic buckling play a dominant role in design. Future work should consider other forms of shell such as cones and domes as well as thinner cylindrical shells. Recent work in China [244] proposed that, when designing externally pressurised steel and titanium hulls with unusual geometries ($R/t>150$ and $L_c/R<2.6$), General Instability modes with more than one half-wave along the compartment length may become critical. It is also shown in [244] that, in these modes, axial stiffening may become relevant. Thinner shells and smaller compartments are also common in steel offshore structures operating at smaller pressures and it is interesting to note that offshore codes use long-compartment

submarine design criteria to size their frames. For offshore structures, axial and bending loads would have to be considered in addition to external pressure.

Partial safety factors for elastic buckling were not treated in detail as this type of buckling is usually not of direct relevance to the design of relatively stocky shells as those considered here. But elastic buckling may be of direct relevance in the design of thinner shells as indicated by the work on aerospace related structures [227-229].

Structural efficiency, in the sense of withstanding given loads with minimised weight, tends to imply the use of thinner shells. In practice, however, the material selection will largely determine the degree of efficiency achieved. The choice of material depends on a number of factors, cost being often the most important for commercial structures: if the designer is prepared to pay for efficiency (as in the aerospace industry), an improved material may be chosen leading to thin walled structures in which elastic buckling may be dominant.

If the designer is not prepared to pay much for efficiency, less improved materials may be used and stockier structures may be obtained; this has often been the case in marine structures. Things have been changing, however: for instance, in the field of fast transportation, aluminium alloys are largely used. Composite materials of very high yield stress are also being considered for deep water and other marine vessels [11,230], maybe also leading to much thinner structures.

From a historical point of view, until perhaps the last century, structural design and construction was carried out by master builders, based on empirical knowledge and judgement. The empirical rules were well kept secrets. In modern times, the task is carried out by structural engineers and is based on the rational treatment of load and strength. The uncertainties associated with these quantities, however, are still treated empirically. In a broad sense, the codes of practice aim to incorporate updated scientific

knowledge, for loads and resistance, as well as the experience and judgement of authorities in the field, for the treatment of uncertainties, and make both available to the general public.

In this context, the application of Structural Reliability theory aims to be a step further in such an evolutionary process, by treating uncertainty in a scientific basis, reducing the element of empiricism and judgement. For the time being, the failure probability has only a notional value due to the simplifications made in the strength modelling as well as in the reliability calculations. Even so, it does allow the derivation of code formats with partial safety factors which are more rationally based than the usual deterministic safety factors.

Future developments may lead to the failure probability being less notional and more of a real measure of risk for direct assistance to the decision making process (referred to in [176] as a *Level IV* reliability method) and therefore fully materialising the benefits of applying Structural Reliability in design, fabrication and operation. It is interesting to note that some work is under way on methods to treat uncertainty in a rational but non-probabilistic way, for cases in which the limited information available is not sufficient for a proper choice of statistical properties [226,231].

The understanding of structural instability has been realised to be useful to other similar problems in nature.

Leonard Euler himself was not concerned only with structures, but was rather a mathematician fascinated by the calculus of variations and the consequent search for maximums and minimums. He devoted a great deal of work to the application of such methods to many different physical problems. One of such problems was that of determining elastic curves and, as part of it, he determined the bifurcating equilibrium configurations of a compressed elastic column [245]. Although published in the eighteenth century, it remained rather controversial until well in the following century [233], simply because it did not work beyond the elastic range.

Simple as we assume it today, Euler's column equation is very important, as stressed by Bleich [233]: 'structural design is normally concerned with the determination of stresses based upon the tacit assumption that stable equilibrium exists between internal and external forces. This is to say, the equilibrium is such that, within certain limits, any slight change of the loading condition does not produce disproportionate increase of the stresses or elastic distortions of the system. Hence, adherence to a certain stress - the allowable stress - determines the degree of safety of the structure. The buckling problem presents an entirely new aspect - the investigation of the potential unstable equilibrium between external loading and the internal response of the structure'.

Some structural engineers [220,246] recently realised the similarity between the problem of structural instability and other instability problems in nature. The concept of bifurcation of equilibrium, if generalised, could also be useful for treating problems in different fields such as the astrophysics of collapsing stars, population explosions of competing ecological species, the onset of turbulence in a fast-moving fluid, etc. [246]. One may look forward to the contributions that researchers in all these different areas may give to a better understanding of instabilities in general and the possible practical applications which may arise from such work.

6. REFERENCES

1 Faulkner, D.: 'Structural developments in underwater operations', Intl. Shipbuilding Progress, 32, pp. 69-83, 1985

2 Reynolds,T., Lomacky, O., Krenzke, M.: 'Design and analysis of small submersible pressure hulls', Comp. & Struct., 3, pp. 1125-1143, 1973

3 Ramsay, R.: 'Inner space vehicles, design features of deep diving submersibles', Trans. North East Coast Institution of Engineers and Shipbuilders, 85, pp. 13-22, 1968

4 Flemming, N.C.: 'Functional requirements for research/work submersibles', Aeronautical Journal, 72, pp. 123-131, 1968

5 Wenk, E., DeHart, R.C., Mandel, P., Kissinger, R.: 'An oceanographic research submarine of aluminium for operation at 15000ft.',Trans. RINA, 102, pp. 555-578, 1960

6 Pritzlaff, J.A., Munske, Z.: 'Manned submarines of the world', Naval Engineer's Journal, 77(5), pp. 715-722, 1965

7 Groves, D.: 'Minisubs', Naval Engineer's Journal, 79(2), pp. 249-255, 1967

8 Burcher, R. and Rydill, L.: 'Concepts in submarine design', Cambridge University Press, 1994

9 Freitas, A.: 'Manned submarines for offshore service duties', Proceedings OMAE 91, Vol.I - B, pp. 449-456, ASME, 1991

10 'Submarine super yachts and sports boats', Ship & Boat Intl., pp. 27-33, April 1994, (No author given)

11 Smith, C.S.: 'Design of submersible pressure hulls in composite materials', Marine Structures, 4, pp. 141-182, 1991

12 Morandi, A.C., Das, P.K. and Faulkner, D.: 'An investigation on the application of alternative materials to externally pressurised vessels', Intl. Conf. Structural Materials in Marine Environments, London, 11-12 May 1994

13 Dow, R.S. and Bird, J.: 'The use of composites in marine environments', Intl. Conf. Structural Materials in Marine Environments, London, 11-12 May 1994

14 Hansen, A.B. and Lundh, T.: 'Composite materials in marine structures: Achievements in Norway 1988-1993 and programmes 1994-2000', Intl. Conf. Structural Materials in Marine Environments, London, 11-12 May 1994

15 Faulkner, D. and Das, P.K.: 'A new risk approach for structural design and adequately safe operation of submarines', UDT Conf., Microwave Exhibitions and Publishers Ltd., London, February 1990

16 Faulkner, D.: 'The safe design and construction of steel spheres and end closures of submersibles, habitats and other pressurised vessels', BOSS'79, Vol. 2, pp. 543-556, ICST, London, 1979

17 Faulkner, D.: 'The collapse strength and design of submarines', RINA Intl. Symp. Naval Submarines, London, May 1983

18 Kendrick, S.: 'Externally pressurized vessels', in The Stress Analysis of Pressure Vessels and Pressure Vessel Components, Ed. S.S.Gill, Pergamon Press, London, 1970

19 Kendrick, S.: 'Collapse of stiffened cylinders under external pressure', Proc. IMechE Conf., Vessels under Buckling Conditions, Paper C190/72, pp. 33-42, London, 1972

20 Morandi, A.C.: 'The design of shell combinations in externally pressurised vessels', Paper submitted to J. Marine Structures

21 Pegg, N., Bosman, T.N. and Keuning, P.J.: 'Summary report of the Canada/Netherlands project on determination of overall collapse of imperfect pressure hull compartments', DREA Rep. 94/101, Dartmouth, Canada, March 1994

22 Pegg, N.: 'A numerical study of dynamic pulse buckling of ring stiffened cylinders', Comp. & Struct., 44(6), pp. 1205-1214, 1992

23 Kendrick, S.: 'Vessels to withstand external pressure', in Developments in Pressure Vessel Technology - 4, Ed. by R.W. Nichols, Applied Science Publishers, London, 1983

24 BSI, 'Specification for unfired fusion welded pressure vessels, BS5500, HMSO, London, 1991

25 Faulkner, D.: 'Application of reliability theory in submarine design', in Advances in Marine Structures-2, Ed. C.S. Smith and R.S. Dow, Elsevier Applied Science, 1991

26 Das, P.K., Garside, J.F. and Faulkner, D.: 'Pilot study into the application of reliability analysis to a structural design code for externally pressurised vessels', MoD contract with BMT Ltd., Wallsend, pp. 120, Feb. 1988

27 Faulkner, D. and Das, P.K.: 'Application of reliability theory to structural design and assessment of submarines and other externally pressurised cylindrical structures', in Integrity of Offshore Structures-3, Ed. D. Faulkner, M.J. Cowling and A. Incecik, Elsevier Applied Science, 1991

28 Morandi, A.C., Das, P.K. and Faulkner, D.: 'An outline of the application of reliability based techniques to structural design and assessment of submarines and other externally pressurised cylindrical structures', Rep. NAOE-92-22, NAOE Dept., University of Glasgow, June 1992.

29 Morandi, A.C., Das, P.K. and Faulkner, D.: 'An outline of the application of reliability based techniques to structural design and assessment of submarines and other externally pressurised cylindrical structures', Marine Structures, 7, pp. 173-187, 1994

30 Morandi, A.C., Das, P.K. and Faulkner, D.: 'Reliability based design of submersibles: An investigation on the general instability of externally pressurised vessels', Proceedings OMAE-93, Glasgow, June 1993

31 Morandi, A.C., Das, P.K. and Faulkner, D.: 'Buckling of ring stiffened cylinders Part I: Elastic general instability', Rep. NAOE-93-30, NAOE Dept., University of Glasgow, Nov. 1993

32 Morandi, A.C., Faulkner, D., and Das, P.K., 'Buckling of ring stiffened cylinders Part II: tripping', Rep. NAOE-94-19, NAOE Dept., University of Glasgow, Mar. 1994

33 Morandi, A.C., Faulkner, D., and Das, P.K., 'Frame tripping in ring stiffened externally pressurised cylinders'. Paper submited to Marine Structures, 1994

34 Morandi, A.C., Faulkner, D., and Das, P.K., 'Buckling of ring stiffened cylinders Part III: collapse prediction', Rep. NAOE-94-26, NAOE Dept., University of Glasgow, Mar. 1994

35 ABAQUS Manual, Version 5-2, Hibbit, Karlsson & Sorensen Inc., 1991

36 Morandi, A.C., Das, P.K. and Faulkner, D.: 'On the application of reliability based methods to the structural design and assessment of submersibles and other externally pressurised vessels', in Structural Safety and Reliability, Ed. G.I. Schuëller, M. Shinozuka, J.T.P. Yao, A.A. Balkema, Rotterdam, 1994

37 Morandi, A.C., Das, P.K. and Faulkner, D.: 'Buckling of ring stiffened cylinders: a Level I design procedure', Rep. NAOE-94-30, NAOE Dept., University of Glasgow, Mar. 1994

38 Faulkner, D.: 'Ring frame design procedures for orthogonally stiffened cylindrical shells', Rep. NAOE-92-20, NAOE Dept., University of Glasgow, May 1992

39 Faulkner, D.: 'Efficient design of orthogonally stiffened cylinders', Tensioned Buoyant Platforms Seminar, London, 25-26 May 1993

40 Commission of the European Communities, 'Eurocode no.3: design of steel structures - Part 1: general rules and rules for buildings', Draft, November 1990

41 Det Norske Veritas, 'Buckling strength analysis of mobile offshore units', Classification Note 30.1, Oct. 1987

42 Odland, J.: 'Buckling resistance of unstiffened and stiffened circular cylindrical shell structures', Norwegian Maritime Research, 6(3), pp. 2-22, 1978

43 Germanischer Lloyd, 'Rules for the classification and construction of offshore technology - Part 1, underwater technology', Ch. 1-3, 1991

44 API, 'Bulletin on stability design of cylindrical shells', API Bul 2U first Ed., May 1987

45 Rule Case Committee, 'Model code for structural design of tension leg platforms (draft)', CONOCO-ABS Rule Case Comitee, ABS, New York, 1983

46 American Petroleum Institute, 'Recommended practice for planning, designing and constructing fixed offshore platforms', API RP 2A, Draft, 1989

47 American Petroleum Institute, 'Specification for fabrication of structural steel pipe ', API Spec 2B, 1977

48 Kendrick, S.: ' Ring-Stiffened cylinders under external pressure', in Shell Structures, Stability and Strength, ed. R. Narayanan, Elsevier Applied Science, London, 1985

49 Kendrick, S.. private communication, Aug. 1992

50 Kendrick, S.: 'The technical basis of the external pressure section of BS5500', J. Press. Vessel Tech., 106, pp. 143-149, 1984

51 Kendrick, S.: 'The buckling under external pressure of ring stiffened circular cylinders', Transactions RINA, 107, pp. 139-156, 1965

52 Kendrick, S.: 'The buckling under external pressure of circular cylindrical shells with evenly spaced equal strength circular ring frames - part I', Rep. NCRE R211, Dunfermline, Scotland, Feb. 1953

53 Kendrick, S.: 'The buckling under external pressure of circular cylindrical shells with evenly spaced equal strength circular ring frames - part II', Rep. NCRE R243, Dunfermline, Scotland, Sep. 1953

54 Kendrick, S.: 'The buckling under external pressure of circular cylindrical shells with evenly spaced equal strength circular ring frames - part III', Rep. NCRE R312, Dunfermline, Scotland, Sep. 1953

55 Kendrick, S.: 'The local instability of ring frames', Rep. NCRE R255, Dunfermline, Scotland, Mar. 1957

56 Kendrick, S.: 'How safe are design codes?' in Marine and Offshore Safety, Ed. P.A. Frieze, R.C. Mac Gregor and I.E. Winkle, Elsevier Applied Science, London, 1984

57 Kendrick, S.: 'Design for external pressure using general criteria', Int. J. Mech. Sci., 24(4), pp. 209-218, 1982

58 Kendrick, S.: 'Design of submarine structures', in Advances in Marine Structures, Ed. C.S.S. Smith and J.D. Clarke, Elsevier Applied Science, London, 1986

59 Kendrick, S.: 'Shape imperfections in cylinders and spheres: their importance in design and methods of measurement', J. Strain Anal. Des., 12(2), pp. 117-122, 1977

60 Kendrick, S.: 'The influence of shape imperfections and residual stresses on the collapse of stiffened cylinders', Paper C10/79, IMechE, 1979

61 Faulkner, D.: 'Effects of residual stresses on the ductile strength of plane welded grillages and of ring stiffened cylinders', J. Strain Anal. Des., 12(2), pp. 130-139, 1977

62 Faulkner, D.: 'Proof testing of submarine structures', Hull Committee, DSAC-MTB, Oct. 1984

63 Faulkner, D.: 'Residual strains measured during the welding of frame 59 in Valiant', NCRE Internal Technical Memo. TGO/M2, Sep. 1962

64 Creswell, D.J., Dow, R.S.: 'The application of nonlinear analysis to ship and submarine structures', in Advances in Marine Structures, Ed. C.S.S. Smith and J.D. Clarke, Elsevier Applied Science, London, 1986

65 Creswell, D.J.: 'Elastic overall instability of ring stiffened cylindrical shells - part I', Rep. NCRE R643A, Dunfermline, Scotland, Nov. 1976

66 Creswell, D.J.: 'Elastic overall instability of ring stiffened cylindrical shells - part II', Rep. NCRE R78643B, Dunfermline, Scotland, Jun. 1978

67 Creswell, D.J.: 'Elastic overall instability of ring stiffened cylindrical shells - part III', Rep. NCRE R643C, Dunfermline, Scotland, Aug. 1978

68 Wilson, L.B.: 'The deformation under uniform pressure of a circular cylindrical shell supported by equally spaced circular ring frames', Reps. NCRE R337A, R337B and R337C, Dunfermline, Scotland, Dec. 1956

69 Wilson, L.B.: 'The plastic deformation of a circular cylindrical shell supported by identical equally spaced circular ring frames under uniform external pressure', Trans. RINA, 110, pp. 115-125, 1968

70 Wilson, L.B.: 'The elastic deformation of a circular cylindrical shell supported by equally spaced circular ring frames under uniform external pressure, Trans. RINA, 108, pp. 63-74, 1966

71 Bryant, A.R.: 'Hydrostatic pressure buckling of a ring stiffened tube', Rep. NCRE R306, Dunfermline, Scotland, Oct. 1954

72 Smith, C.S. and Kirkwood, W.: 'Influence of initial deformations and residual stresses on inelastic flexural buckling of stiffened plates and shells', in Steel Plated Structures, Ed. P.J. Dowling, J.E. Harding and P.A. Frieze, Crosby Lockwood Staples, London, 1977

73 Graham, D., Keron, I., Mitchell, G., Creswell, D.: 'DRA Structural research on submarines and submersibles', Charles Smith Memorial Conference, DRA, Dunfermline, Scotland, July 1992

74 Reynolds, T.E., Blumenberg, W.F.: 'General instability of ring-stiffened cylindrical shells subjected to external hydrostatic pressure', DTMB 1324, Jun. 1959

75 Reynolds, T.M.: 'Inelastic lobar buckling of cylindrical shells under external hydrostatic pressure', DTMB 1392, Aug. 1960

76 Krenzke, M.A., Kiernan, T.J.: 'Structural development of a titanium oceanographic vehicle for operating depths of 15000 and 20000 ft', DTMB 1677, Sep. 1963

77 Krenzke, M.A.: 'Effect of initial deflections and residual welding stresses on elastic behaviour and collapse pressure of stiffened cylinders subjected to external hydrostatic pressure', DTMB 1327, April 1960

78 Krenzke, M.A.: 'Structural aspects of hydrospace vehicles', Naval Engineer's Journal, 77(4), pp. 597-606, 1965

79 Blumenberg, W.F., Reynolds, T.E.: 'Elastic general instability of ring-stiffened cylinders with intermediate heavy frames under external hydrostatic pressure', DTMB 1588, Dec. 1961

80 Blumenberg, W.F.: 'The effect of intermediate heavy frames on the elastic general instability strength of ring-stiffened cylinders under external hydrostatic pressure', DTMB 1844, Feb. 1965

81 Lunchick, M.E.: 'Plastic axisymmetric buckling of ring-stiffened cylindrical shells fabricated from strain hardening materials and subjected to external hydrostatic pressure', DTMB 1393, Jan. 1961

82 Lunchick, M.E.: 'The influence of residual rolling stresses on the strength of cylindrical pressure vessels under external loading', J. Eng. Ind., ASME, pp. 275-280, May 1970

83 Lunchick, M.E., Overby, J.A.: 'Yield strength of machined ring-stiffened cylindrical shell under hydrostatic pressure', Proc. Soc. Exp. Mech., 18(1), pp. 178-185, 1960

84 Galletly, G.D., Reynolds, T.E.: 'A simple extension of Southwell's method for determining the elastic general instability pressure of ring-stiffened cylinders subject to external hydrostatic pressure', Proc. Soc. Exp. Mech., 13(2), pp. 141-152, 1956

85 Galletly, G.D., Slankard, R.C., Wenk, E.: 'General instability of ring-stiffened cylindrical shells subject to external hydrostatic pressure - a comparison of theory and experiments', J. Applied Mech., 25, pp. 259-266, 1958

86 Galletly, G.D., Bart, R.: 'Effects of boundary conditions and initial out-of-circularity on the strength of thin-walled cylinders subjected to external hydrostatic pressure', J. Applied Mech., 23, pp. 351-358, 1956

87 Nash, W.A.: 'Buckling of initially imperfect cylindrical shells', J. Applied Mech., 24, pp. 125-130, 1957

88 Nash, W.A.: 'Buckling of multiple-bay ring-stiffened cylindrical shells subject to hydrostatic pressure', J. Applied Mech., 20, pp. 469-474, 1953

89 Bodner, S.R.: 'General instability of a ring-stiffened, circular cylindrical shell', J. Applied Mech., 24, pp. 269-279, 1957

90 Bodner, S.R.: 'General instability of a ring-stiffened, circular cylindrical shell under hydrostatic pressure', Journal of Applied Mechanics, 24(2), Jun. 1957

91 Pulos, J.G., Salerno, V.L.: 'Axisymmetric elastic deformations and stresses in a ring-stiffened, perfectly circular cylindrical shell under external hydrostatic pressure', DTMB 1497, Sep. 1961

92 Kennard, E.H.: 'Tripping of T-shaped stiffening rings on cylinders under external pressure', DTMB 1079, Nov. 1959

93 Kaminsky, E.L.: 'General instability of ring-stiffened cylinders with clamped ends under external pressure by Kendrick's method', DTMB 855, Jun. 1954

94 Boichot, L. and Reynolds, T.E.: 'Inelastic buckling tests of ring-stiffened cylinders under hydrostatic pressure', DTMB 1992, May 1965

95 Ball Jr., W.E.: 'Formulas and curves for determining the elastic general-instability pressures of ring-stiffened cylinders', DTMB 1570, Jan. 1962

96 Kirsten, A.F., Wenk, E.: 'Observation of snap-through action in thin cylindrical shells under external pressure', Proc. Soc. Exp. Mech., 14(1), pp. 205-214, 1956

97 Pulos, J.G. and Krenzke, M.A.: 'Recent developments in pressure hull structures and materials for hydrospace vehicles', DTMB 2137, Dec. 1965

98 Von Sanden, K., Gunther, K.: 'The strength of cylindrical shells, stiffened by frames and bulkheads, under uniform external pressure on all sides', DTMB Translation 38, Mar. 1952

99 Kempner, J. and Salerno, V.L.: 'Analysis of the inelastic behaviour of transversely reinforced cylindrical shells under hydrostatic pressure', Polytechnic Institute of Brooklyn, Rep. 172, Aug. 1950

100 Lunchick, M.E.: 'Plastic pre-buckling stresses for ring-stiffened cylindrical shells under external pressure', DTMB 1448, Jan. 1961

101 Wenk, E., Slankard, R.C., Nash, W.A.: 'Experimental analysis of the buckling of cylindrical shells subjected to external hydrostatic pressure', Proc. Soc. Exp. Mech., 12(1), 1954

102 Kirsten, A.F., Slankard, R.C.: 'An experimental investigation of the shell instability strength of a machined, ring-stiffened cylindrical shell under hydrostatic pressure (Model BR-4A)', DTMB 997, April 1956

103 Slankard, R.C.: 'Tests of the elastic stability of a ring-stiffened cylindrical shell, Model BR-4 subjected to hydrostatic pressure', DTMB 876, Feb. 1955

104 Adamchak, J.C.: 'Design equations for tripping of stiffeners under inplane and lateral loads', DTNSRDC Rep. 79/064, Oct. 1979

105 Palermo, P.: 'Experimental stress analysis goes deep', Naval Engineer's Journal, 87(4), pp. 67-82, 1975

106 Dunham, F.W., Heller, S.R.: 'Comparative behaviour of submarine pressure hull structures of different scales under uniform external pressure', Naval Engineer's Journal, 75(2), pp. 397-404, 1963

107 Barry, T.M., Ballowm L.D.: 'Elastic instability of relatively thick circular cylindrical shells subject to hydrostatic pressure', 76(4), Naval Engineer's Journal, pp. 621-631, 1964

108 Gerard, G.: ' Plastic stability theory of stiffened cylinders under hydrostatic pressure', Journal of Ship Research, 6(2), pp. 1-7, Oct. 1962

109 Milligan, R., Lakshmikantham, C. and Gerard, G.: 'General instability of shallow-stiffened orthotropic cylinders under hydrostatic pressure', Journal of Ship Research, 11(1), pp. 269-279, March 1967

110 Ross, C.T.F.: 'The collapse of ring-reinforced cylinders under uniform external pressure', Trans. RINA, 107, 1965, pp. 375-394

111 Koga, T., Morimatsu, S.: 'Bifurcation buckling of circular cylindrical shells under uniform external pressure', AIAA Journal, 27(2), pp. 242-246, 1989

112 Lee, L.H.N.: 'Inelastic asymmetric buckling of ring stiffened cylindrical shells under external pressure', AIAA Journal, 12(8), pp. 1051-1056, 1974

113 Midgley, W.R., Johnson, A.E.: 'Experimental buckling of internal integral ring-stiffened cylinders', Proc. Soc. Exp. Str. Anal., 24(1), pp.145-153, 1967

114 Yamaki, N., Otono, K.: 'Experiments on the post-buckling behaviour of circular cylindrical shells under hydrostatic pressure', Exp. Mechanics, 13(7), pp. 299-304, 1973

115 Yamaki, N., Otono, K.: 'Experiments on the postbuckling behaviour of circular cylindrical shells under hydrostatic pressure', Proc. Soc. Exp. Mech., 30(2), pp. 299-304, 1973

116 Singer, J.: 'Buckling, vibration and post-buckling of stiffened metal cylindrical shells', Proc. BOSS'76, Vol. I, Trondheim, Norway, 1976

117 Budianski, B. and Amazigo, J.C.: 'Initial postbuckling behaviour of cylindrical shells under external pressure', J. Math. Phys., 47, pp. 223-235, 1968

118 Hutchinson, J.W. and Amazigo, J.C.: 'Imperfection sensitivity of eccentrically stiffened cylindrical shells', AIAA J., 5, pp. 392-401, 1967

119 Ellinas, C.P., Supple, W.J., Walker, A.C.: 'Buckling of offshore structures', Prepared for the U.K. Dept. of Energy by J.P. Kenny & Partners Ltd., Granada, London, 1984

120 Harding, J.E., Dowling, P.J.: 'Recent research on the behaviour of cylindrical shells used in offshore structures', in Steel Structures, ed. M.N. Pavlovic, Elsevier Applied Science, London 1986

121 Vojta, J.: 'Buckling of ring and stringer and ring (only) stiffened steel cylinders - large scale tests', CBI Industries, Plainfield, January 1982

122 Health and Safety Executive (UK), 'Buckling of offshore structural components', OTH/90/329, J.P. Kenny & Partners Ltd., London, 1992

123 Sridharan, S.,Walker, A.C., Andrinocou, A.: 'Local plastic collapse of ring stiffened cylinders', Proc. Inst. Civil Engs., 71(2), pp. 341-368, 1981

124 Walker, A.C., McCall, S., Thorpe, T.W.: 'Strength of damaged ring and orthogonally stiffened shells - part I: plain ring stiffened shells', Thin Walled Structures, 5, pp. 425-453, 1987.

125 Walker, A.C., McCall, S., Thorpe, T.W.: 'Strength of damaged ring and orthogonally stiffened shells - part II: T-ring and orthogonally stiffened shells', 6, pp. 19-50, 1988

126 Tsang, S.K., Harding, J.E.: 'Buckling behaviour under pressure of cylindrical shells reinforced by light ring stiffeners', Proc. Inst. Civil Engs., 79(2), pp. 365-382, 1985

127 Tsang, S.K., Harding, J.E.: 'A mechanism approach for the prediction of the collapse strength of ring-stiffened cylinders under axial compression and external pressure', Thin Walled Structures, 2, pp. 325-353, 1984

128 Tsang, S.K., Harding, J.E.: 'A plastic mechanism formulation for the general instability of ring stiffened cylinders under pressure dominated loadings', Intl. J. Mech. Sci., 27, pp. 409-422, 1985

129 Estefen, S.F., Harding, J.E.: 'Ring stiffener behaviour and its interaction with cylindrical panel buckling', Proc. Inst. Civil Engs., 75(2), pp. 243-264, 1983

130 Croll, J.G.A.: 'Elasto-Plastic buckling of pressure and axial loaded cylinders', Proc. Inst. Civil Engs., 73(2), pp. 633-652, 1982

131 Croll, J.G.A.: 'Lower bound elasto-plastic buckling of cylinders', Proc. Inst. Civil Engs., 71(2), pp. 235-262, 1981

132 Croll, J.G.A.: 'Stiffened cylindrical shells under axial and pressure loading', in Shell Structures, Stability and Strength, ed. R. Narayanan, Elsevier Applied Science, London, 1985

133 Frieze, P.A, Sands, G.: 'CONOCO/ABS Ring stiffened cylinder tests - final report', Rep. NAOE-84-24, NAOE Dept., University of Glasgow, Mar. 1984.

134 Frieze, P.A.: 'The experimental response of flat-bar stiffeners in cylinders under external pressure', Charles Smith Memorial Conference, DRA, Dunfermline, July 1992

135 Chryssanthopoulos, M.K., Baker, M.J., Dowling, P.J.: 'Imperfection modelling for buckling analysis of stiffened cylinders', J. Str. Div. ASCE, 117(7), pp. 1998-2018, 1991

136 Seleim, S.S., Roorda, J.: 'Buckling behaviour of ring-stiffened cylinders; experimental study', Thin Walled Structures, 3, pp. 203-222, 1986

137 Seleim, S.S., Roorda, J.: 'Theoretical and experimental results on the post-buckling of ring-stiffened cylinders', Mech. Struc. & Mach., 15(1), pp. 69-87, 1987

138 Gonçalves, P.B., Batista, R.C.: 'Buckling and sensitivity estimates for ring-stiffened cylinders under external pressure', Int. J. Mech. Sc., 27(1), pp. 1-11, 1985

139 Miller, C.D., Kinra, K.: 'External pressure tests of ring fabricated steel cylinders', proc. OTC 81, Vol. III, pp. 371-386, 1981

140 Esslinger, M., Geier, B.: 'Flat bar steel ring stiffeners on cylinders subjected to external pressure', Thin-Walled Structures, 15, pp. 249-269, 1993

141 Louca, L.A. and Harding, J.E.: 'Torsional buckling of ring-stiffeners in cylindrical shells subjected to external pressure' Proc. Inst. Civil Eng., 104, pp. 219-230, 1994

142 Morihana, H., Inoue, K., Takenaka, M., Yamauchi, Y., Nakamura, K. and Baba, K.: 'Research on general instability of cylindrical shells reinforced by ring stiffeners under uniform pressure (2nd. Report)', J. Soc. Naval Arch. Japan, 168, pp. 431-440, Dec. 1990, (In Japanese)

143 Homma, Y., Mitsuhashi, T., Ikegami: 'General instability of ring-stiffened shells subjected to hydrostatic pressure', J. Soc. Naval Arch. Japan, 162, pp. 307-312, Dec. 1987 (In Japanese).

144 Homma, Y., Hoshino, Y.: 'Shell buckling of circular shells with initial deflections (2nd. Report)', J. Soc. Naval Arch. Japan, 162, pp. 313-319, Dec. 1987 (In Japanese).

145 Homma, Y.: 'Axisymmetric collapse of circular cylindrical shells subjected to hydrostatic pressure', J. Soc. Naval Arch. Japan, 147, pp. 238-243, Jun. 1980 (In Japanese).

146 Homma, Y., Ishida, S.: 'Shell buckling of circular shells with initial deflections (1st. Report)', J. Soc. Naval Arch. Japan, 158, pp. 395-405, Dec. 1985 (In Japanese).

147 Yokota, K., Yamauchi, Y., Baba, K., Nanba, N. and Urabe, Y.: 'Research on general instability of cylindrical shells reinforced by ring stiffeners under uniform pressure (1st. Report)', J. Soc. Naval Arch. Japan, 158, pp. 406-419, Dec. 1990 (In Japanese).

148 Yamamoto, Y., Homma, Y., Oshima, K., Mishiro, Y., Terada, H., Yoshikawa, T., Morihana, H., Yamauchi, Y. and Takenaka, M.: 'General instability of ring-stiffened shells under external pressure', Marine Structures, 2, pp. 133-149, 1989

149 Bosman, T.N., Pegg, N.G., Keuning, P.J.: 'Experimental and numerical determination of the nonlinear overall collapse of imperfect pressure hull compartments', RINA Intl. Symp. Naval Submarines, London, May 1993

150 Bushnell, D.: 'Computerized buckling analysis of shells', Martinius Nijhoff Publishers, Dordrecht, 1985

151 Bushnell, D.: 'Buckling of shells - pitfall for designers', AIAA Jnl., 19(9), pp. 1183-1226, Sep. 1981

152 Bushnell, D.: 'Plastic buckling of various shells', J. Press. Vessel Tech., 104, pp. 51-72, 1984

153 Bushnell, D.: 'Stress, stability and vibration of complex branched shells of revolution', Comp. & Struct., 4, pp. 399-435, 1974

154 Bushnell, D.: 'BOSOR5 - program for buckling of elastic-plastic complex shells of revolution including large deflections and creep', Comp. & Struct., 6, pp. 221-239, 1976

155 Bushnell, D.: 'Analysis of ring-stiffened shells of revolution under combined thermal and mechanical loading', AIAA J., 9(3), pp. 401-410, 1971

156 Bushnell, D.: 'Effect of ring out-of-plane bending stiffness on thermal buckling prediction for ring-stiffened cylinders', AIAA J., 9(8), pp. 1653-1654, 1971

157 Bushnell, D.: 'Effect of cold bending and welding on buckling of ring stiffened cylinders', Comp. & Struct., 12, pp. 291-307, 1980

158 Bushnell, D.: 'Buckling of elastic-plastic shells of revolution with discrete elastic-plastic ring stiffeners', Int. J. Sol. Struct., 12, pp. 51-66, 1976

159 Bushnell, D.: 'Computerized analysis of shells - governing equations', Comp. & Struct., 18(3), pp. 471-536, 1984

160 Bushnell, D.: 'A strategy for the solution of problems involving large deflections, plasticity and creep', Int. J. Num. Meth. Eng., 11, pp. 683-708, 1977

161 Bushnell, D.: 'Evaluation of various analytical models for buckling and vibration of stiffened shells', AIAA J., 11(9), pp. 1283-1291, 1973

162 Riks, E.: 'Progress in collapse analysis', Journal of Pressure Vessel Technology, 109(1), pp. 33-41, 1987

163 Crisfield, M.A.: 'A fast incremental/iterative solution procedure that handles snap-through', Comp. & Struct., 13, pp. 55-62, 1981

164 Lam,W.F., Morley, C.T.: 'Arc-length method for passing limit points in structural calculation', J. Str. Div. ASCE, 118(1), pp. 169-187, 1992

165 Moradi, B., Parsons, J.D.: 'A comparison of techniques for computing the buckling loads of stiffened shells', Comp. & Struct., 46(3), pp. 505-514, 1992

166 Subbiah, J.: 'Non-Linear Analysis of geometrically imperfect stiffened shells of revolution', Journal of Ship Research, 32(1), pp. 29-36, March 1988

167 Subbiah, J., Natarajan, R.: 'Stability analysis of ring-stiffened shells of revolution', Journal of Ship Research, 26(2), pp. 125-134, June 1982

168 Subbiah, J., Natarajan, R.: 'Stability analysis of ring stiffened shells of revolution', Comp. & Struct., 14(5-6), pp. 479-490, 1981

169 Subbiah, J., Natarajan, R.: 'Stability analysis of ring stiffened shells of revolution', Comp. & Struct., 13, pp. 497-503, 1981

170 Park, C.M., Yim, S.J.: 'Ultimate strength analysis of ring-stiffened cylinders under hydrostatic pressure', Proceedings OMAE 93, Vol. I, pp. 399-404, ASME, 1993

171 Code of practice for design of steel bridges, BS 5400, Part 3, 1982

172 CIRIA (Construction Industry Research and Information Association), 'Rationalisation of Safety and Serviceability Factors in Structural Codes', CIRIA Report 63, London, 1977

173 Commission of the European Communities, 'Eurocode no.2: design of concrete structures - Part 1: general rules and rules for buildings', Draft, October 1991

174 Commission of the European Communities, 'Eurocode no.4: design of composite steel and concrete structures - Part 1.1: general rules and rules for buildings', Draft, March 1992

175 Thoft-Christensen, P. and Baker, M. J.: 'Structural reliability theory and its applications', Springer-Verlag, Berlin, 1982

176 Madsen, H.O., Krenk, S. and Lind, N.C.: 'Methods of structural safety', Prentice-Hall Inc., Englewood Cliffs, 1986

177 Benjamin, J.R. and Cornell, C.A.: 'Probability statistics and decision for civil engineers', Mc Graw Hill, New York, 1970

178 Hasofer, A.M. and Lind, N.C.: 'Exact and invariant second-moment code format', Journal Eng. Mech. Div. ASCE, 100, pp. 111-121, 1974

179 Rackwitz, R. and Fiessler, B.: 'Structural reliability under combined random load sequences', Comp. & Struct., 9, pp. 489-494, 1978

180 Fiessler, B., Neuman, H.-J. and Rackwitz, R.: 'Quadratic limit states in structural reliability', Journal Eng. Mech. Div. ASCE, 105, pp. 661-676, 1979

181 Madsen, H.O.: 'First order vs. second order reliability analysis of series structures', Structural Safety, 2(3), pp. 207-214, 1984

182 Hochenbichler, M., Gollwitzer, S. Kruse, W. and Rackwitz, R.: 'New light on first and second order reliability methods', Structural Safety, 4(4), pp. 267-284, 1986

183 Der Kiureghian, A., Lin, H.Z. and Hwang, S.J.: 'Second order reliability approximations', Journal Eng. Mech. Div. ASCE, 113(8), pp. 1208-1228, 1987

184 Der Kiureghian, A. and De Stefano, M.: 'Efficient algorithm for second order reliability analysis', Journal Eng. Mech. Div. ASCE, 117(2), pp. 2904-2925, 1991

185 Breitung, K.: 'Asymptotic approximations for multimodal integrals', Journal Eng. Mech. Div. ASCE, 110(3), pp. 357-366, 1984

186 Tvedt, L.: 'Two second order approximations to the failure probability', Veritas Report RDIV/20-004-83, Det norske Veritas, Oslo, 1983

187 Ditlevsen, O.: 'Narrow reliability bounds for structural systems', Journal of Structural Mechanics, 7(4), pp. 435-454, 1979

188 Schuëller, G.I. and Stix, R.: 'A critical appraisal of methods to determine failure probabilities', Structural Safety, 4, pp. 293-309, 1987

189 Bjerager, P.: 'On computational methods for structural reliability analysis', Structural Safety, 9, pp. 79-96, 1990

190 Pulido, G.E., Jacobs, T.L. and Lima, E.C.P.: 'Structural reliability using Monte Carlo simulation with variance reduction techniques on elastic-plastic structures', Comp. and Struct., 43(3), pp. 419-430, 1992

191 Melchers, R.E.: 'Search based importance sampling', Structural Safety, 9(2), pp. 117-128, 1990

192 Melchers, R.E.: 'Importance sampling in structural systems', Structural Safety, 6(1), pp. 3-10, 1989

193 Melchers, R.E.: 'Radial importance sampling for structural reliability', Journal Eng. Mech. Div. ASCE, 116(1), pp. 189-209, 1990

194 Fu, G.: 'Variance reduction in simulation for first order problems', in Structural Safety and Reliability, Ed. G.I. Schuëller, M. Shinozuka, J.T.P. Yao, A.A. Balkema, Rotterdam, 1994

195 Wang, G.S. and Ang, A. H.-S.: 'Adaptive Kernel method for evaluating structural system reliability', in Structural Safety and Reliability, Ed. G.I. Schuëller, M. Shinozuka, J.T.P. Yao, A.A. Balkema, Rotterdam, 1994

196 Yonezawa, M. and Okuda, S.: 'An improved importance sampling density estimation for structural reliability assessment', in Structural Safety and Reliability, Ed. G.I. Schuëller, M. Shinozuka, J.T.P. Yao, A.A. Balkema, Rotterdam, 1994

197 Bucher, C.G.: 'Adaptative sampling - an iterative fast Monte Carlo procedure', Structural Safety, 5(2), pp. 119-126, 1988

198 Ditlevsen, O., Olesen, R. and Mohr, G.: 'Solution of a class of load combination problems by directional simulation', Structural Safety, 4(2), pp. 95-110, 1986

199 Puppo, A.H. and Bertero, R.D.: 'Evaluation of probabilities using orientated simulation', Journal Eng. Mech. Div. ASCE,118(6), pp. 1683-1706, 1992

200 Shao, S. and Murotsu, Y.: 'Reliability of complex structural systems using an efficient directional simulation', in Structural Safety and Reliability, Ed. G.I. Schuëller, M. Shinozuka, J.T.P. Yao, A.A. Balkema, Rotterdam, 1994

201 Shooman, M.L.: 'Probabilistic reliability: an engineering approach', Mc Graw Hill, New York, 1968

202 Harbitz, A.: 'An effective sampling method for probability of failure calculation', Structural Safety, 3(2), pp. 109-115, 1986

203 Sweeting, T.J. and Finn, A.F.: 'A Monte Carlo method based on first and second order reliability approximations', Structural Safety, 11(3-4), pp. 203-213, 1992

204 Hochenbichler, M., Rackwitz, R. and Ruediger: 'Improvement of second order reliability estimates by importance sampling', Journal of Eng. Mech., 114(2), pp. 2195-2198, 1988

205 Sharp, J.V., Kam, J.C. and Birkinshaw, M.: 'Review of criteria for inspection and maintenance of North Sea structures', Proceedings OMAE-93, Vol. II, Glasgow, June 1993

206 'How safe is safe enough', Plenary Discussion of ICOSSAR'93, in Structural Safety and Reliability, Ed. G.I. Schuëller, M. Shinozuka, J.T.P. Yao, A.A. Balkema, Rotterdam, 1994

207 Bea, R.G.: 'Reliability based requalification criteria for offshore platforms', Proceedings OMAE-93, Vol. II, Glasgow, June 1993

208 Faulkner, D., Birrel, N.D. and Stiansen, S.G.: 'Development of a reliability based code for the structure of tension leg platforms'. OMAE Special Symposium, New Orleans, Feb. 1986

209 Faulkner, D.: 'Development of a code for the structure design of compliant deep water platforms'. OMAE Special Symposium, New Orleans, Feb. 1986

210 Mansour, A., Lin, M., Hovem, L. and Thayamballi, A.: 'Probability-Based ship design (Phase 1) - A demonstration', Report to the Ship Structure Committee, SSC-368, Washington, U.S. Coast Guard, Sep. 1992

211 Brown, C.B.: 'A fuzzy safety measure', Journal Eng. Mech. Div. ASCE, 105, pp. 855-872, 1979

212 Yunlong, Z., Fujimoto, Y. and Iwata, M.: 'On reliability assessment of framed structures based on Monte Carlo simulation - Application of importance sampling and Neumann Expansion', Journal Soc. Naval Arch. Japan, 167, pp. 199-204, June 1990

213 Murotsu, Y., Okada, H., Hibi, S., Niho, O. and Kaminaga, H.: 'A system for collapse and reliability analysis of ship structures using a spatial plate element model', Proceedings OMAE-93, Vol. II, Glasgow, June 1993

214 Sigurdson, G., Skjong, R., Skallerud, B. and Amdahl, J.: 'Probabilistic collapse analysis of jackets', in Structural Safety and Reliability, Ed. G.I. Schuëller, M. Shinozuka, J.T.P. Yao, A.A. Balkema, Rotterdam, 1994

215 Maymom, G.: 'Direct computation of the design point of a stochastic structure using a finite element code', Structural Safety, 14, pp. 185-202, 1994

216 Sarras, T.A., Diekman, R.M., Matthies, H.G. and Moore, C.S.: 'Stochastic finite elements: An interface approach', Proceedings OMAE-93, Vol. II, Glasgow, June 1993

217 Muzeau, J.-P., Lemaire, M., Besse, P., Locci, J.-M.: 'Evaluation of reliability in case of complex mechanical behaviour', Proceedings OMAE-93, Vol. II, Glasgow, June 1993

218 Lee, J.-S., Krakovski, M.B., Yakubovich, A.N.: 'Investigation of response surface for reliability analysis of structural systems', Proceedings OMAE-93, Vol. II, Glasgow, June 1993

219 Lee, J.-S., Krakovski, M.B.: 'System reliability analysis using response surface and Monte Carlo approaches', in Structural Safety and Reliability, Ed. G.I. Schuëller, M. Shinozuka, J.T.P. Yao, A.A. Balkema, Rotterdam, 1994

220 Shinozuka, M.: 'Computational stochastic mechanics: Recent and future developments', in Structural Safety and Reliability, Ed. G.I. Schuëller, M. Shinozuka, J.T.P. Yao, A.A. Balkema, Rotterdam, 1994

221 Vanmarcke, E., Shinozuka, M., Nakagiri, S., Schuëller, G.I. and Grigoriu, M.: 'Random fields and stochastic finite lements', Structrual Safety, 3, pp. 143-166, 1986

222 Lee, J.-S.: 'Application of stochastic finite element method to system reliability analysis of offshore structures', in Structural Safety and Reliability, Ed. G.I. Schuëller, M. Shinozuka, J.T.P. Yao, A.A. Balkema, Rotterdam, 1994

223 Wall, F.J., Deodatis, G. and Shinozuka, M.: 'Variability response functions and upper bounds of response variability of 2D stochastic systems', in Structural Safety and Reliability, Ed. G.I. Schuëller, M. Shinozuka, J.T.P. Yao, A.A. Balkema, Rotterdam, 1994

224 Breitung, K., Ibrahim, Y.: 'Problems of statistical inference in structural reliability', in Structural Safety and Reliability, Ed. G.I. Schuëller, M. Shinozuka, J.T.P. Yao, A.A. Balkema, Rotterdam, 1994

225 Ditlevsen O.: 'Distribution arbitrariness in structural reliability', in Structural Safety and Reliability, Ed. G.I. Schuëller, M. Shinozuka, J.T.P. Yao, A.A. Balkema, Rotterdam, 1994

226 Ben-Haim, Y.: 'A non-probabilistic concept of reliability', Structural Safety, 14(4), pp. 227-246, 1994

227 Bushnell, D.: 'Computerized buckling analysis of shells', Martinius Nijhoff Publishers, Dordrecht, 1985

228 Elishakoff, I. and Arbocz, J.: 'Reliability of axially compressed cylindrical shells with random axisymmetric imperfections', Intl. Journal of Solids and Structures, 18(7), pp. 563-585, 1982

229 Elishakoff, I., Von Manen, S., Vermeulen, P.G. and Arbocz, J.: 'First order second moment analysis of the buckling of shells with random imperfections', AIAA Journal, 25(8), pp. 1113-1117, 1987

230 Kimpara, I.: 'Use of advanced composite materials in marine vehicles', Marine Structures, 4(2), pp. 117-128, 1991

231 Elishakoff, I., Cai, G.Q. and Starnes Jr., J.H.: 'Probabilistic and convex models of uncertainty in buckling of structures', in Structural Safety and Reliability, Ed. G.I. Schuëller, M. Shinozuka, J.T.P. Yao, A.A. Balkema, Rotterdam, 1994

232 Shanley, F.R.: 'Inelastic Column Theory', J. Aero. Sci., 14(5),1947, pp. 261.

233 Bleich, F.: 'Buckling Strength of Metal Structures', McGraw-Hill Inc., 1952.

234 Johnston, B.G.: 'Guide to stability design criteria for metal structures', John Wiley & Sons Inc., New York, 1976

235 Beedle, L.S.: 'Stability of metal structures - a world view', Structural Stability Research Council, Bethlehem, USA, 1991.

236 Seide, P.: 'A reexamination of Koiter's theory of initial postbuckling behaviour and imperfection sensitivity of structures', in Thin Shell Structures, Ed. Y.C. Fung and C.C. Sechler, Prentice Hall Inc., New Jersey, 1974

237 Donnell, L.H.: 'Effect of imperfections on buckling of thin cylinders under external pressure', J. Applied Mech., 23, pp. 569-575, 1956

238 Franitza, S.: 'Strength aspects of the design of submarine pressure hulls', Naval Forces, 10, Special Supplement V, pp. 89-92, 1989

239 Faulkner, D., Adamchack, J.C., Snyder, G.J., Vetter, M.F.: 'Synthesis of Welded Grillages to Withstand Compression and Normal Loads', Comp. & Struct., 3, pp. 221-246, 1973

240 Shama, M.A.: 'Cold forming residual stresses and their effect on the accuracy of post-forming operations', European Shipbuilding, 19(2), pp. 23-26, 1970

241 Khaw, T.K.: 'Buckling strength of imperfect ring-stiffened cylinders under combined loads', PhD Thesis, NAOE Dept., Glasgow University, 1980

242 Hu, Z.S.: 'A Finite element assessment of the buckling strength equations of stiffened plates', SNAME Ship Structures Symposium'93, Virginia, USA, Nov. 1993

243 Hu, S.Z., Birkemoe, P.C., Prion, H.G.L.: 'Finite element modelling of imperfections and residual stresses in fabricated tubular columns', in Design of Marine and Offshore Structures, Ed. T.K.S. Murthy, J.A. Alaez, Elsevier Applied Science, 1992

244 Zuoshui, X. and Jiping, X.: 'On the overall stability of submarine circular cylindrical shells with large diameters and thin thicknesses', Shipbuiding of China, 2, pp. 82-88, May 1994 (in Chinese)

245 Euler, L.: 'Methodus inveniendi lineas curvas maximi minimive proprietate gaudentes (Appendix, De curvis elasticis)', Marcum Michaelem Bousquet, Lausanne and Geneva, 1744

246 Thompson, J.M.T.: 'Instabilities and catastrophes in science and engineering', John Wiley & Sons, Chichester, 1982

Four centuries BC: Aristotle wrote of diving bells for divers -30m

Until 1934: Man had reached only 183m

1934: Bebe & Barton reached 923m in a lowered cast steel bathysphere

1945-1970: Intense scientific and military research:

- 1960, Picard & Walsh reached 19910m with the Trieste I (Ni-Cr-Mo Bathysphere)
- Nuclear powered naval submarines, (>225m) (Quenched & Tempered Steels)
- Deep Submergence Rescue Vehicle, (5000 ft) (Titanium tri-sphere)

1970- : Commercial applications:

- Inspection and repair of cables, pipelines and other underwater installations: submersibles may work close to the installation in a weather-independent environment, without relying on long guide wires and umbilicals
- Oceanographic surveying (Scientific/Environmental)
- Exploration of sunken vessels (Titanic, e.g.)
- Recreational (Touristic submersibles, e.g.)

Figure 1 - Inner Space Exploration and Exploitation - Brief History

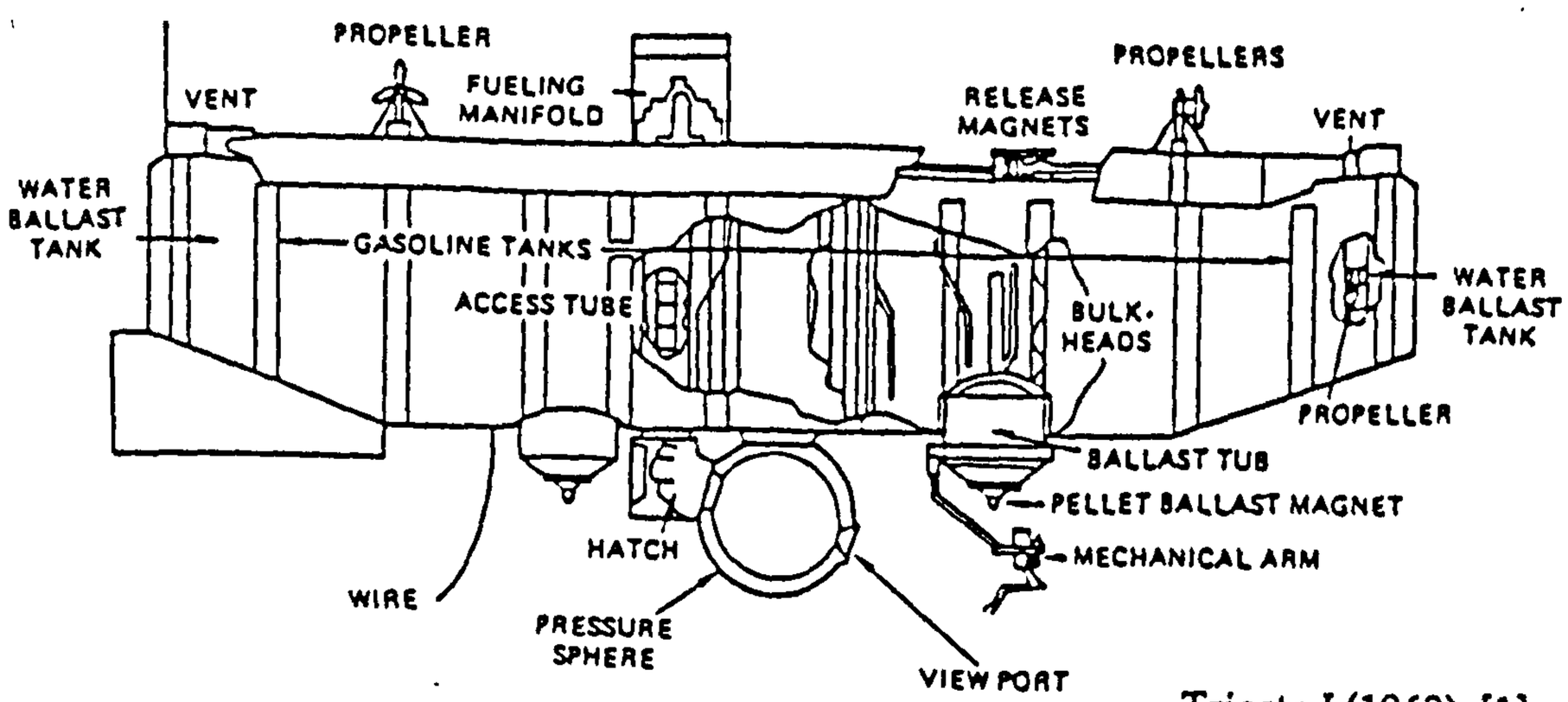

Trieste I (1960), [1]

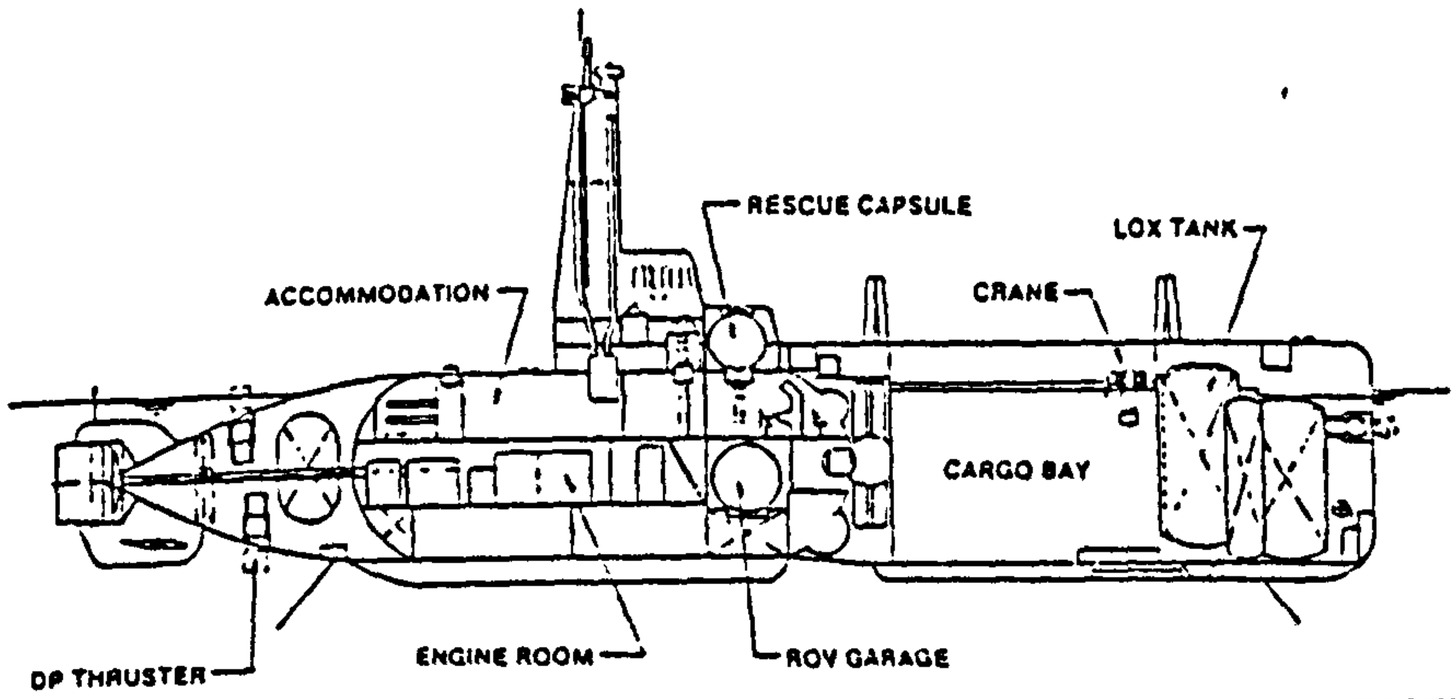

450m

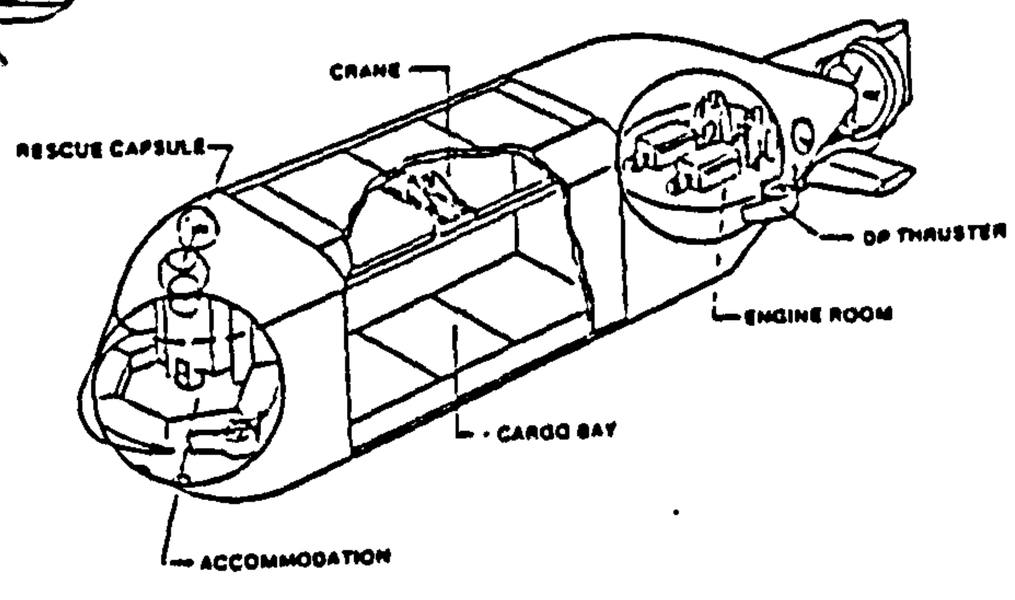

Offshore Service Submarines (1991) [9]

1500m

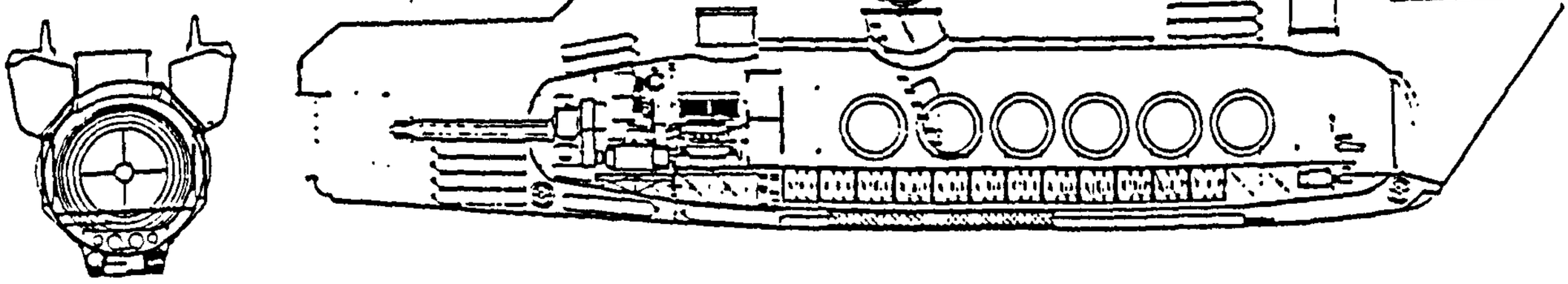

General arrangement of Nomad with passenger space laid out as a yacht. The faired yacht hull encloses the pressure hull.

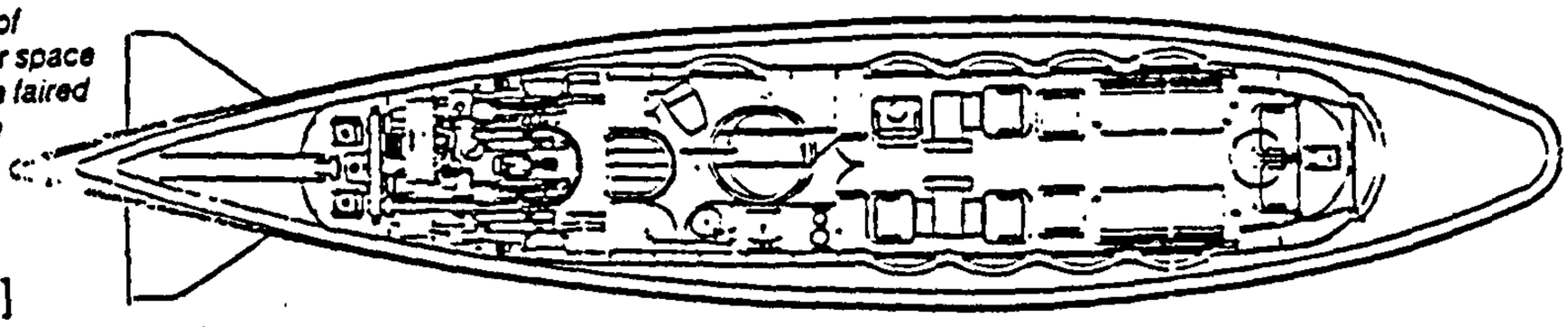

Nomad 1000 (1994) [10]

Figure 2 - Possible Concepts of Submersible Vehicles

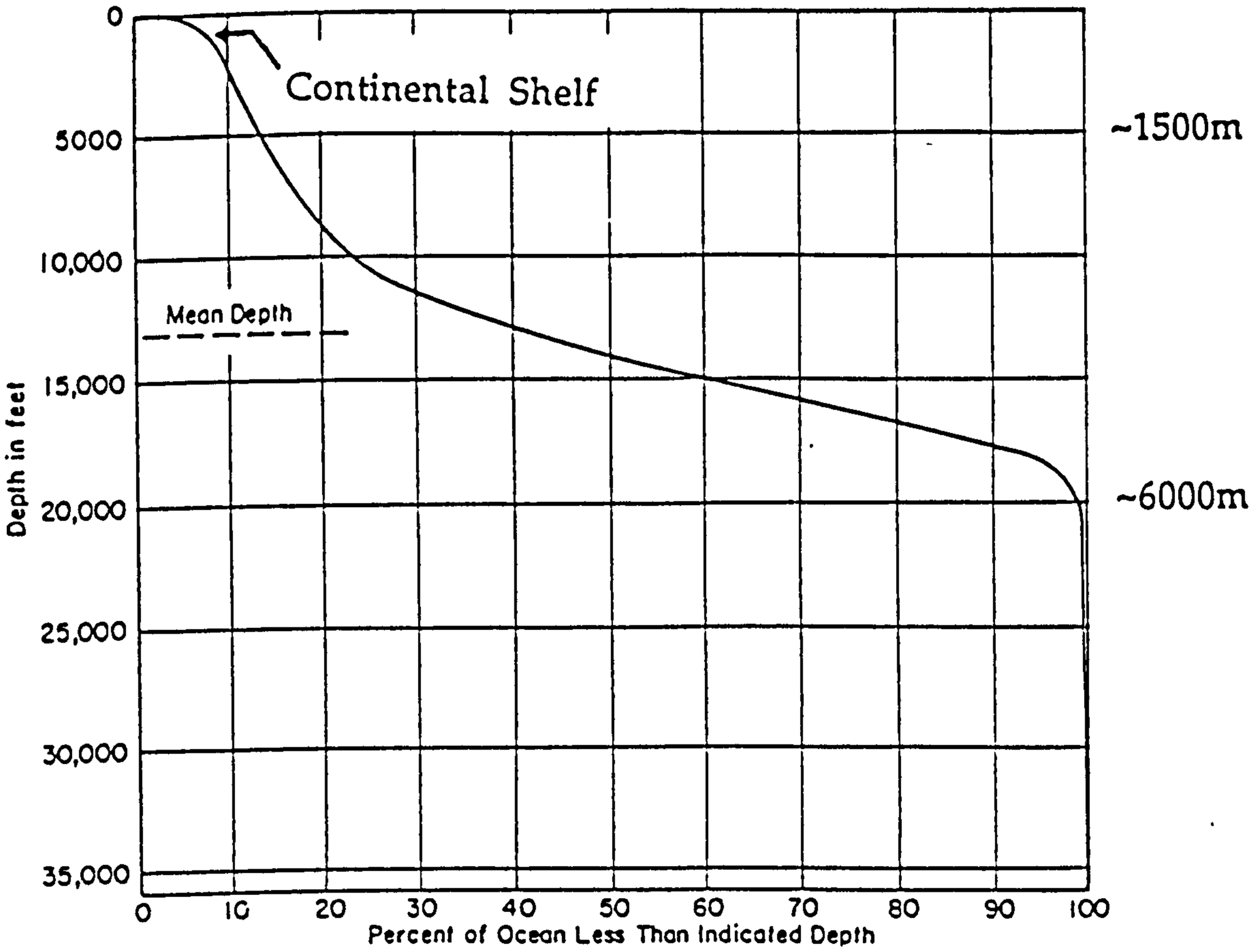

Figure 3 - Distribution of Ocean Depth, [76]

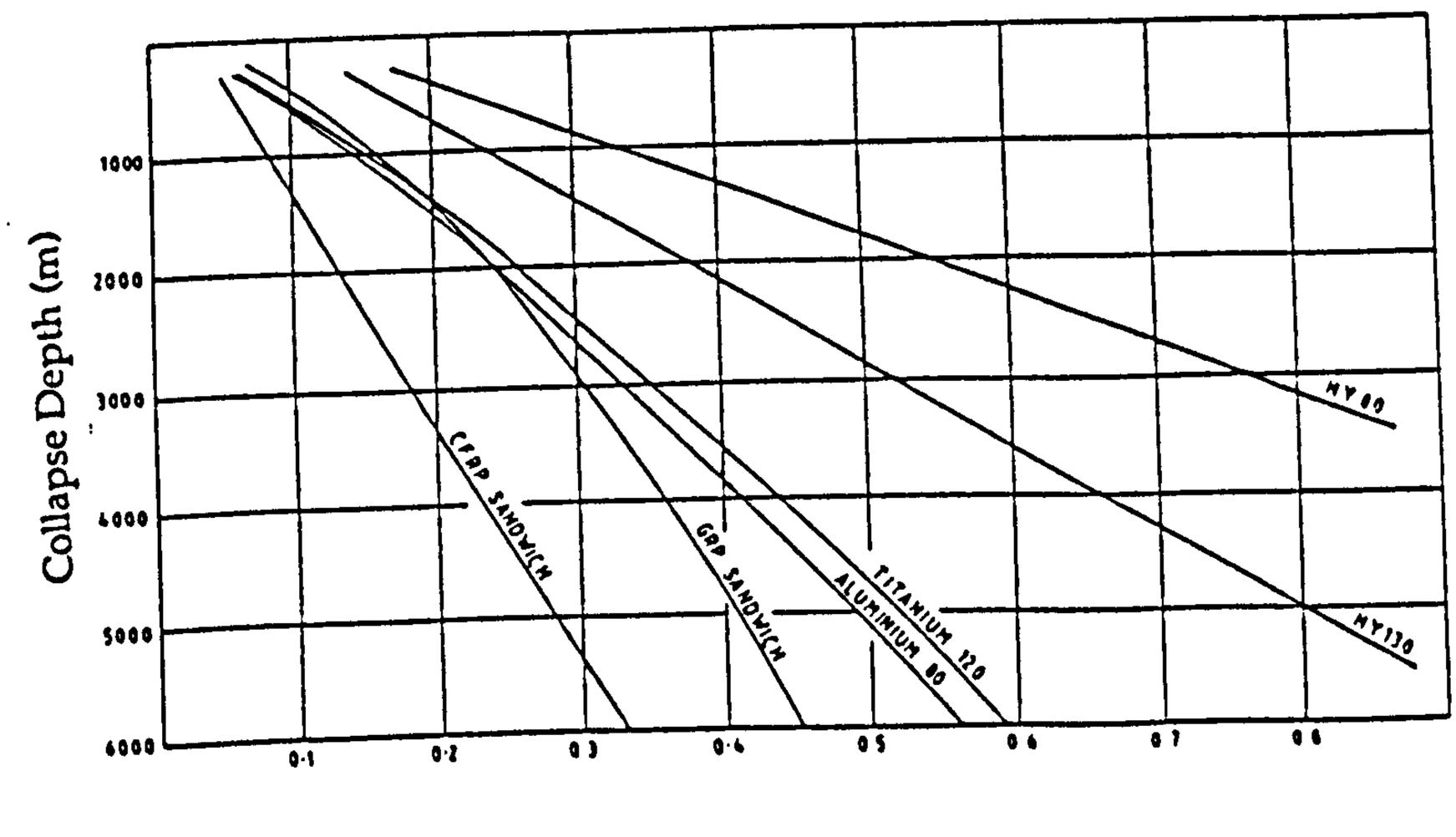

Figure 4 - Collapse Depth vs. W/Δ for Stiffened Cylinders, [11]

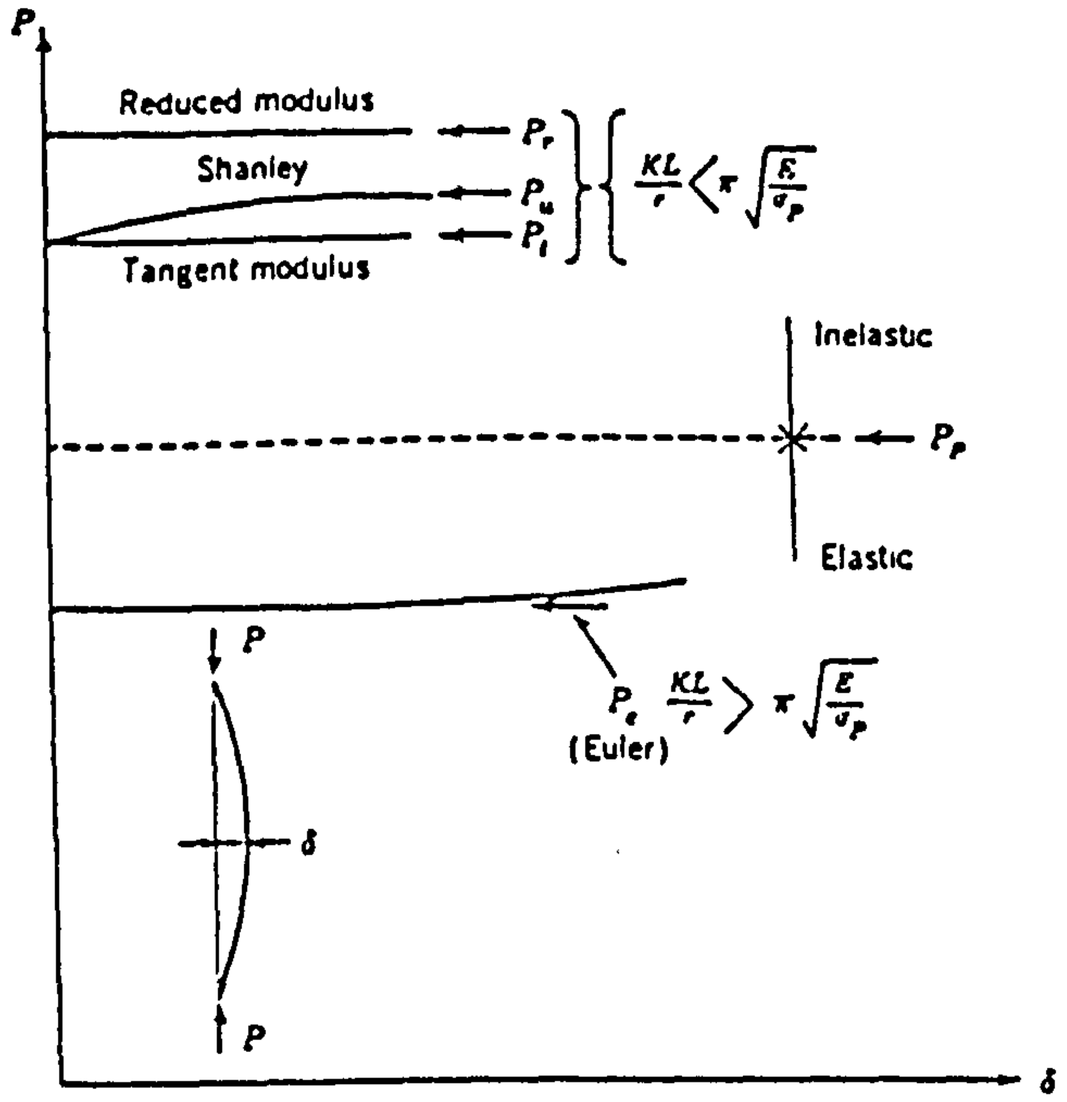

Figure 5 - Bifurcation Buckling, [234]

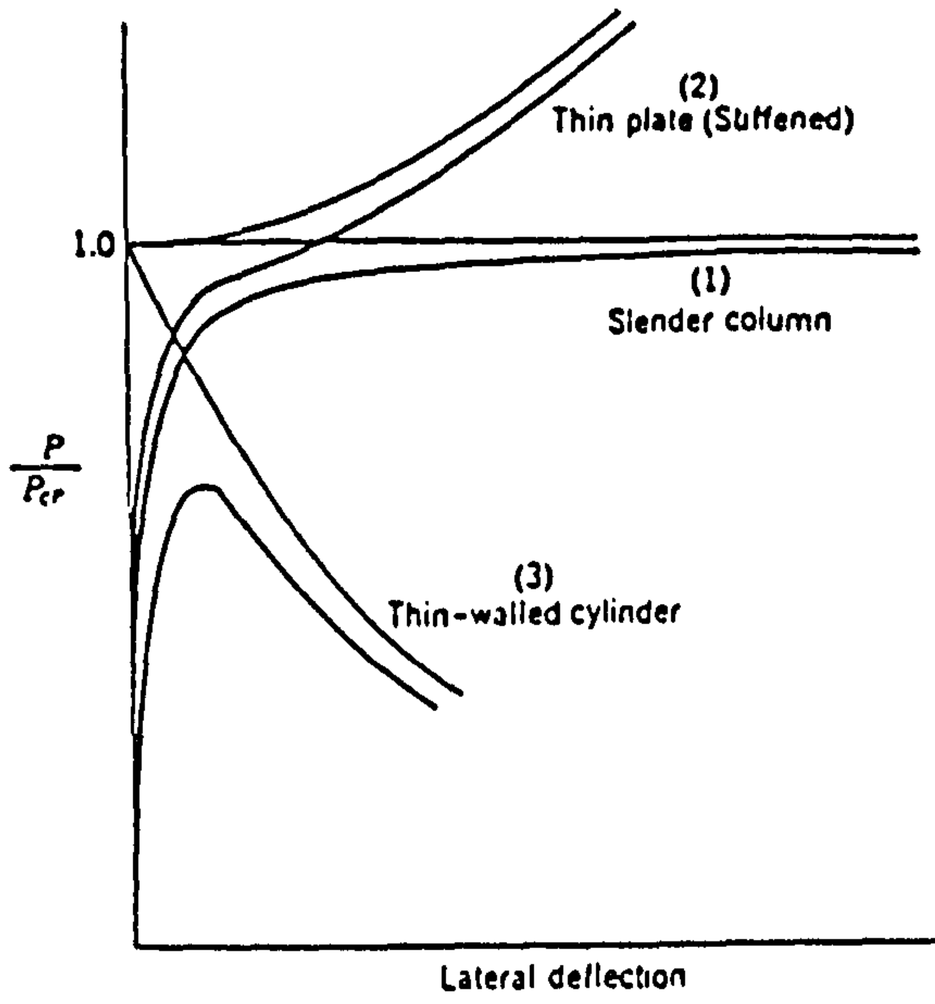

Figure 6 - Post Buckling Behaviour in the Elastic Range, [234]

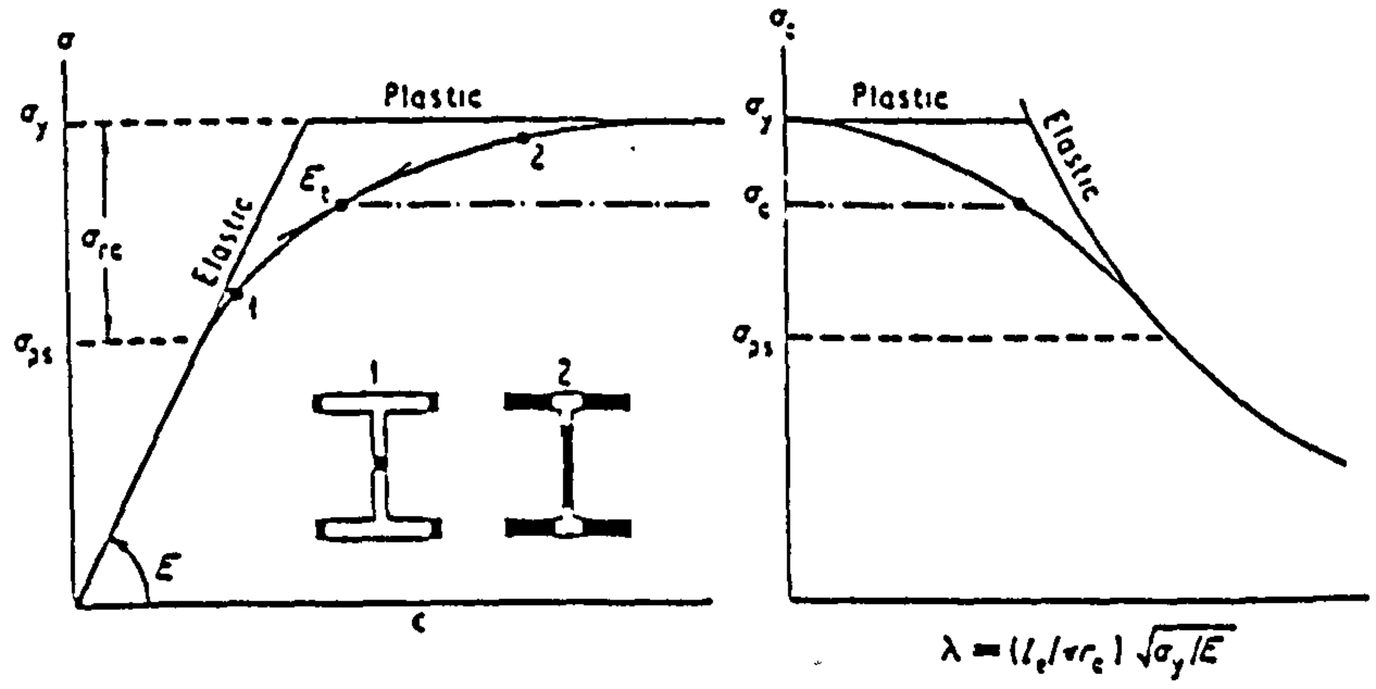

Fig. 7a - Rolled-Steel Column Strength

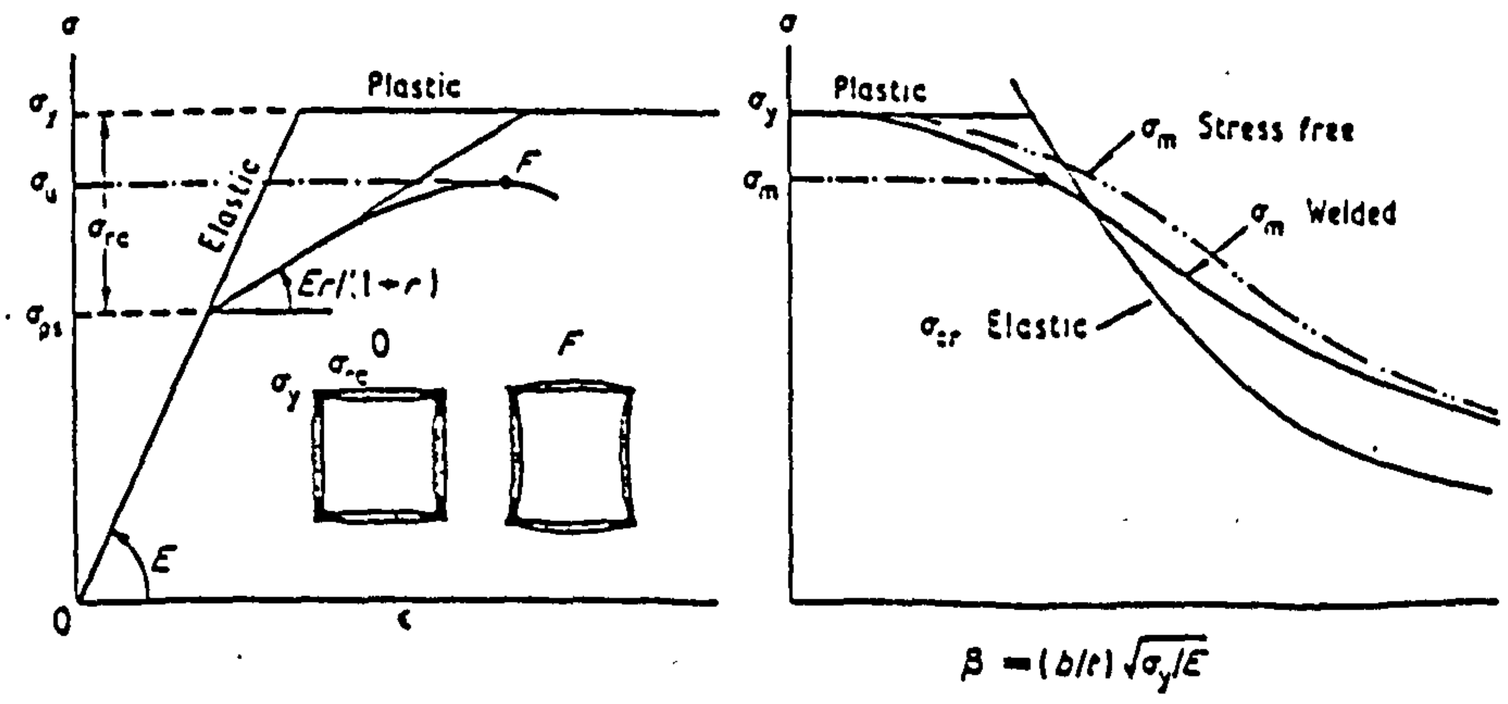

Fig. 7b - Welded Box-Column Strength

Figure 7 - Structural Proportional Limit, [61]

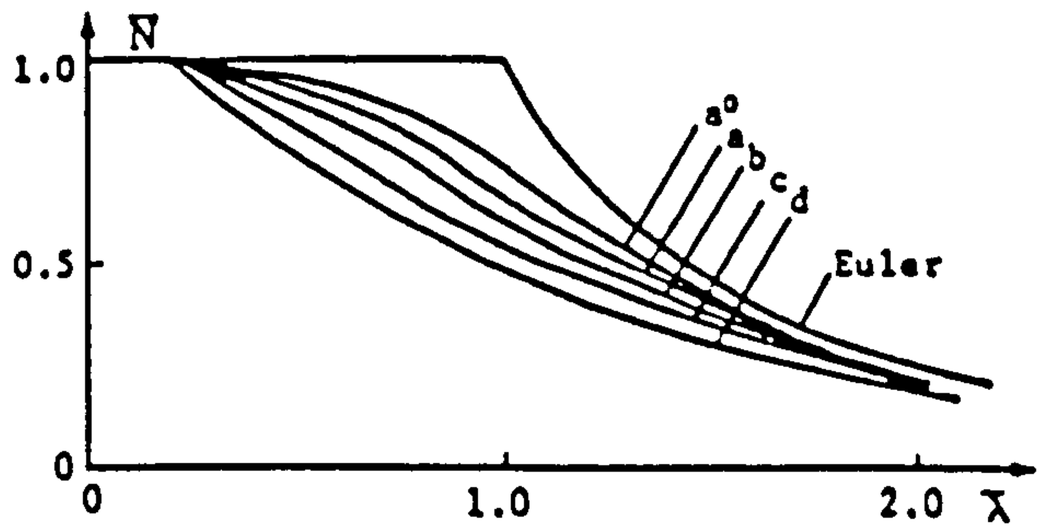

European column curves for steel

Cross section		buckling perpendicular to axis	buckling curve
hollow section Any increase in the yield strength which might be caused by a cold forming process shall be ignored 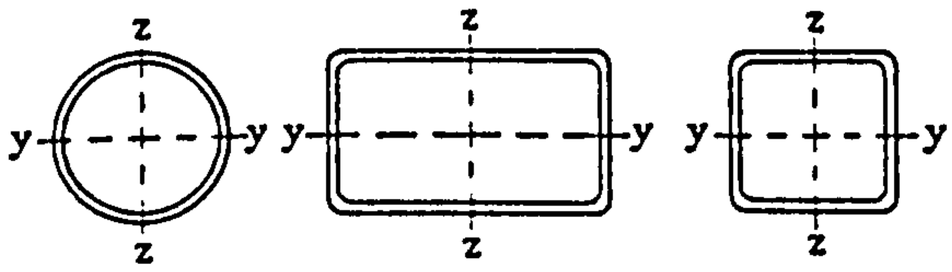		y – y z – z	a
welded box sections 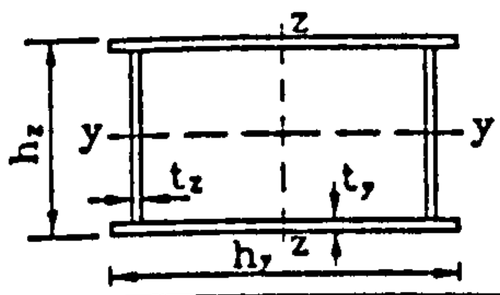		y – y z – z	b
	thick welds and $h_y/t_y < 30$ $h_z/t_z < 30$	y – y z – z	c
rolled I-sections 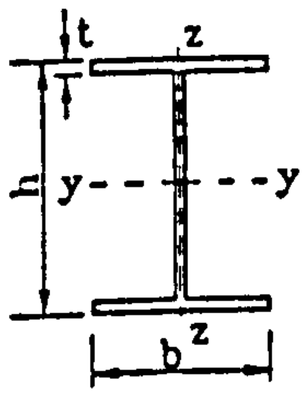	$\frac{h}{b} > 1.2$; $t \leq 40$ mm	y – y z – z	a (a_o) b (a)
	$\frac{h}{b} > 1.2$; $40 < t \leq 80$mm and $\frac{h}{b} \leq 1.2$; $t \leq 80$ mm	y – y z – z	b (a) c (b)
	$t > 80$ mm	y – y z – z	d d
welded I-sections 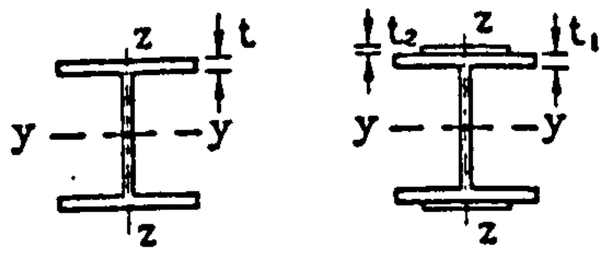	$t_1 \leq 40$ mm	y – y z – z	b c
	$t_1 > 40$ mm	y – y z – z	c d
U-, L-, T- and solid sections 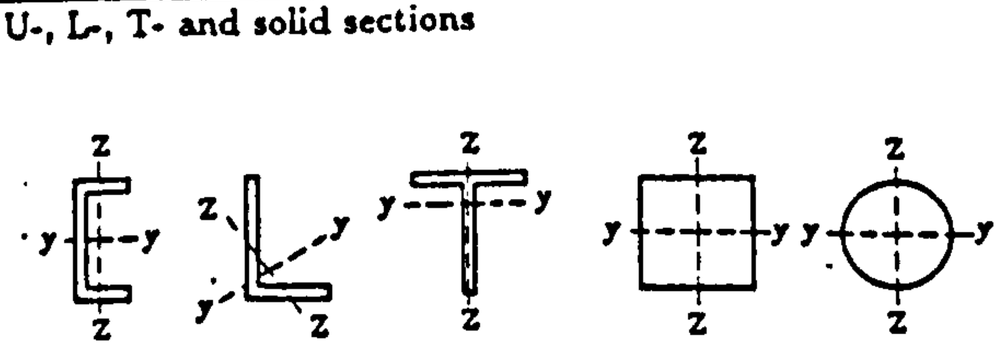		y – y z – z	c

Sections not contained in this table shall be classified analogously.

The buckling curves put in brackets may be assumed for high-strength steels with $f_y \geq 430$ N/mm^2 and $t \leq 40$ mm.

For transmission towers and similar structures where sufficient experimental data exist, alternative procedures can be used.

Figure 8 - ECCS Column Curves, [40]

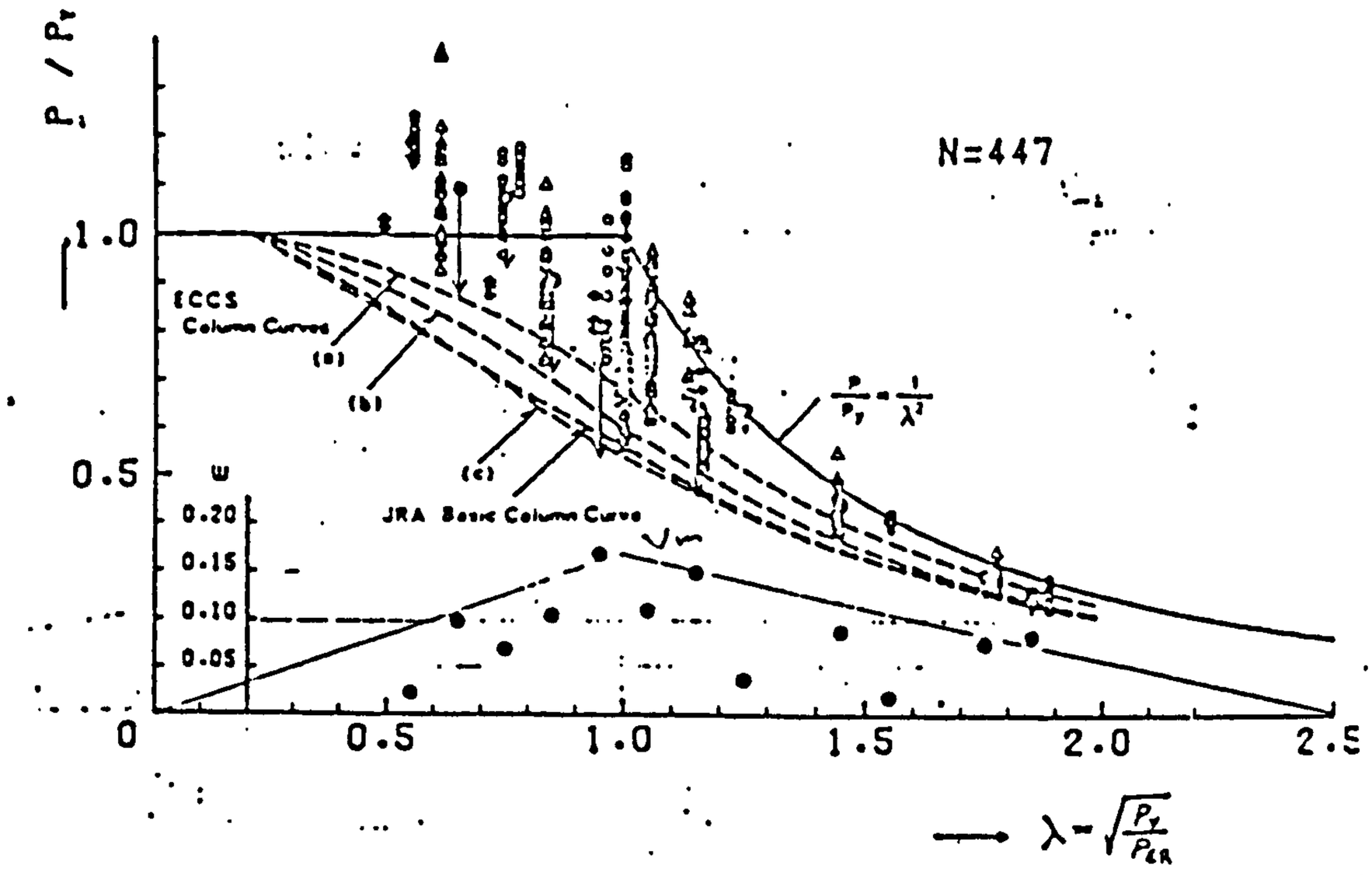

Scatter of Test Results by ECCS Column Test (using nominal P_y)

Figure 9 - Column Test Results

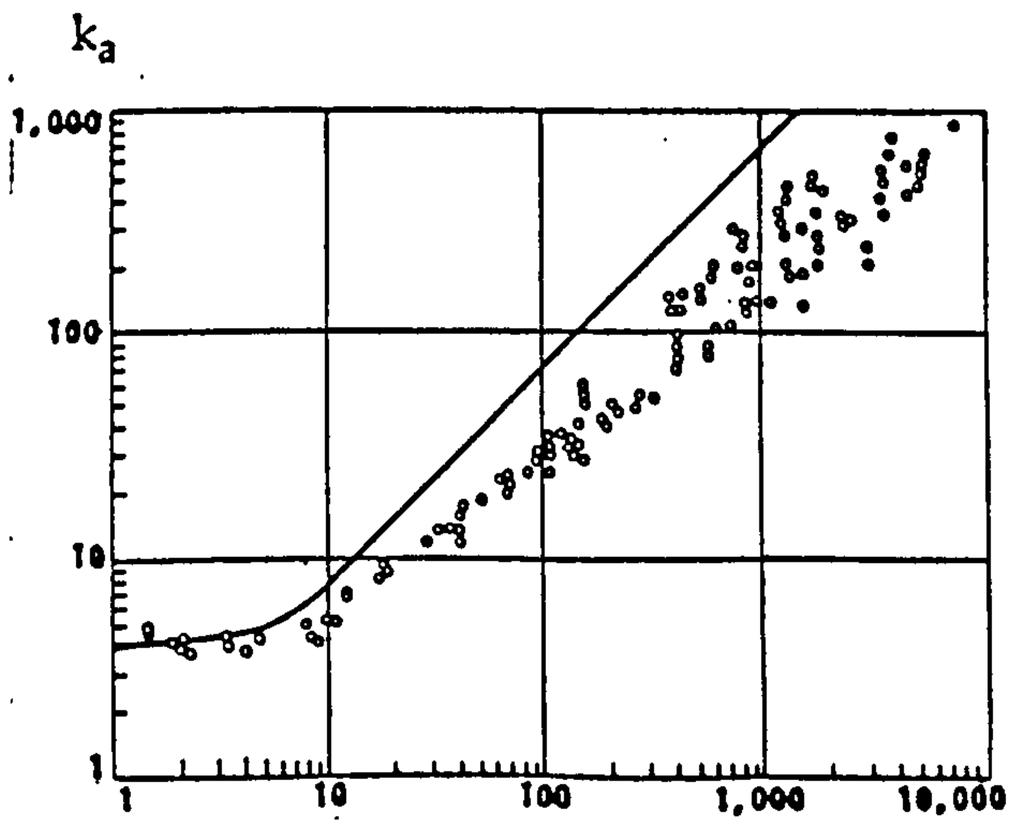

Figure 10 - Comparison between Test and Theory Cylinders under Axial Comp., [150]

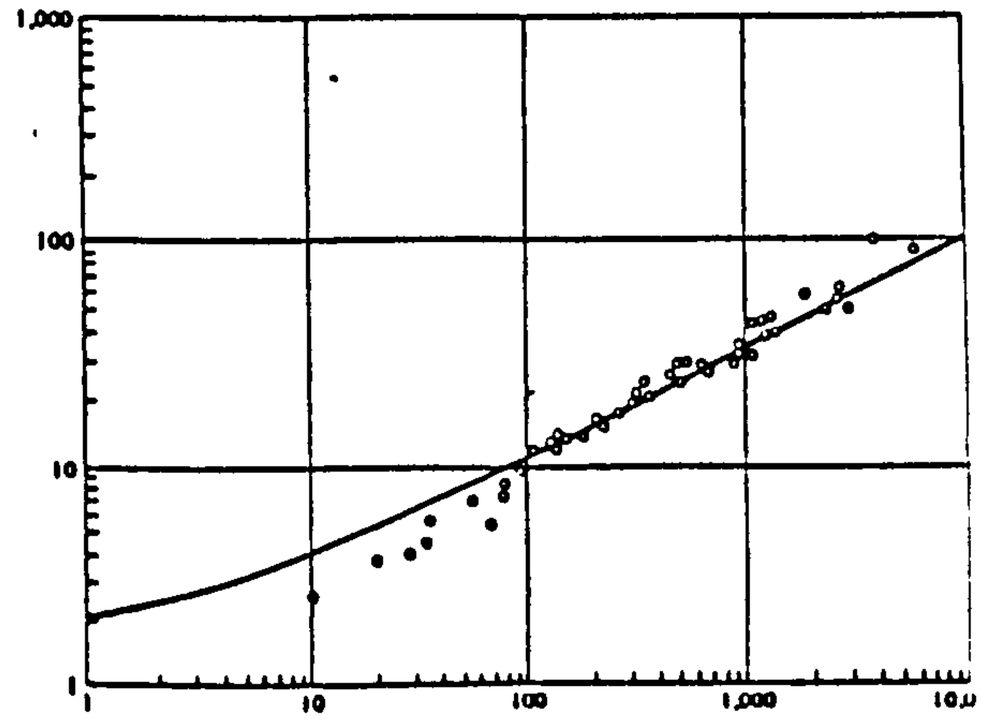

Figure 11 - Comparison between Test and Theory Cylinders under External Pressure, [15(

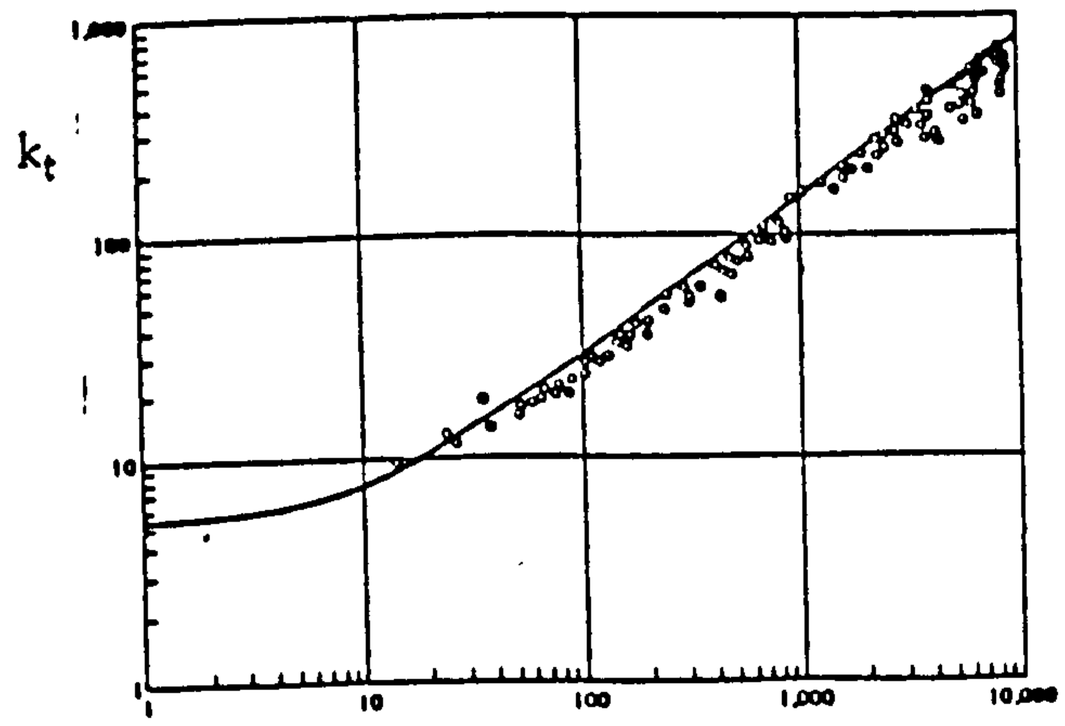

Figure 12 - Comparison between Test and Theory Cylinders under Torsion, [150]

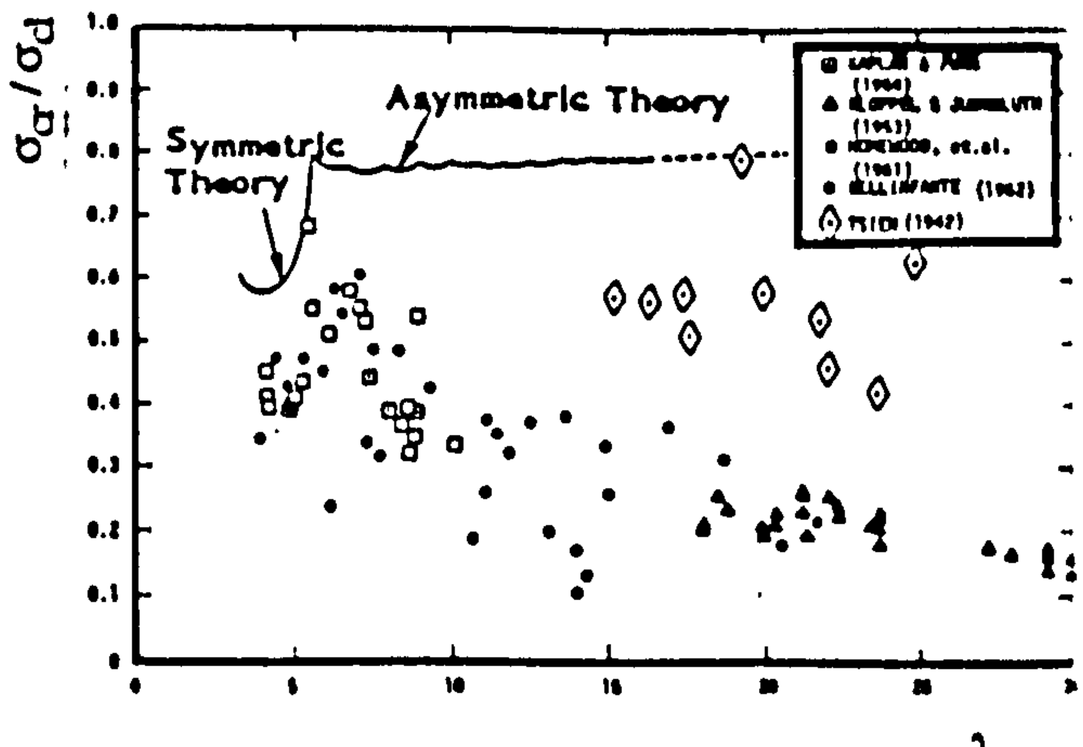

Figure 13 - Comparison between Test and Theory Clamped Spherical Caps, Ext. Pres., [150

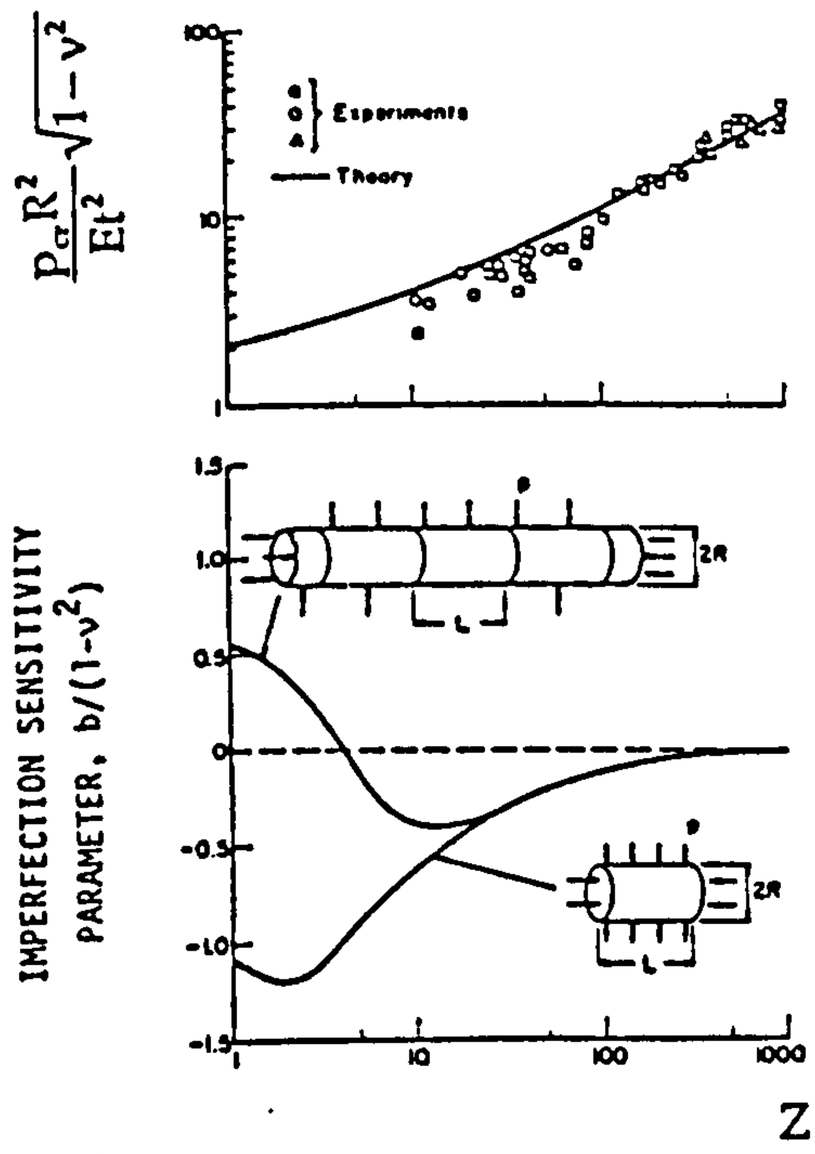

Fig. 14a - Unstiffened and Ring-Stiffened in Interframe Mode, [117]

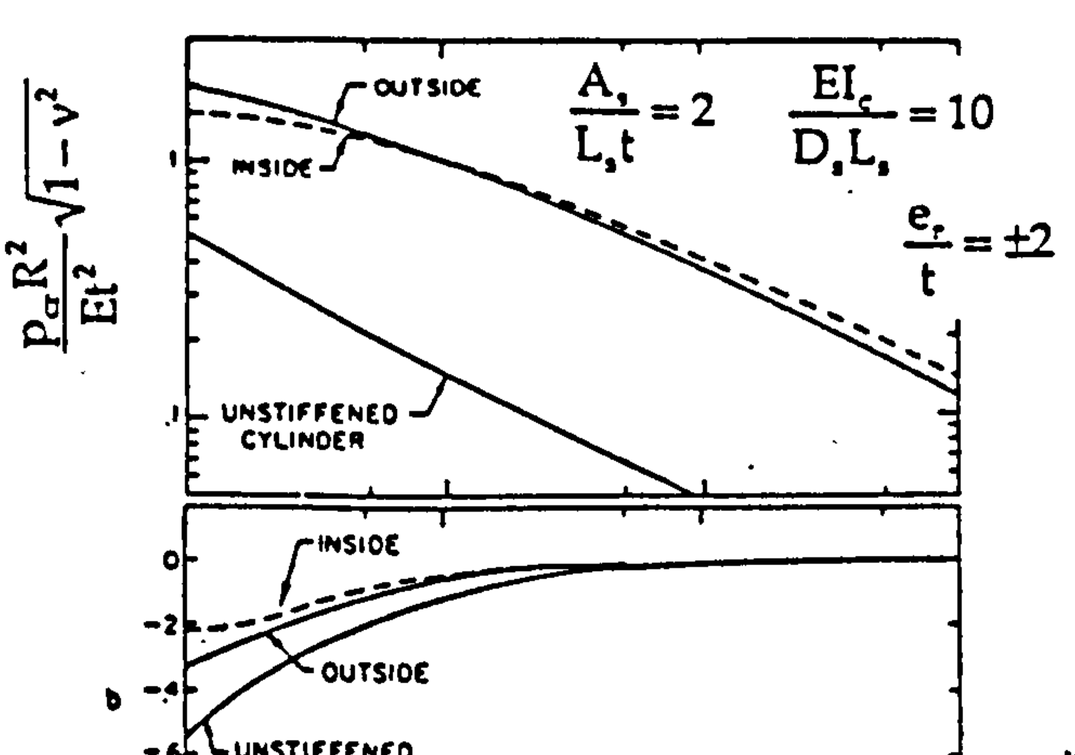

Fig. 14b - Ring-Stiffened in General Instability Mode, [118]

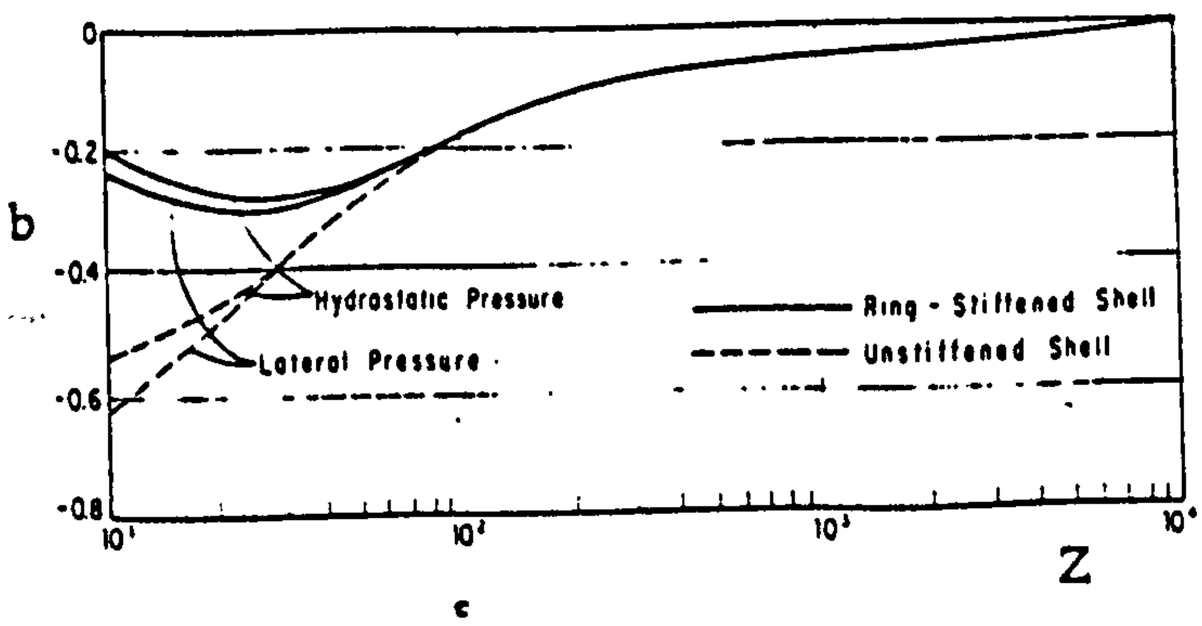

Fig. 14c - Ring-Stiffened in Interframe Mode, [138]

Figure 14 - Post-Buckling Behaviour of Cylinders under External Pressure

Fig. 15a - General Instability

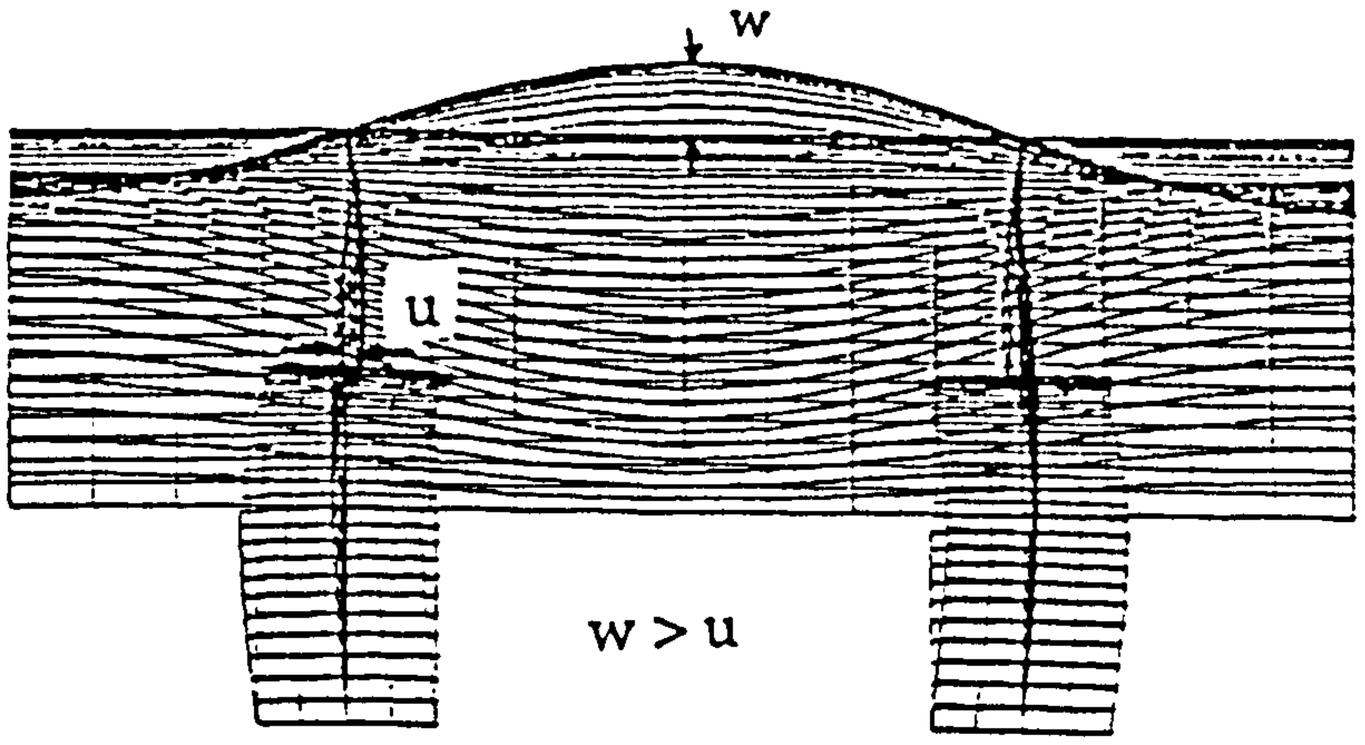

Fig. 15b - Interframe Shell Buckling

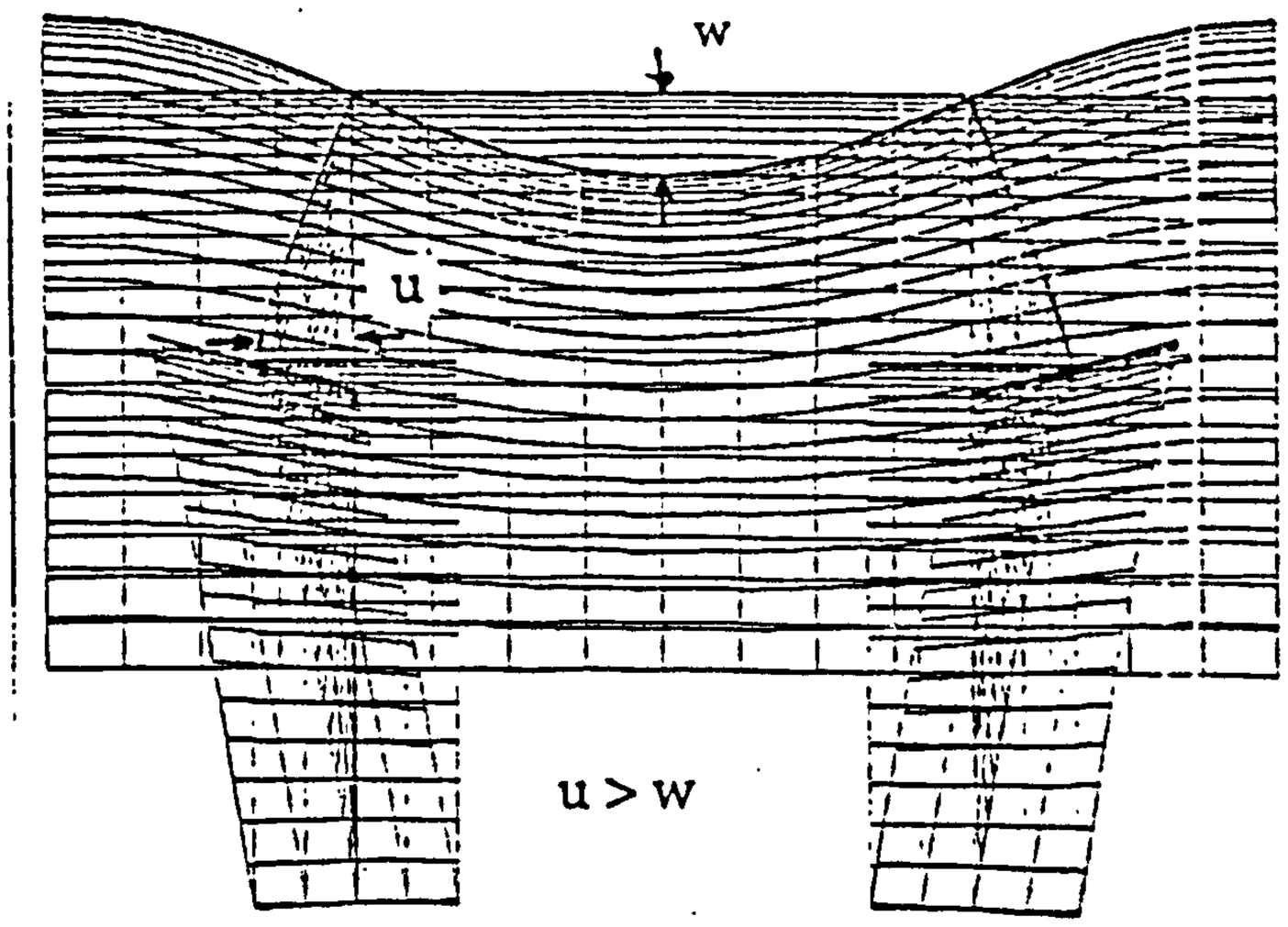

Fig. 15c - Frame Tripping

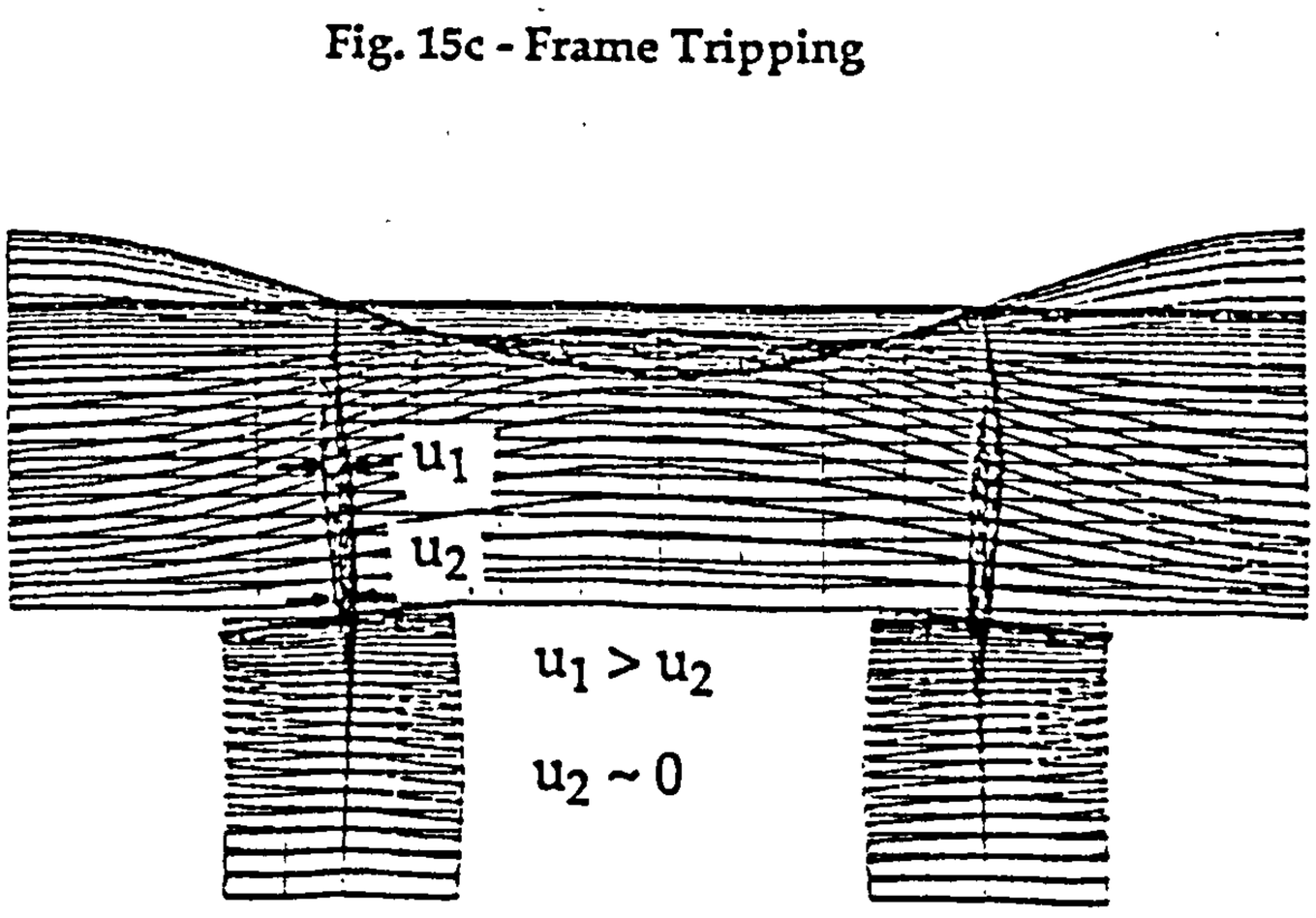

Fig. 15d - Local Buckling of the Web

Figure 15 - Relevant Buckling Modes

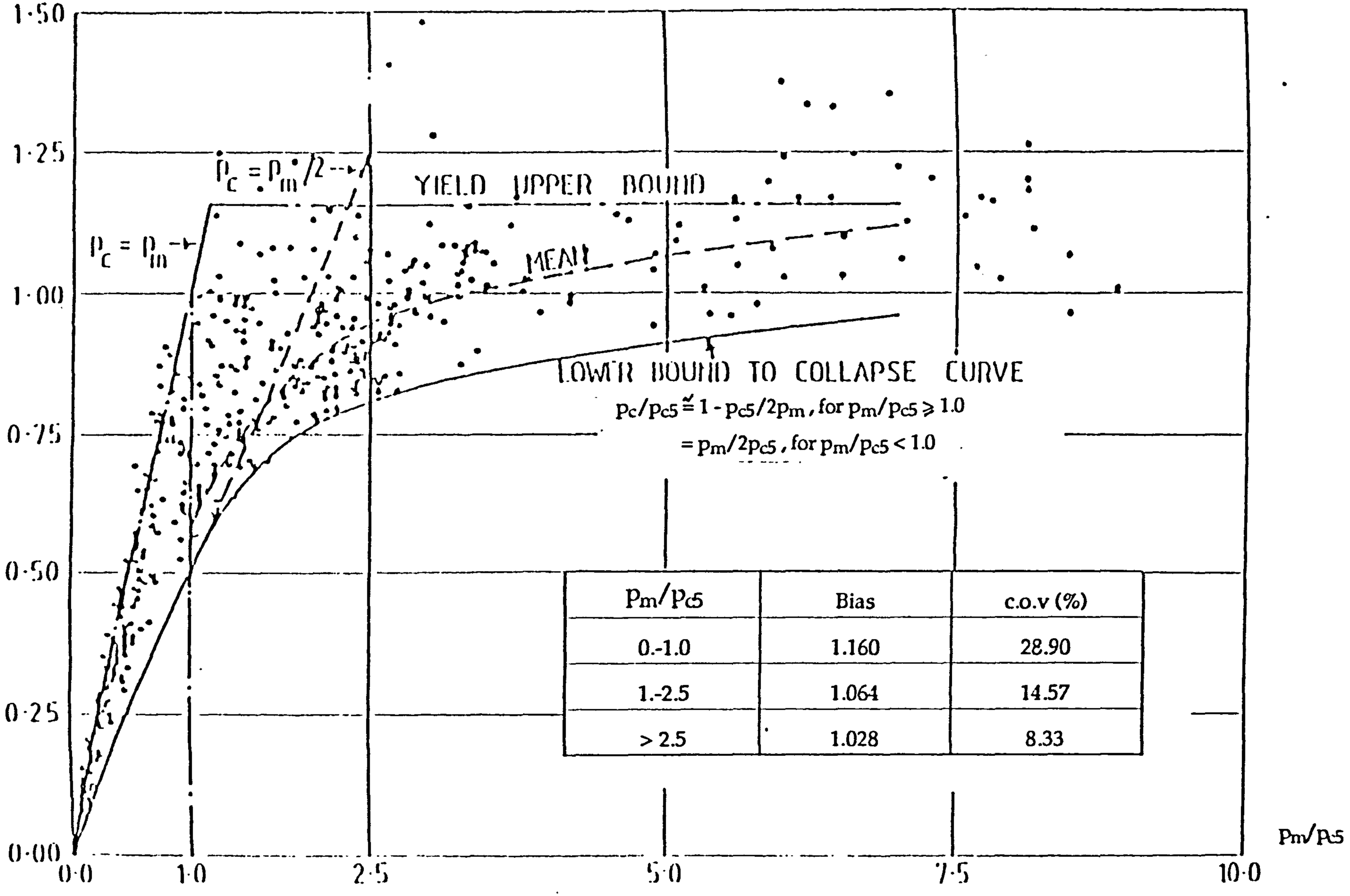

Pm/Pc5	Bias	c.o.v (%)
0.-1.0	1.160	28.90
1.-2.5	1.064	14.57
> 2.5	1.028	8.33

Figure 16 - Plot of Interframe Shell Collapse Results [18] with Bias and COV of the Model Uncertainty (Mean Curve)

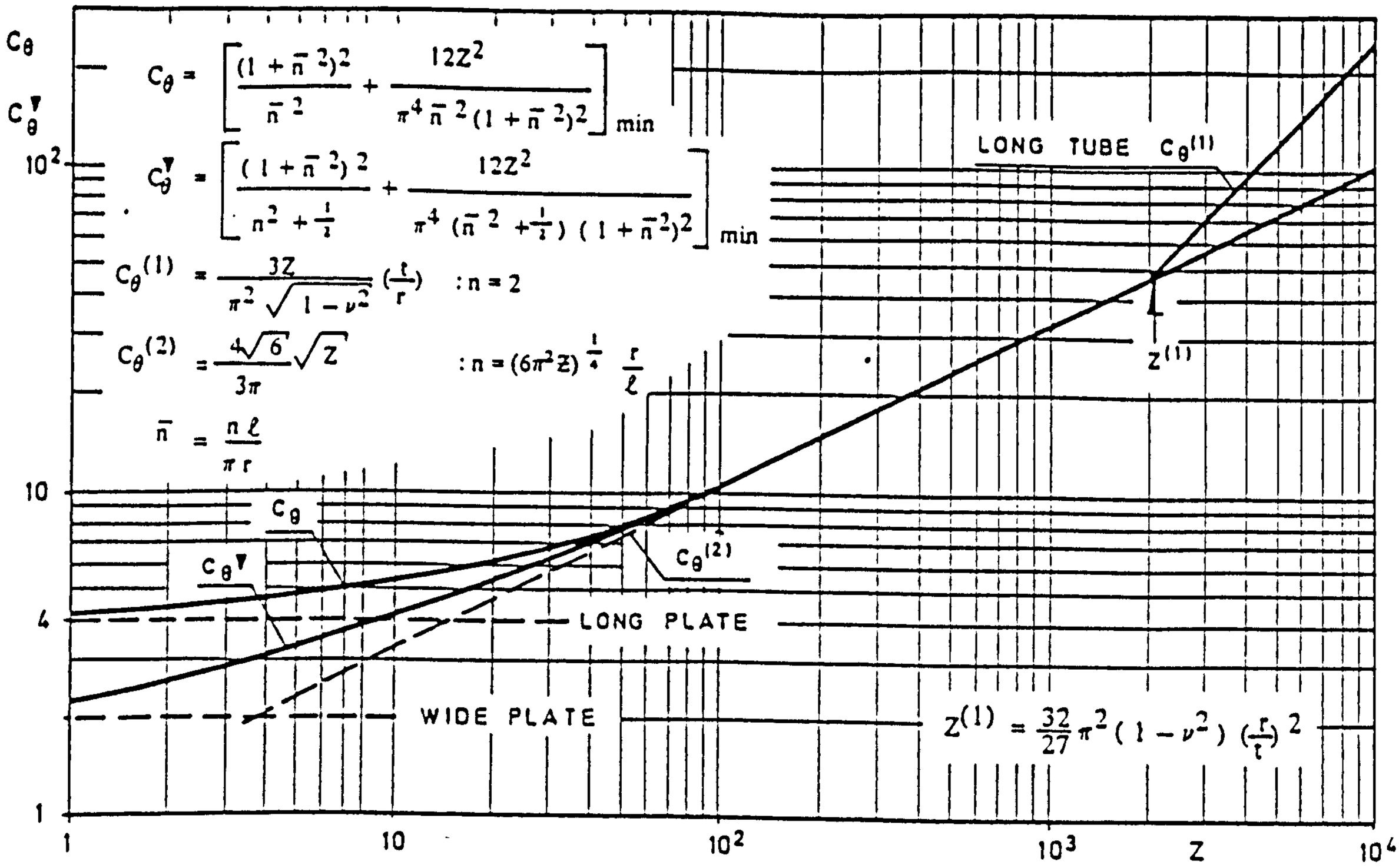

Figure 17 - Buckling Coefficient for Eq. (10), [42]

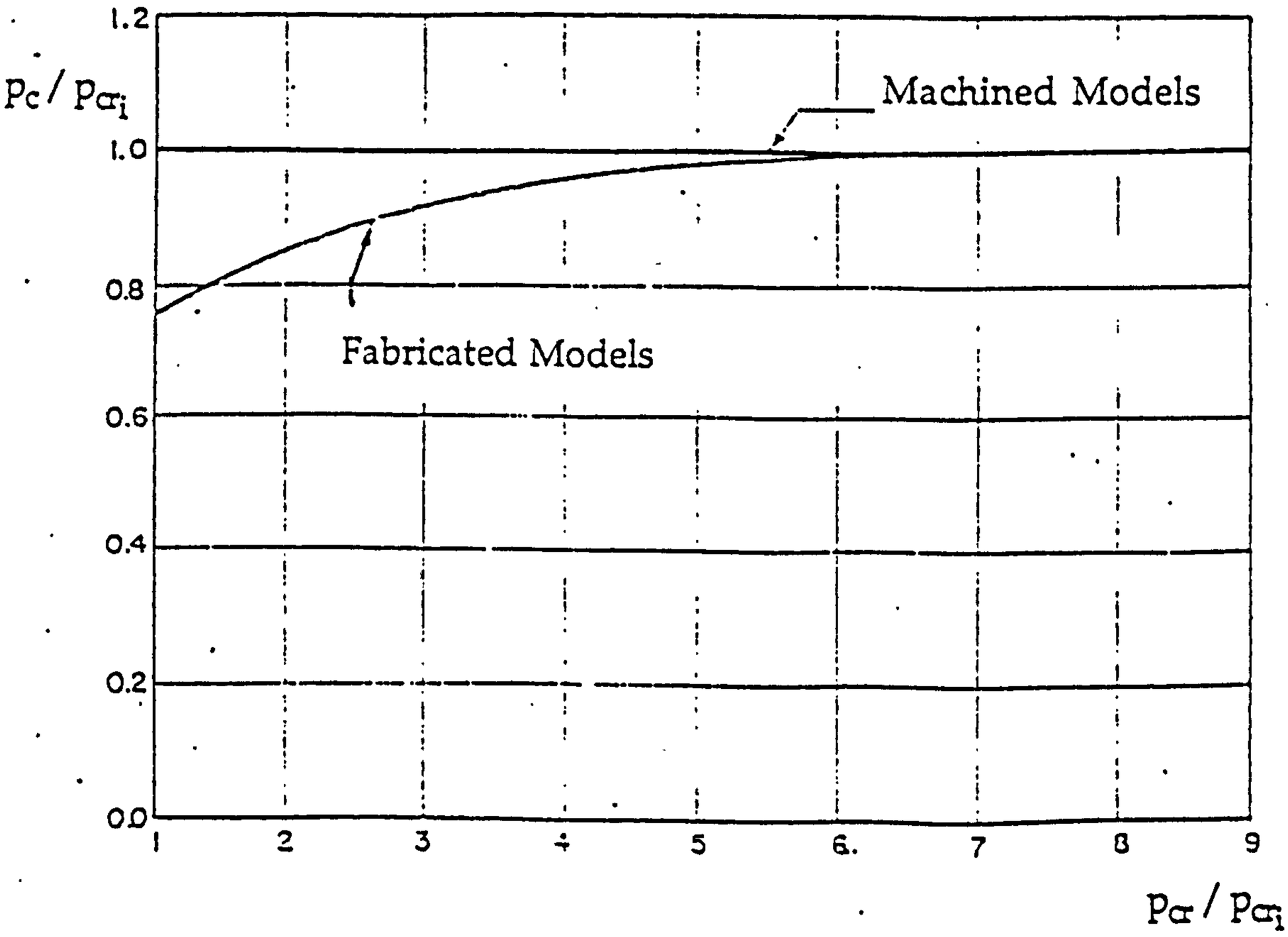

Figure 18 - Empirical Curve for Interframe Shell Collapse, [97]

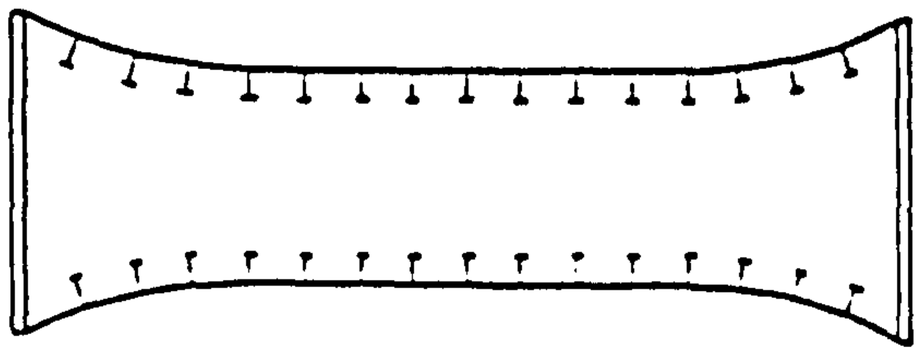

Figure 19 - Critical Buckling Mode for Long Cylinders, [51]

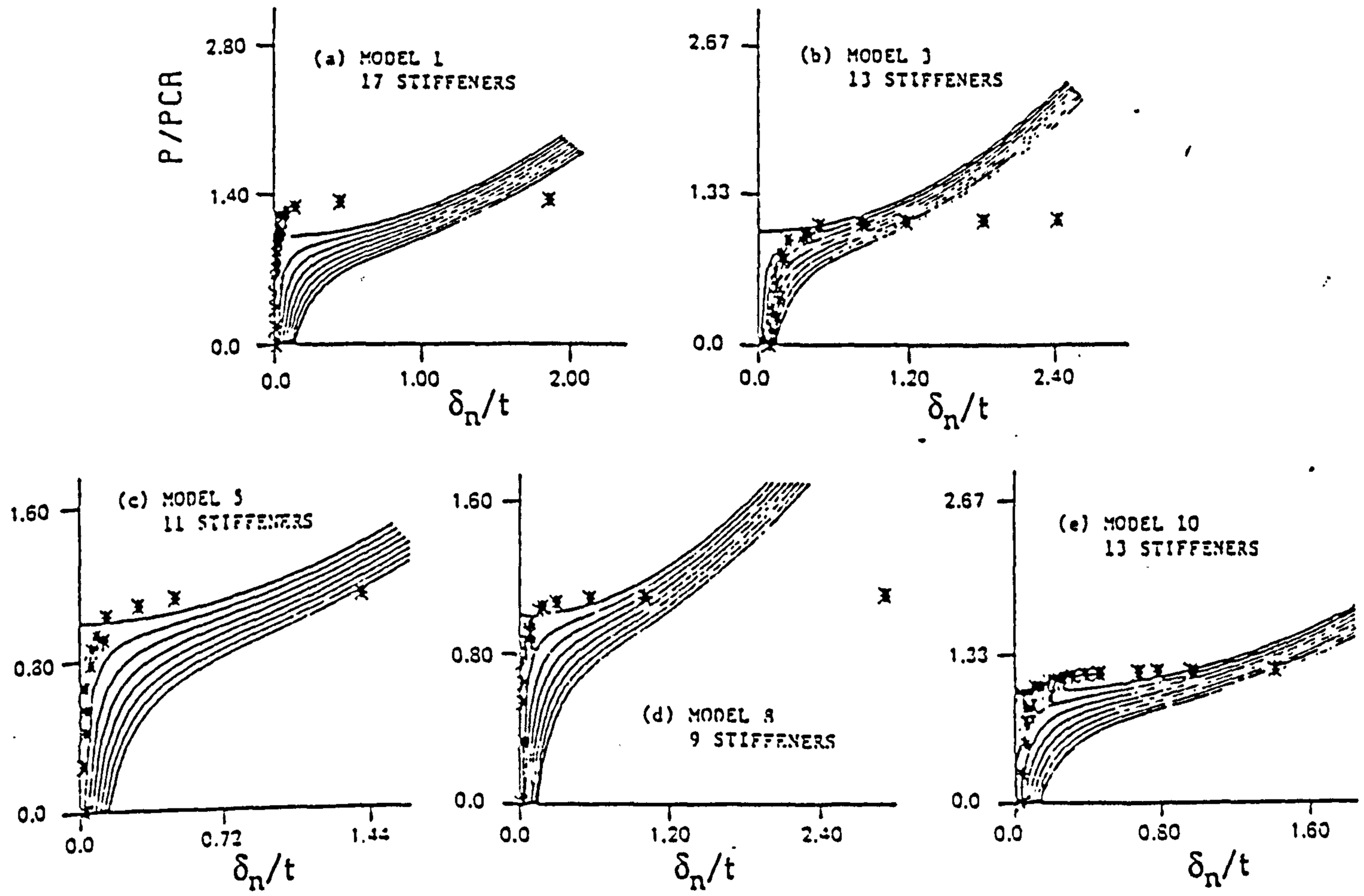

Figure 21 - Experimental Postbuckling Behaviour
Elastic General Instability, [137]

Boundary conditions: 1: Restrained, 0: Free

	Prebuckling						Buckling					
Bound.	u	v	w	uu	vv	ww	u	v	w	uu	vv	ww
B1	0	1	1	0	0	0	*	1	1	*	*	*
B2	0	1	0	1	0	1	0	1	0	1	0	1
B3	1	0	0	0	1	1	1	0	0	0	1	1
B4	0	1	0	1	0	1	**	**	**	**	**	**

*Cases I to V:	Case I:	all free	(simply supported)
	Case II:	vv restr.	
	Case III:	u restr.	(simp. sup.+axial restr.)
	Case IV:	u,vv restr.	
	Case V:	all restr.	(clamped)

**Eigenvalue Analysis: The model has $\pi/2n$ in the circumf. direction.
Anti-symmetry is used: u,w,vv restrained; v,uu,ww free.

Riks Analysis: The model has π/n in the circumf. direction.
Symmetry is used: v,uu,ww restrained; u,w,vv free.

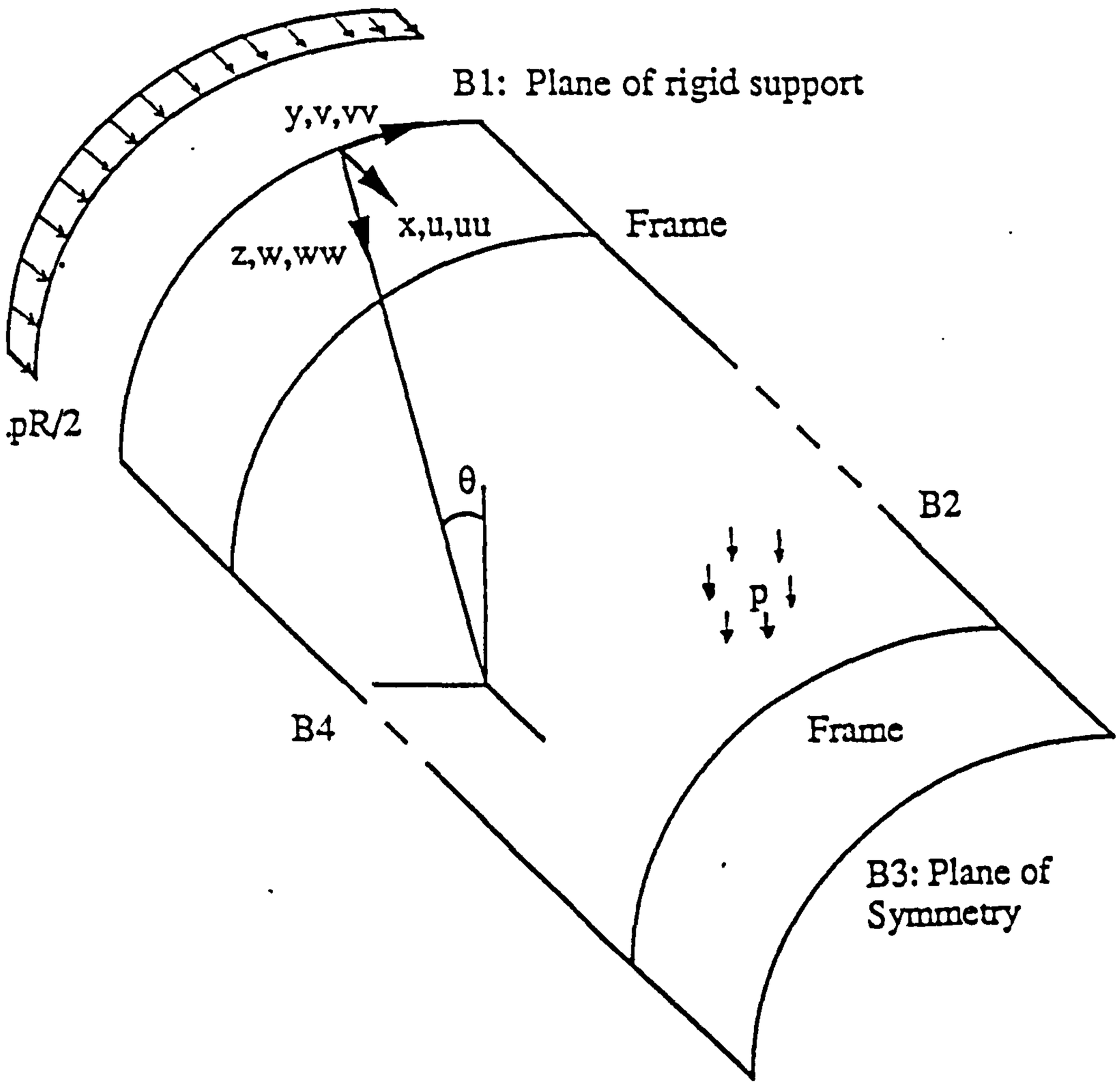

Figure 20 - FE Models for Elastic General Instability

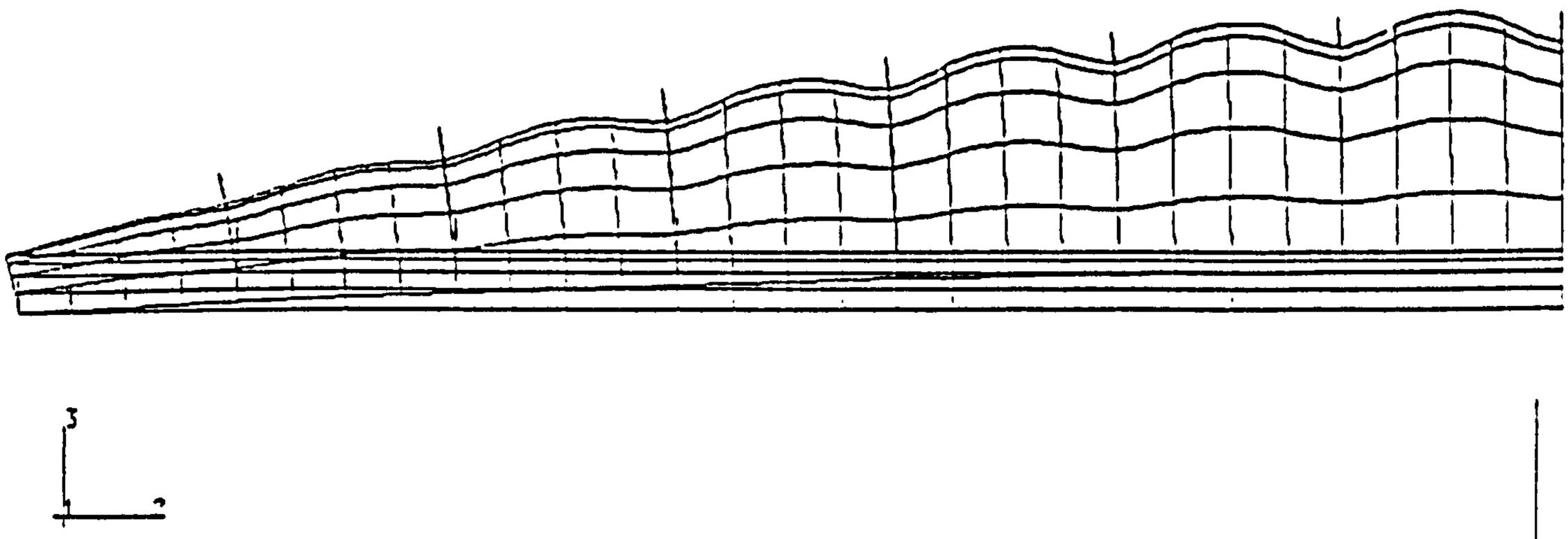

Fig. 22a: Case I

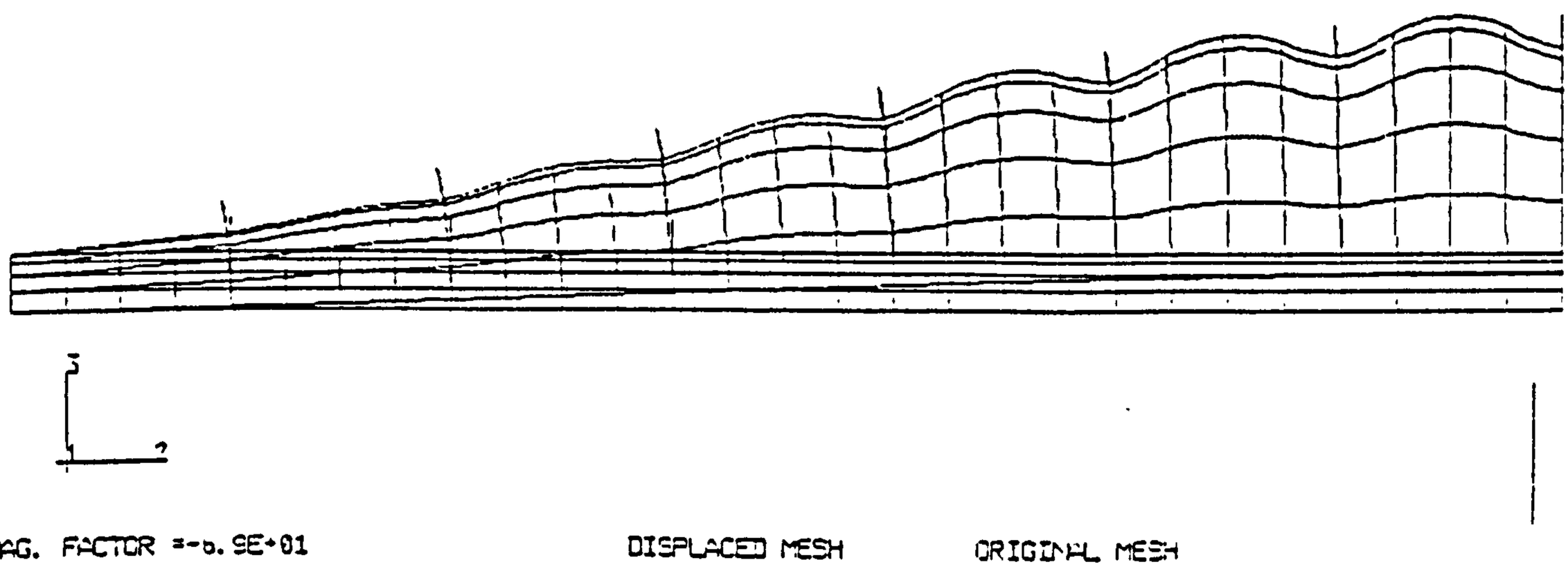

Fig. 22b: Case III

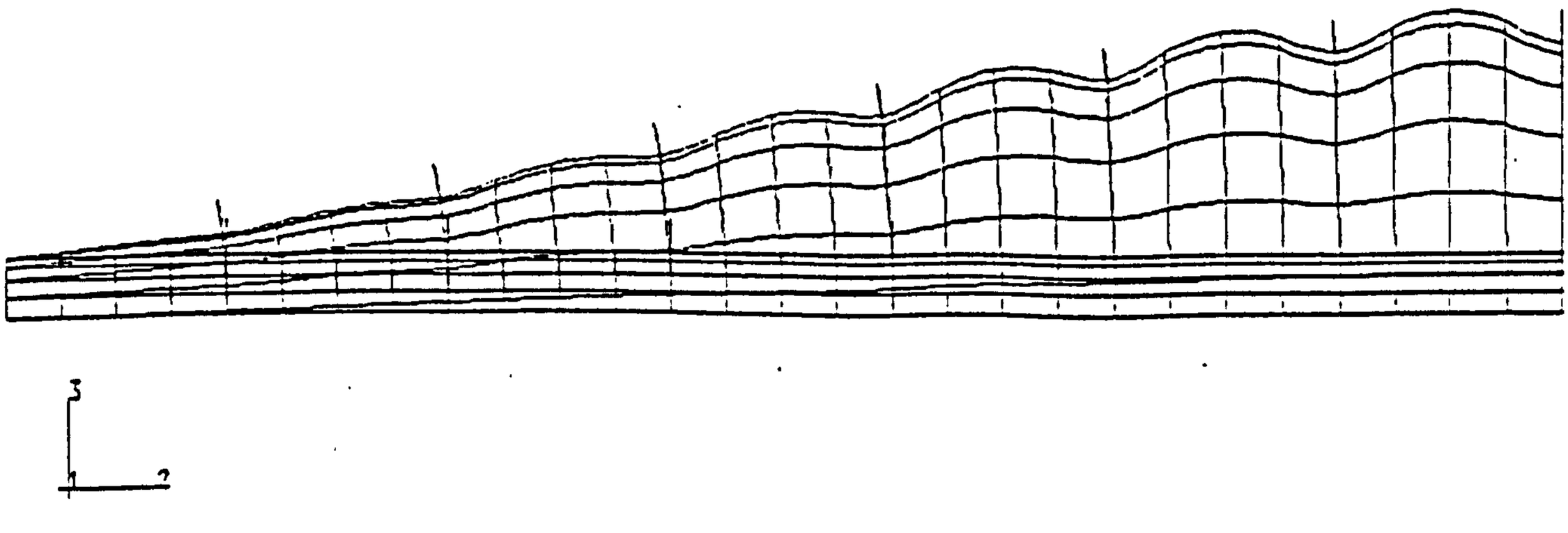

Fig. 22c: Case V

Figure 22 - Buckling Modes from FE Eigenvalue Analysis
Model 3 of [136], Boundary Conditions of Fig. 20

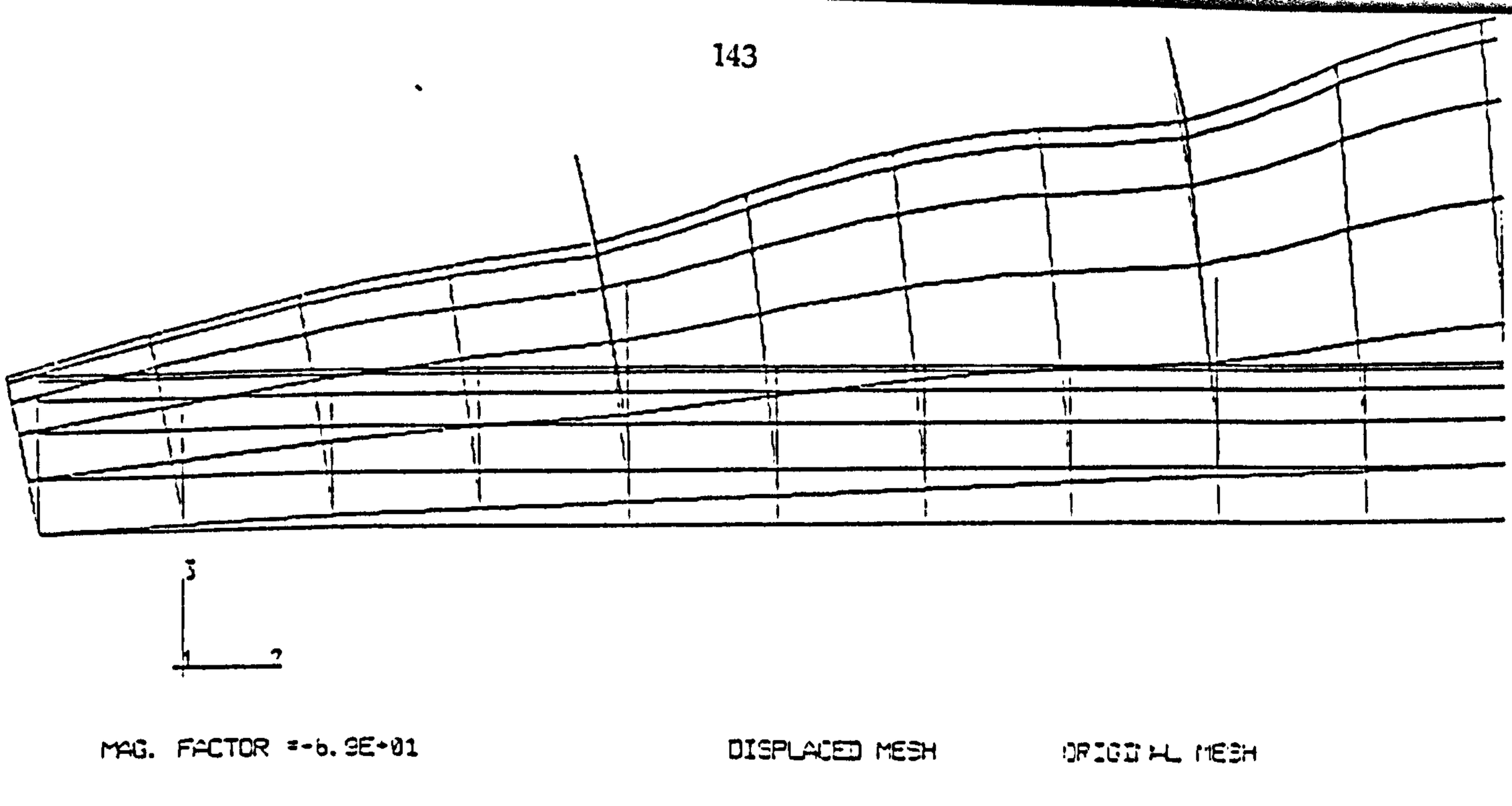

Fig. 23a: Case I

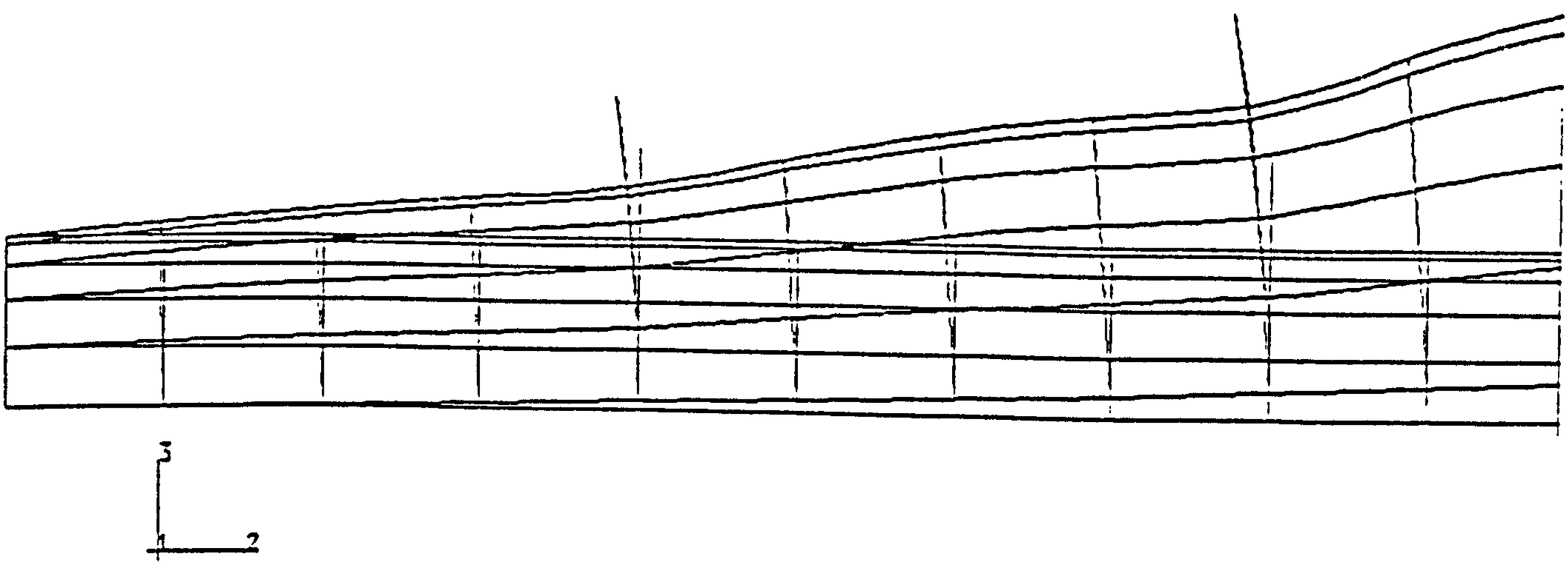

Fig. 23b: Case III

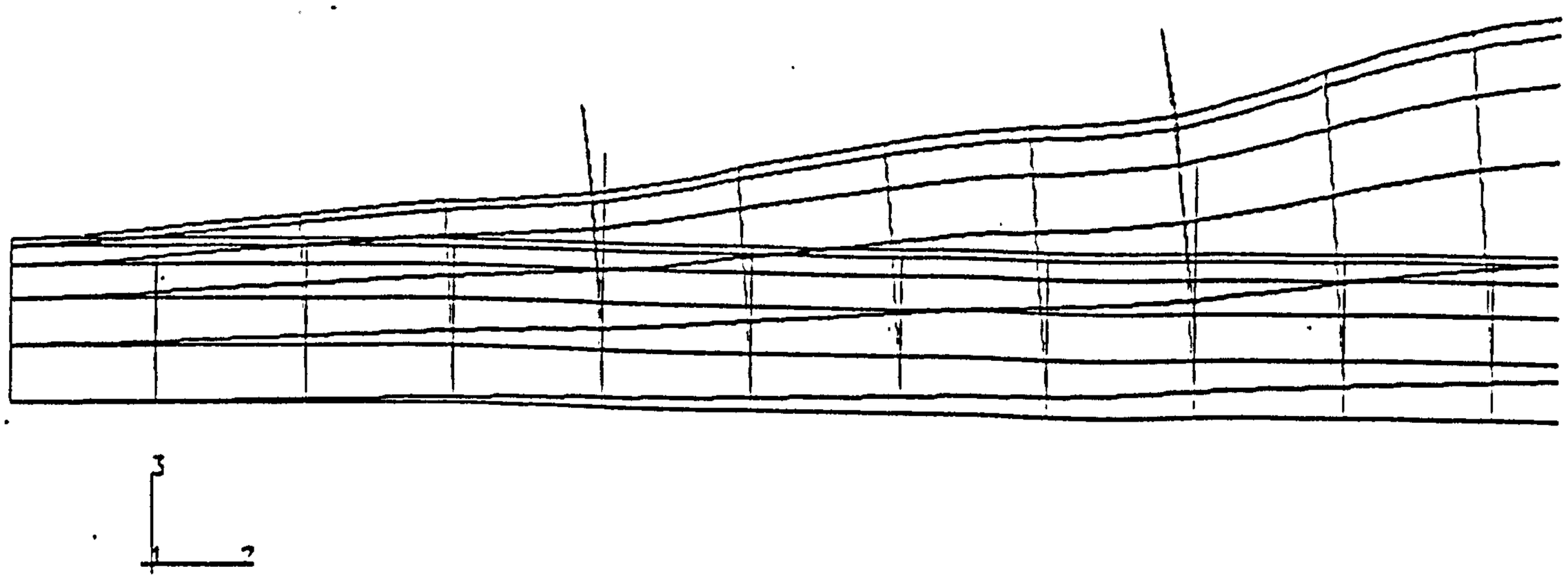

Fig. 23c: Case V

Figure 23 - Buckling Modes from FE Eigenvalue Analysis
Model 3 of [136], Detail

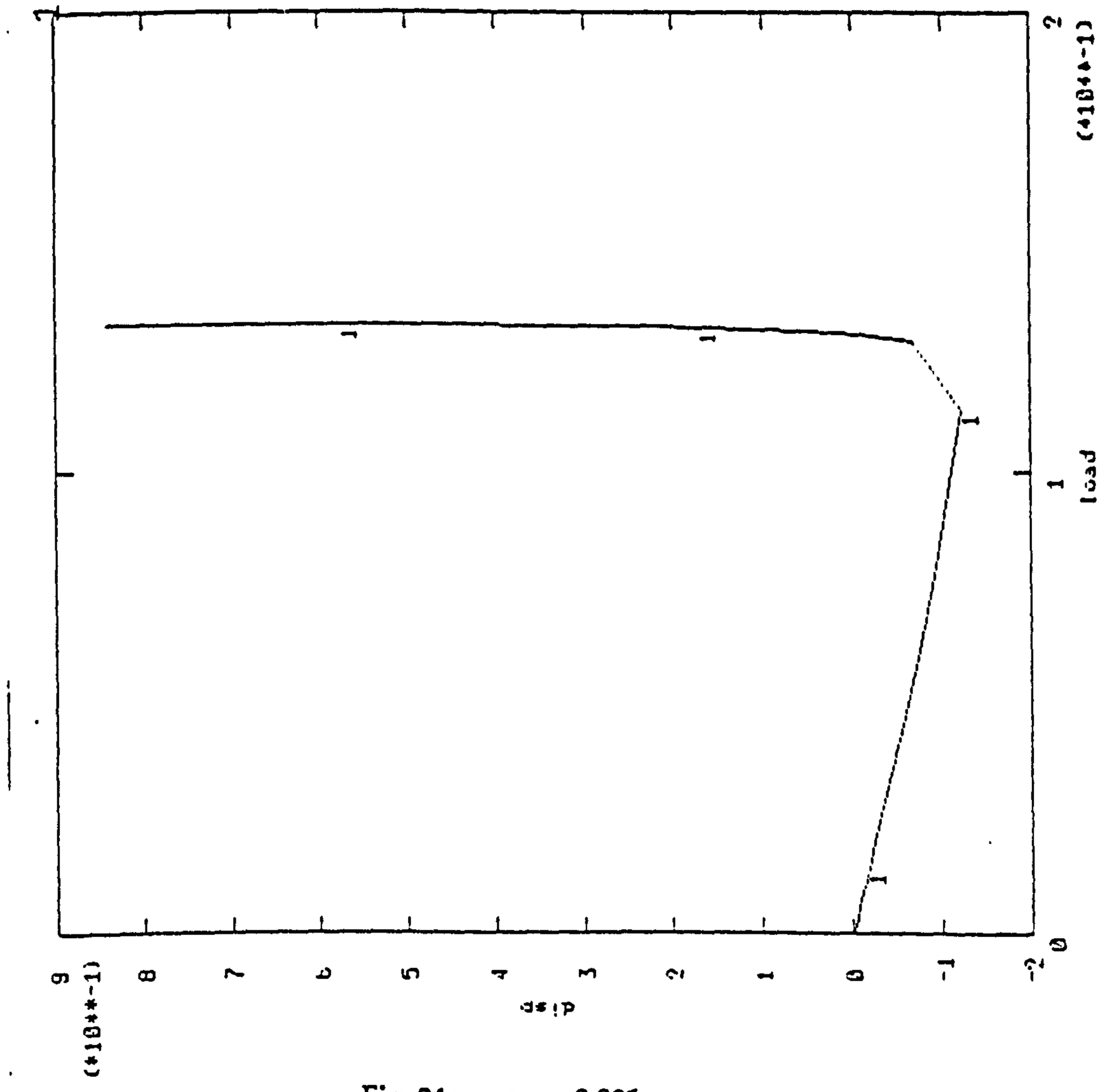

Fig. 24a: o-o-c = 0.001 mm

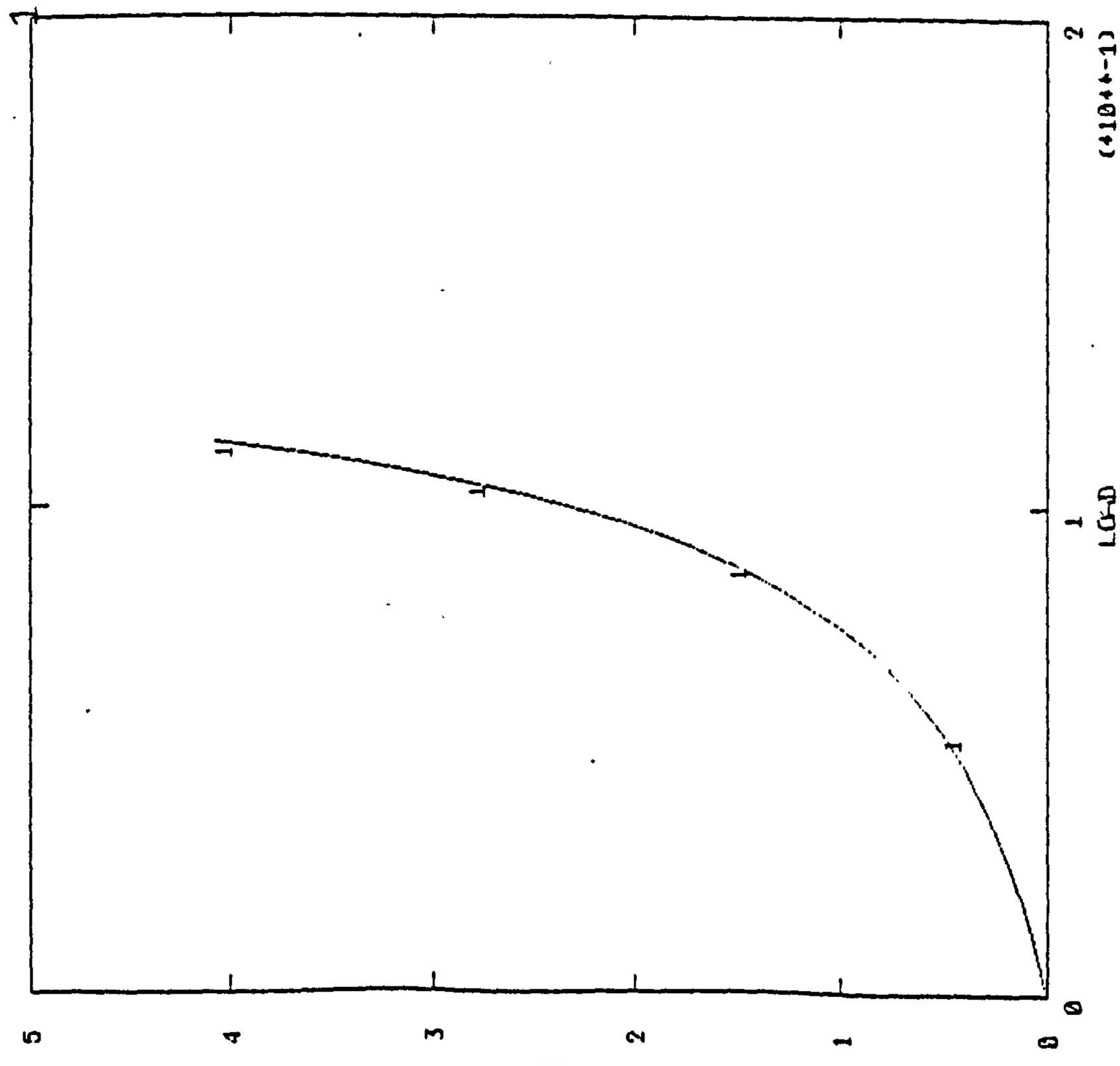

Fig. 24b: o-o-c = 0.9 mm

Figure 24: Postbuckling Behaviour from FE Riks Analysis
Radial Displacement at Mid-Compartment
Model 3 of [136] with Different Initial o-o-c

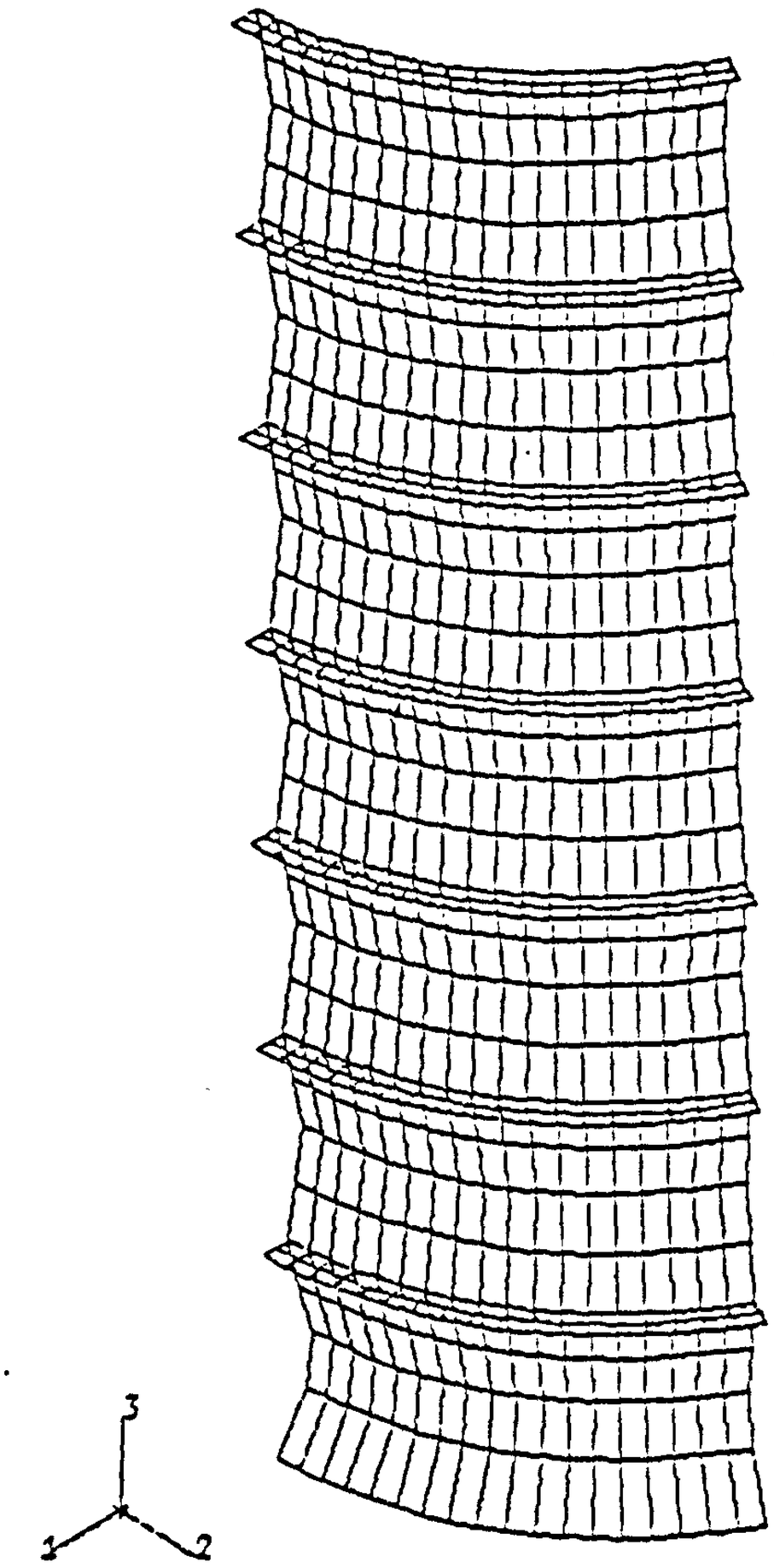

Fig. 25a: p=1.60 N/mm^2

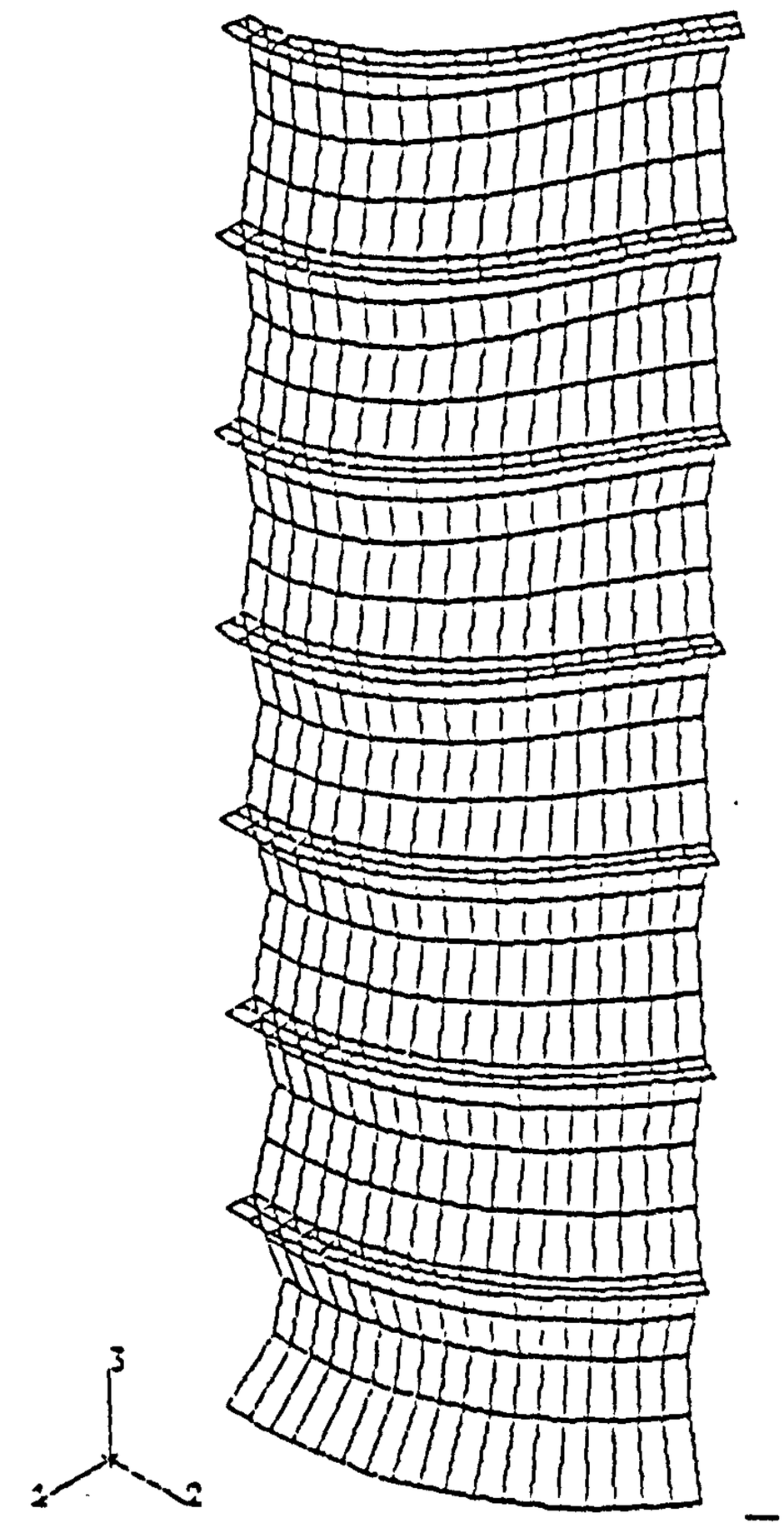

Fig. 25b: p=2.32 N/mm^2

Figure 25: Deformed Shapes from FE Riks Analysis, Model 3 of [136] with o-o-c = 0.001 mm

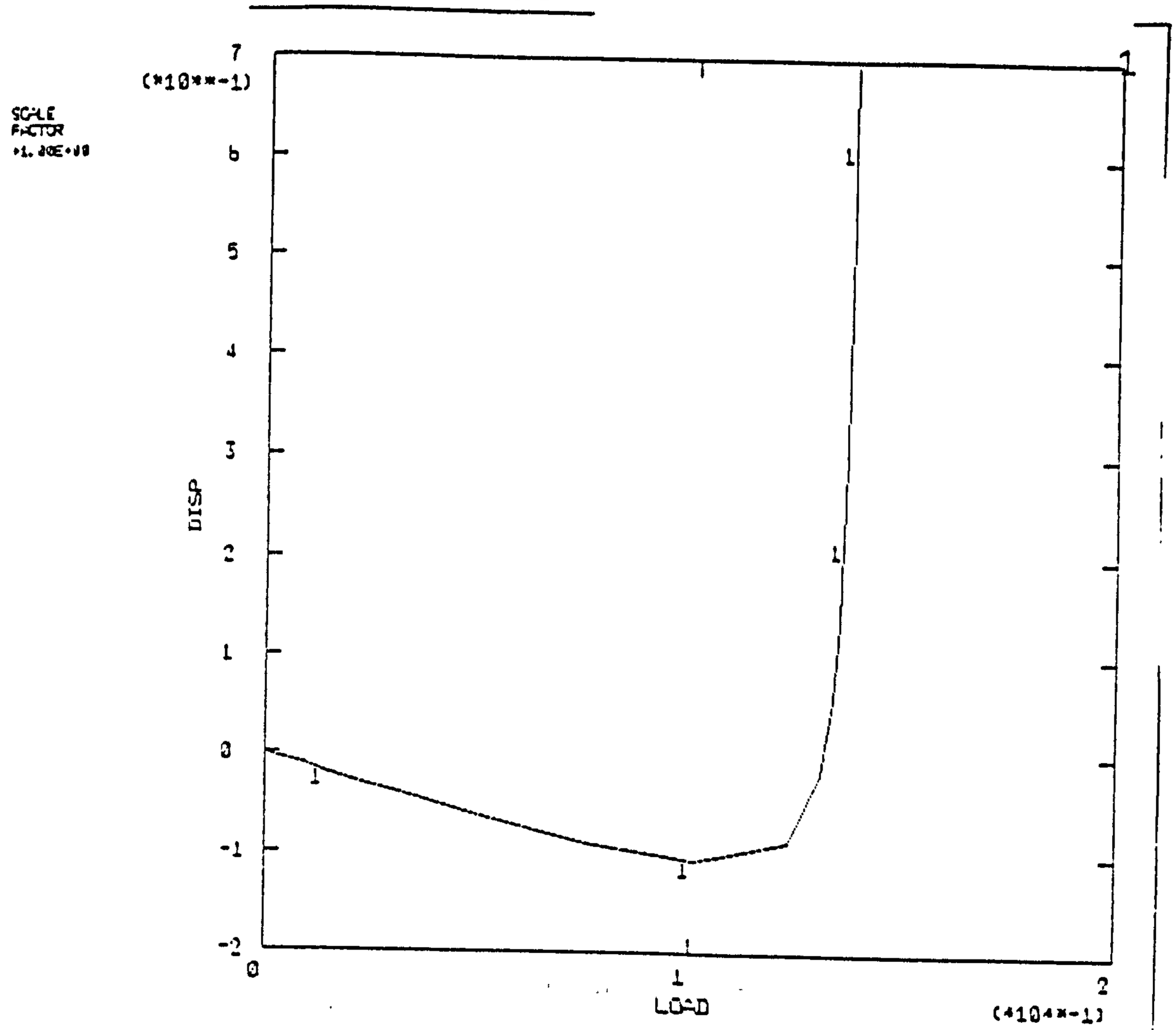

Fig. 26a: Model 1 of [136]

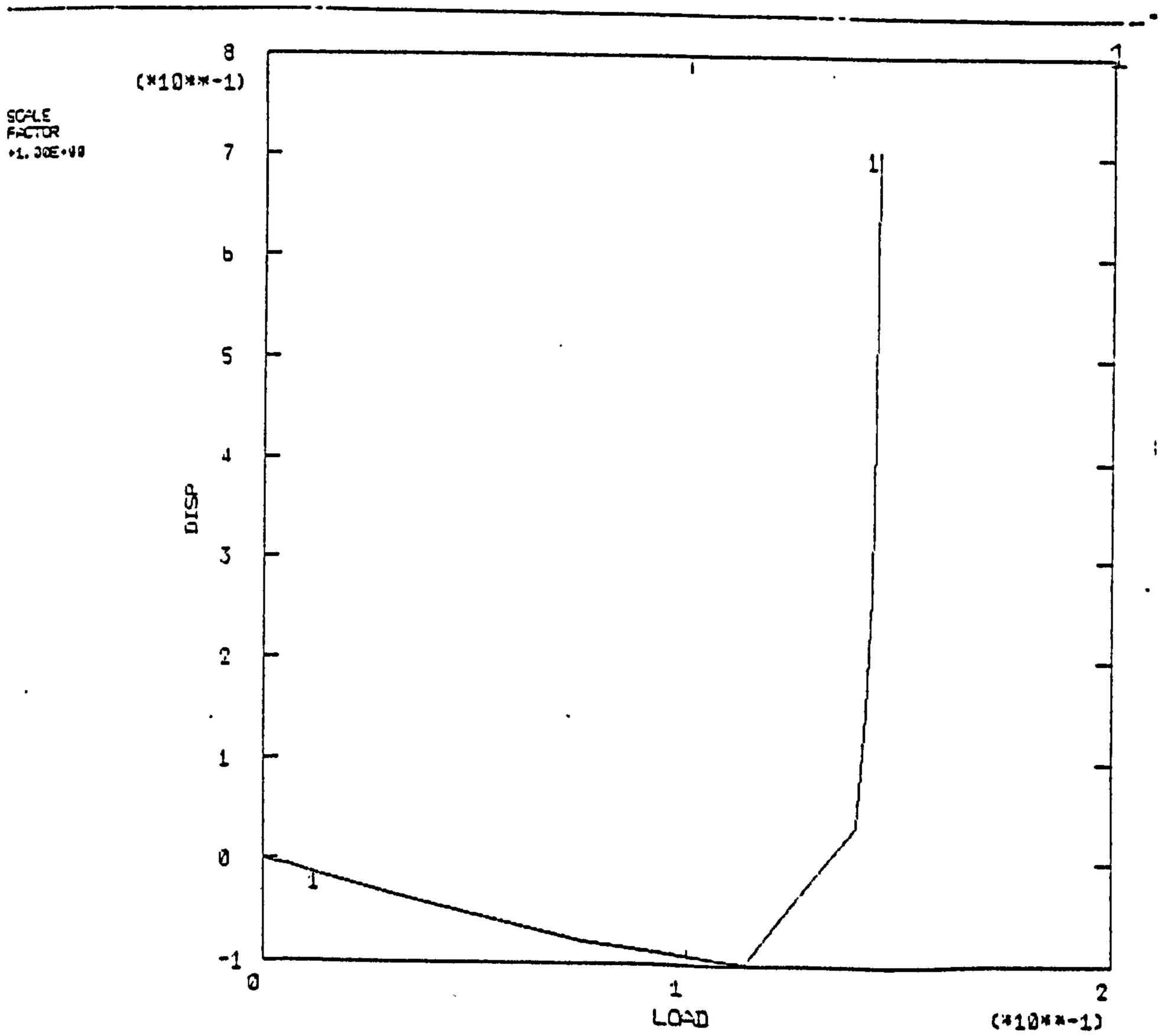

Fig. 26b: Model 3 of [136]

Figure 26: Postbuckling Behaviour from FE Riks Analysis
Radial Displacement at Mid-Compartment

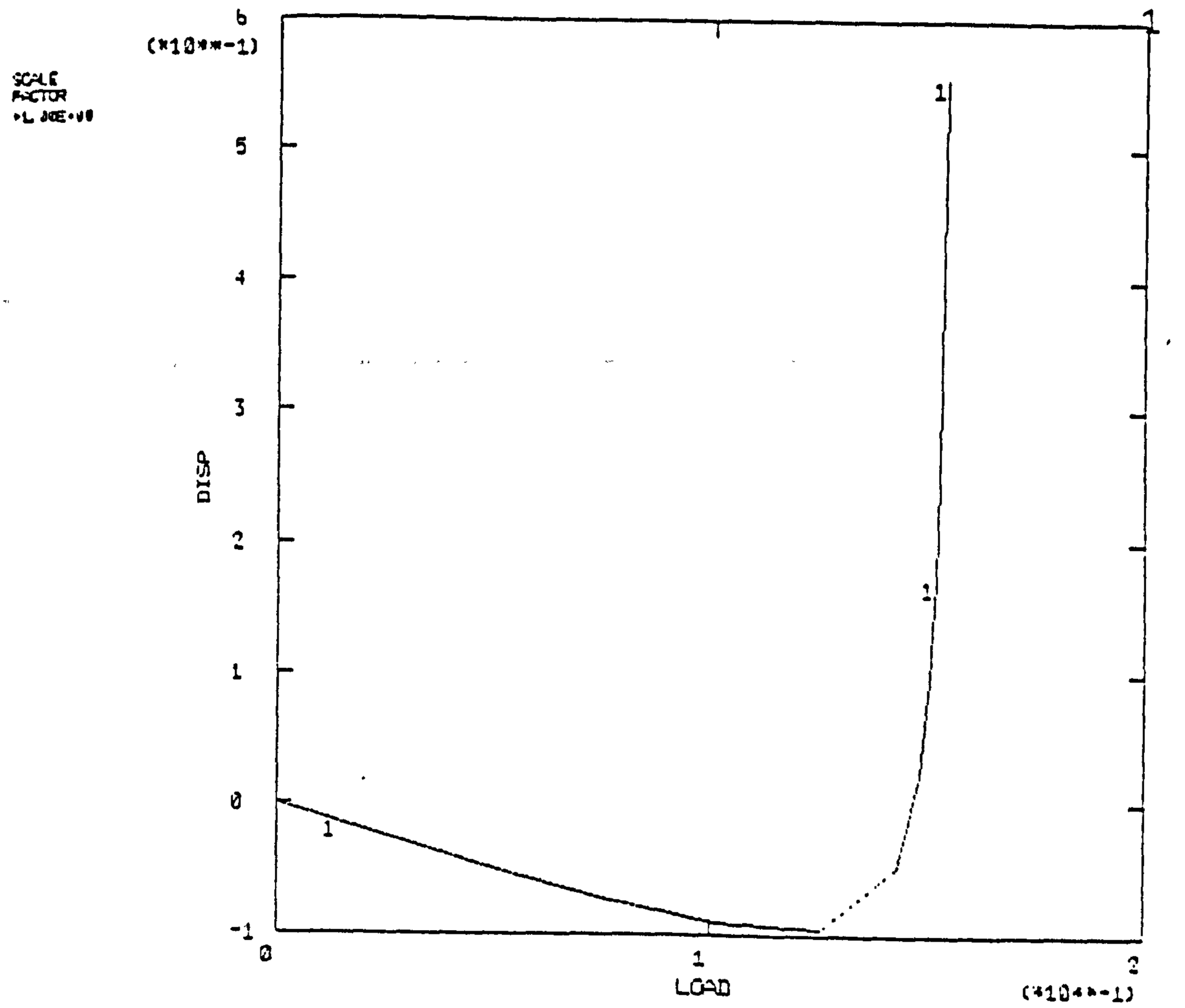

Fig. 26c: Model 5 of [136]

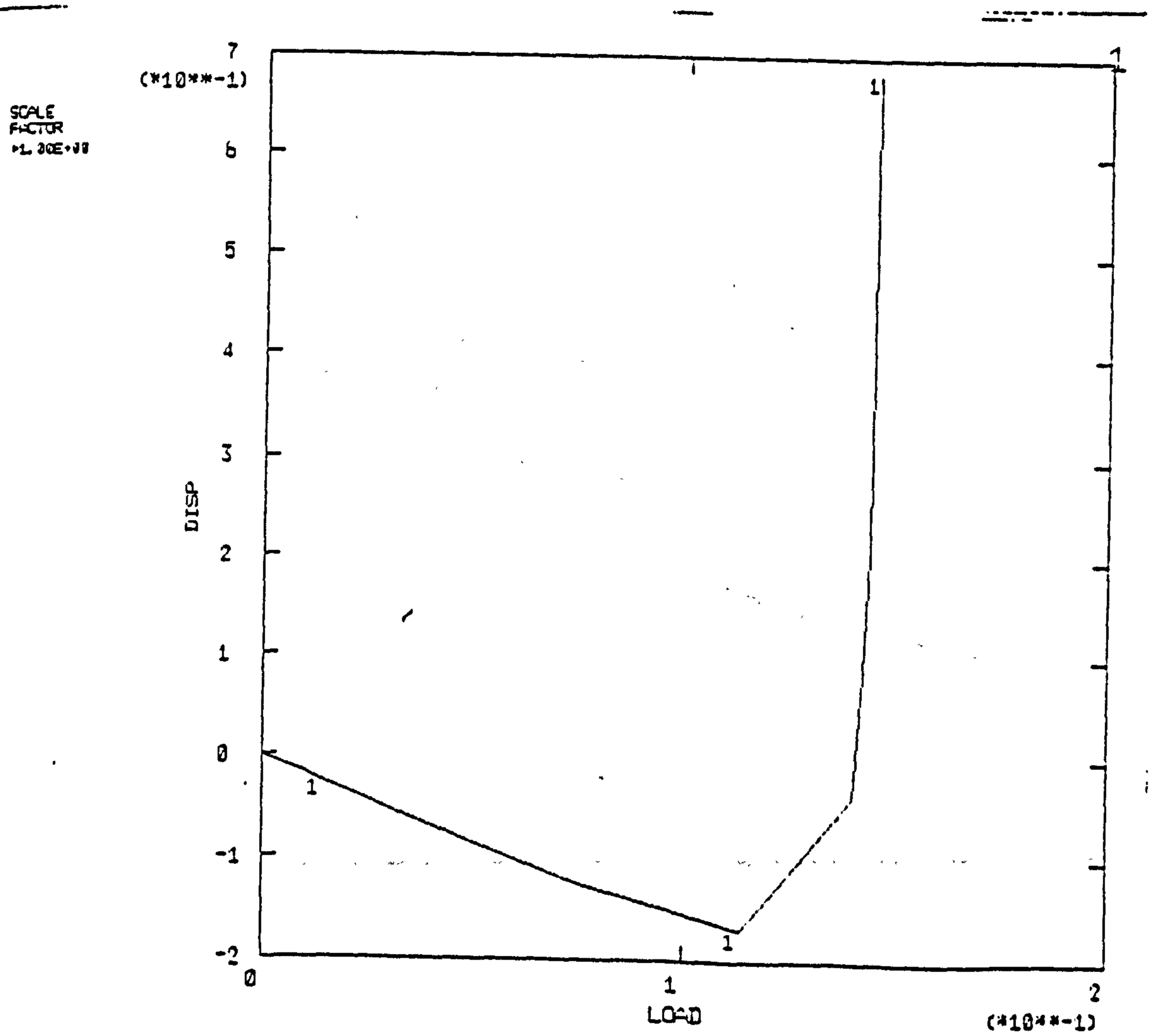

Fig. 26d: Model 8 of [136]

Figure 26: Postbuckling Behaviour from FE Riks Analysis Radial Displacement at Mid-Compartment (Cont.)

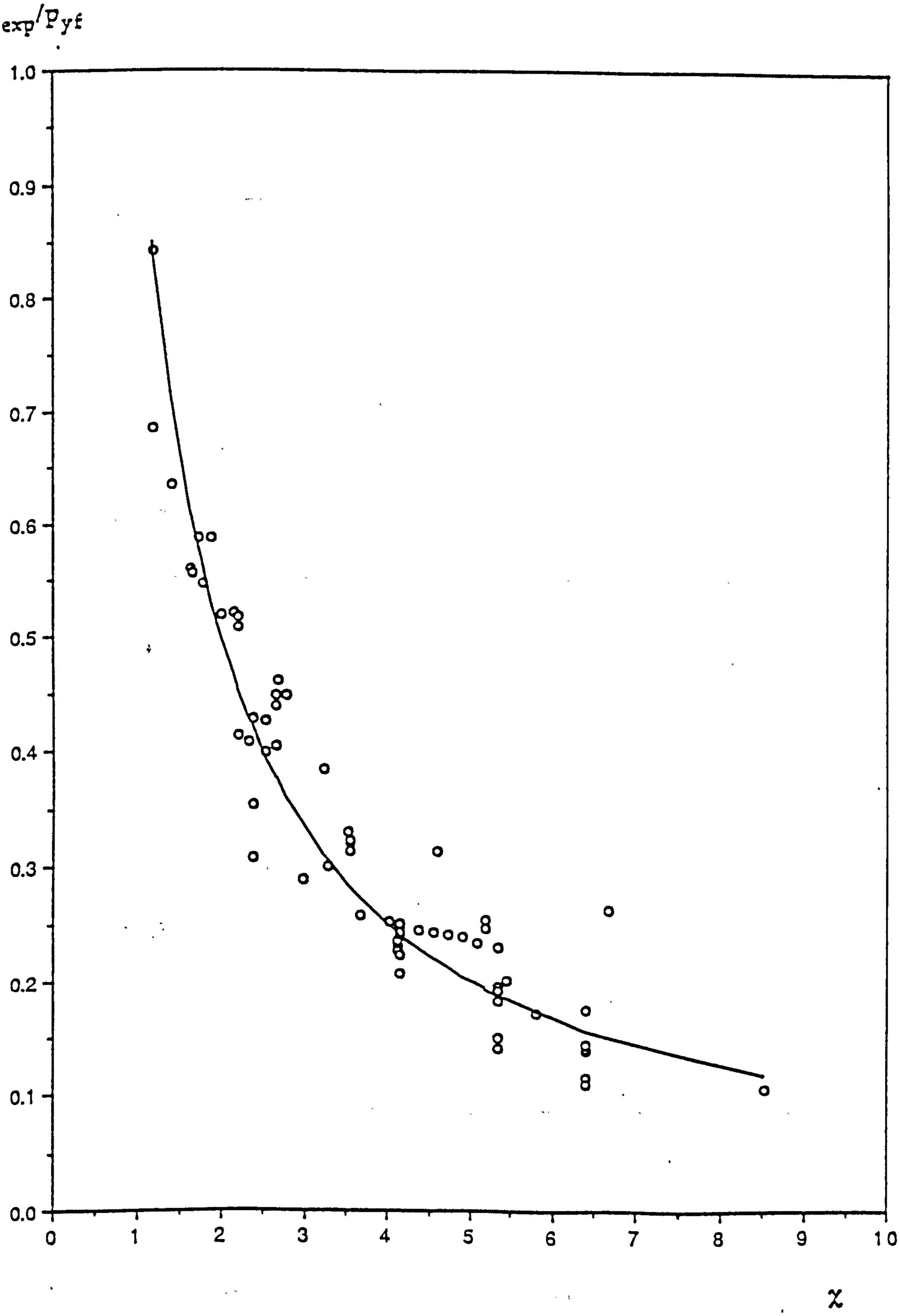

Figure 27: Experimental Data - Elastic General Instability

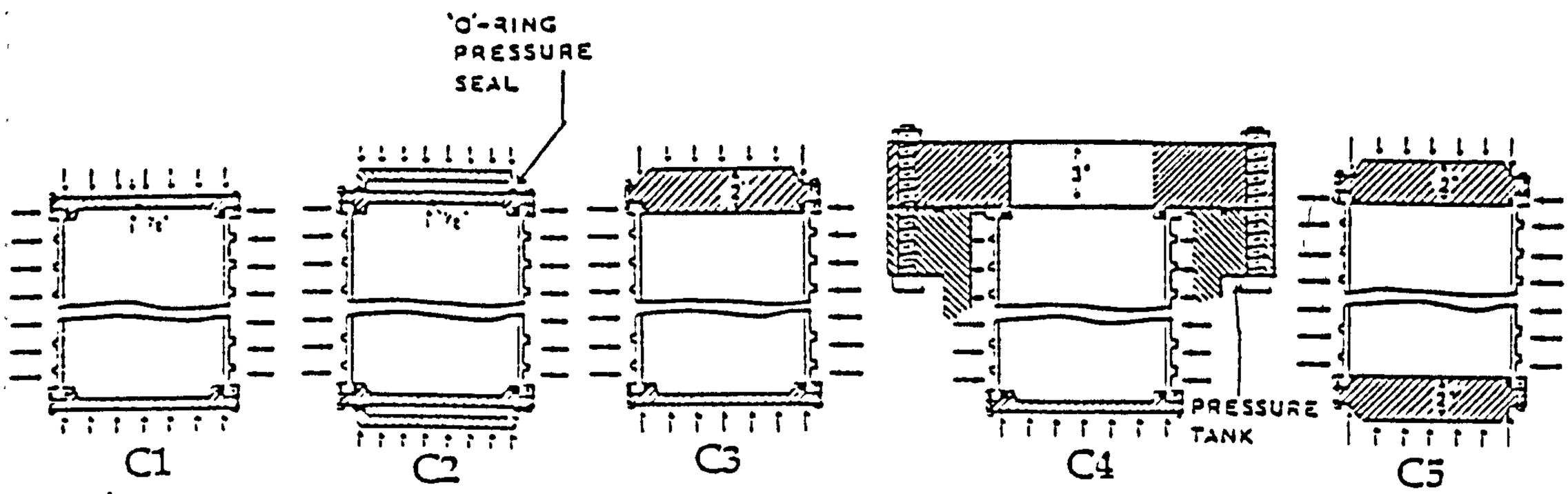

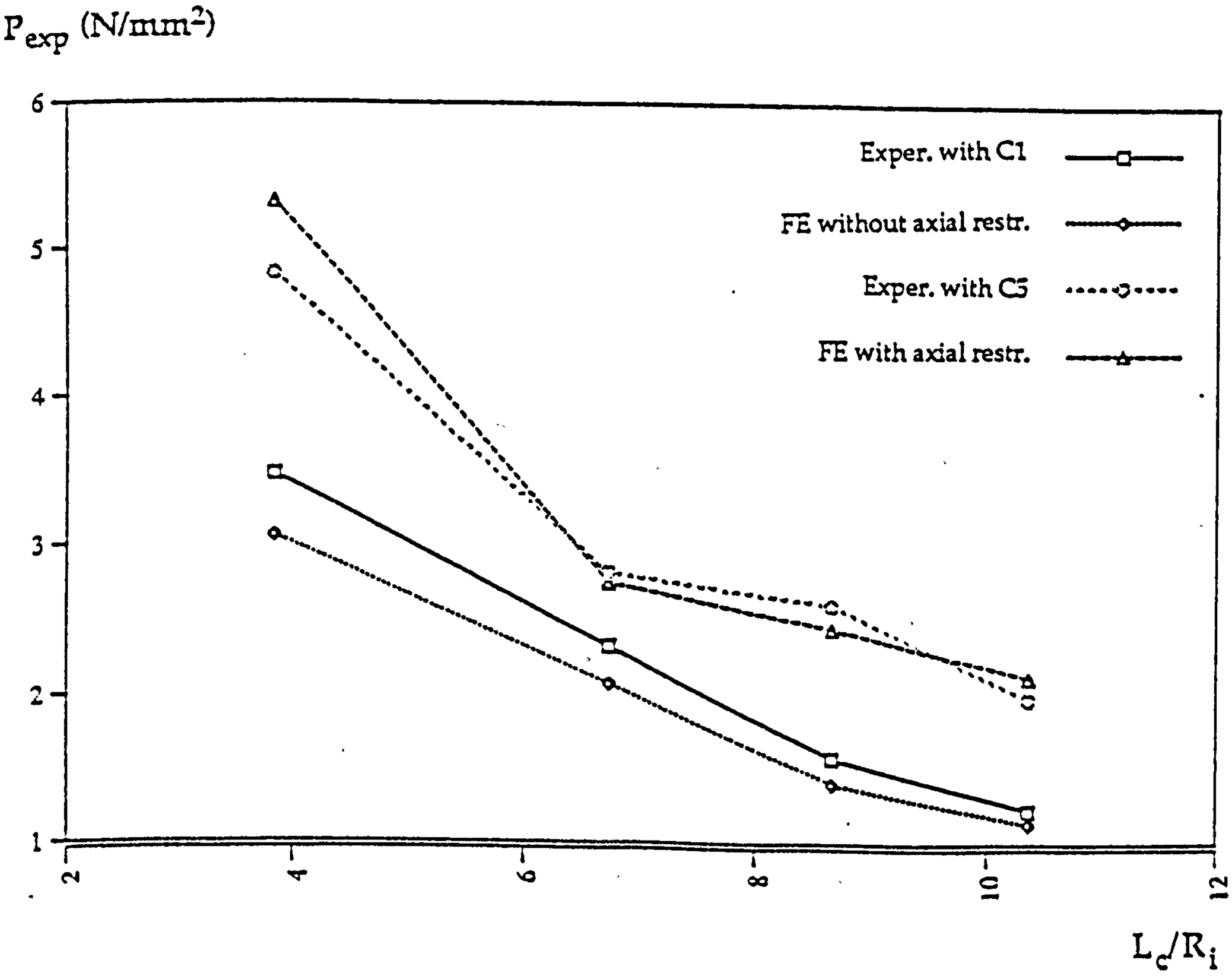

Figure 28: Comparison Experimental vs. FE Results
Elastic General Instability

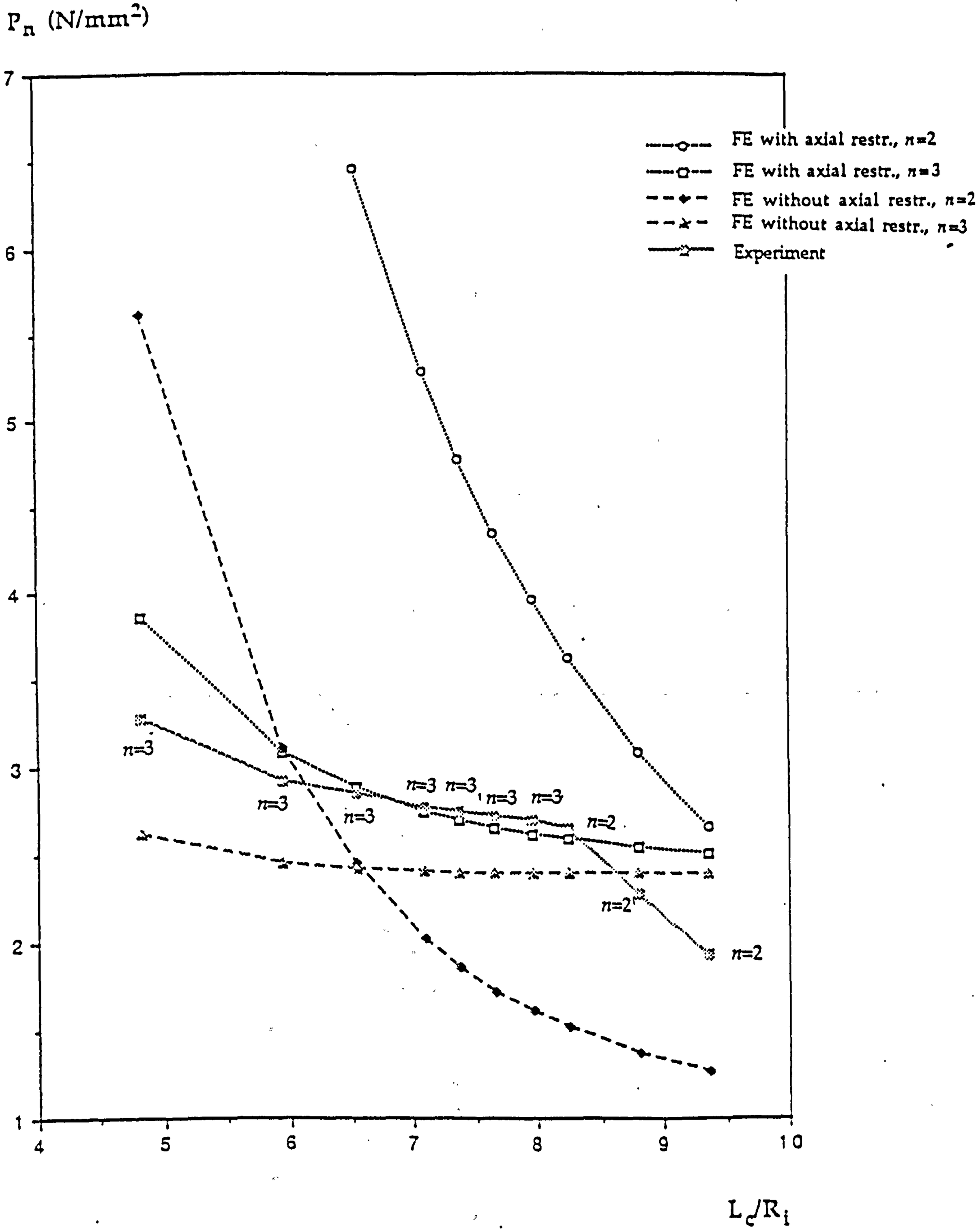

Figure 29: Comparison Experimental vs. FE Results
Models of [74]

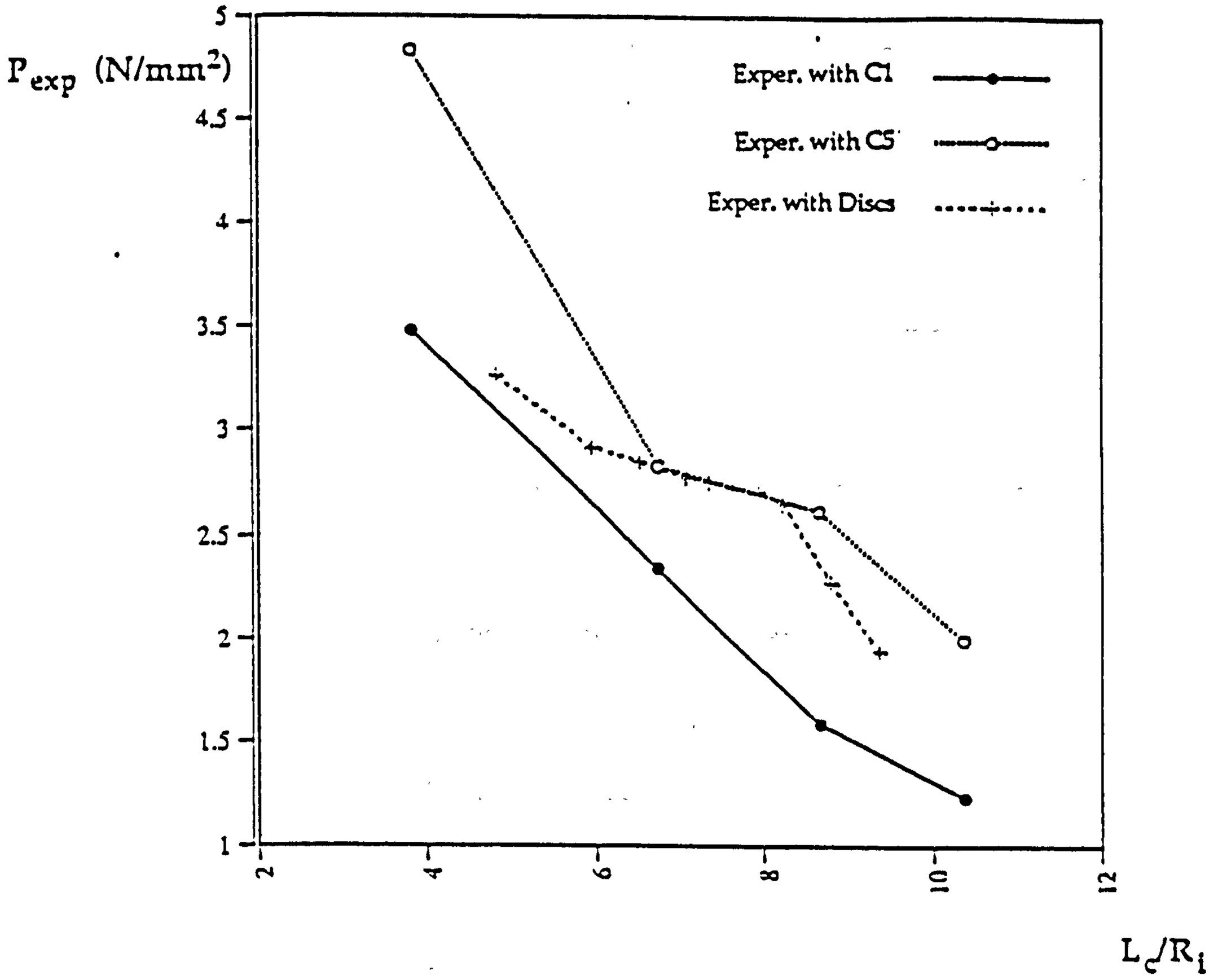

Figure 30: Comparison Experiments of [74] vs. Experiments of [85]

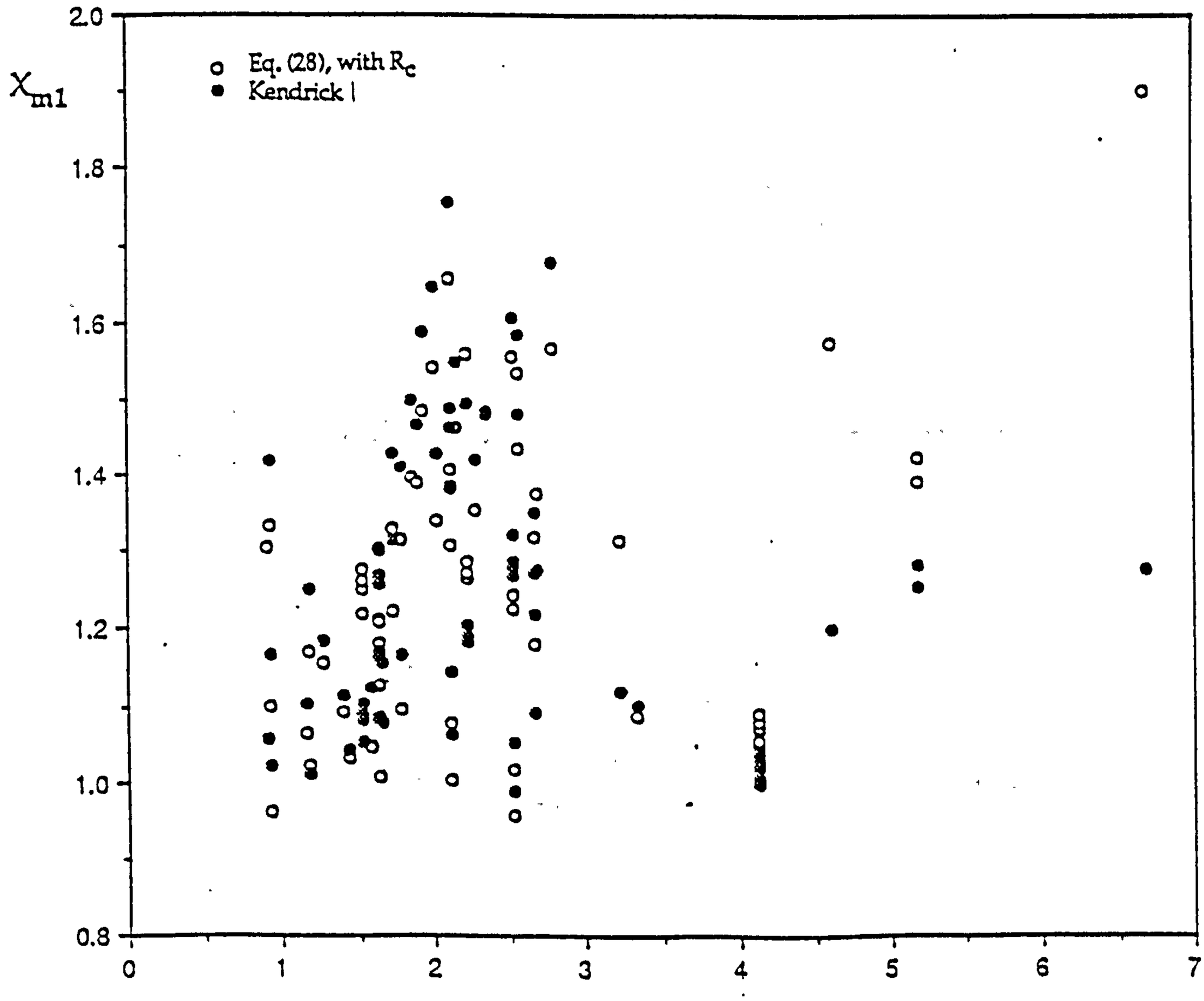

Figure 31: X_{m1} vs. χ, 72 Experimental Results

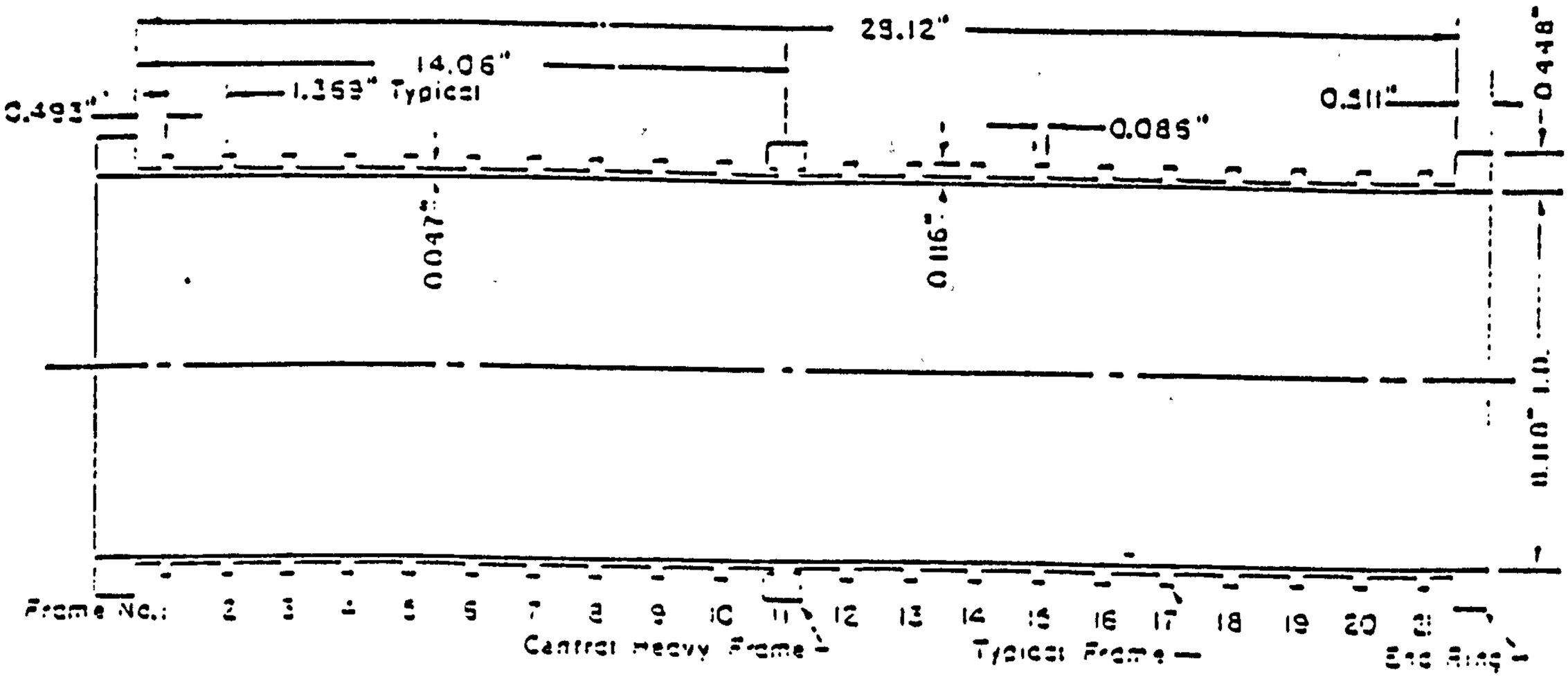

Figure 32: Group A Model, [79]

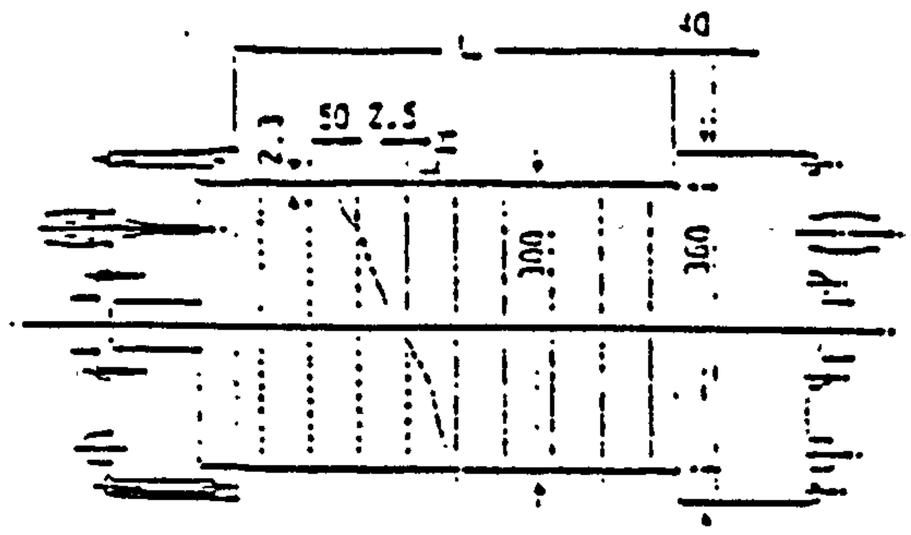

Figure 33: Group B Model, [148]

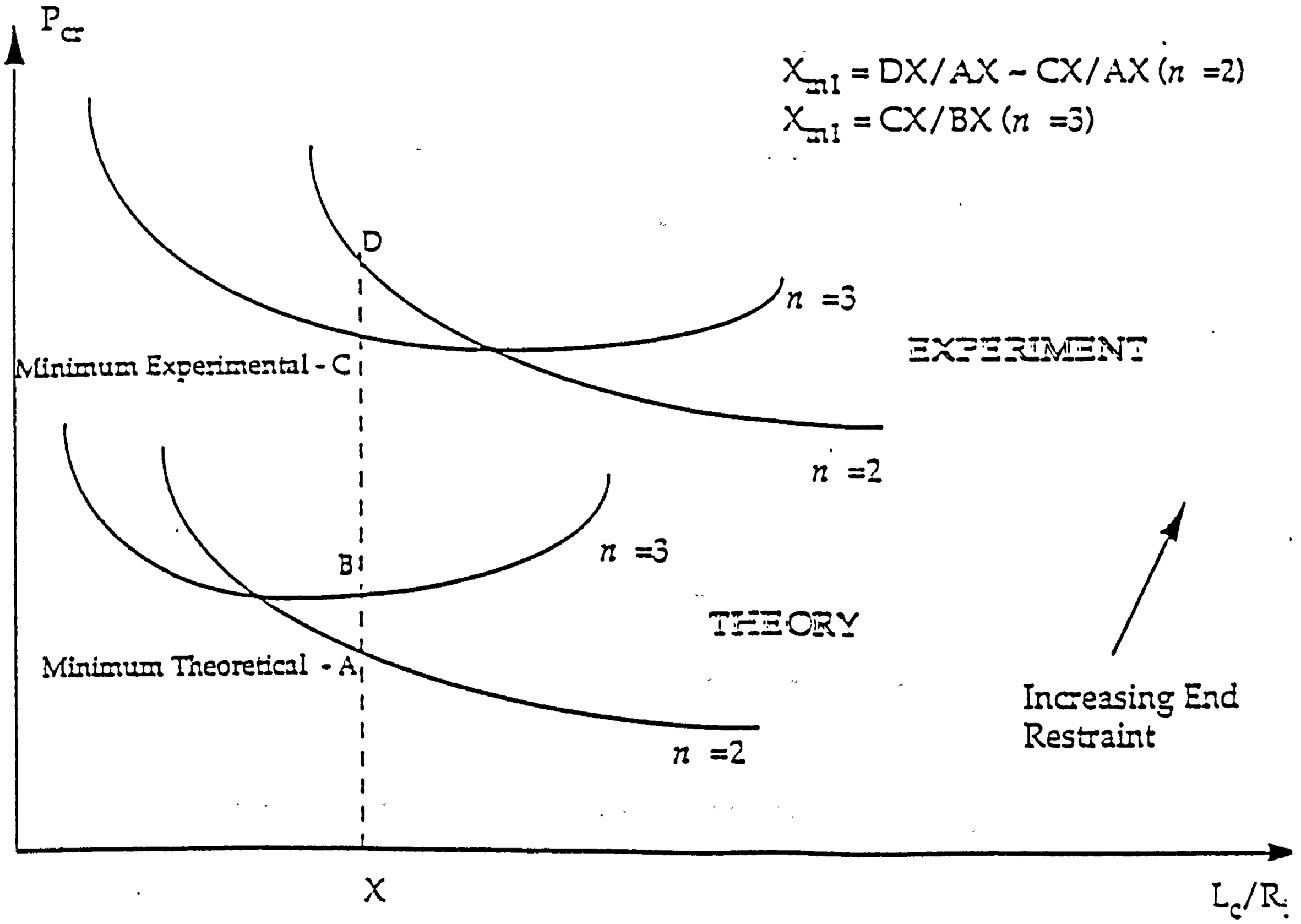

Figure 34: Redefinition of X_{m1} for Group B Models

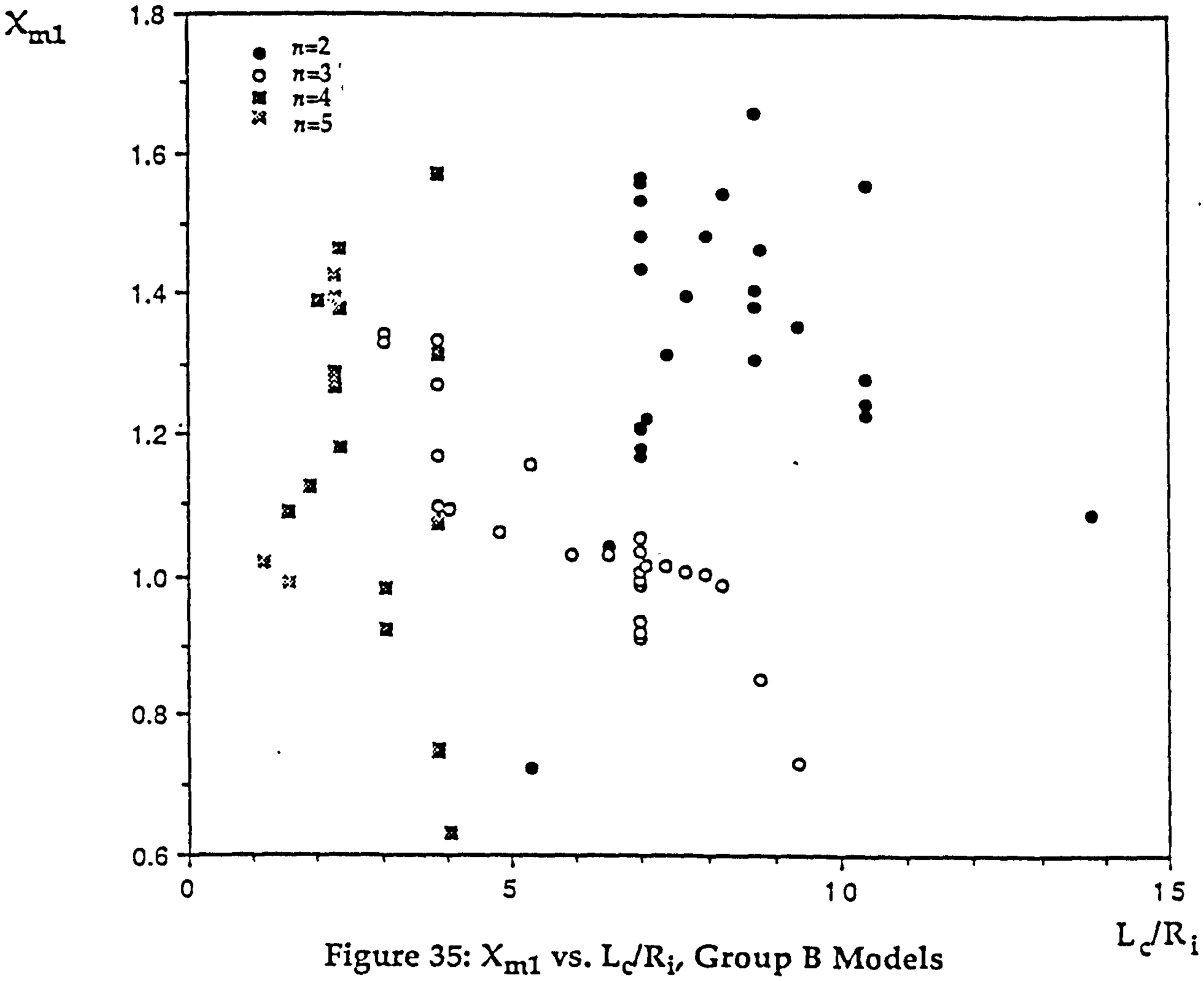

Figure 35: X_{m1} vs. L_c/R_i, Group B Models

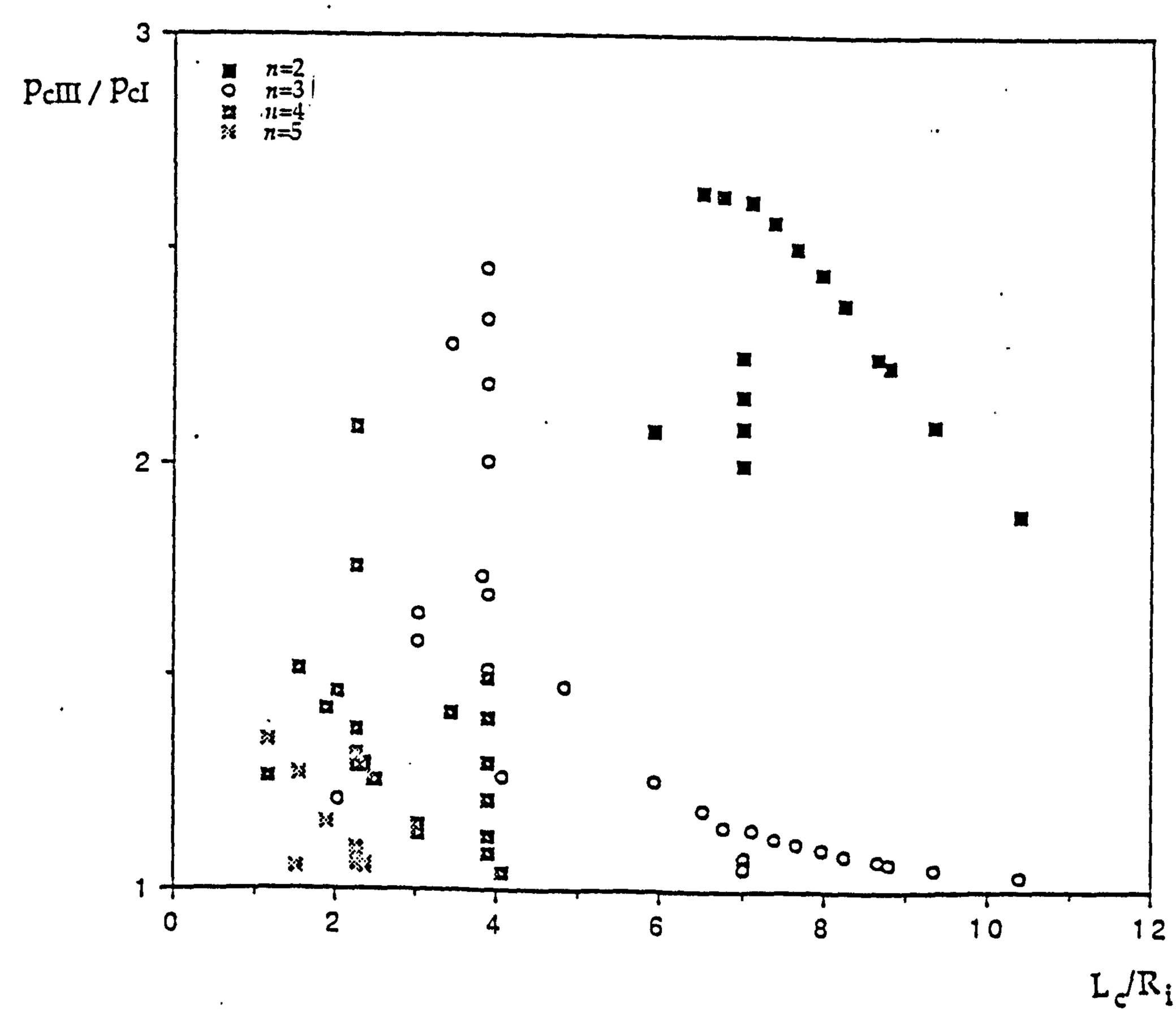

Figure 36: Effect of End Restraint, FE Eigenvalue Analysis

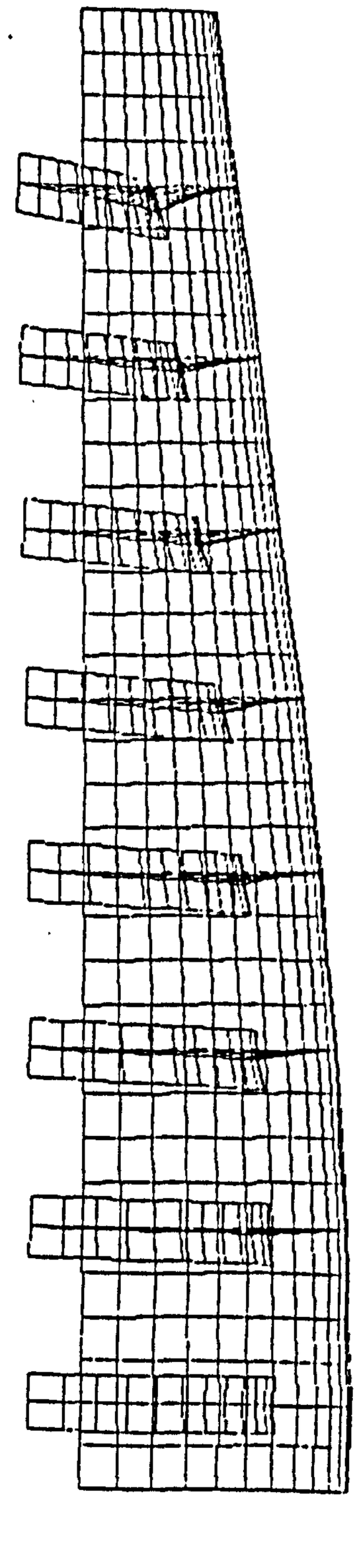

Figure 37: General Instability Buckling Mode from FE Eigenvalue Analysis
Case 3 of Table 6, L_c=1543 mm, n=3, Axial Restrained, p_n = 26.42 N/mm^2

	Prebuckling						Buckling					
Boundary	u	v	w	uu	vv	ww	u	v	w	uu	vv	ww
B1	0	0	0	0	1	1	0	0	0	0	1	1
B2	0	1	0	1	0	1	0	1	0	1	0	1
B3	1	0	0	0	1	1	1	0	0	0	1	1
B4	0	1	0	1	0	1	0	1	-1	1	0	1

Boundary conditions; 1: fixed , 0: free, -1: antisymmetry

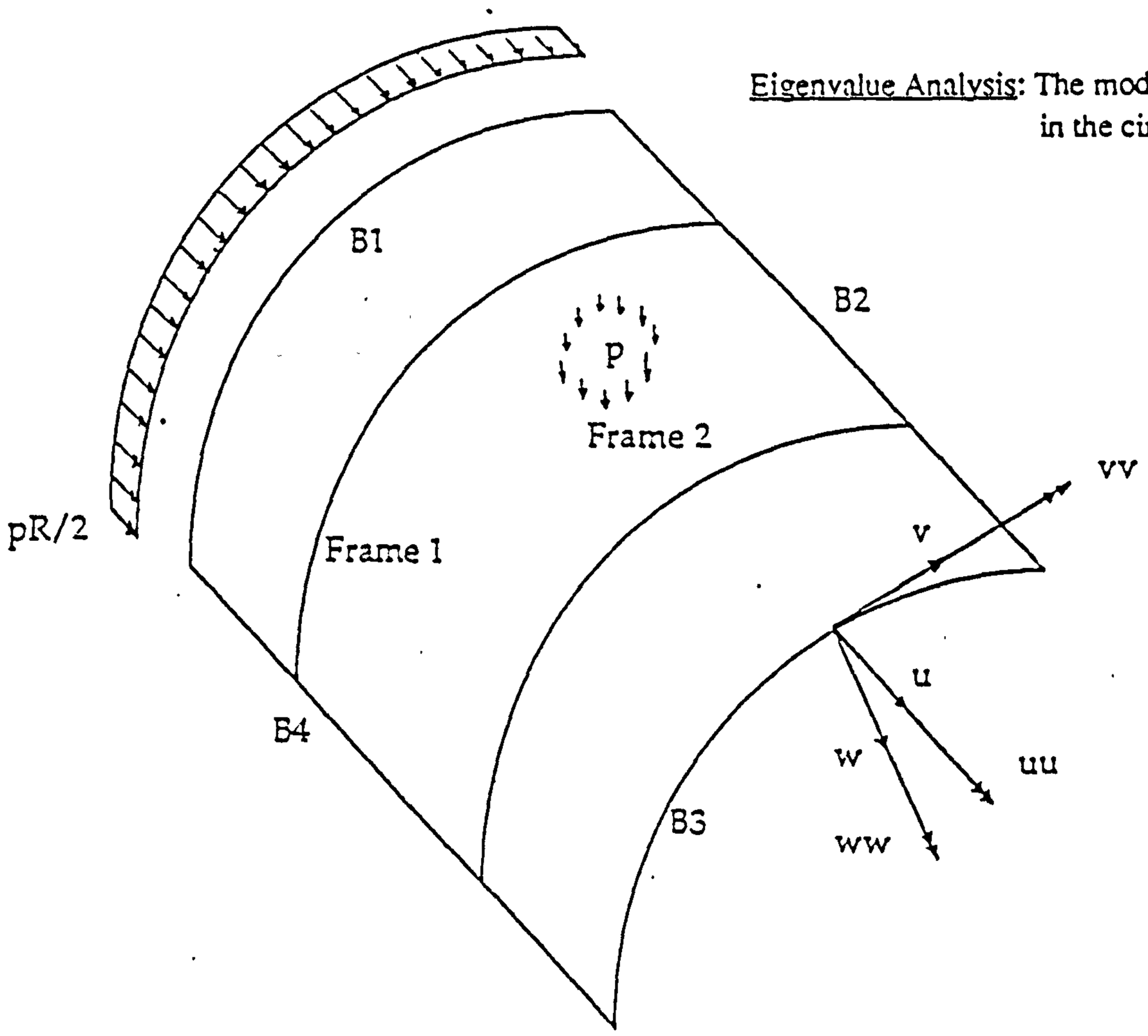

Eigenvalue Analysis: The model has $\pi/2n$ in the circumf. direction.

Figure 38: FE Models for Frame Tripping

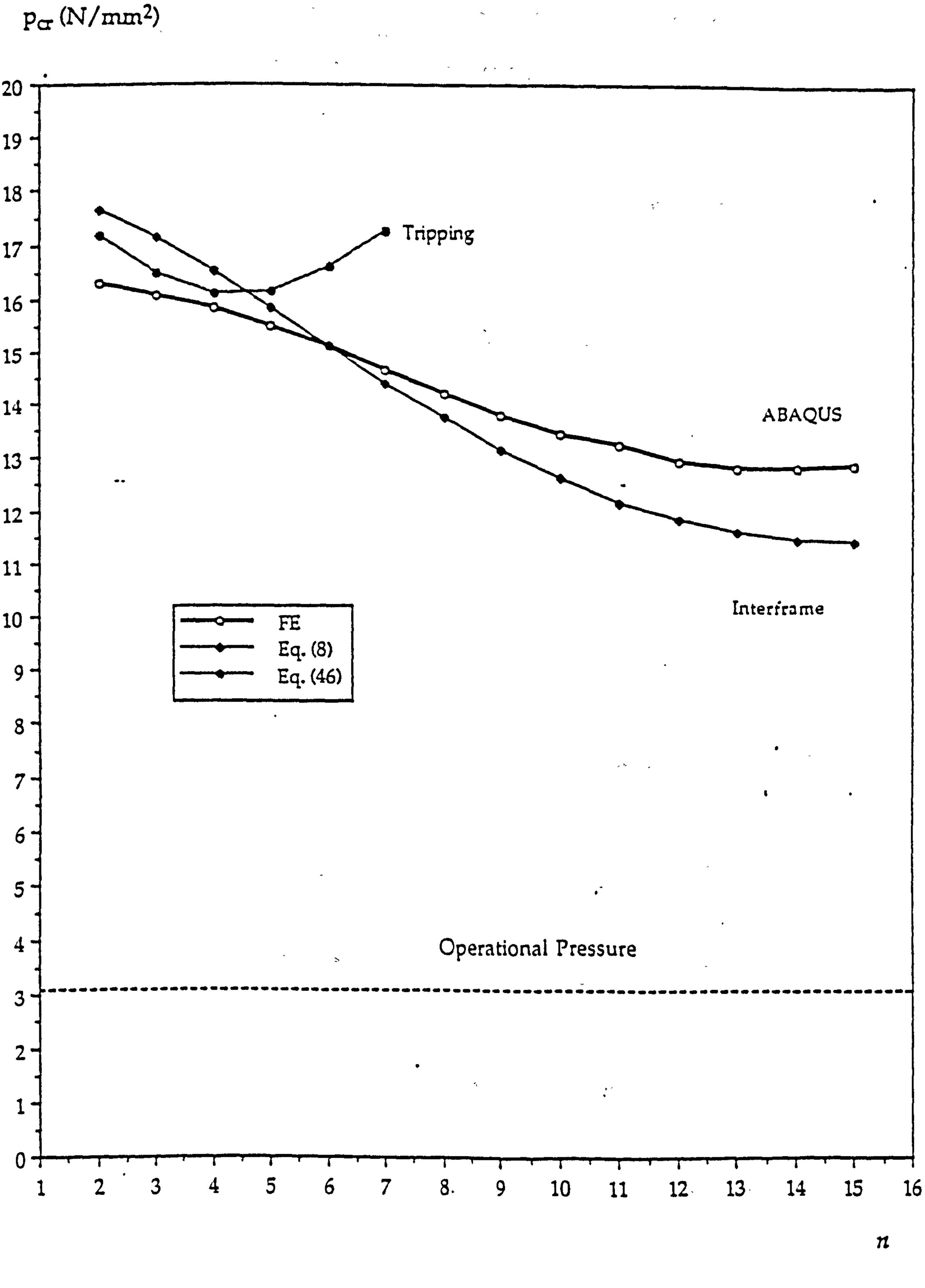

Figure 39: Elastic Buckling Pressures, Case 3 of Table 6

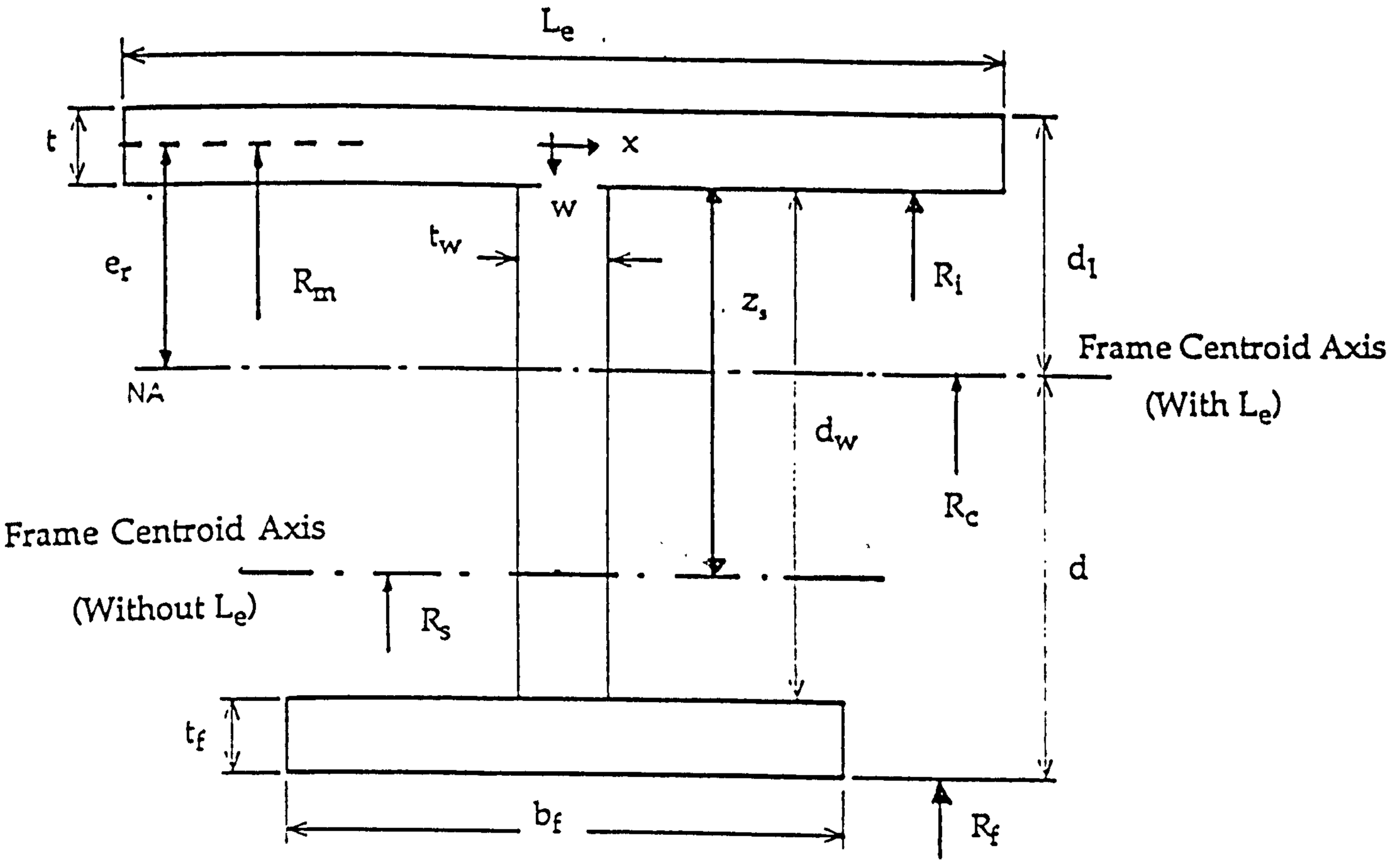

Figure 40: Basic Geometry

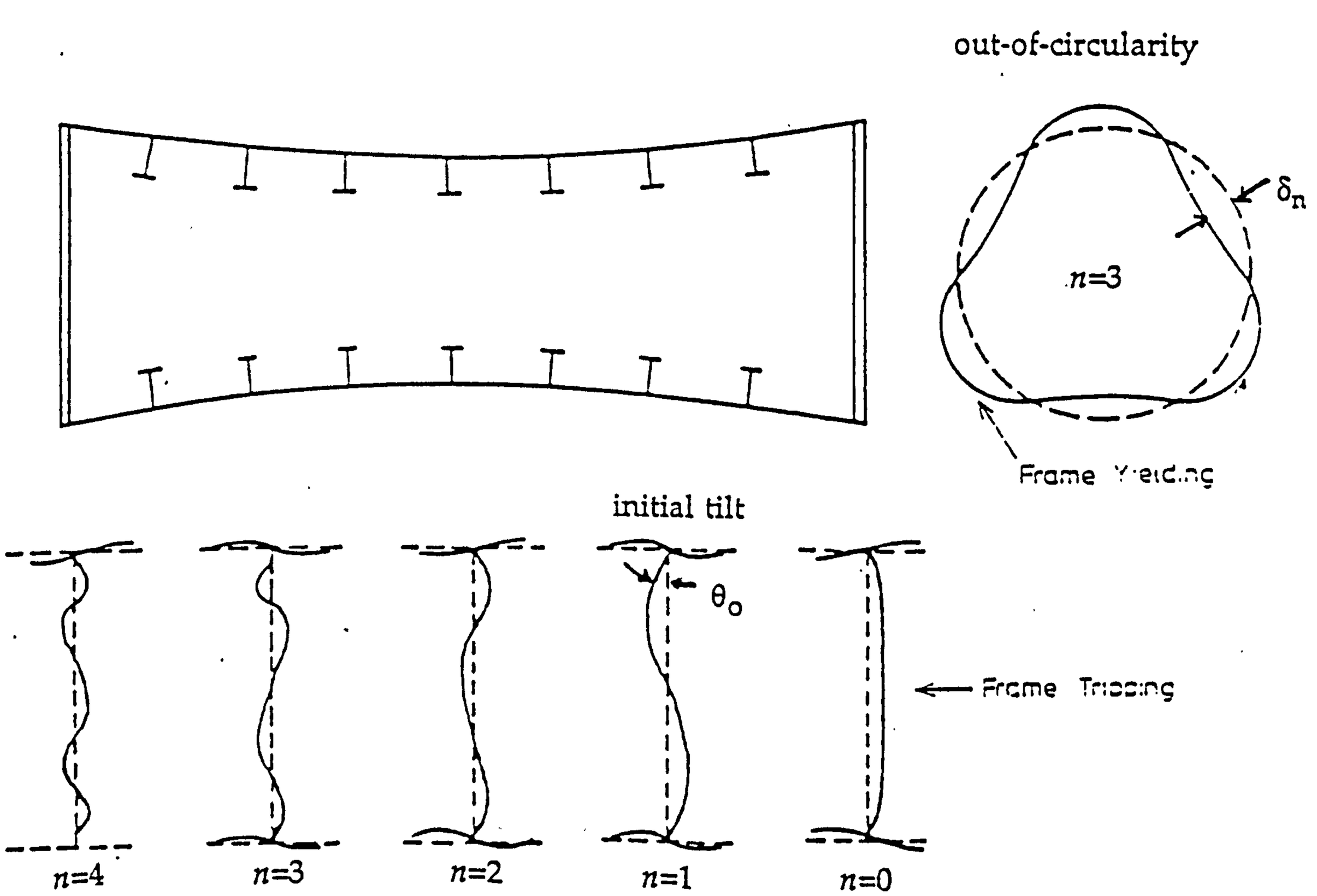

Figure 41: Relevant Imperfections

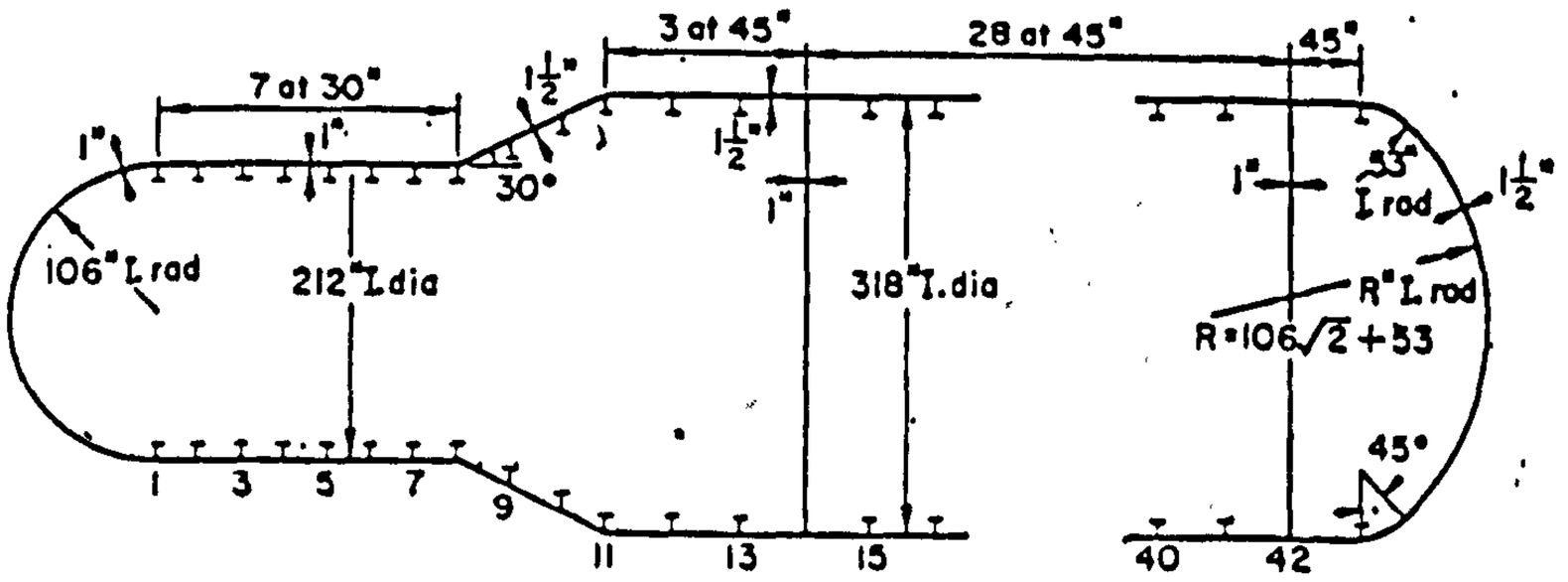

Detail of smaller stiffeners (1 – 8)

Detail of larger stiffeners (9–13, 15–41, 43)

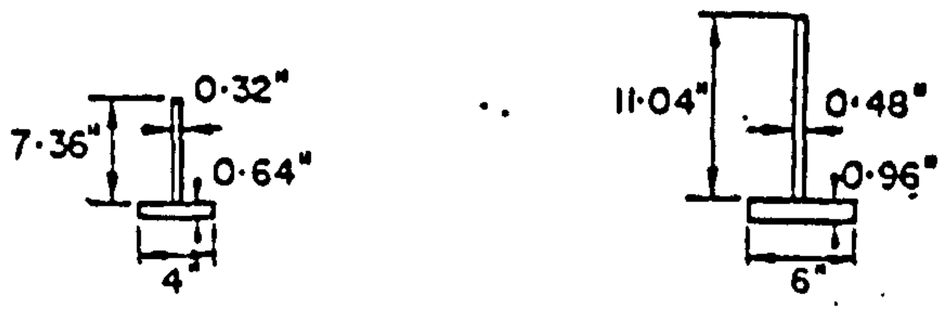

Figure 42: Geometry of Ref. [18], pp. 409

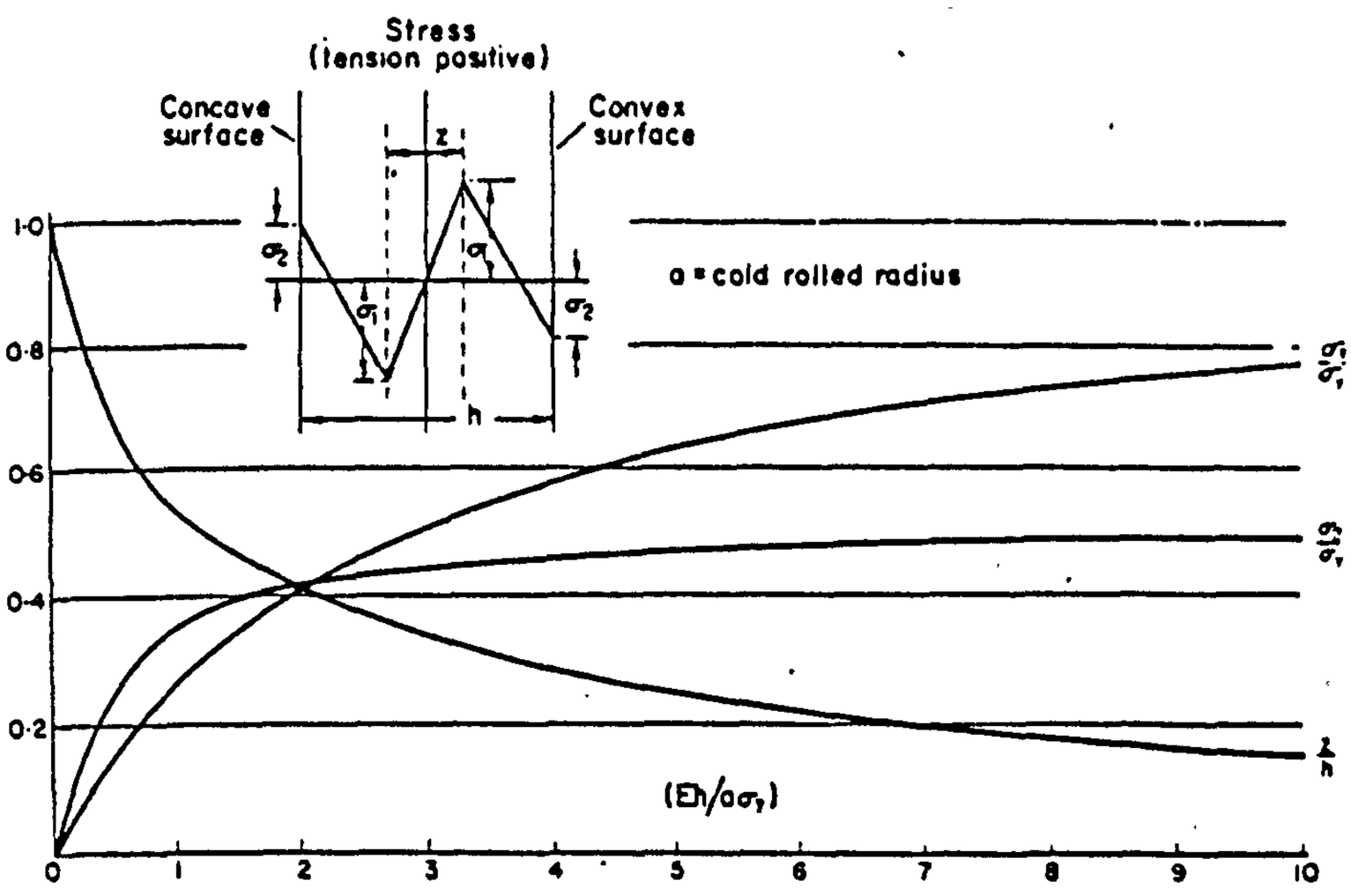

Figure 43: Typical Cold Rolling Residual Stress Distribution, [18]

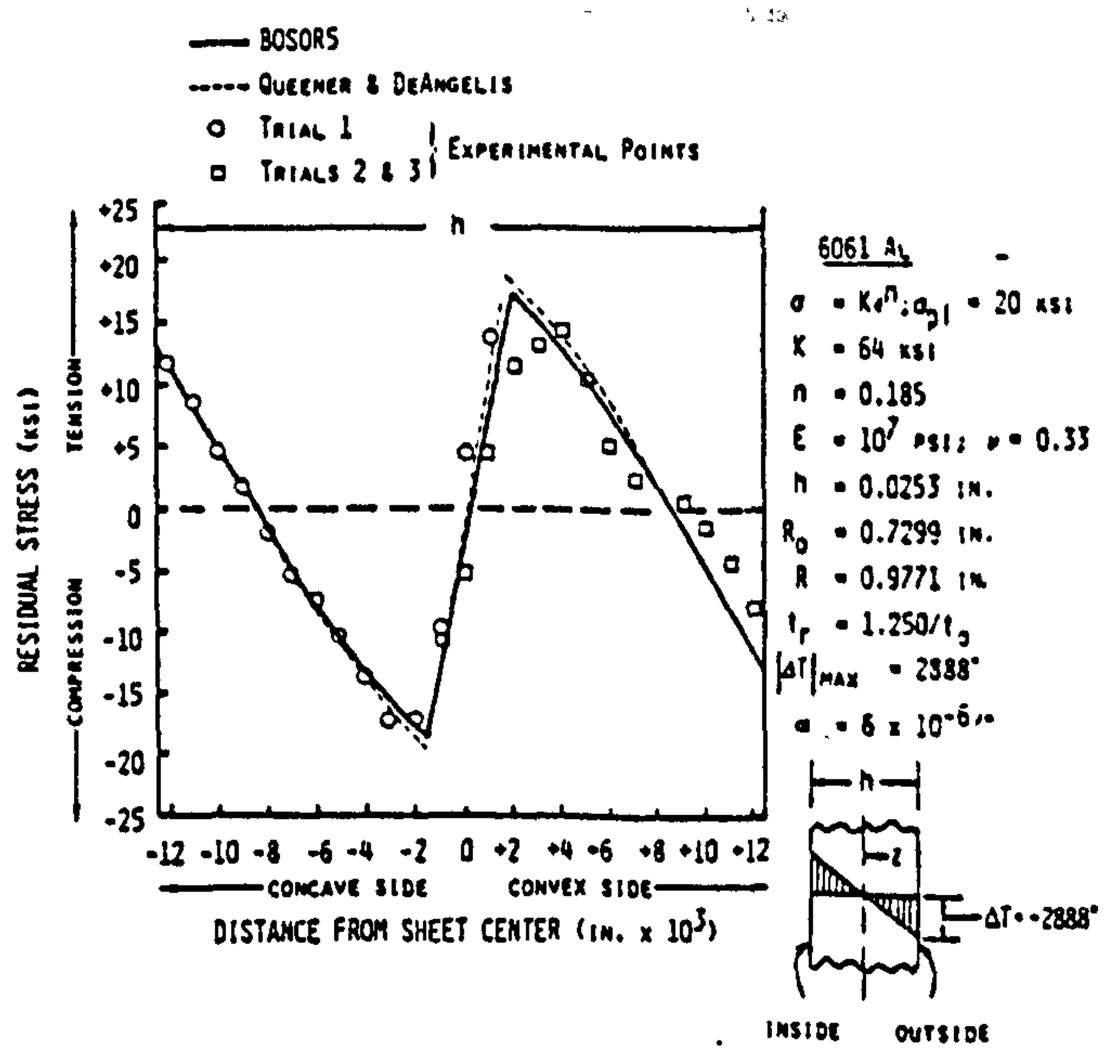

Figure 44: Measured Cold Rolling Residual Stress Distribution, [150]

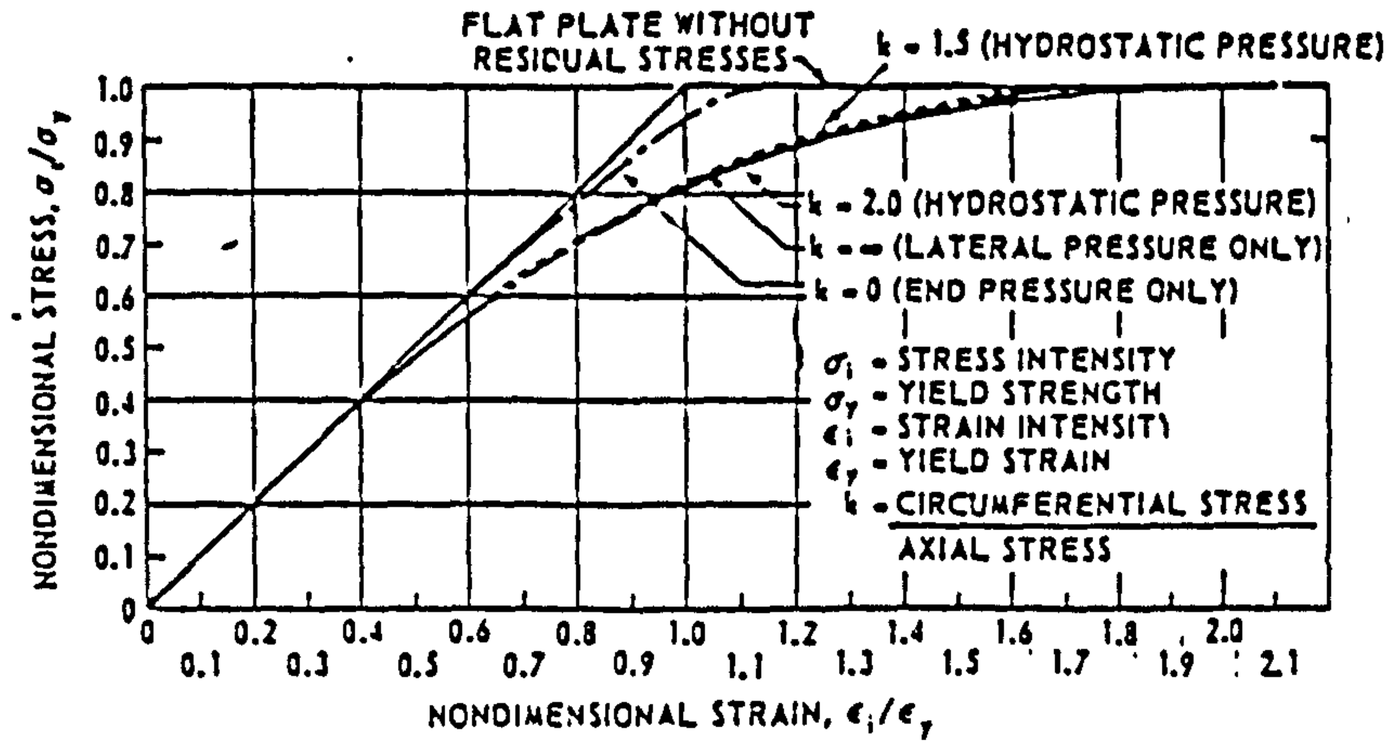

Figure 45: Apparent Stress-Strain Curves, [82]

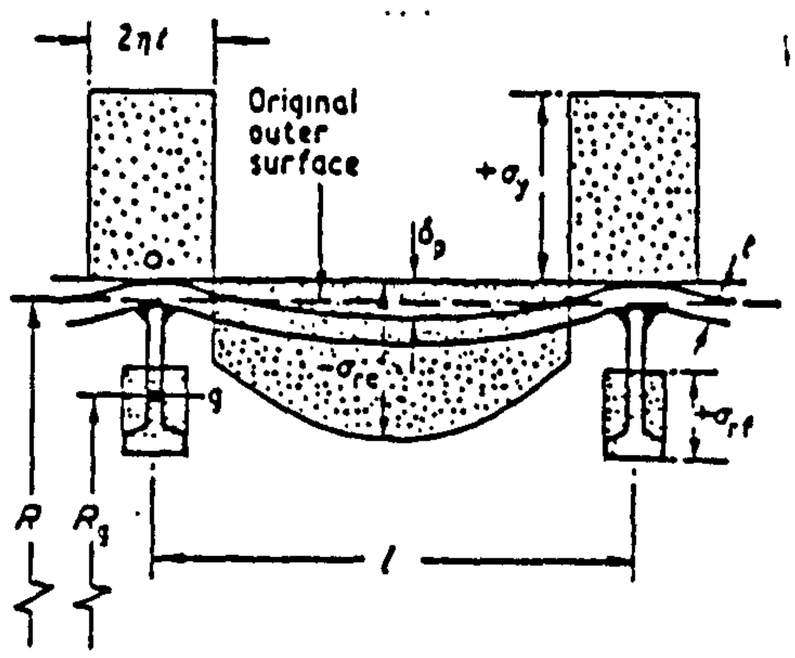

Figure 46: Welding Shrinkage Actions, [61]

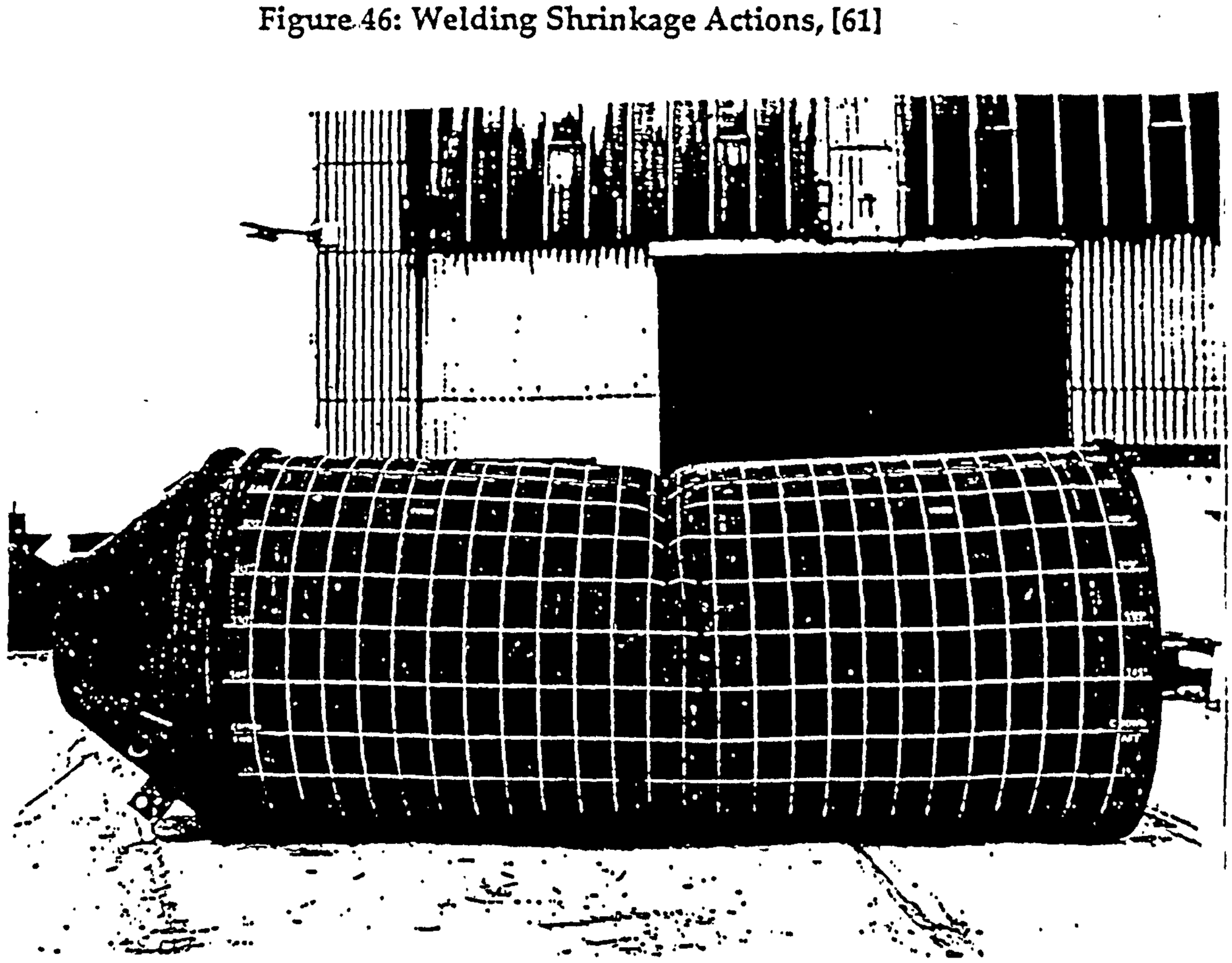

Figure 47: Example of Mode Interactive Collapse, [73]

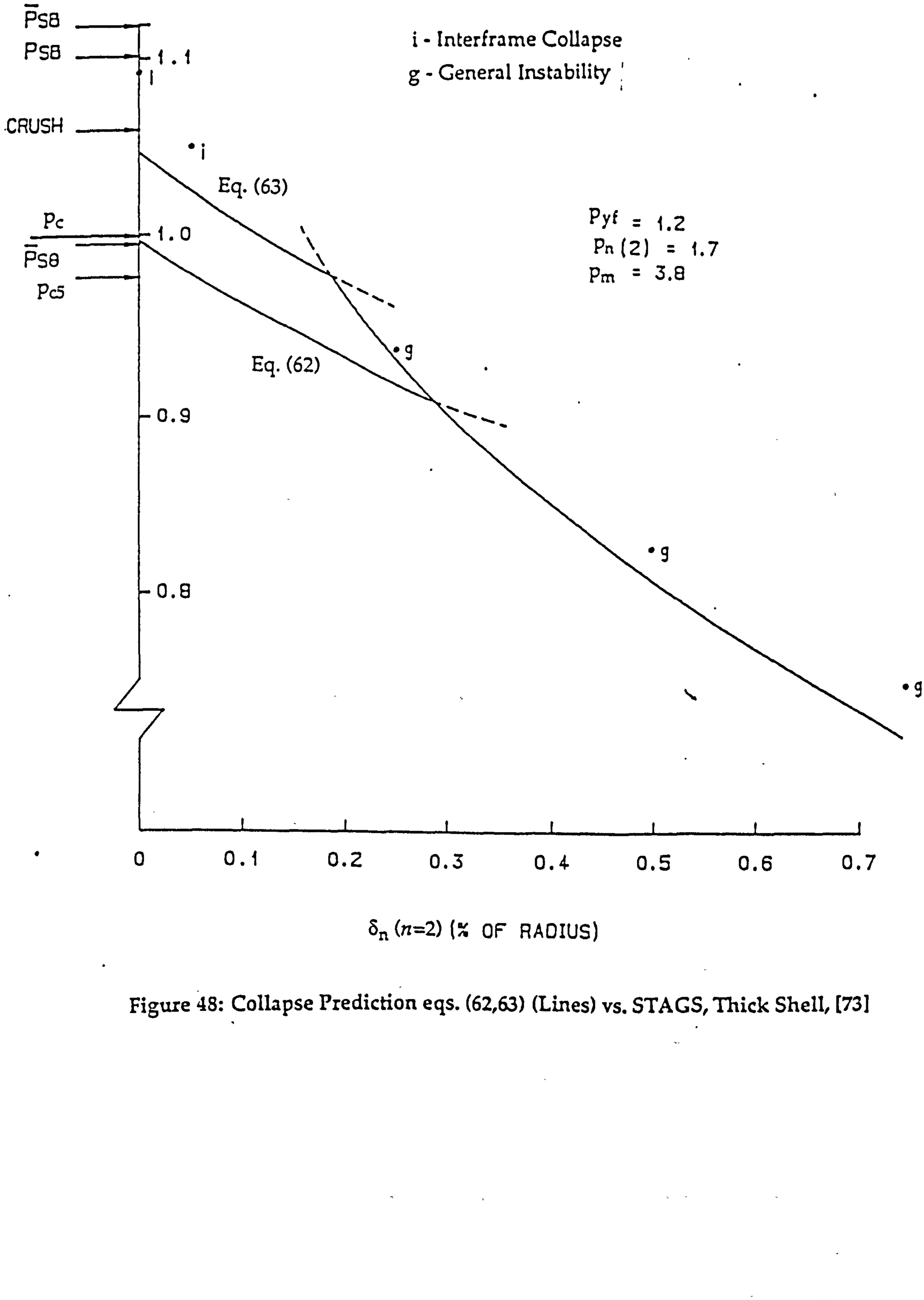

Figure 48: Collapse Prediction eqs. (62,63) (Lines) vs. STAGS, Thick Shell, [73]

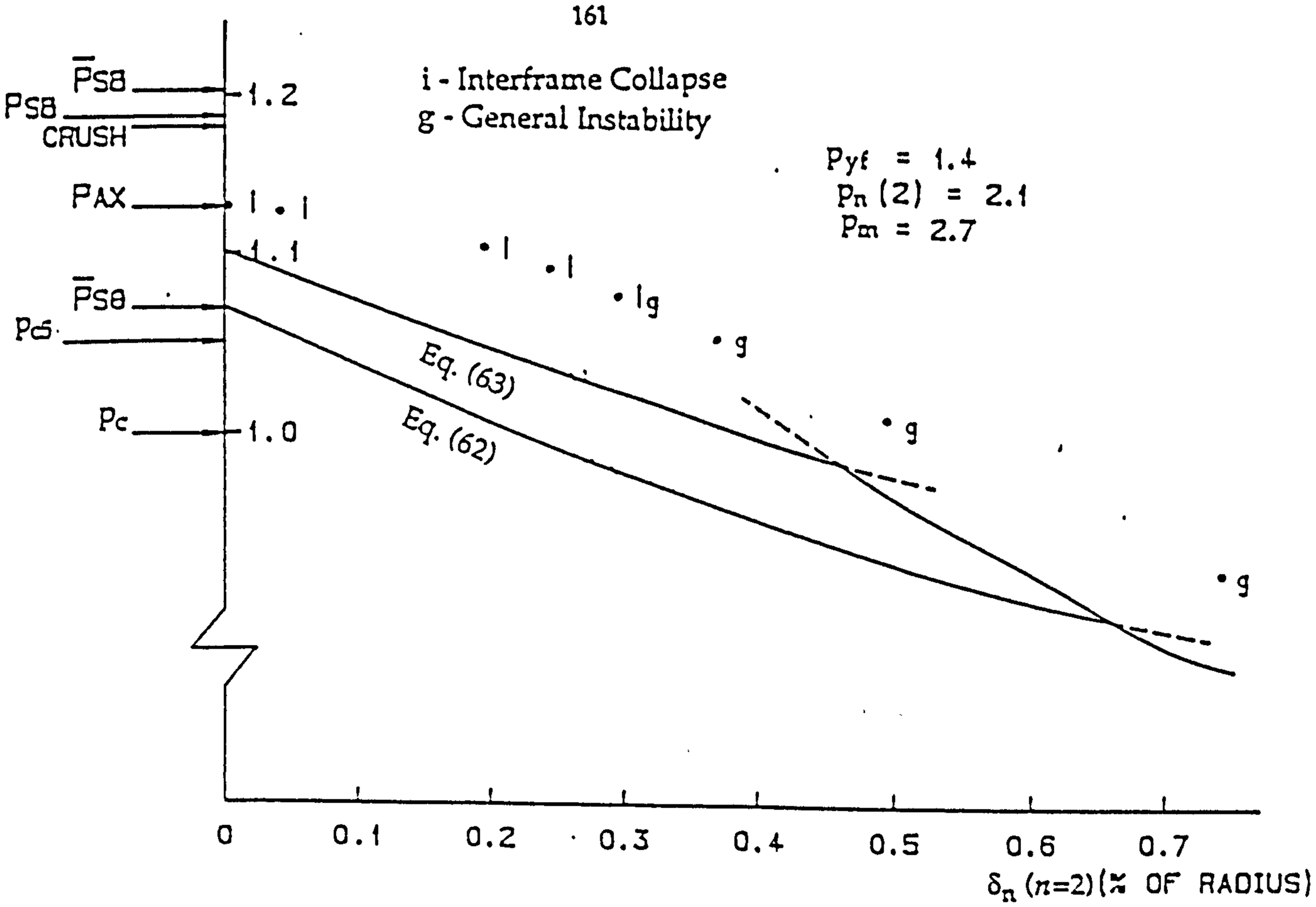

Figure 49: Collapse Prediction eqs. (62,63) (Lines) vs. STAGS, Moder. Thick Shell, [73]

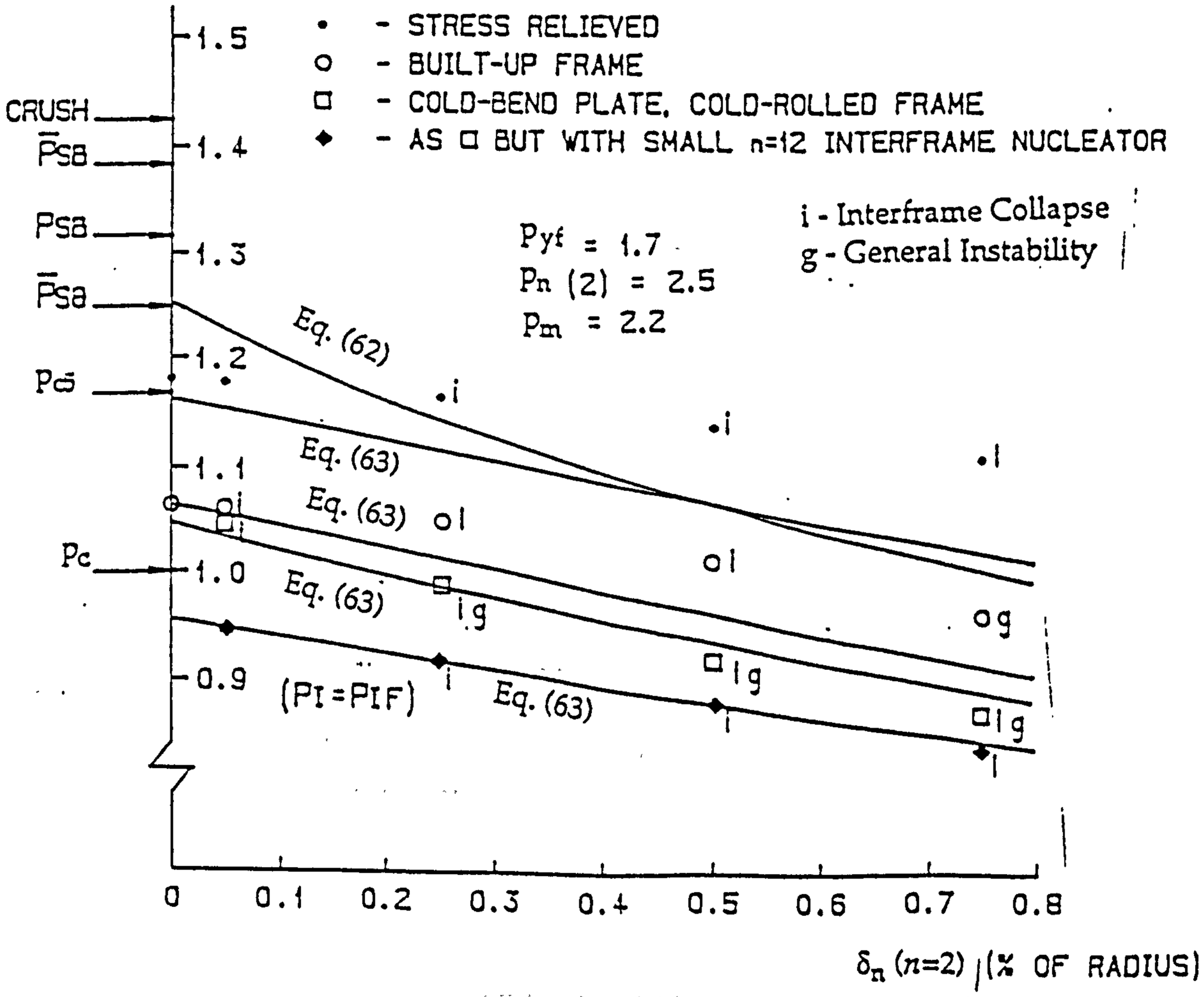

Figure 50: Collapse Prediction eqs. (62,63) (Lines) vs. STAGS, Thin Shell, [73]

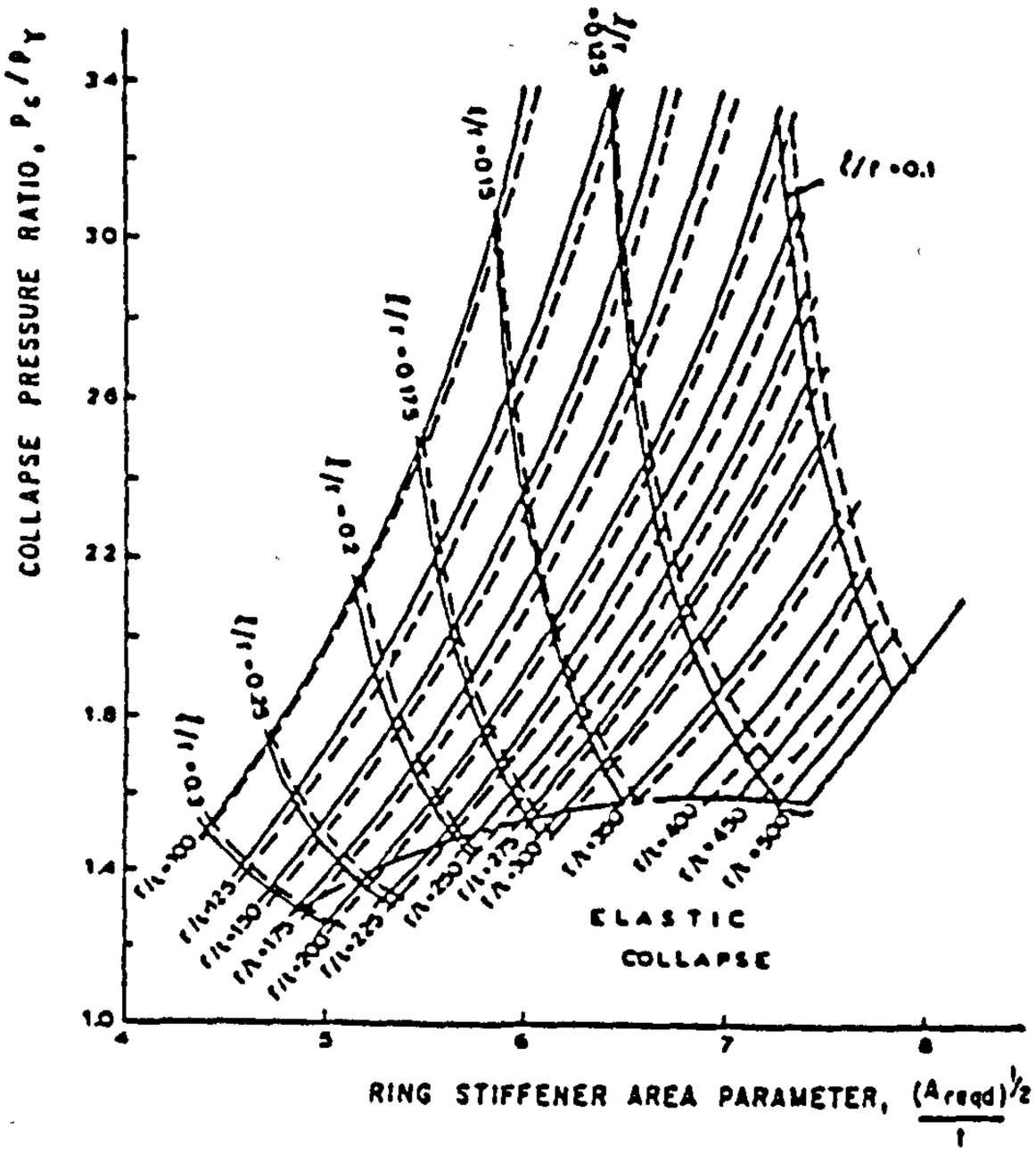

Figure 51: Effect of Stiffener Size on Load-Carrying Capacity, [122]

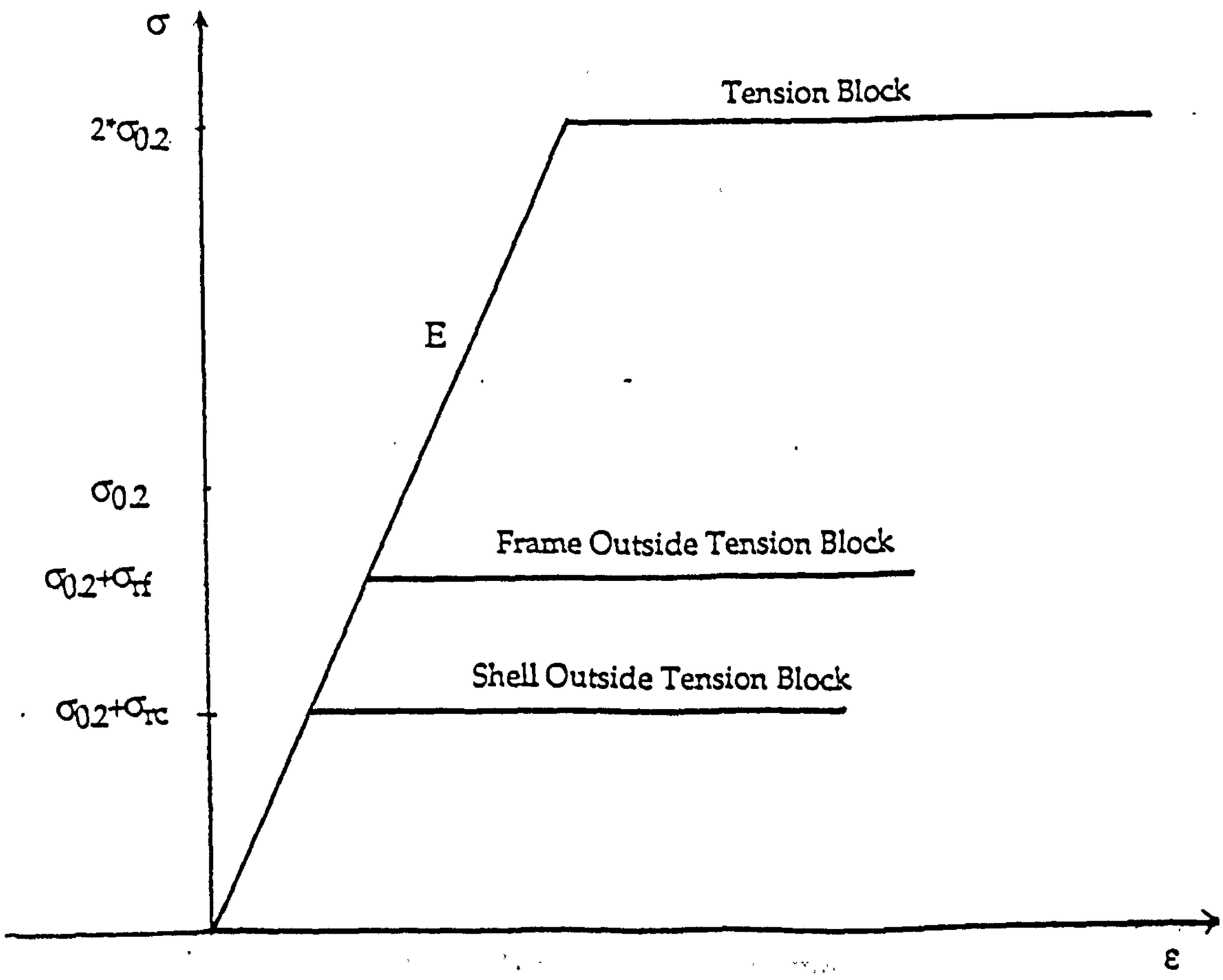

Figure 54: Modelling of Residual Stresses by means of a Modified Stress-Strain Curve

Boundary	u	v	w	uu	vv	ww
B1	0	0	0	0	1	1
B2	0	1	0	1	0	1
B3	1	0	0	0	1	1
B4	0	1	0	1	0	1

Riks Analysis: The model has π/n in the circumf. direction.

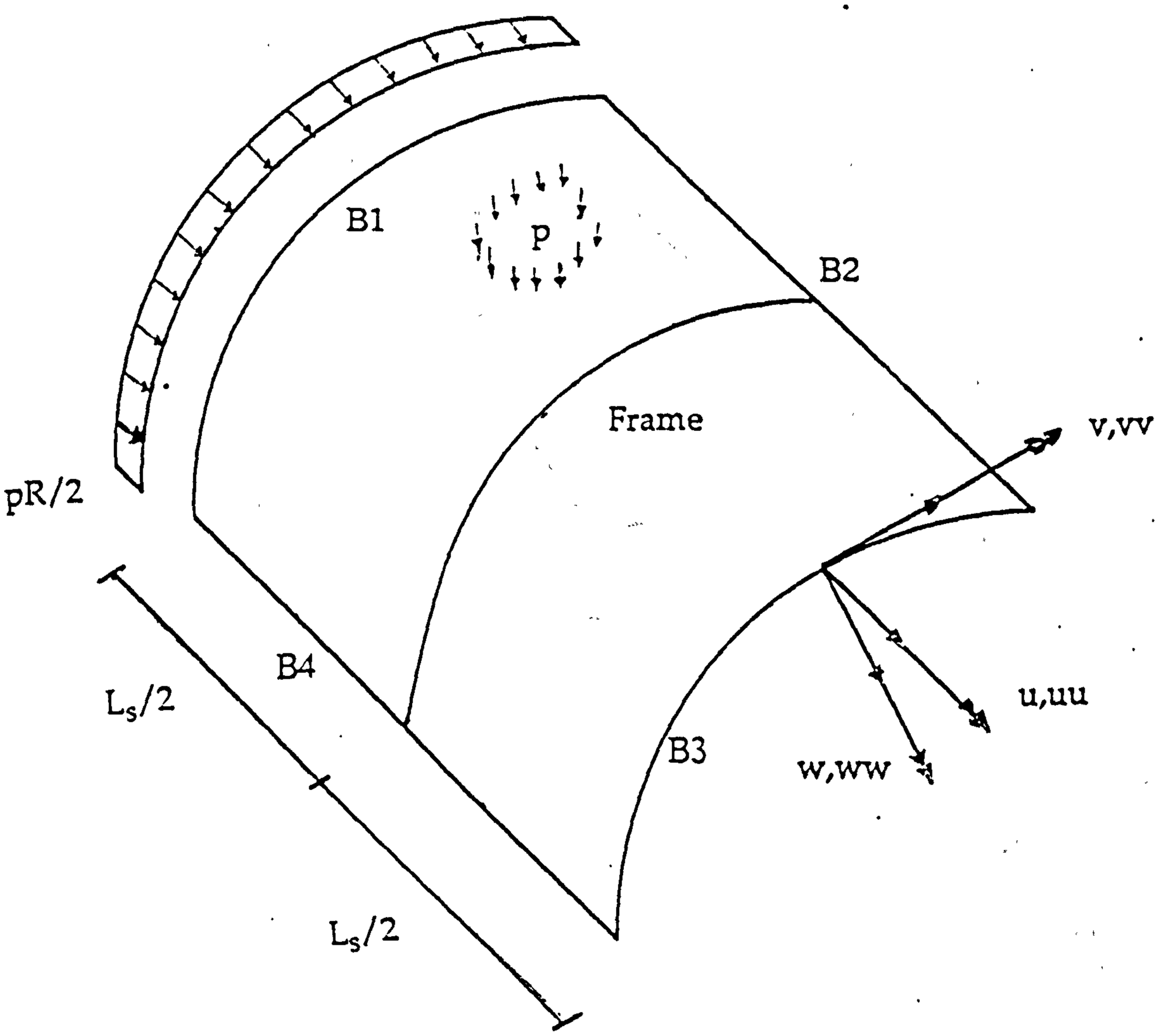

Figure 52: FE models - Infinite Compartments

Boundary	u	v	w	uu	vv	ww
B1	0	1	1	0	0	0
B2	0	1	0	1	0	1
B3	1	0	0	0	1	1
B4	0	1	0	1	0	1

Riks Analysis: The model has π/n in the circumf. direction.

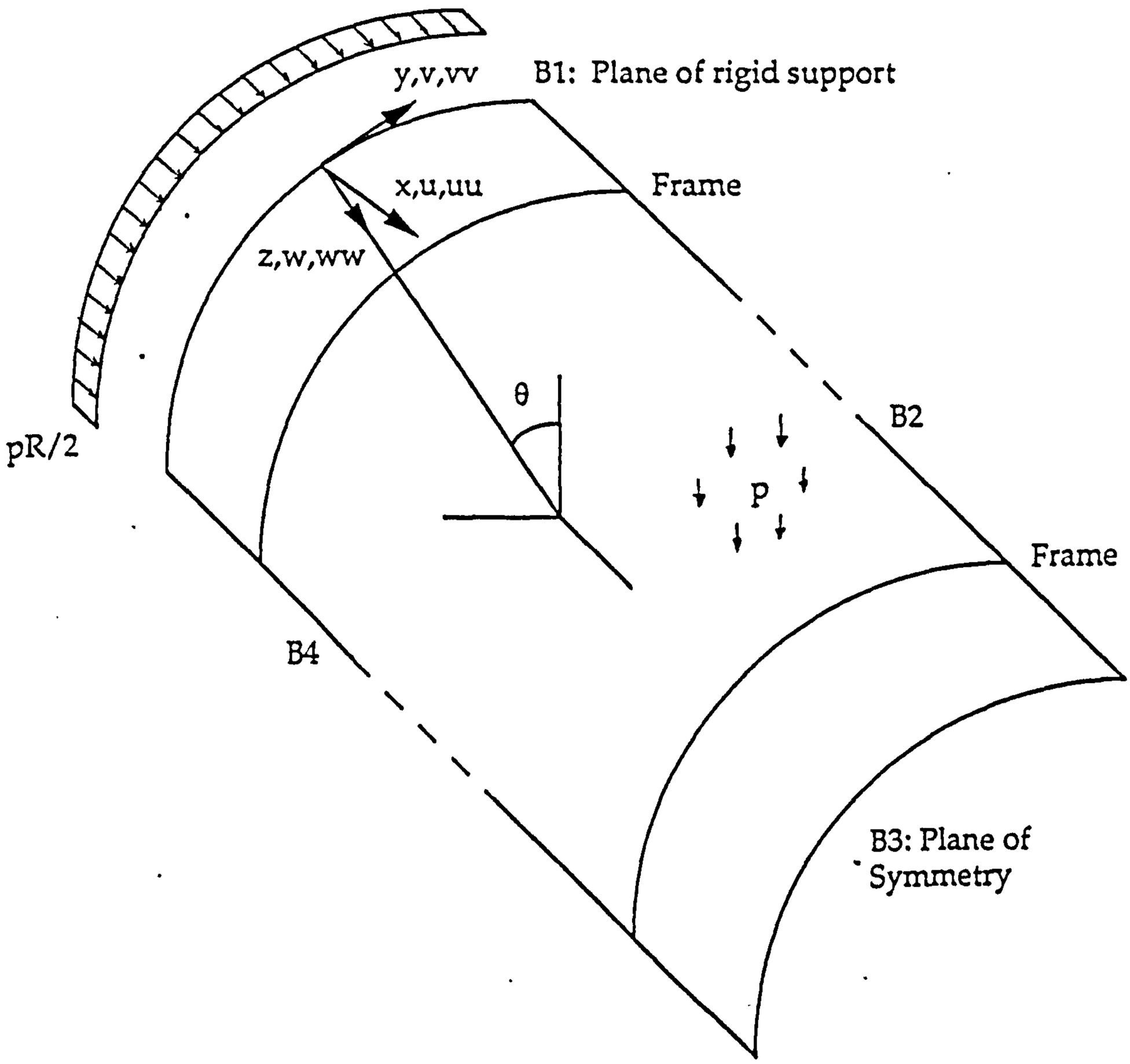

Figure 53: FE models - Finite Compartments

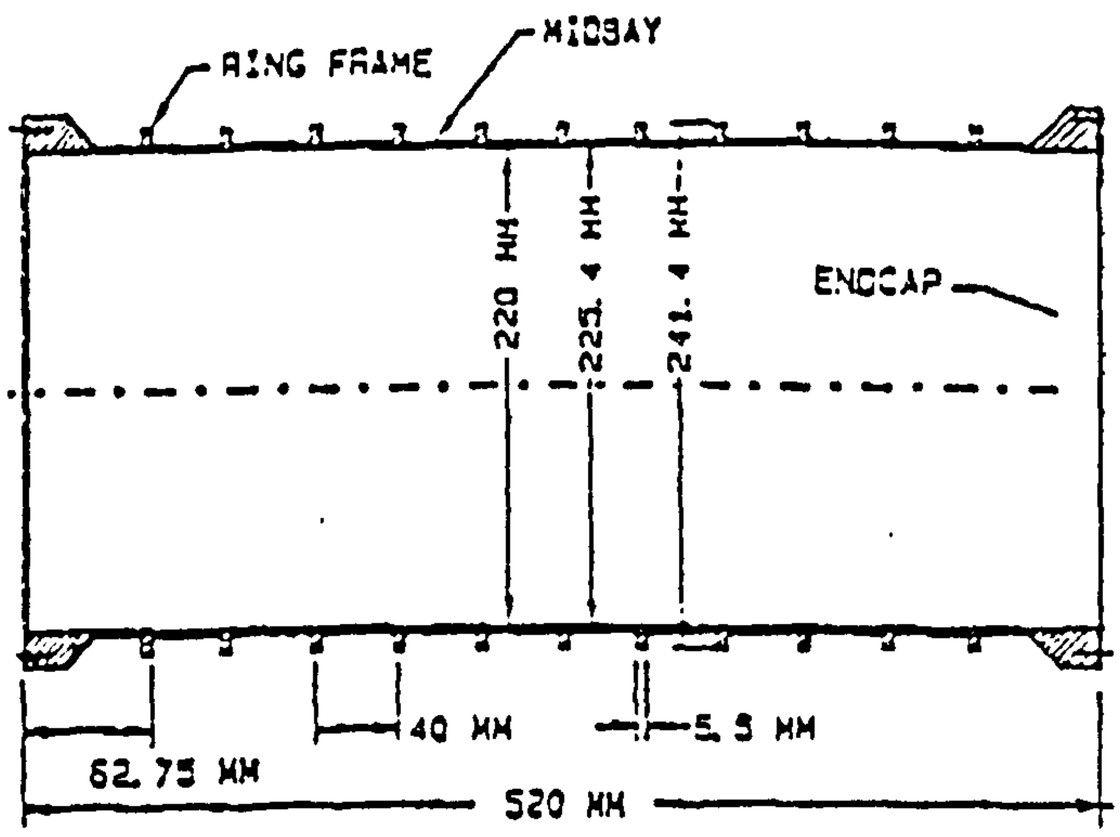

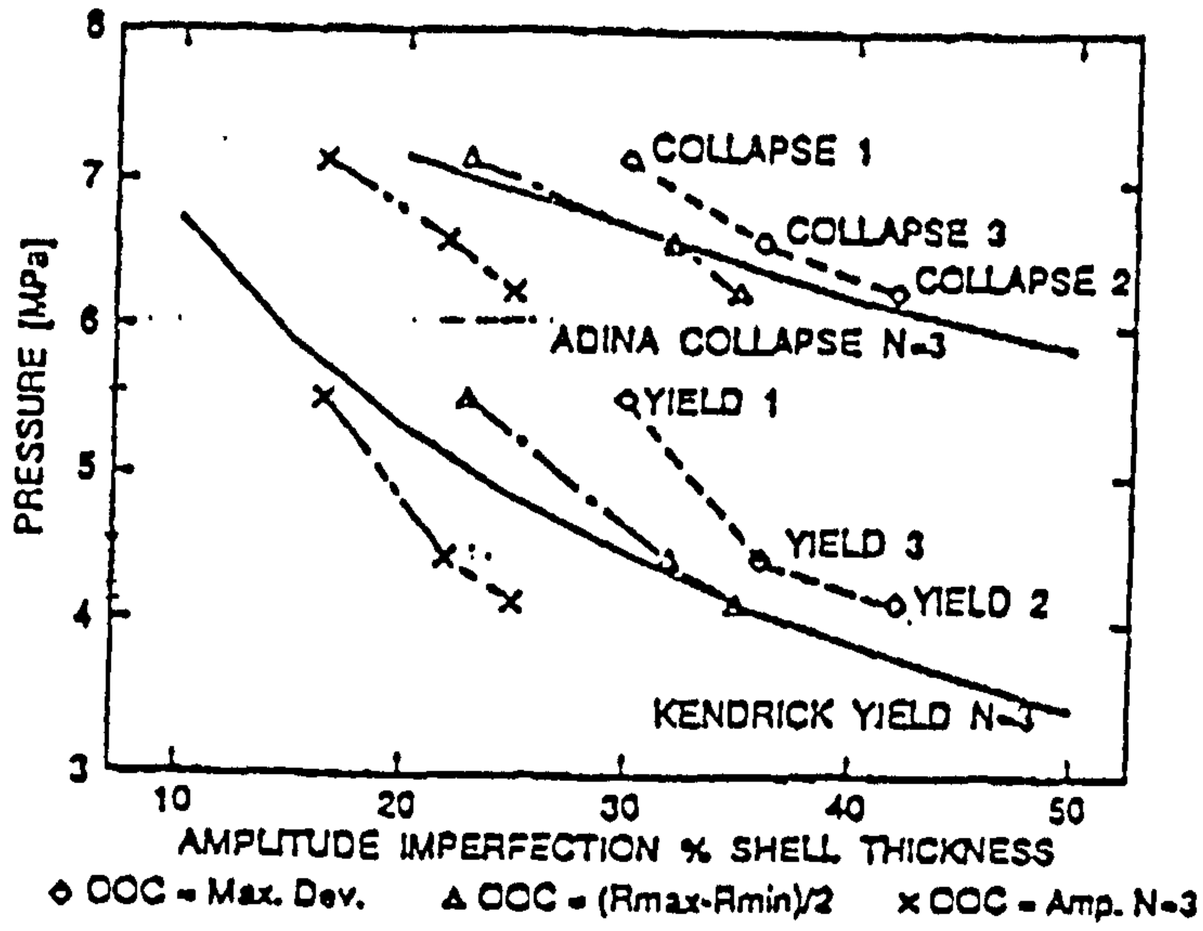

Figure 55: Experiments of Bosman et al. [149]

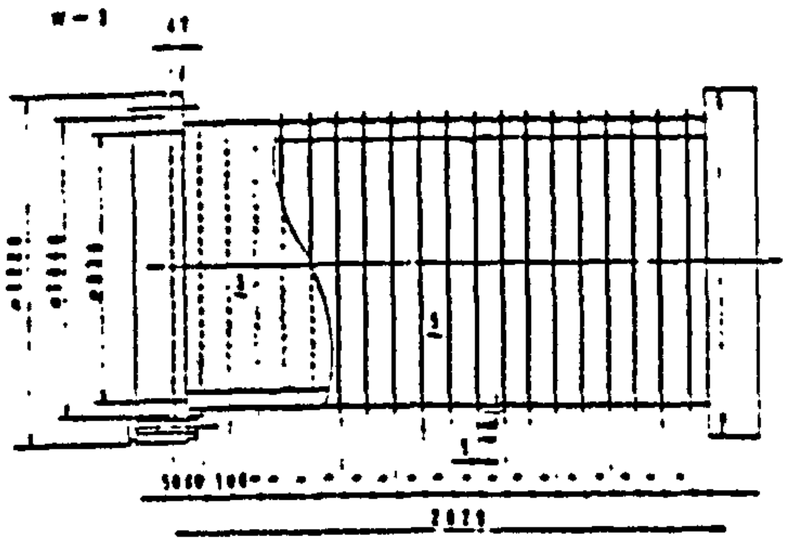

(単位：mm)

Figure 56: Experiments of Morihana et al. [142]

供試番号			M－3	W－3	W－1**
製造方式			機械加工	溶接組立	溶接組立
使用材料	円筒部	種別	60kgf／mm² 級 調質高張力鋼	60kgf／mm² 級 調質高張力鋼	60kgf／mm² 級 調質高張力鋼
	補強フレーム	種別	60kgf／mm² 級 調質高張力鋼	60kgf／mm² 級 調質高張力鋼	60kgf／mm² 級 調質高張力鋼
形状寸法	外径	Do (mm)	500.0	1000.0	1000.0
	板厚	t (mm)	2.5	5.0	5.0
	全長	L (mm)	960.5	1920.0	1920.0
	平均径	Dm (mm)	497.5	995.0	995.0
	フレームスペース	ℓ (mm)	50.0	100.0	100.0
	フレーム型式		F.B.(外)**	F.B.(外)**	F.B.(外)**
	フレーム寸法**	(mm)	14.5×2.5	40×5	24×5

※1：外面付を示す。　※3：第1列で溶接したもの。

※2：高さ×板厚を示す。

Figure 57: Numerical Analysis of Esslinger [140]

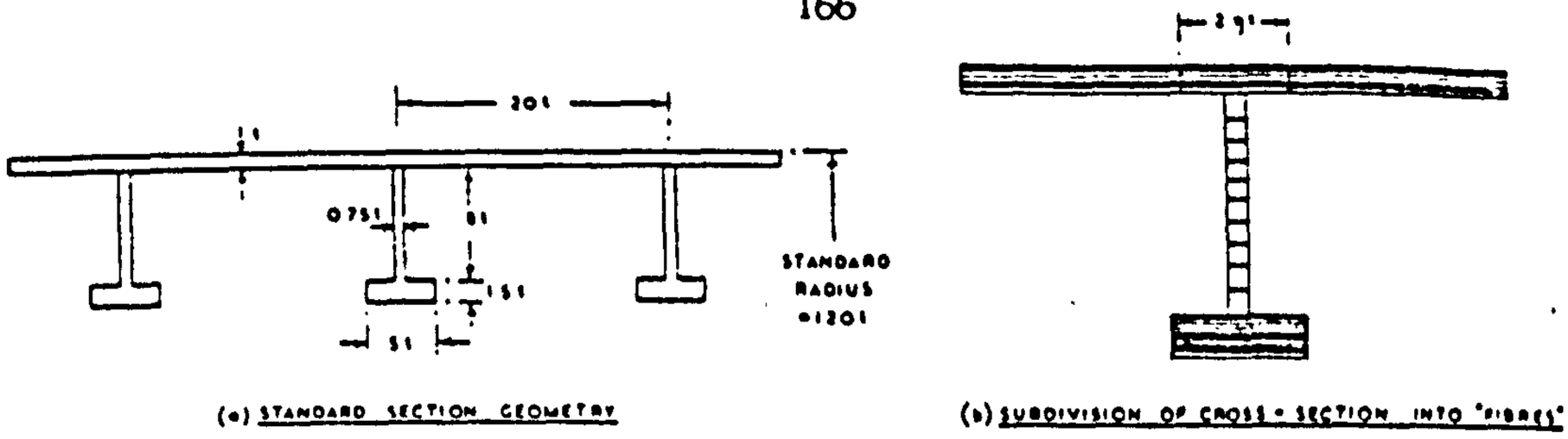

Geometry of ring-stiffened cylinders

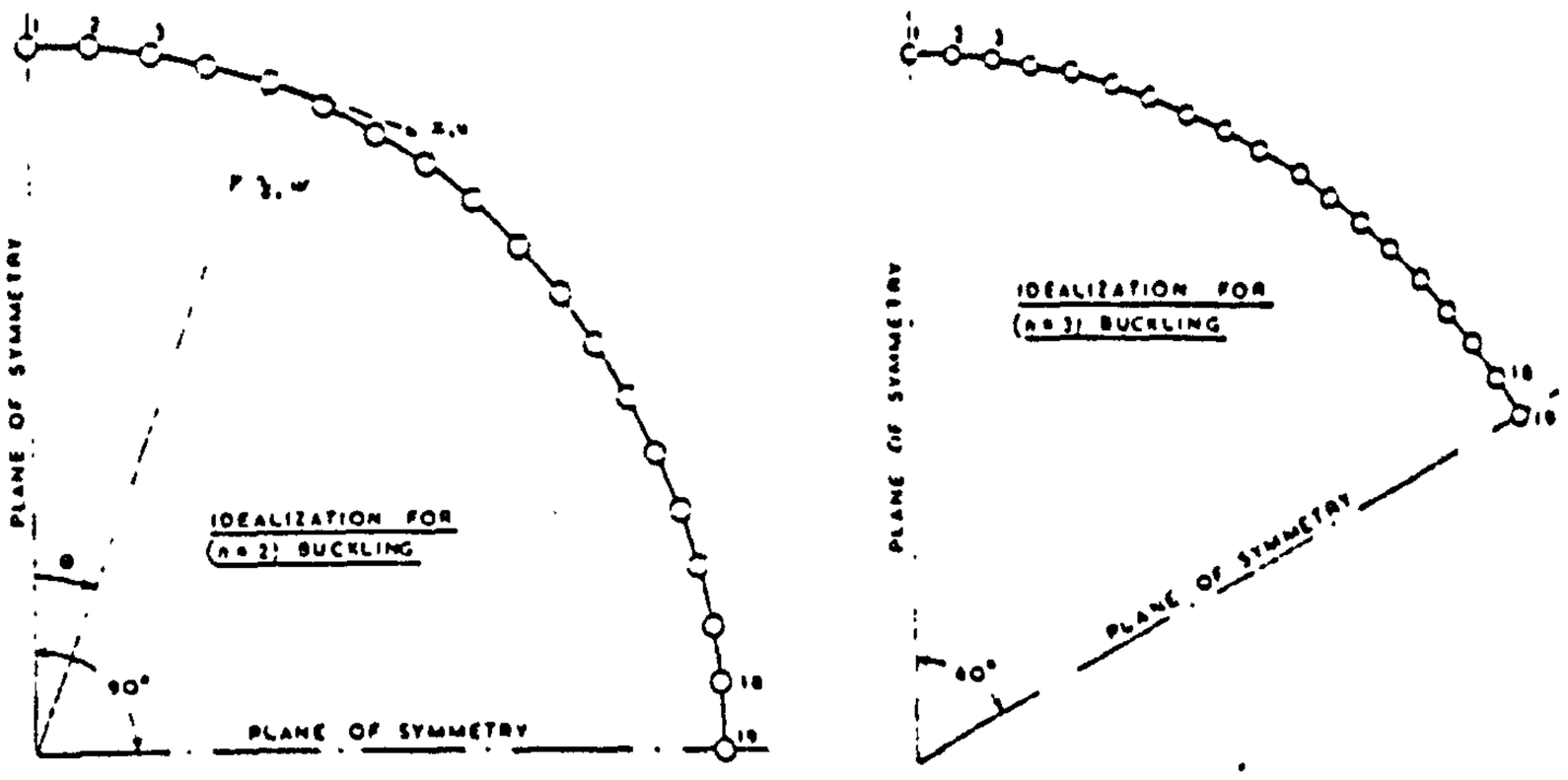

Ring frame finite element idealisation

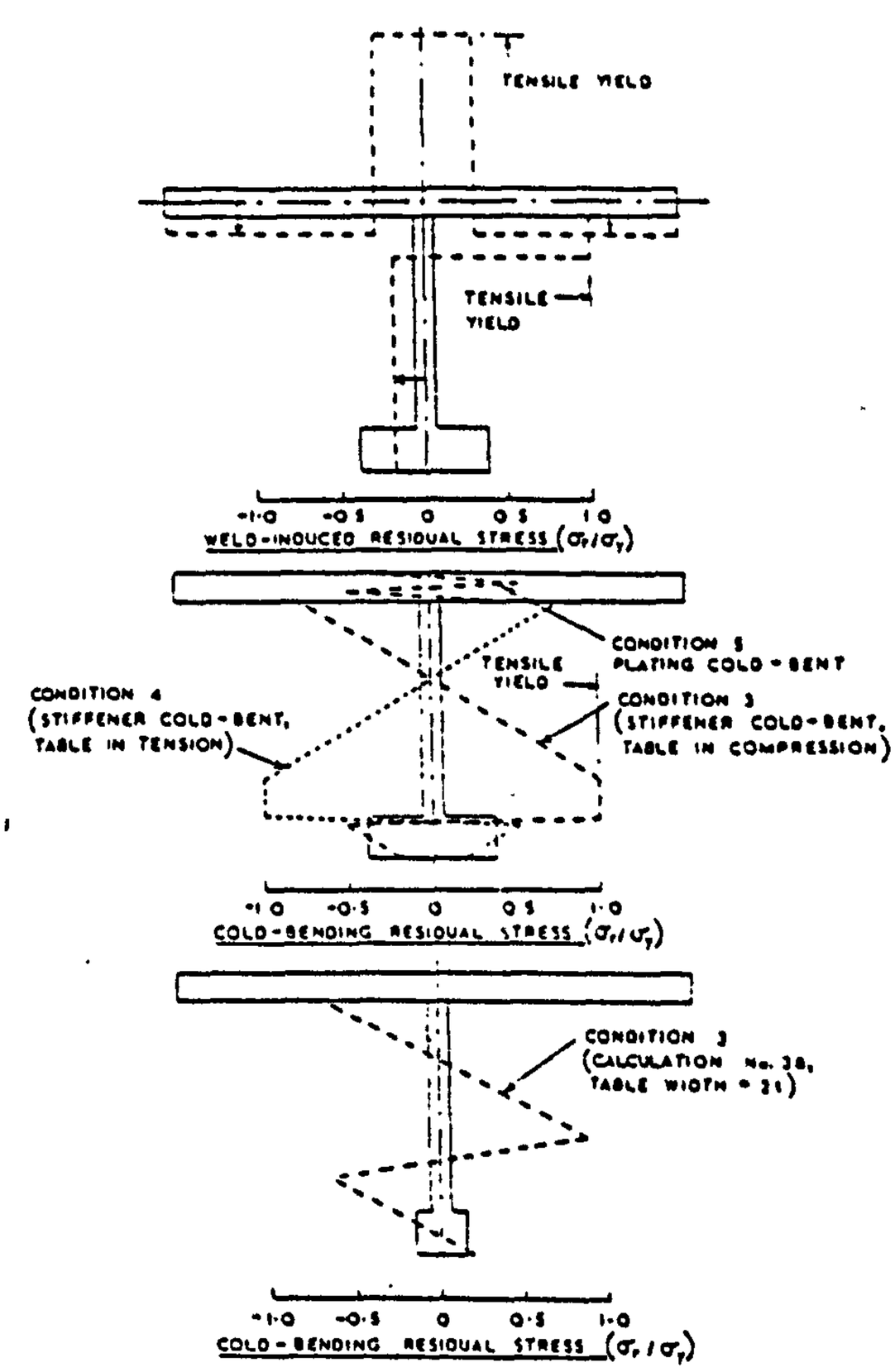

Residual stress distributions in ring-stiffened cylinders

Figure 58: Numerical Analysis of Smith and Kirkwood [72]

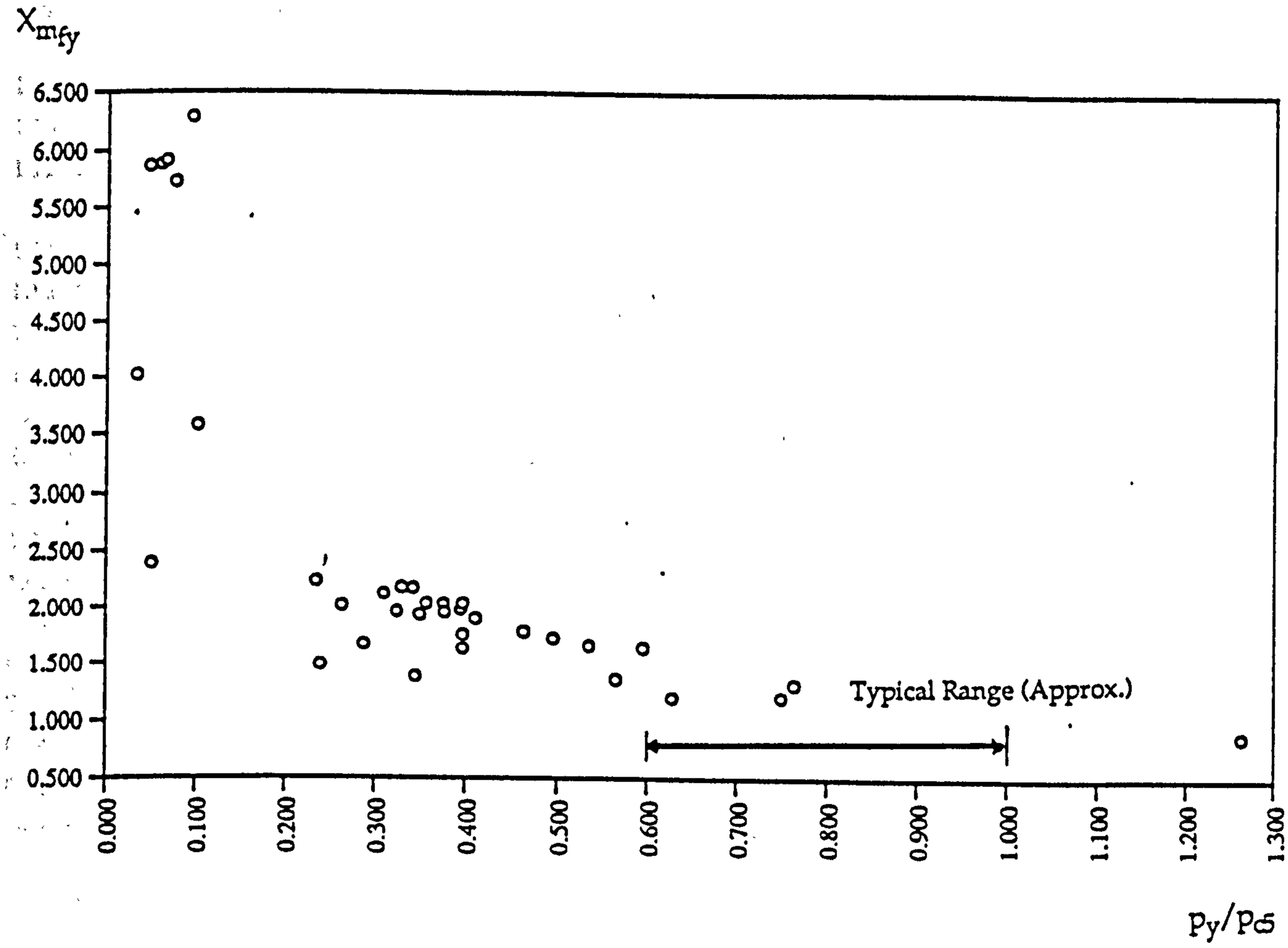

Figure 59: $X_{m_{fy}}$ vs. p_y/p_{cs}, 35 Fabricated Models Failing by General Instability

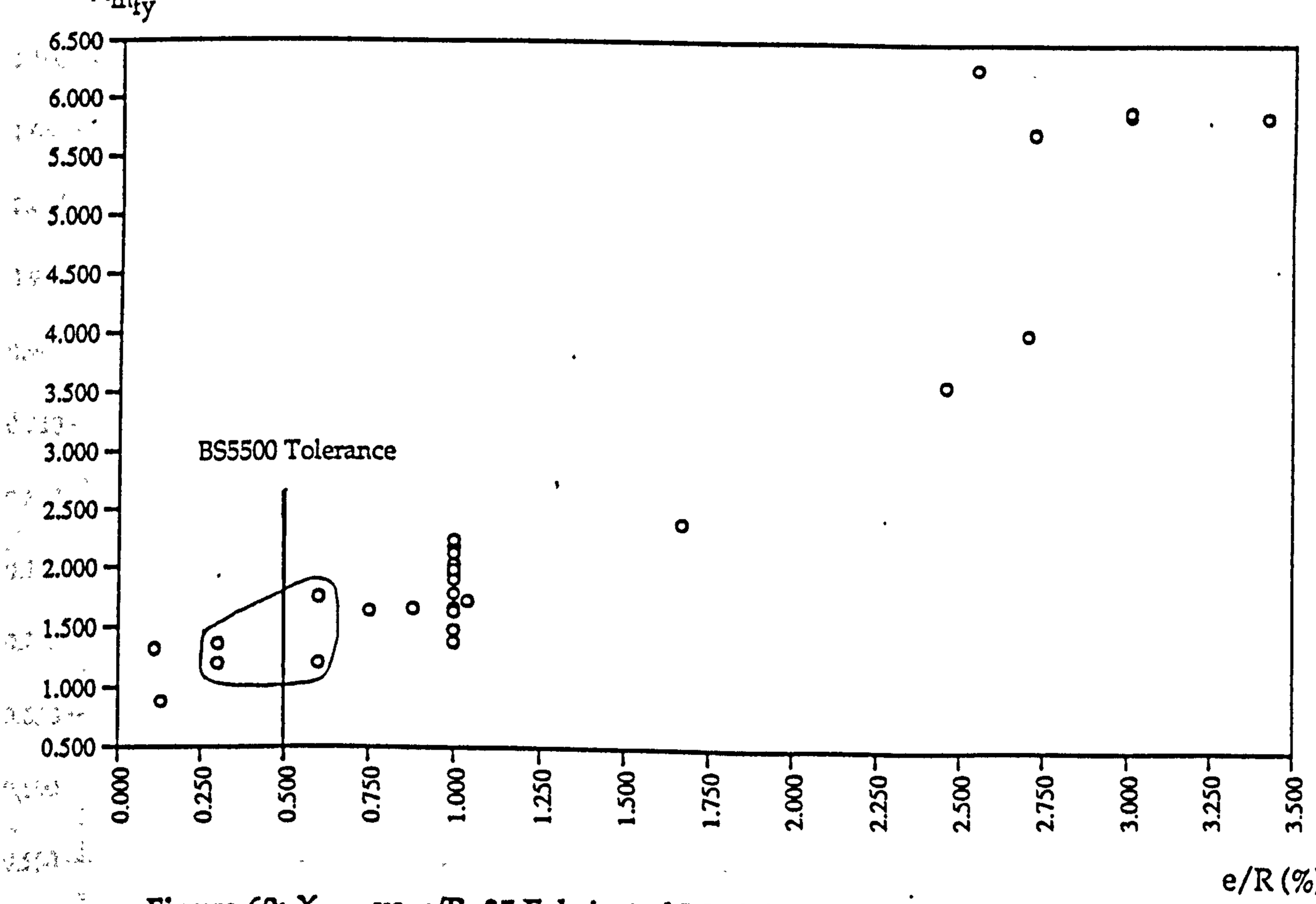

Figure 60: $X_{m_{fy}}$ vs. e/R, 35 Fabricated Models Failing by General Instability

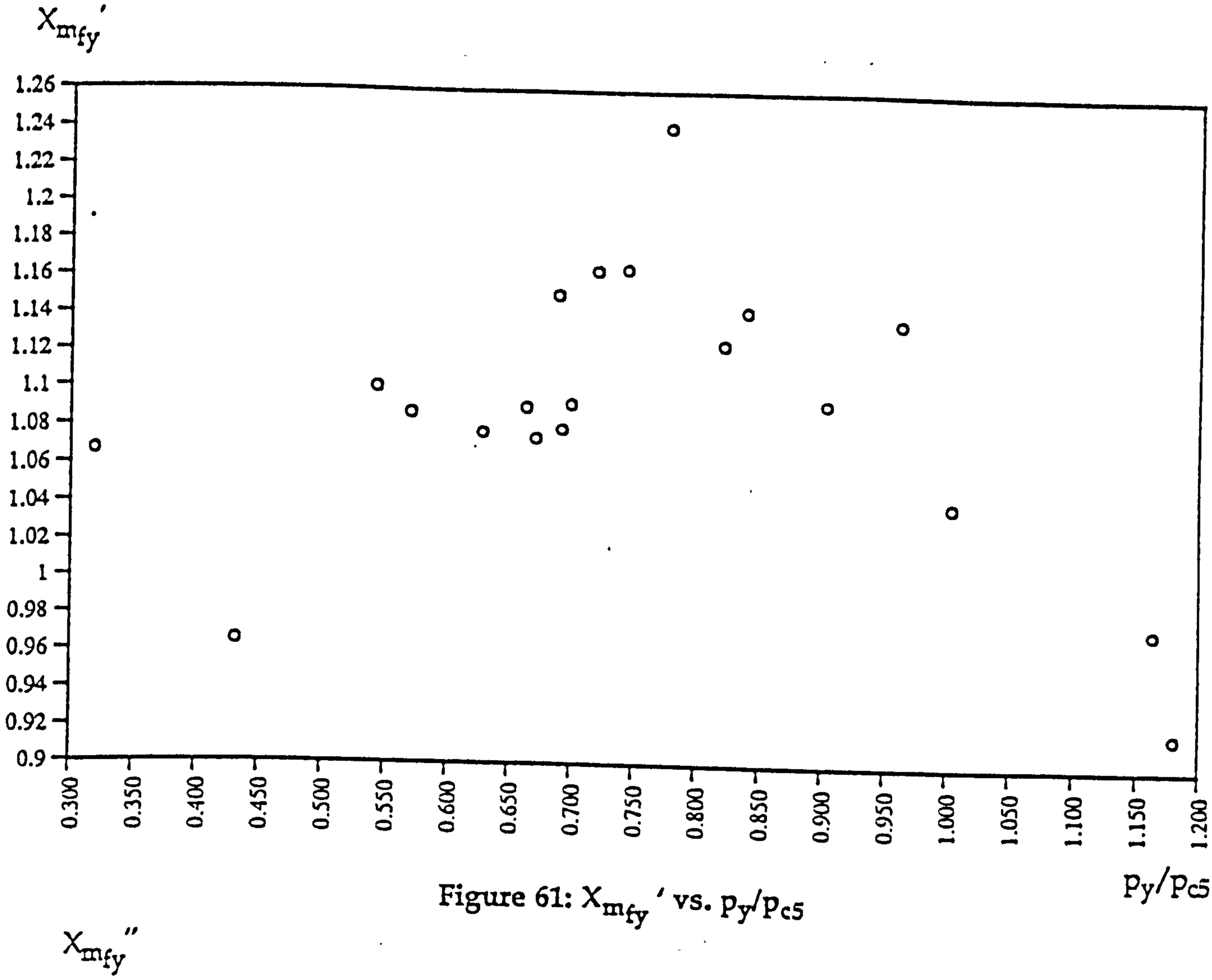

Figure 61: X_{mfy}' vs. p_y/p_{c5}

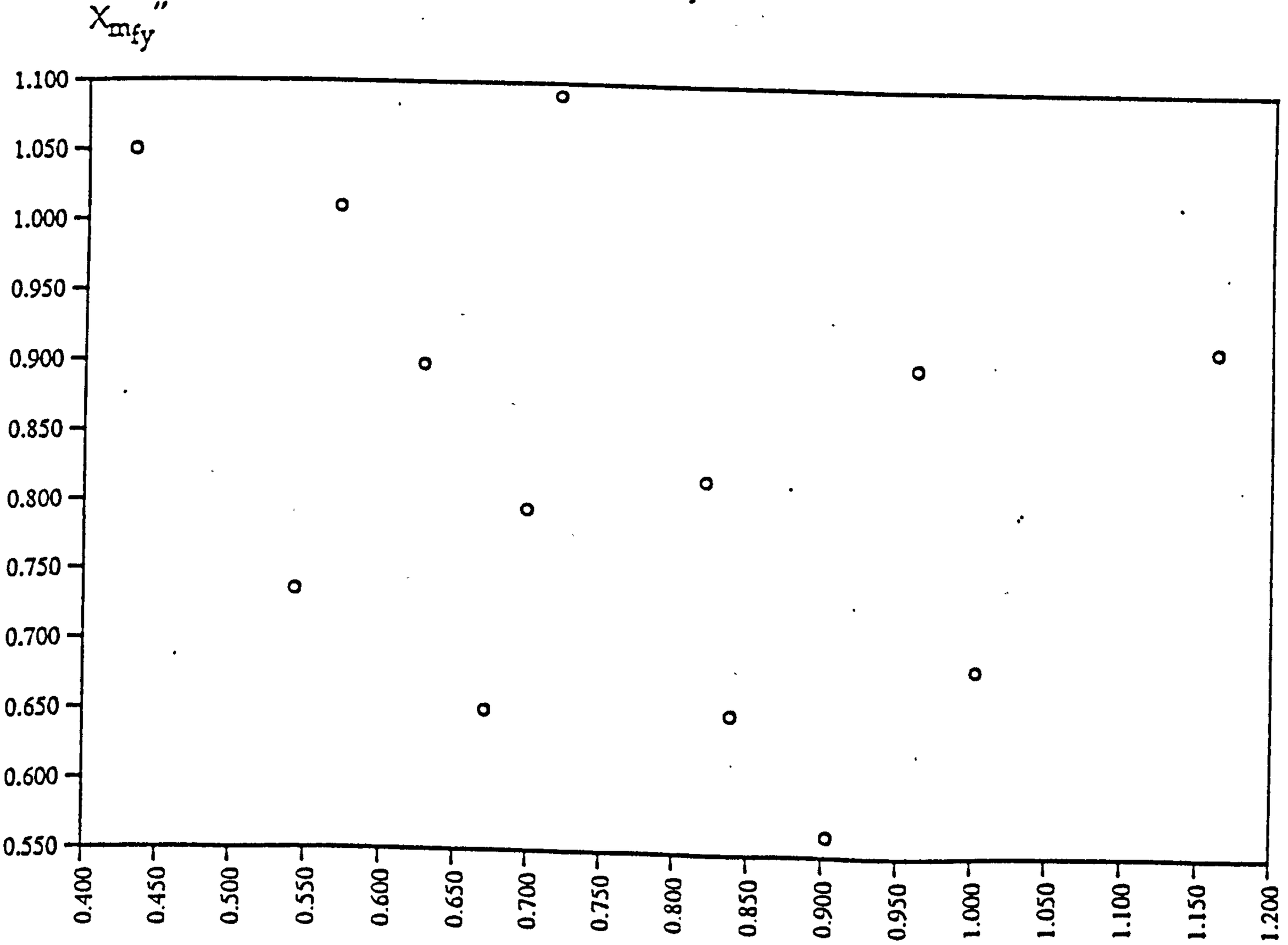

Figure 62: X_{mfy}'' vs. p_y/p_{c5}

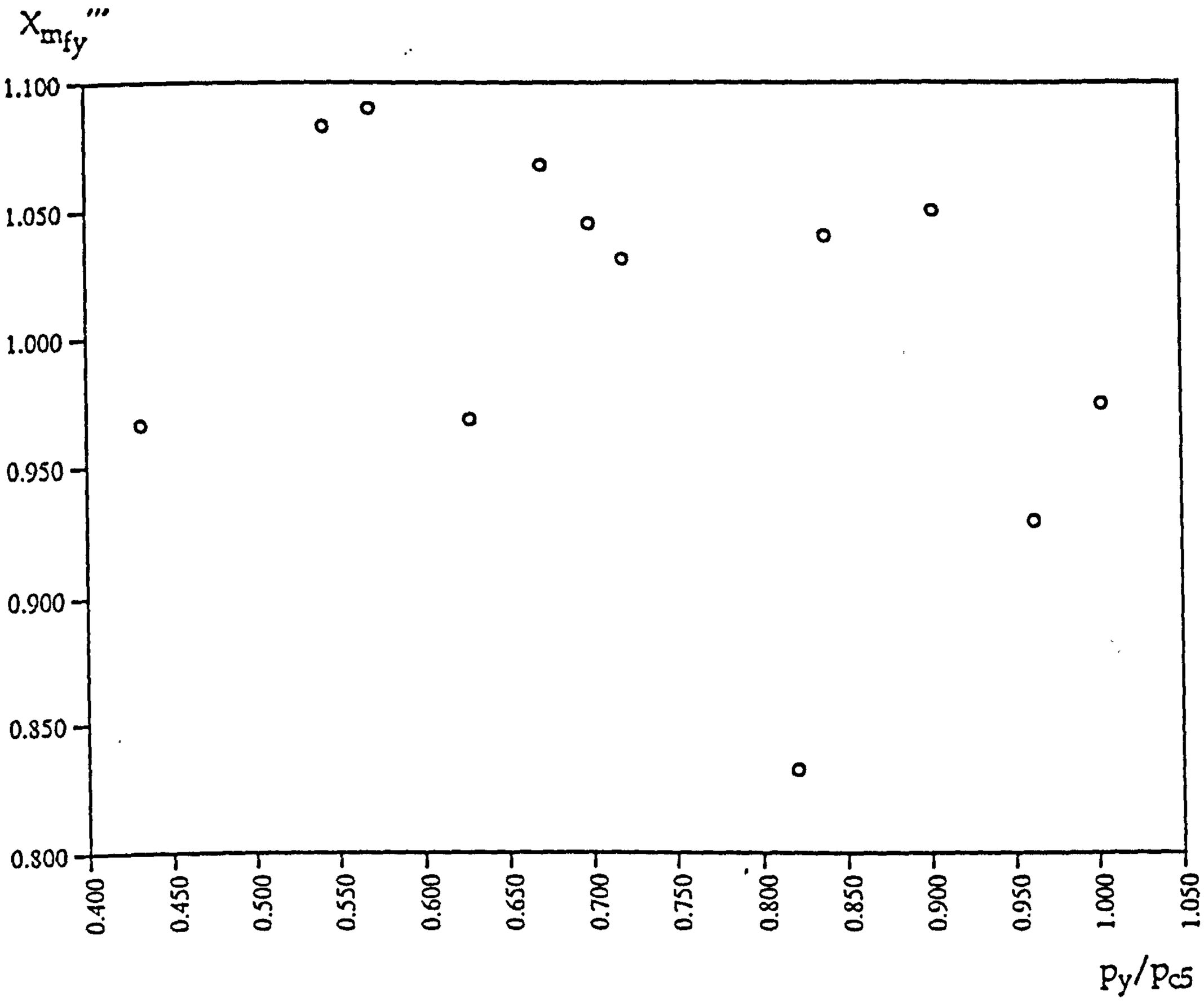

Figure 63: X_{mfy}''' vs. p_y/p_{c5}

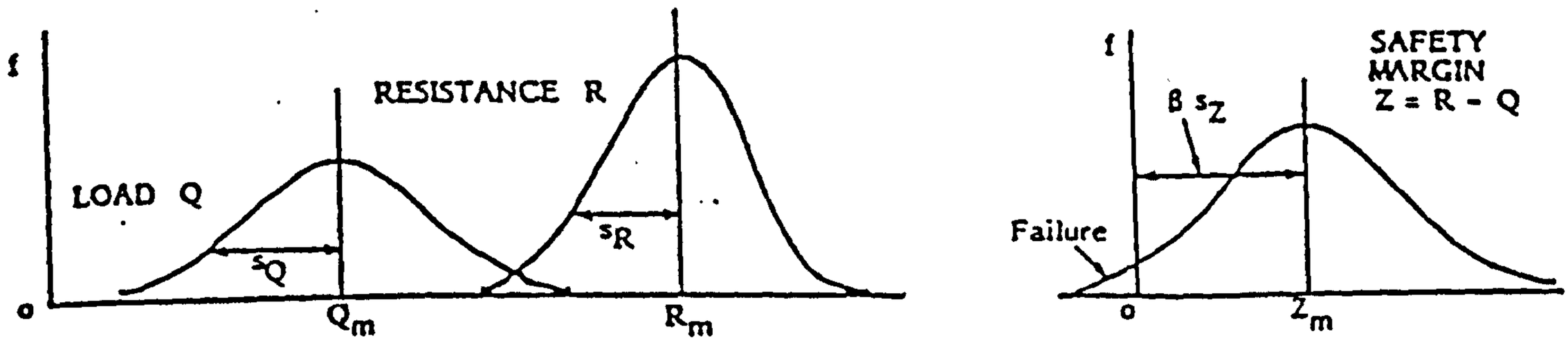

The notional probability of failure is then given by:

$$p_f = \Phi(-\beta)$$

Figure 64: Idealisations of Loading, Strength and Safety Margin Distributions, [25]

$$Z=R-Q \Rightarrow g(X_1, X_2,\ldots,X_n) \quad \begin{matrix} <0 \text{ Safe} \\ \geq 0 \text{ Unsafe} \end{matrix} \Rightarrow p_f = \int_{x1}\ldots\int_{xn}\underset{\text{Dom.}}{} f(x_1, x_2,\ldots, x_n)dx_1dx_2\ldots dx_n$$

Analytical Methods (Level II)

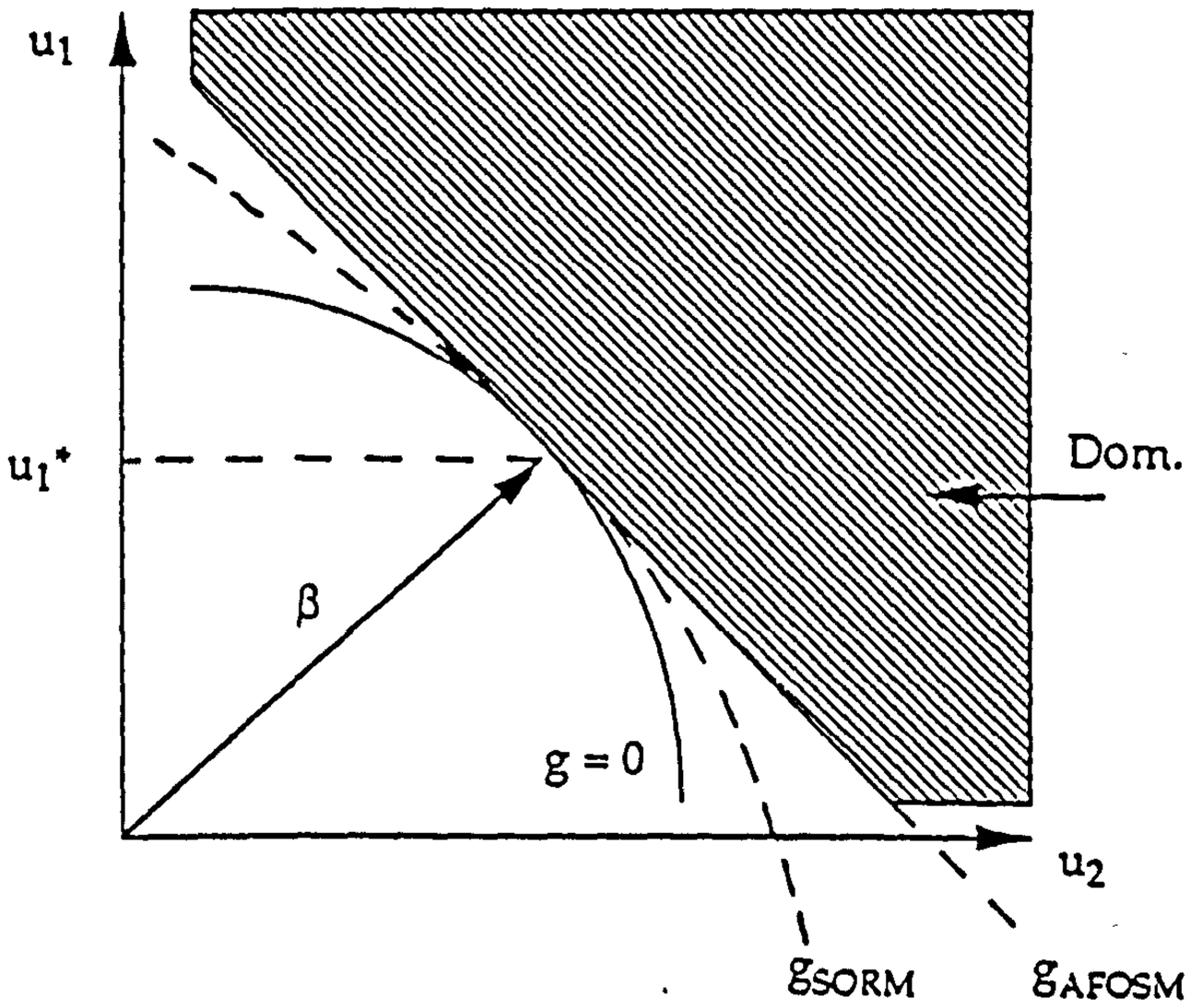

AFOSM: $g=0, -\beta+\sum c_i u_i$

$p_f = \Phi(-\beta)$

SORM: $g=0, -\beta+\sum \kappa_i u_i^2$

$p_f \sim \Phi(-\beta)\prod(1+\beta\kappa)^{-1/2}$

or Tvedt's integral [186]

Problems:
- Multiple modes
- Highly curved g

Simulation Methods (Level III)

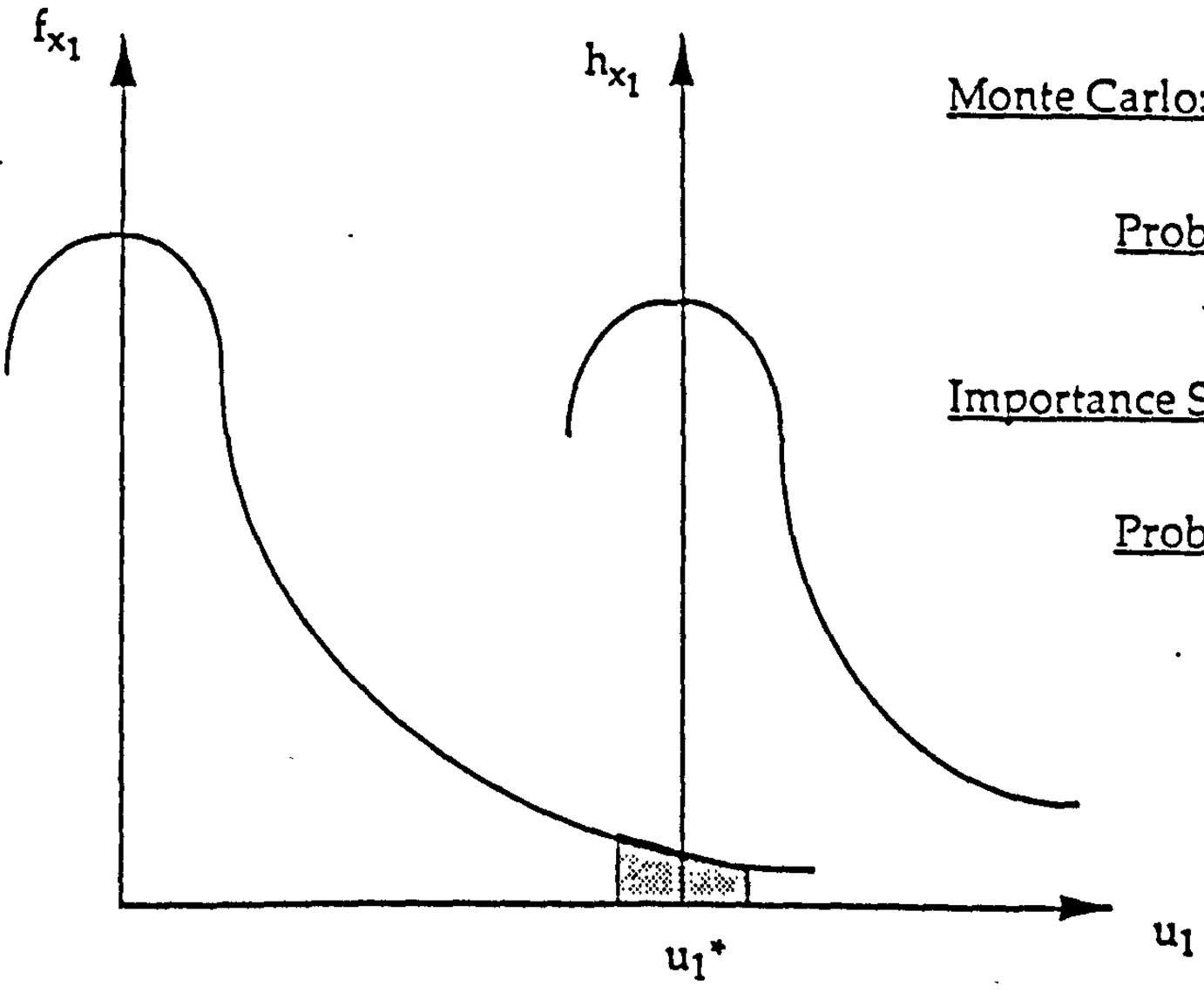

Monte Carlo: $p_f = \dfrac{\text{number of failures}}{\text{number of samples}}$

Problem: number of samples $> \dfrac{100}{p_f}$

Importance Sampling: Use of h_{x_1}

Problems:
- Multiple Modes
- Choice of h_{x_1}

Figure 65: Reliability Methods

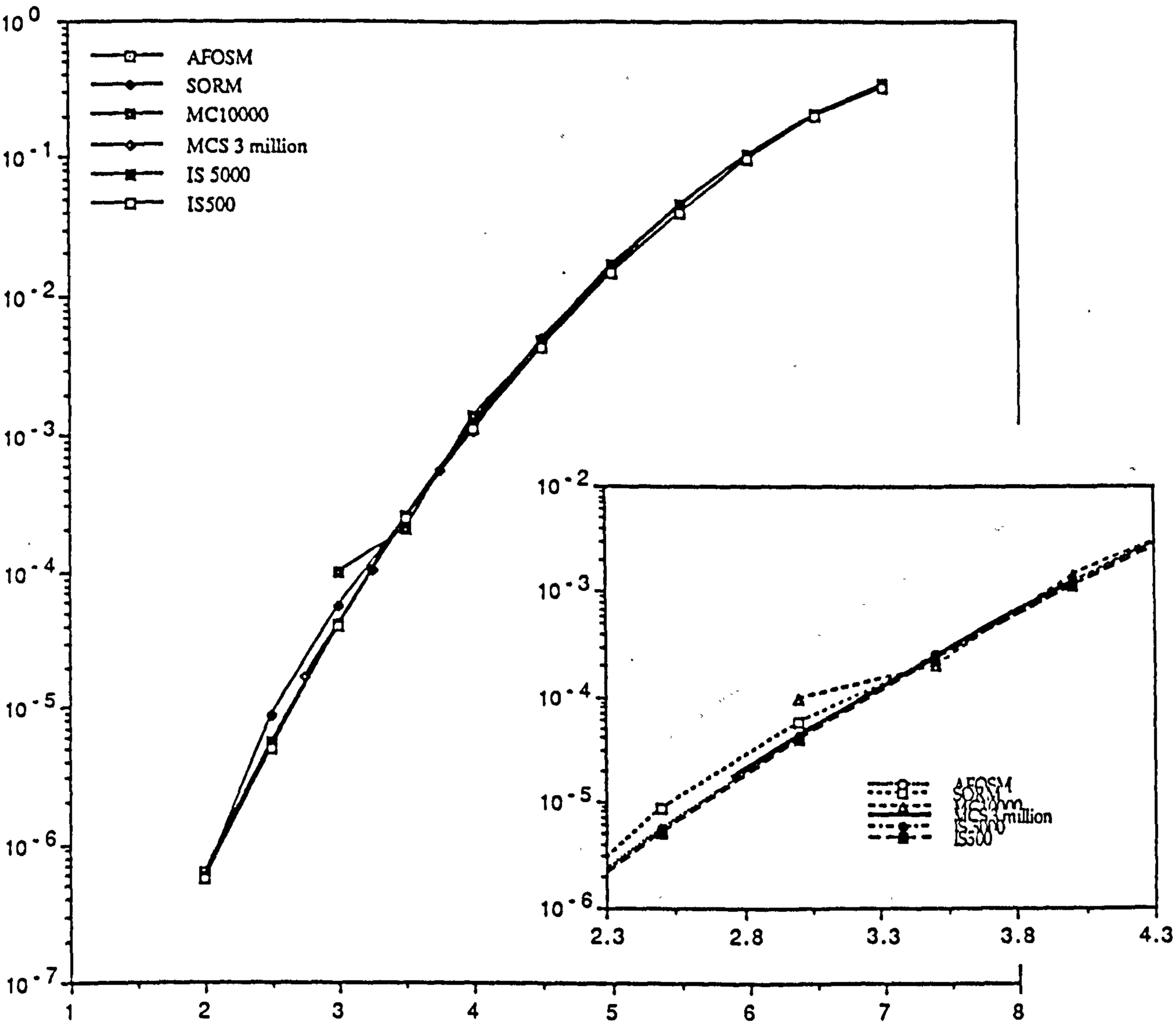

p (N/mm²)	AFOSM	SORM	MC 10000	MC 3.10⁶	IS 5000	IS 500
2.00	6.18E-07	5.52E-07			5.80E-07	5.60E-07
2.50	5.48E-06	8.67E-06			5.30E-06	4.95E-06
3.00	4.04E-05	5.67E-05	1.00E-04	4.20E-05	4.17E-05	3.96E-05
3.50	2.50E-04	2.40E-04	2.00E-04	2.42E-04	2.56E-04	2.39E-04
4.00	1.21E-03	1.11E-03	1.40E-03	1.23E-03	1.25E-03	1.14E-03
4.50	4.87E-03	5.06E-03	4.70E-03		4.93E-03	4.35E-03
5.00	1.63E-02	1.63E-02	1.57E-02		1.66E-02	1.45E-02
5.50	4.56E-02	4.62E-02	4.49E-02		4.49E-02	3.99E-02
6.00	1.04E-01	1.05E-01	1.04E-01		1.04E-01	9.84E-02
6.50	2.04E-01	2.03E-01	2.06E-01		2.04E-01	1.98E-01
7.00	3.44E-01	3.41E-01	3.43E-01		3.44E-01	3.23E-01

Figure 66: Comparison of Reliability Methods, Case 3, Tripping

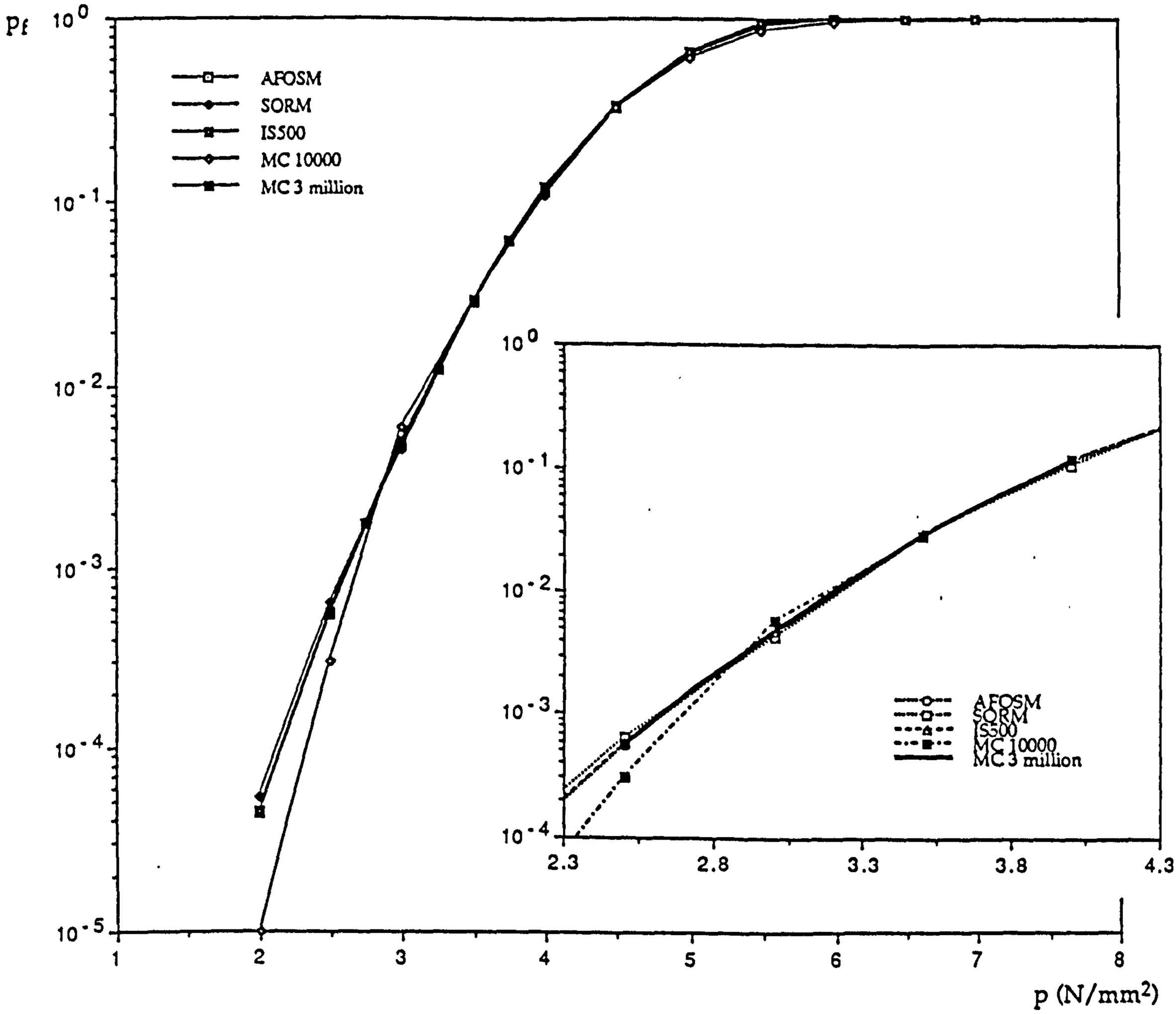

p (N/mm²)	AFOSM	SORM	IS 500	MC 10000	MC 3.10⁶
2.00	4.28E-05	5.28E-05	4.36E-05	1.00E-05	
2.50	5.42E-04	6.33E-04	5.65E-04	3.00E-04	5.50E-04
3.00	4.74E-03	4.45E-03	4.95E-03	6.00E-03	4.86E-03
3.50	2.88E-02	2.93E-02	2.96E-02	2.91E-02	2.89E-02
4.00	1.15E-01	1.07E-01	1.18E-01	1.19E-01	1.16E-01
4.50	3.21E-01	3.18E-01	3.28E-01	3.21E-01	
5.00	6.00E-01	6.04E-01	6.07E-01	6.07E-01	
5.50	8.05E-01	8.09E-01	8.11E-01	8.45E-01	
6.00	9.42E-01	9.46E-01	9.47E-01	9.57E-01	
6.50	9.89E-01	9.93E-01	9.91E-01	9.93E-01	
7.00	9.99E-01	1.00E+00	1.00E+00	9.99E-01	

Figure 67: Comparison of Reliability Methods, Case 3, Total Failure Probability

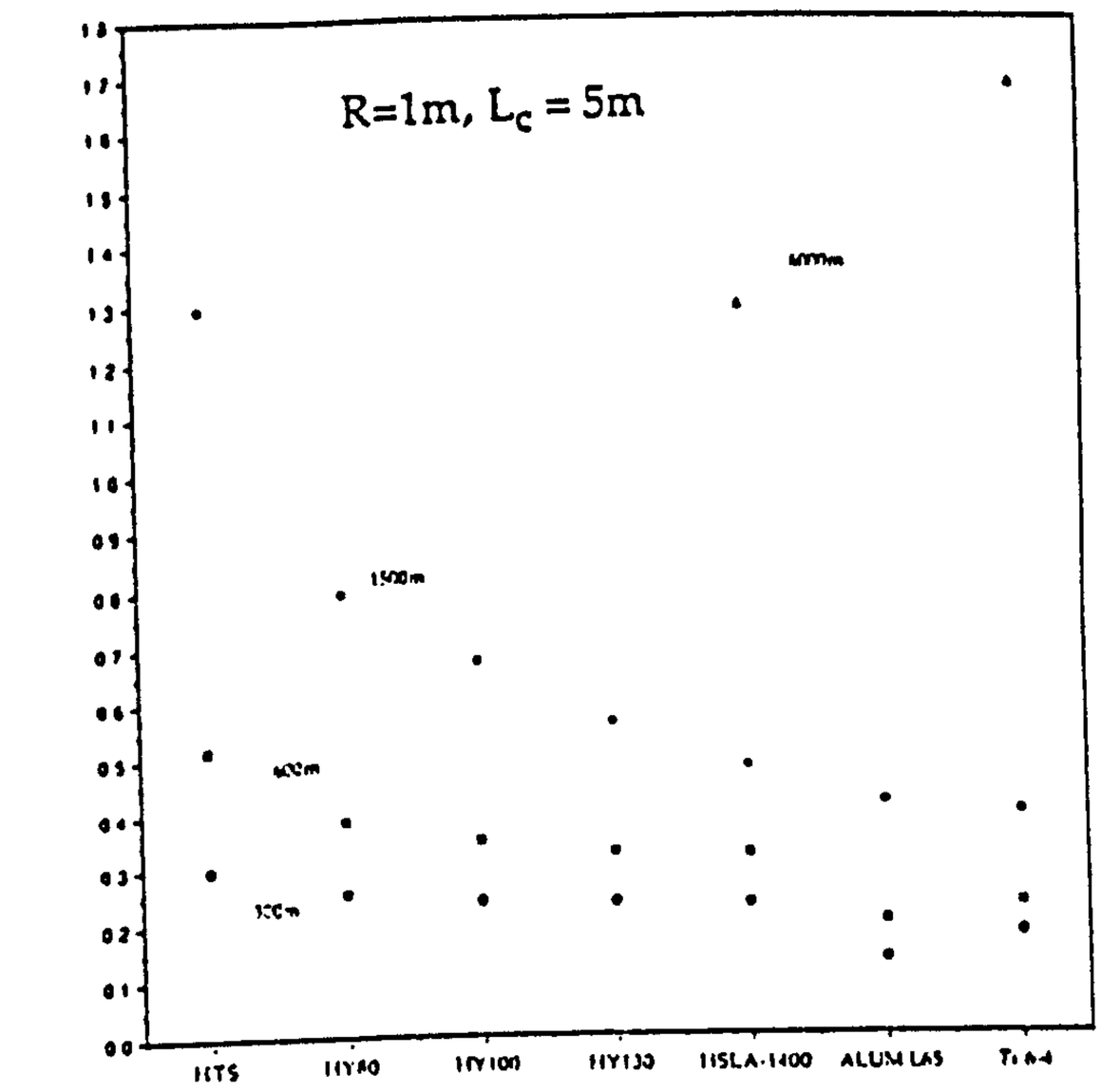

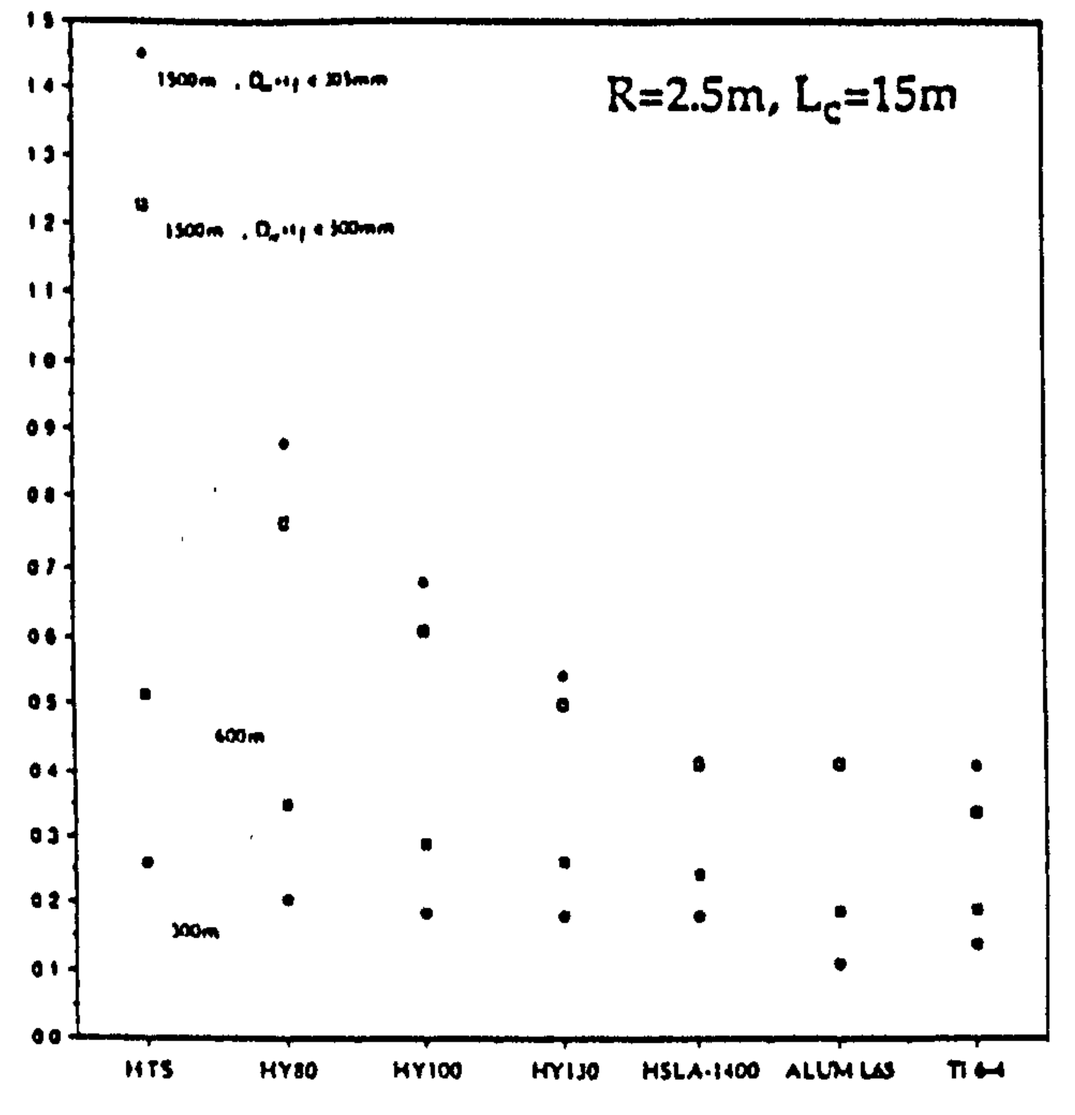

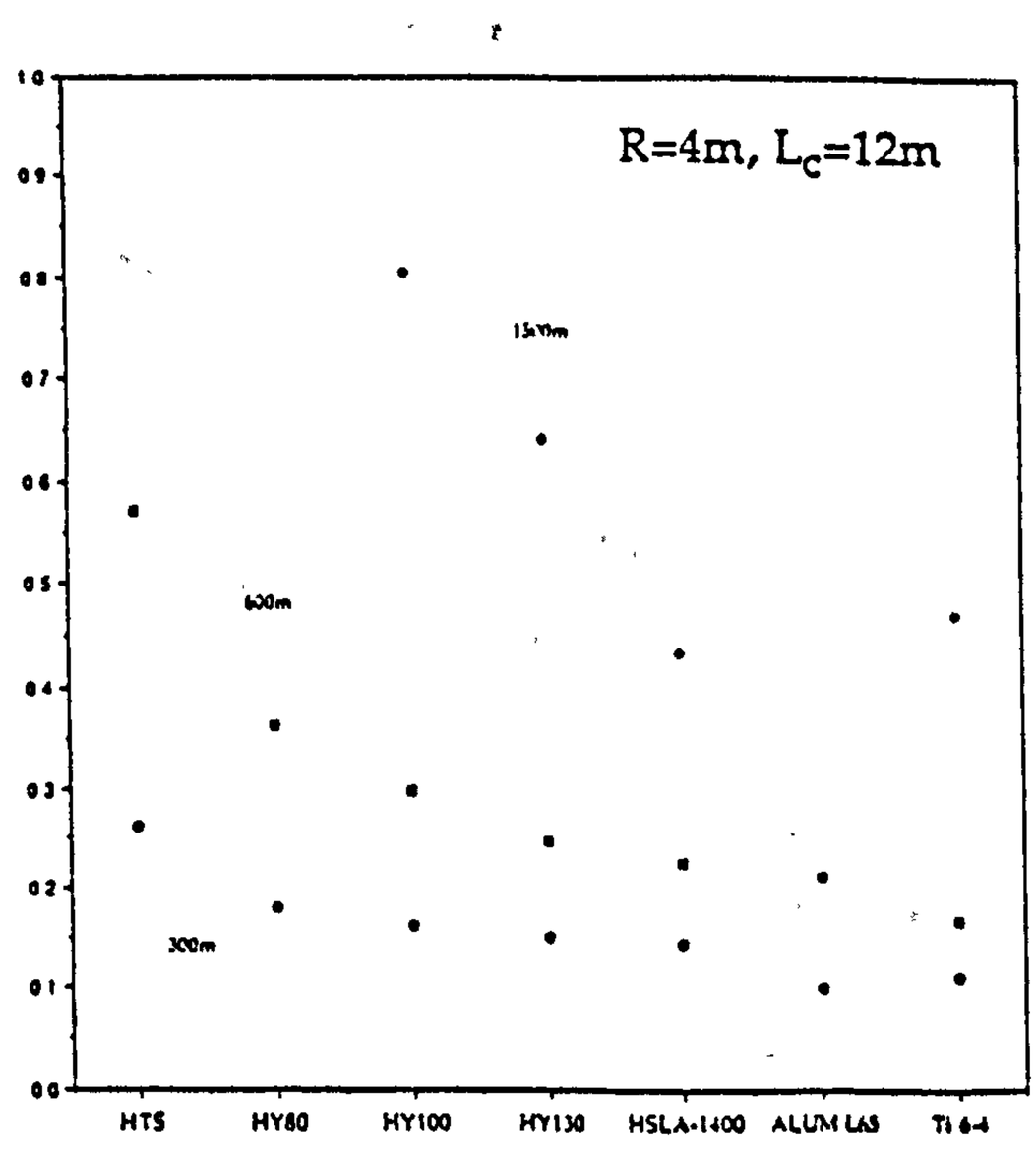

Figure 68: Results of Optimisation Studies [12]

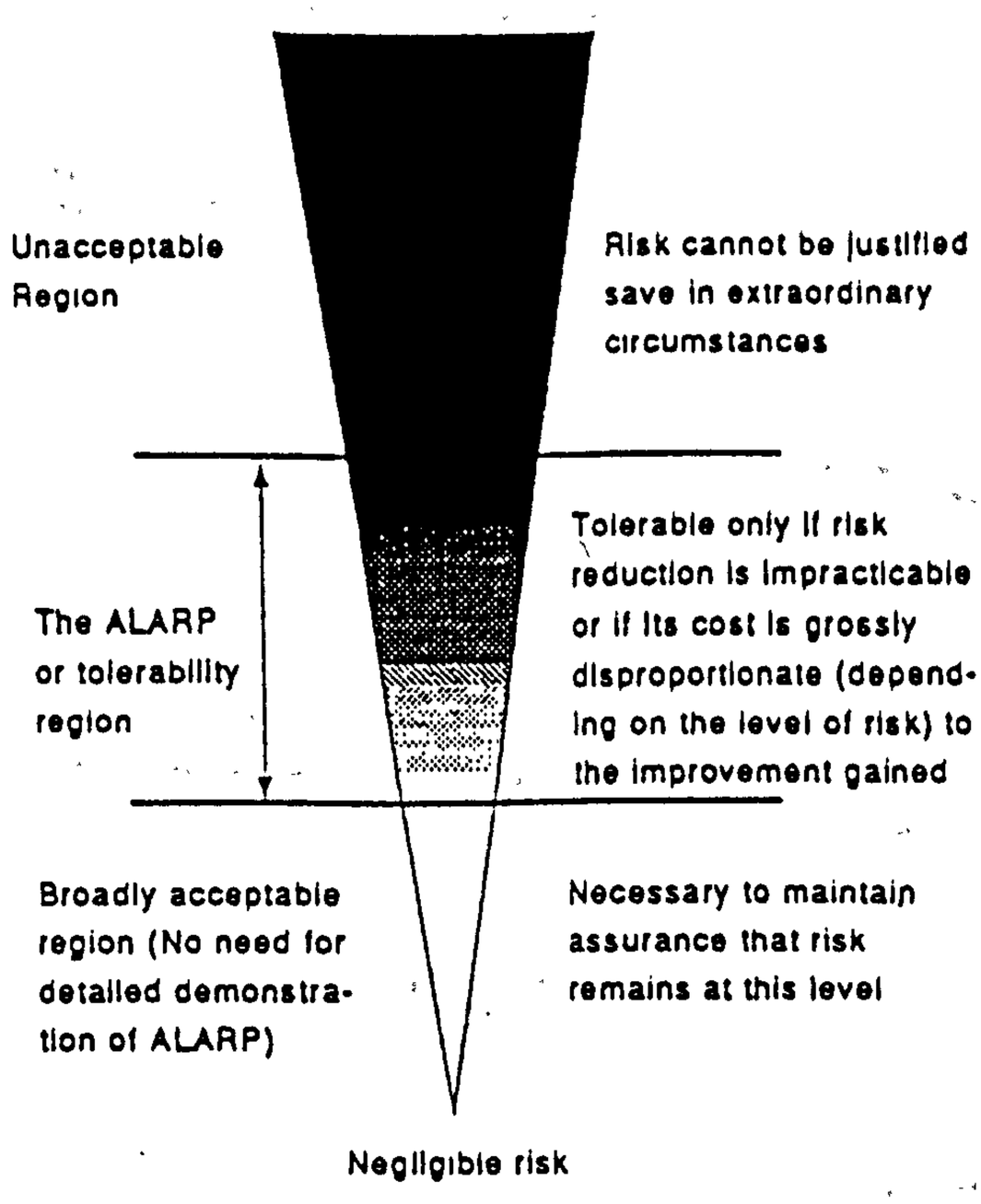

Figure 69: ALARP Principle [205]

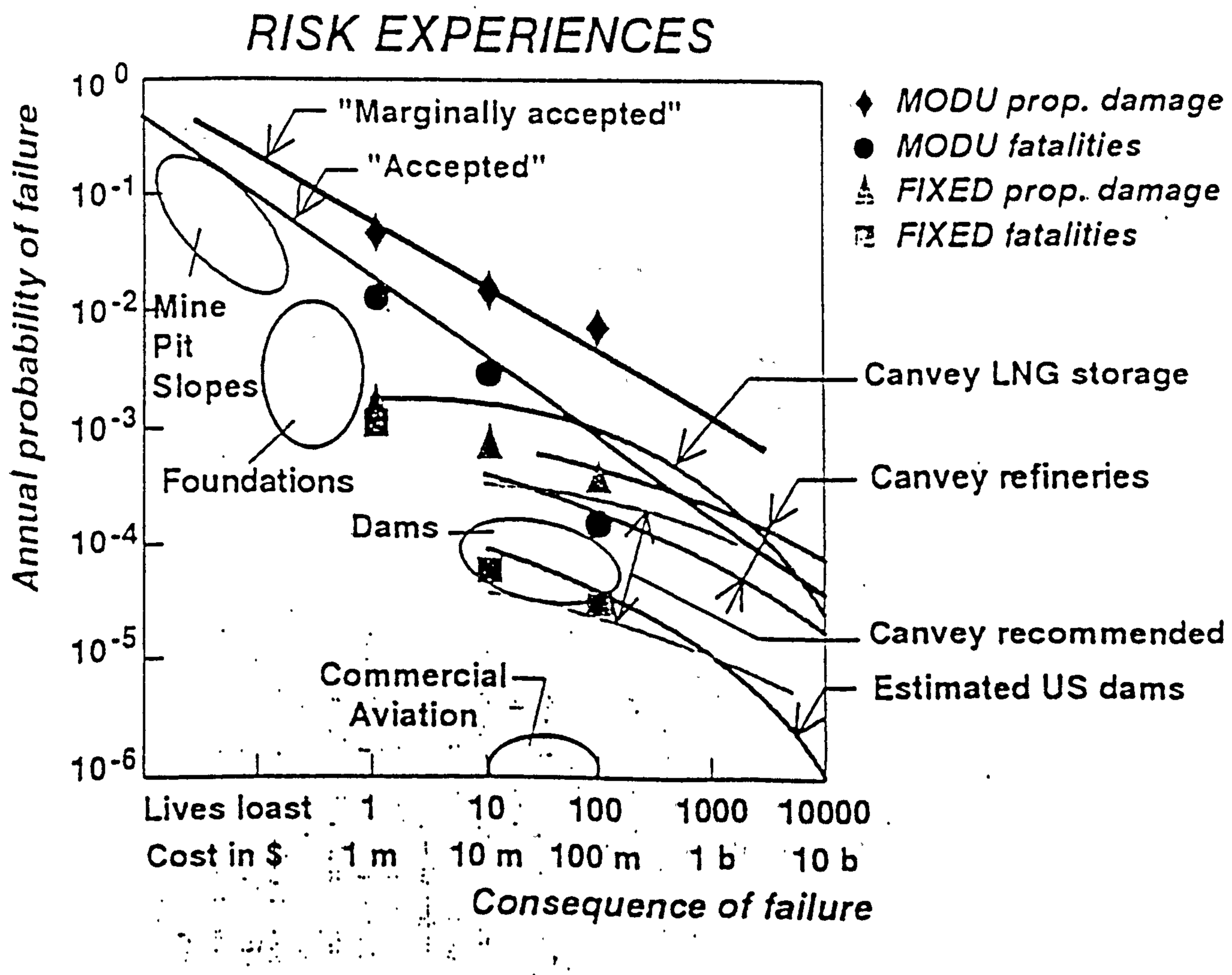

Figure 70: Risk Experiences [206]

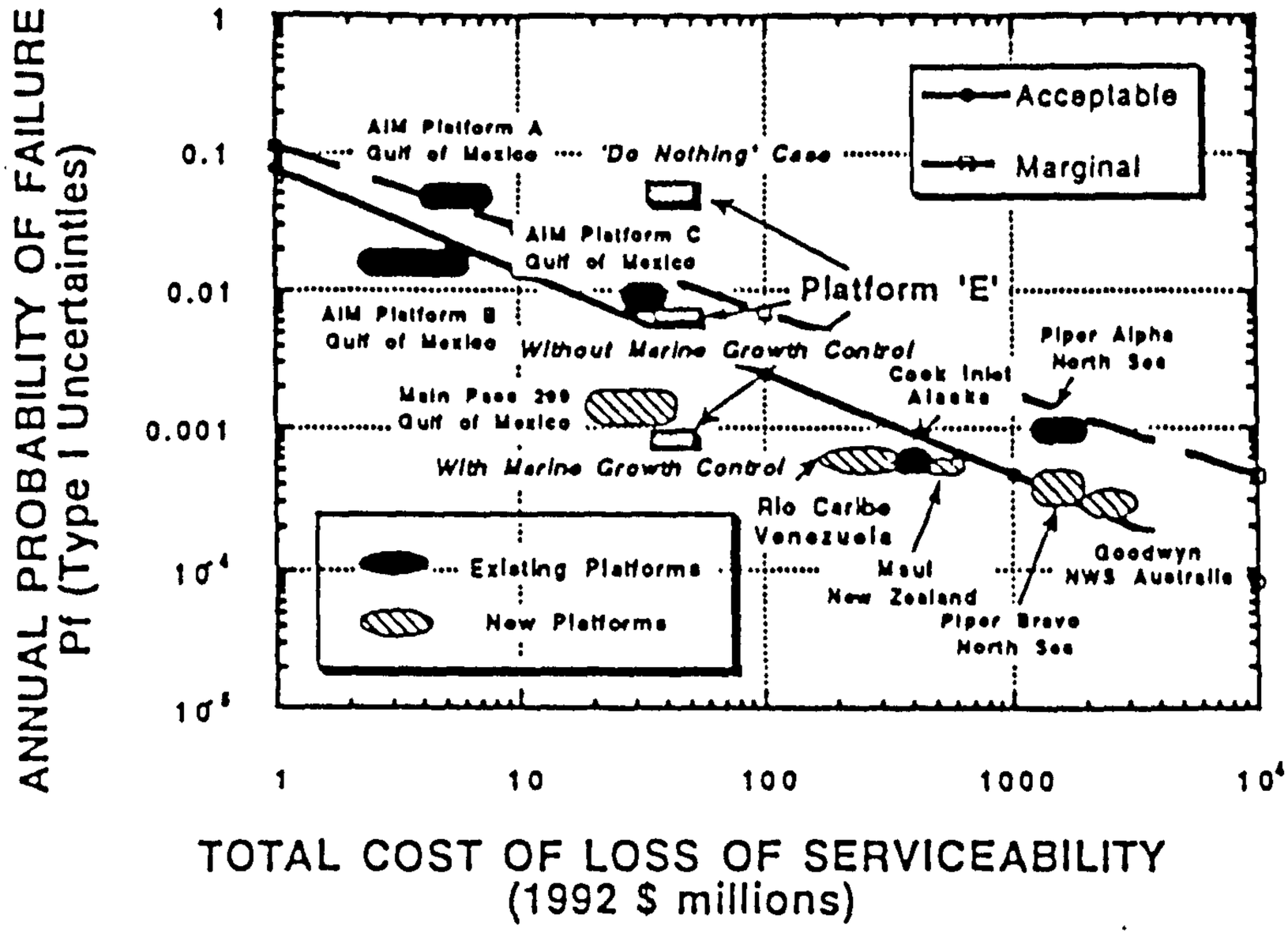

Figure 71: Risk Levels due to Natural Uncertainties Only [207]

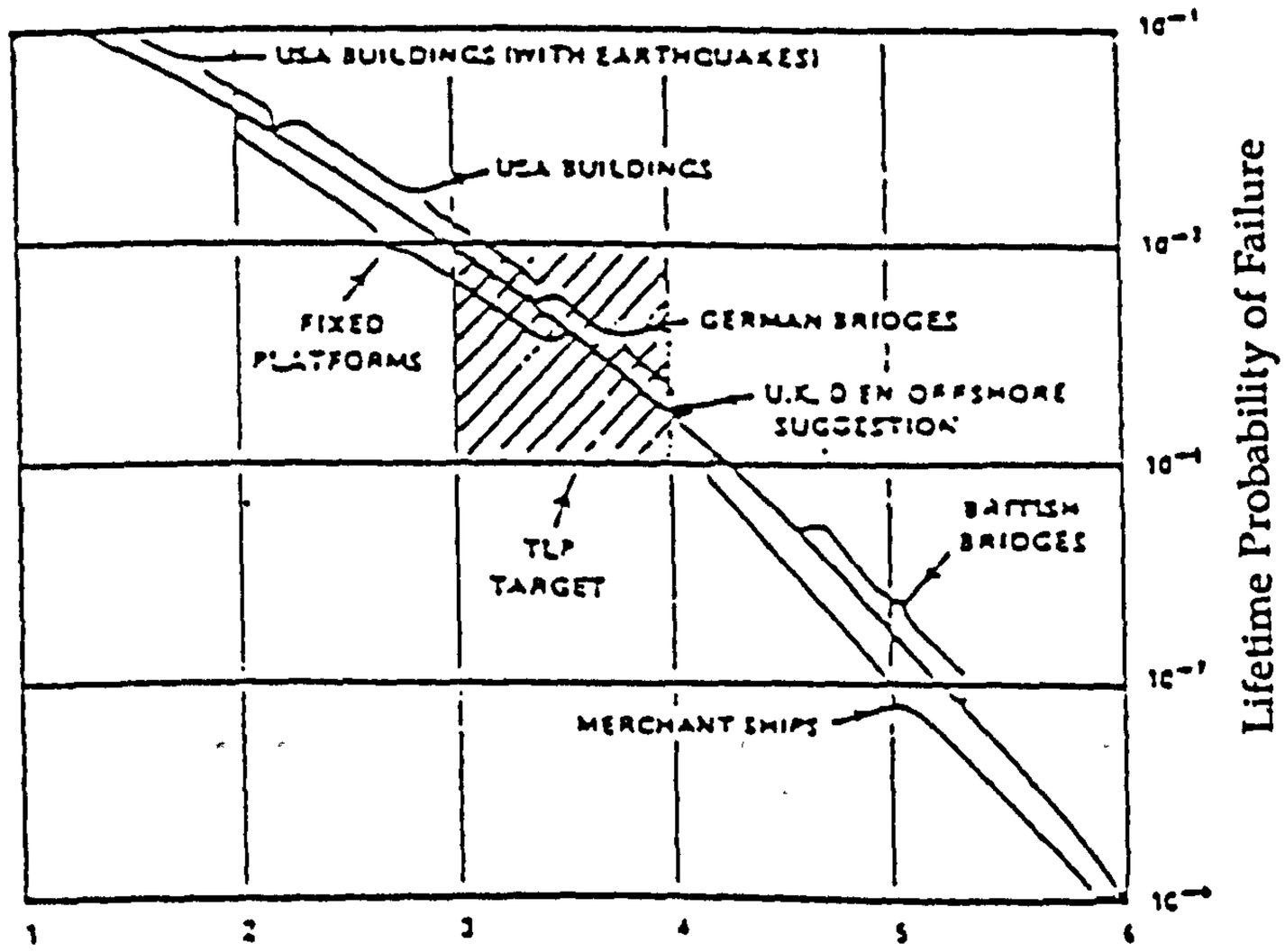

Figure 72: Safety Levels for Various Structures [208]

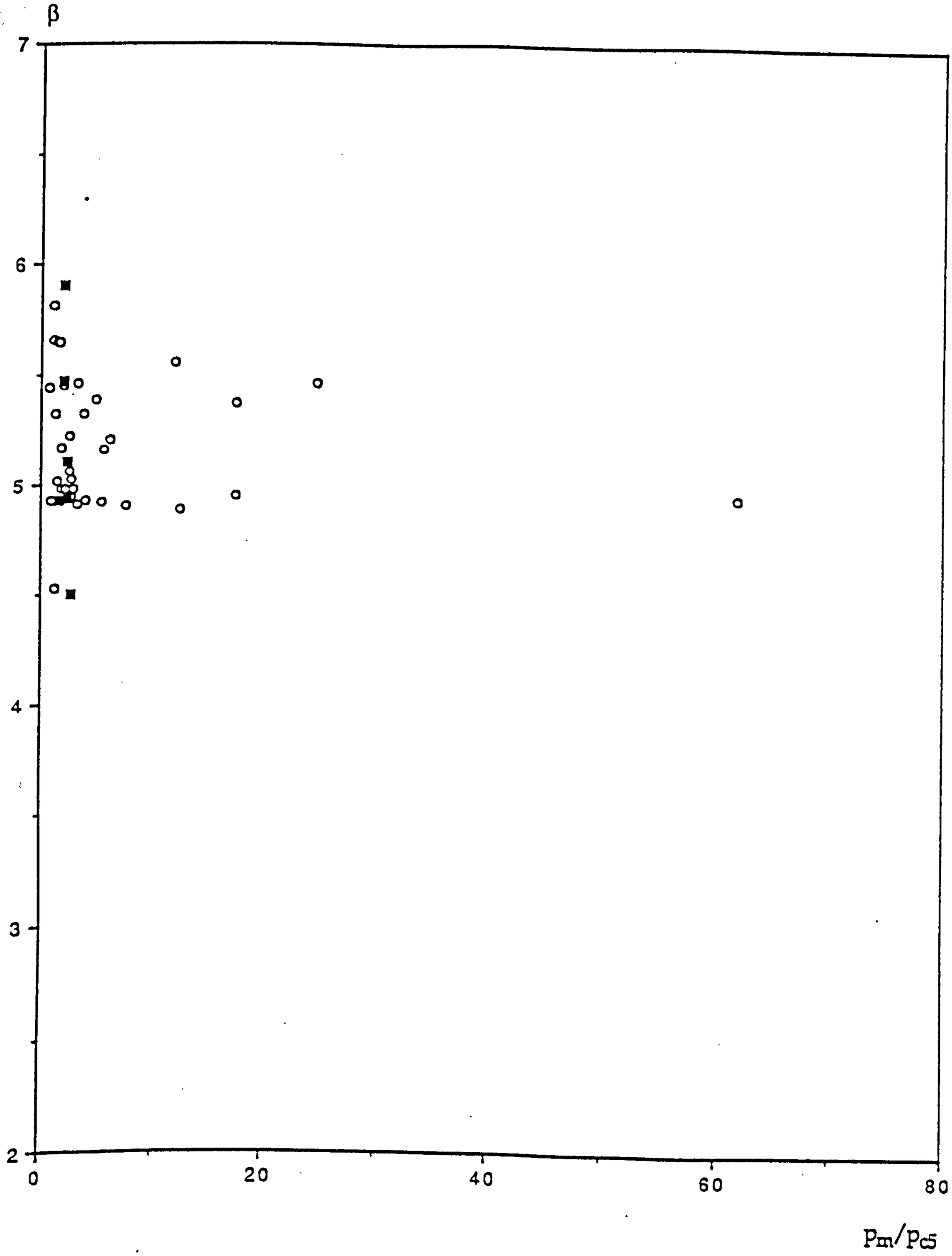

Figure 73: Safety Index, Flange Yield

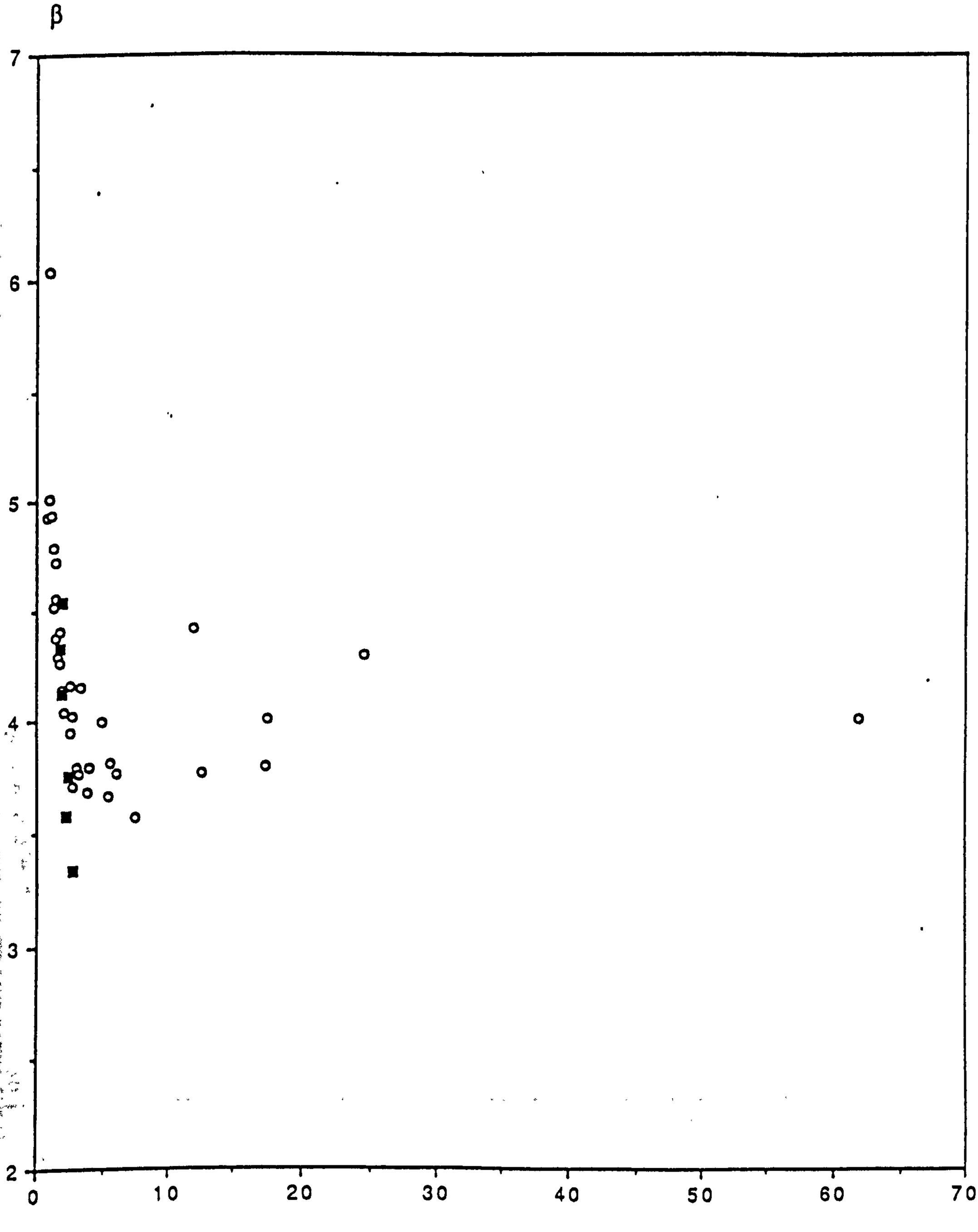

Figure 74: Safety Index, Plate Yield

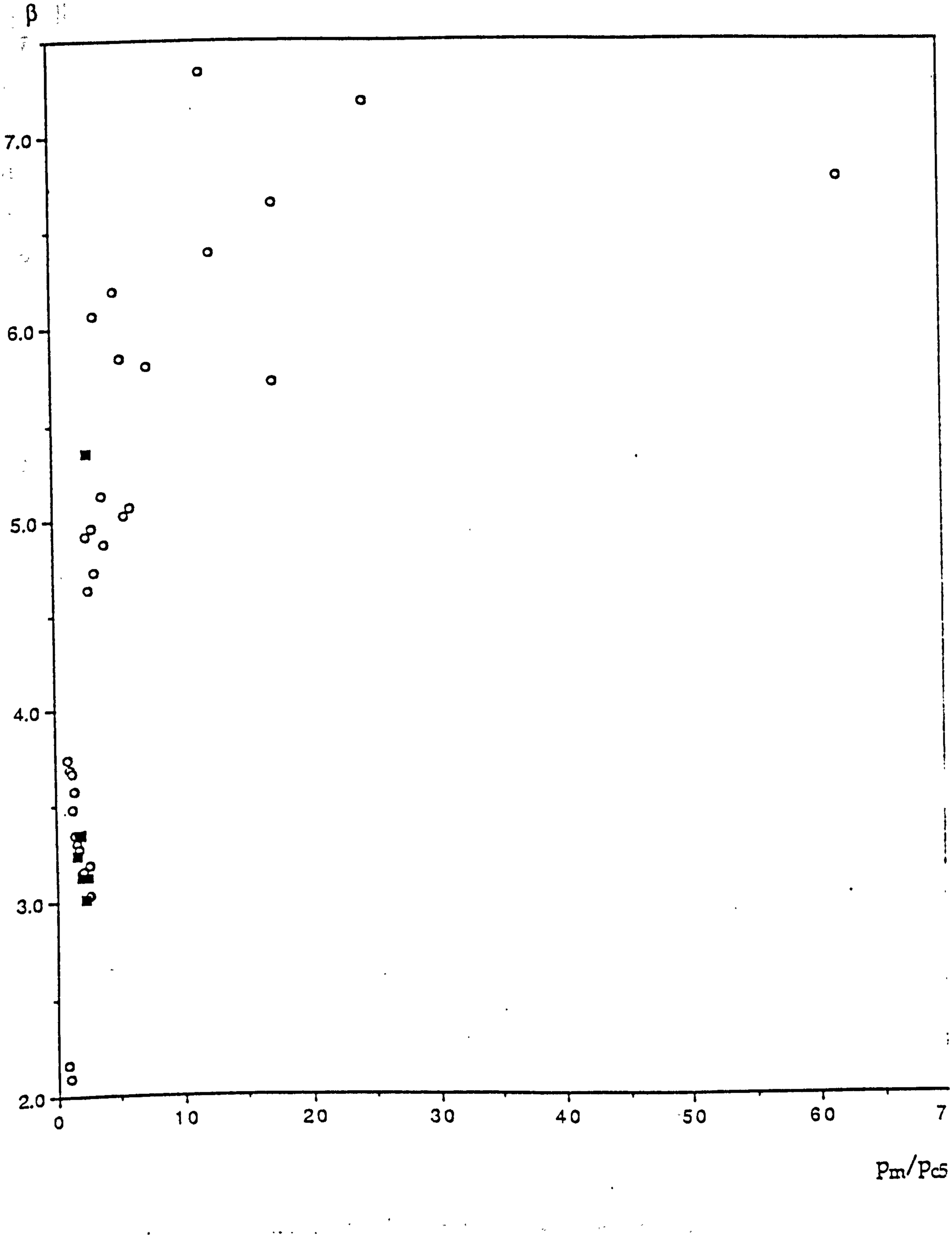

Figure 75: Safety Index, Interframe Shell Collapse

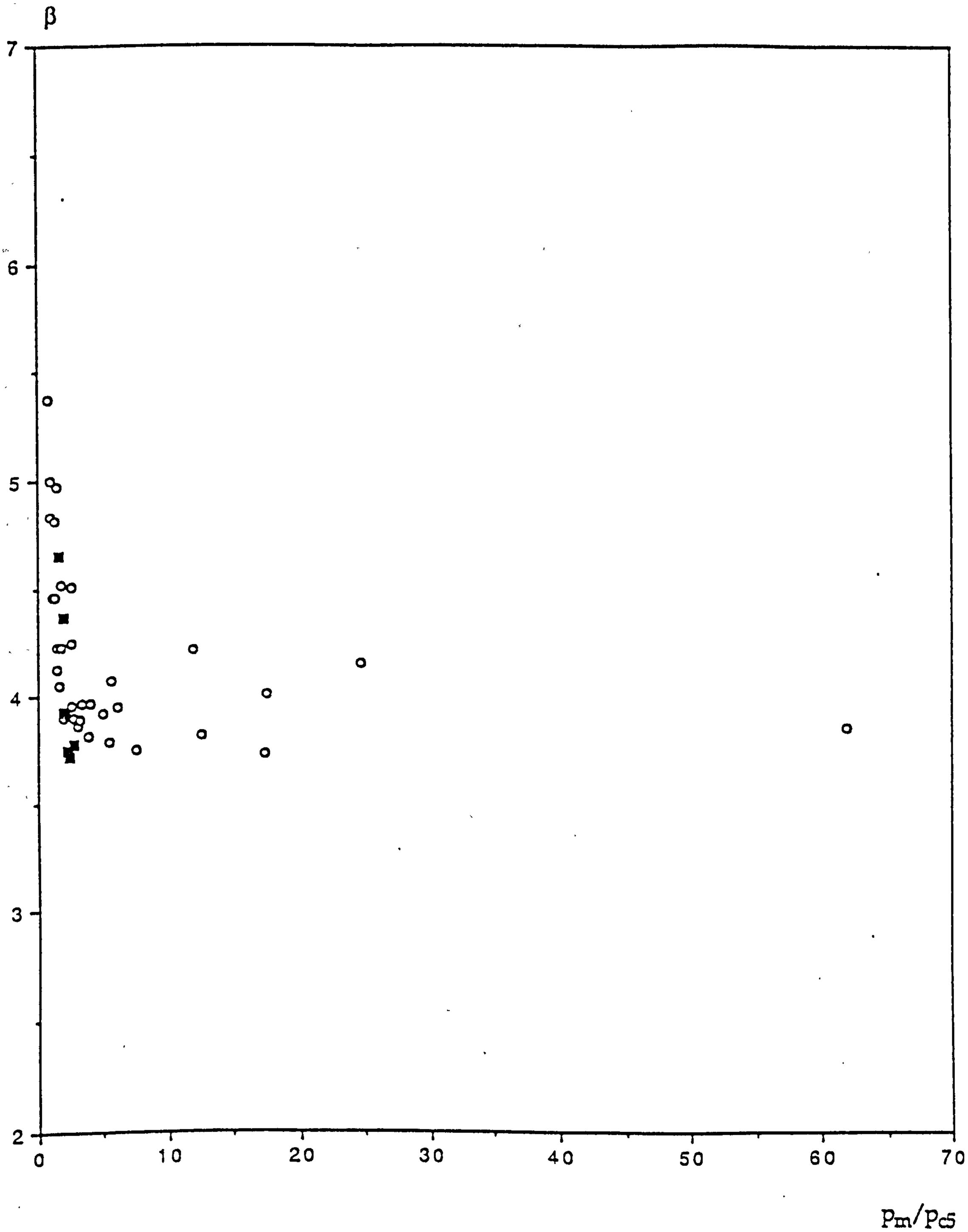

Figure 76: Safety Index, Frame Tripping

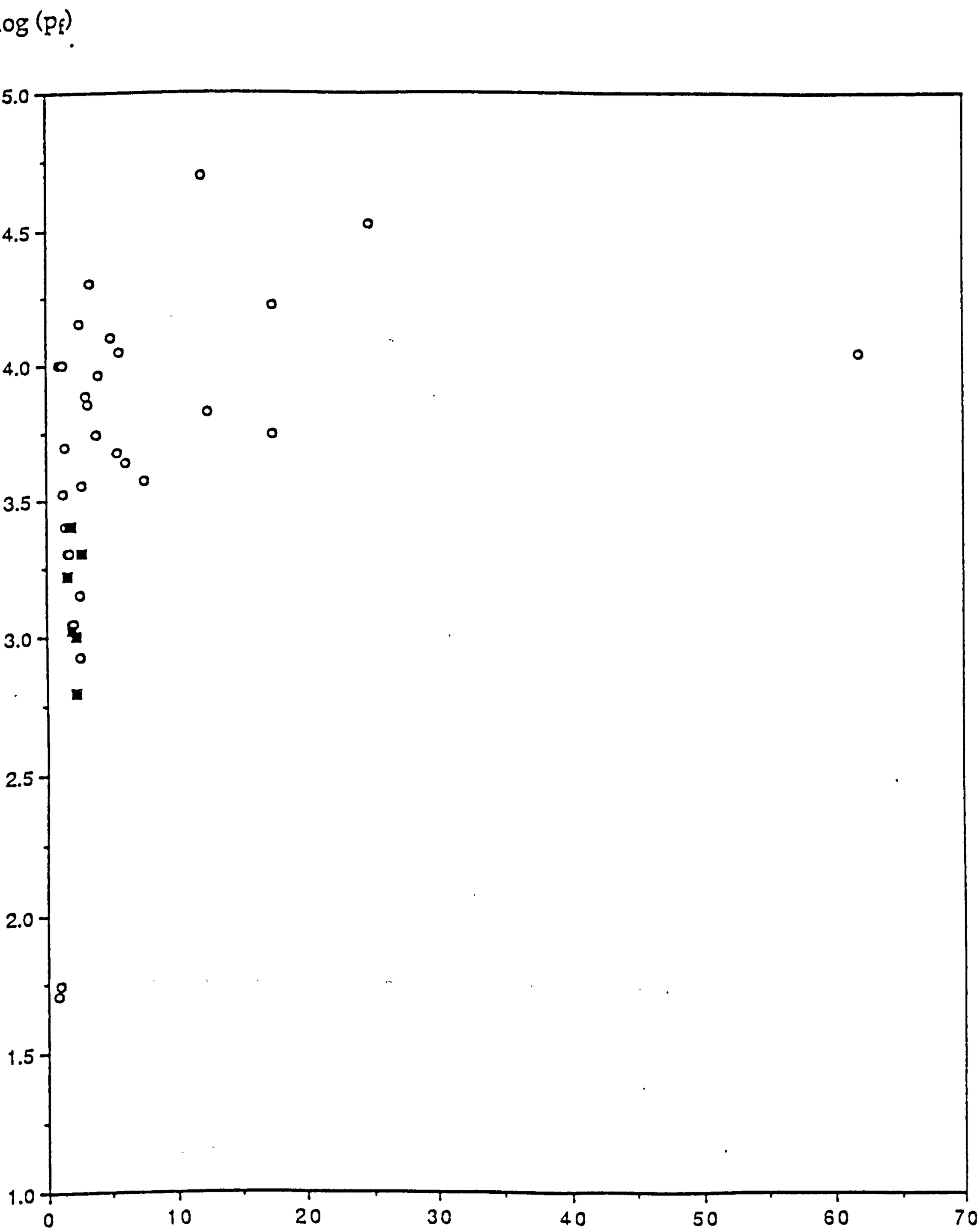

Figure 77: Total Failure Probability

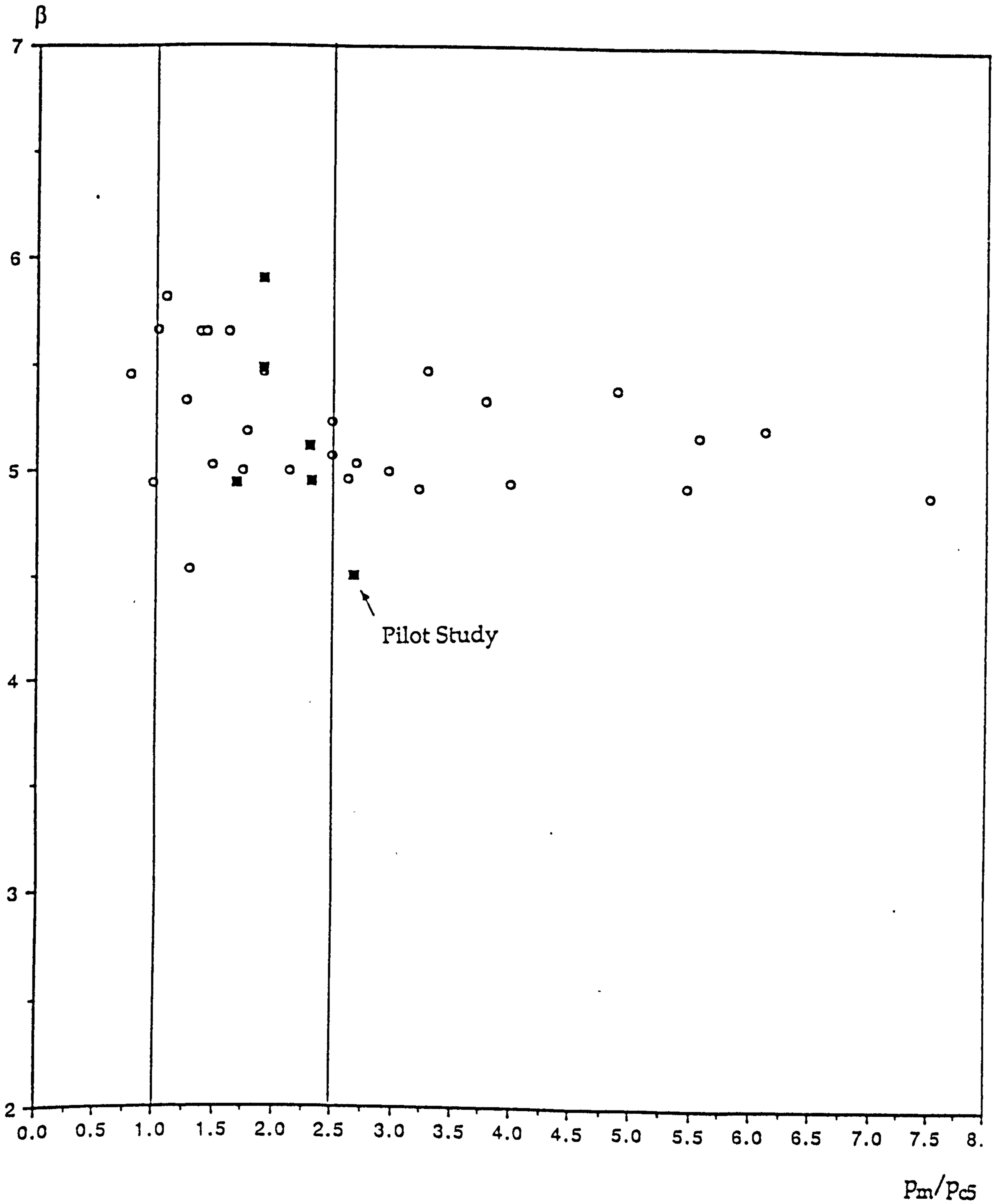

Figure 78: Safety Index, Flange Yield, Designs with $p_m/p_{c5} < 8$.

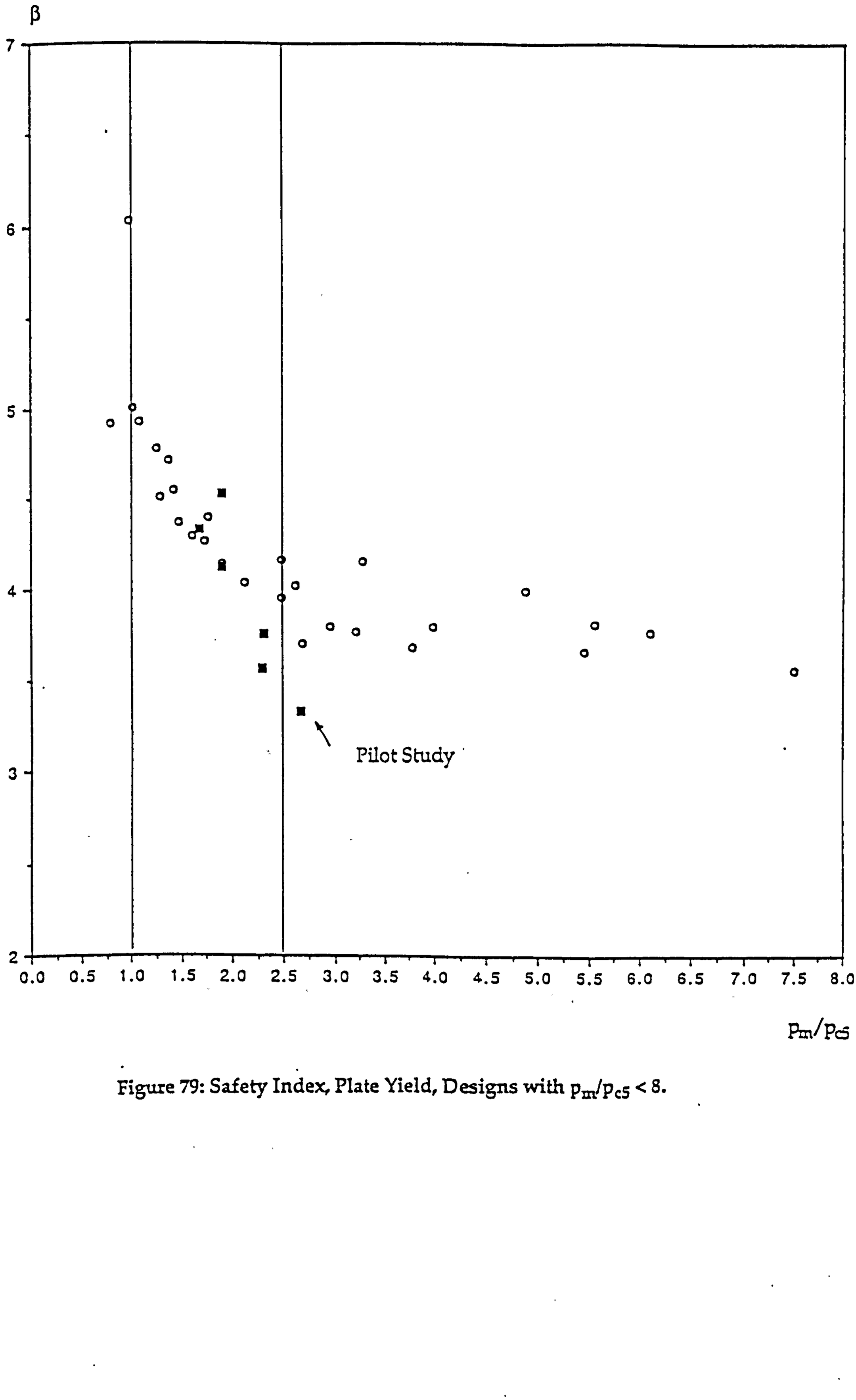

Figure 79: Safety Index, Plate Yield, Designs with $p_m/p_{c5} < 8$.

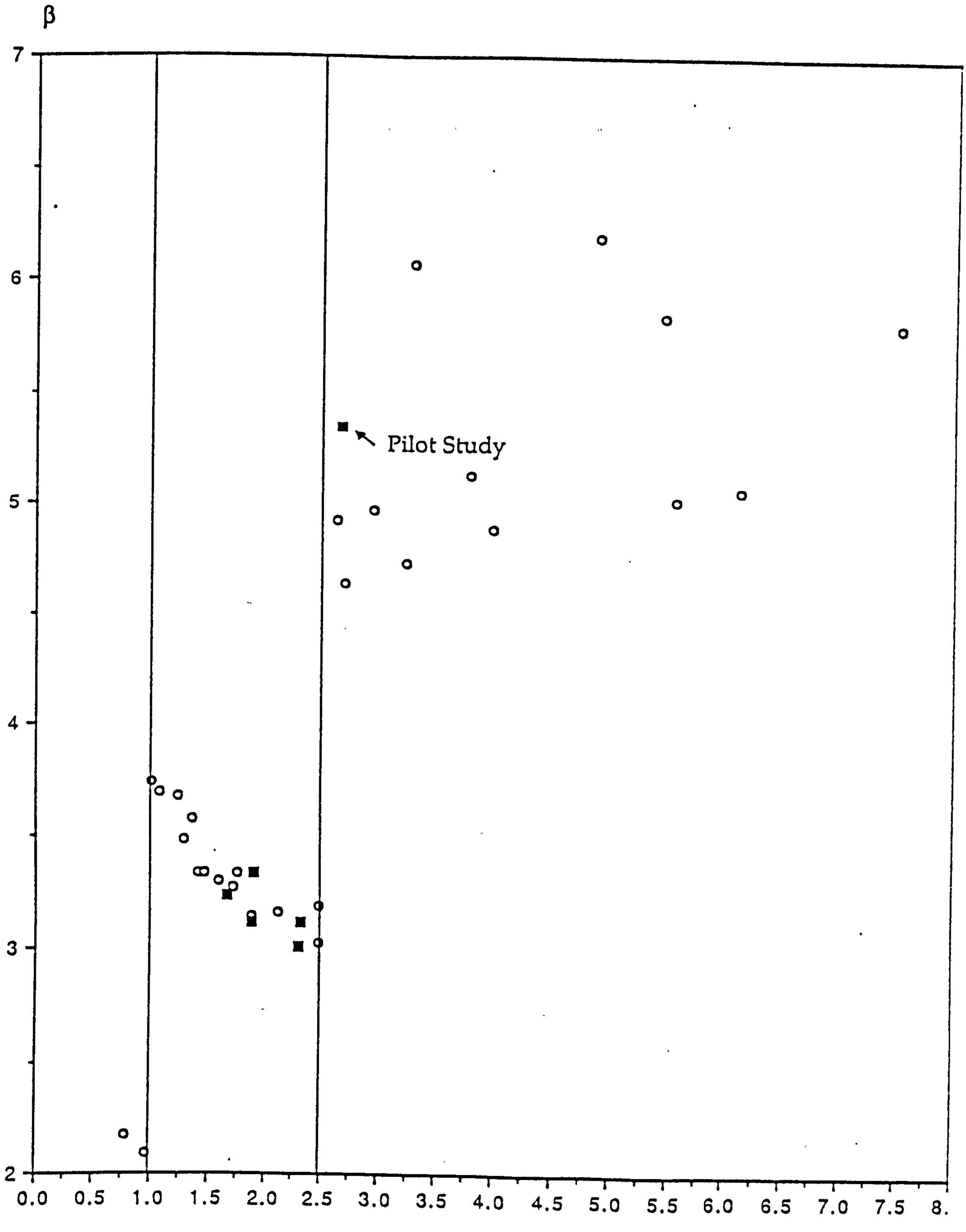

Figure 80: Safety Index, Interframe Shell Collapse, Designs with $p_m/p_{c5} < 8$.

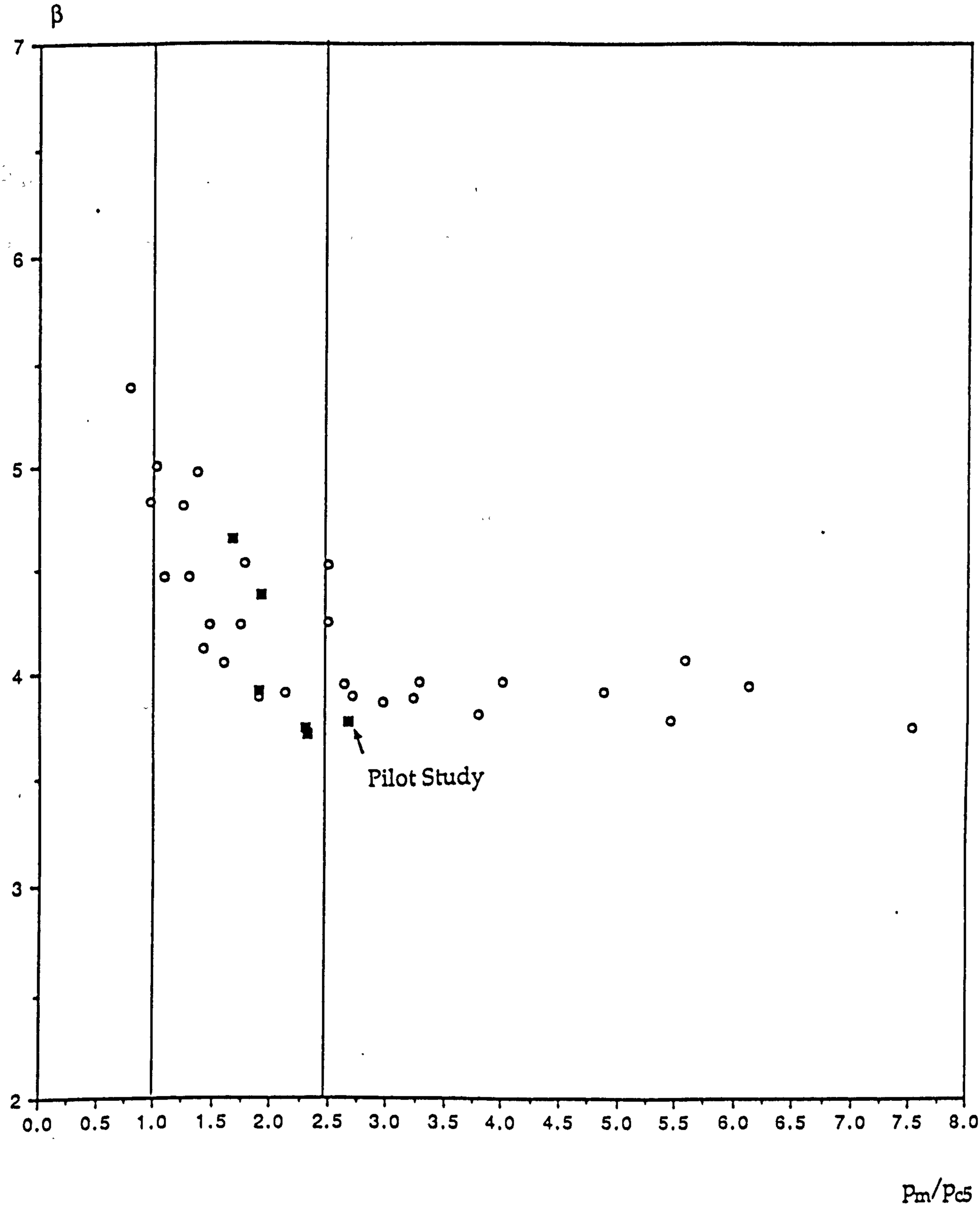

Figure 81: Safety Index, Frame Tripping, Designs with $p_m/p_{c5} < 8$.

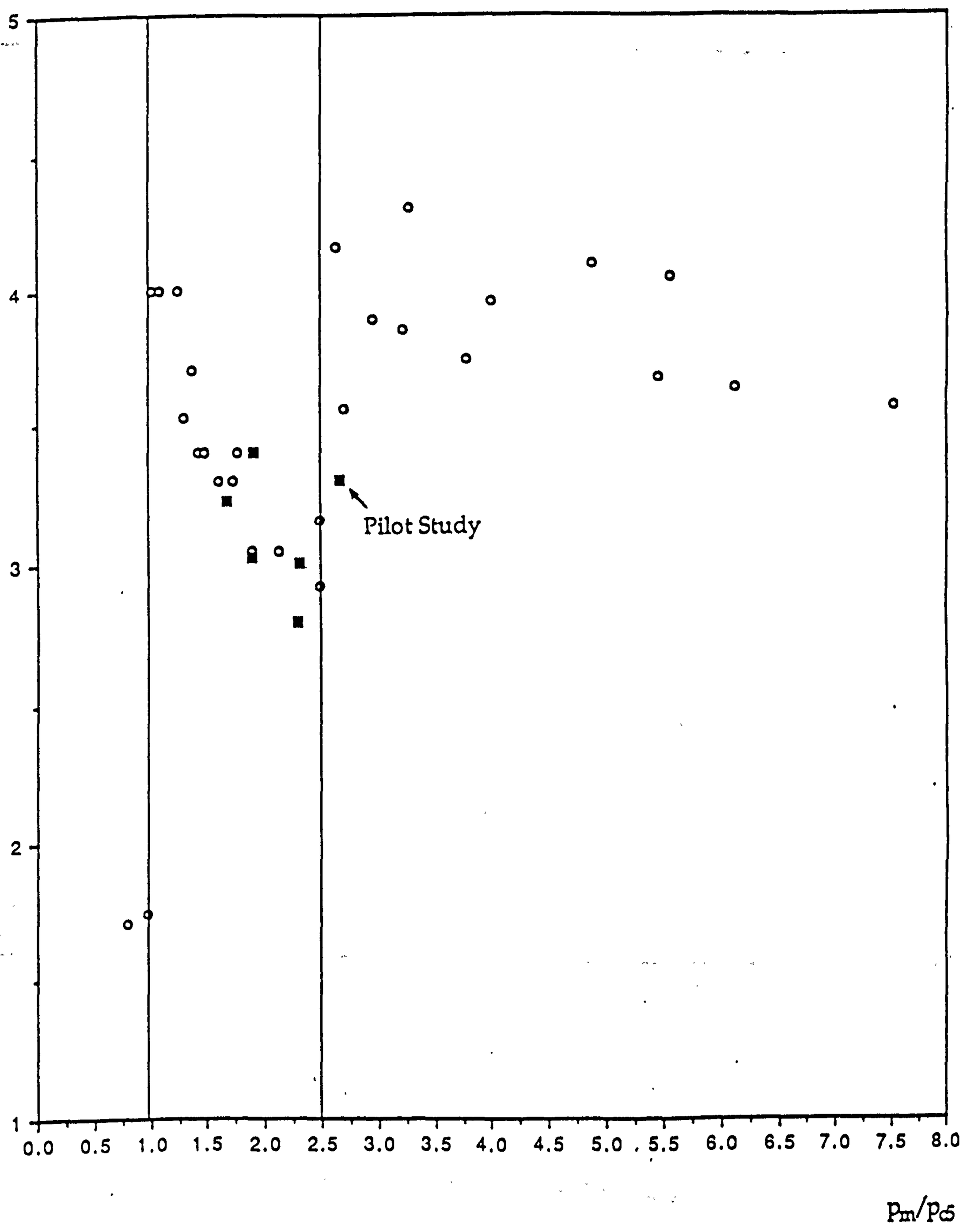

Figure 82: Total Failure Probability, Designs with $p_m/p_{c5} < 8$.

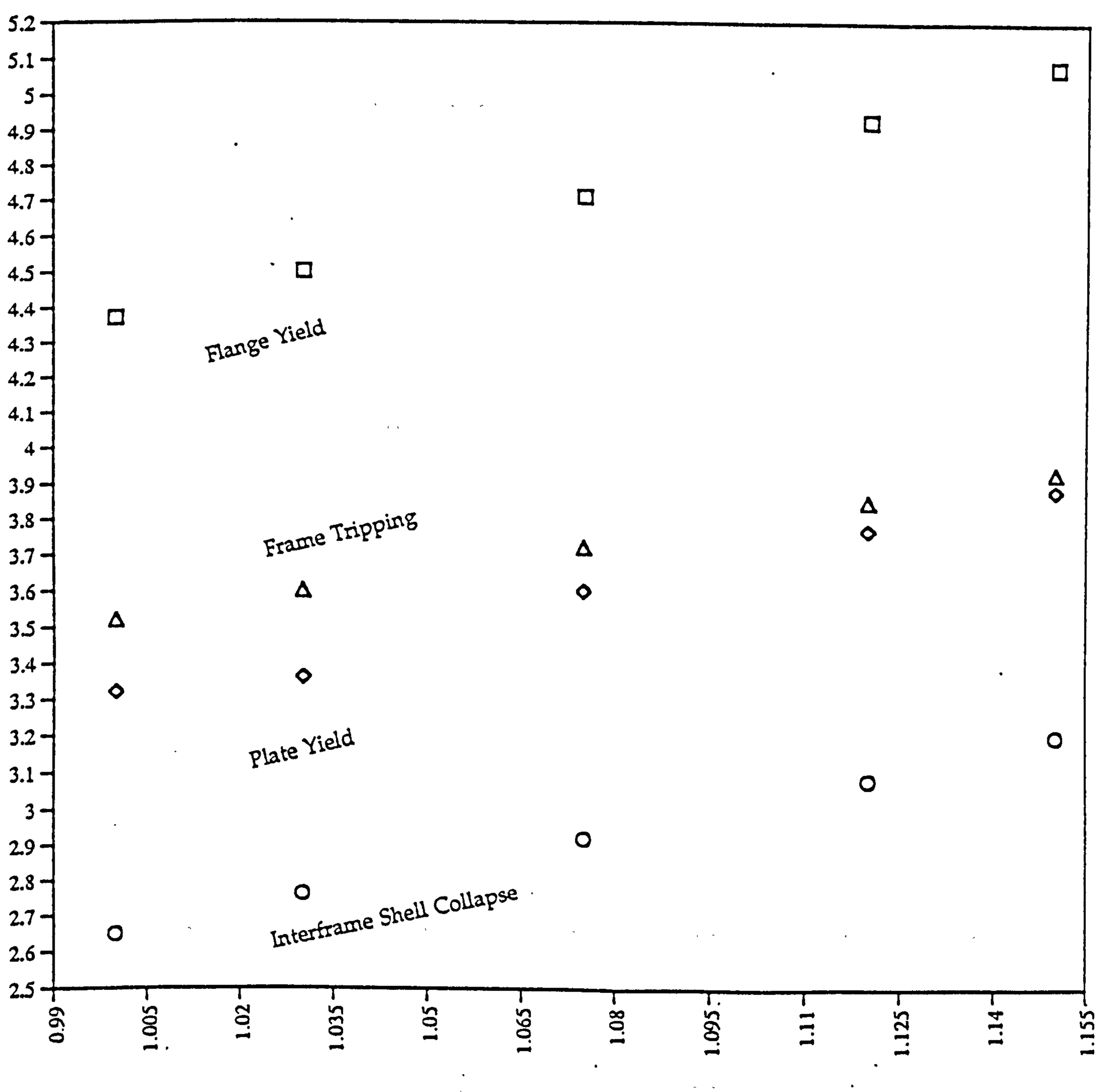

Figure 83: Target β vs. F, Eq. (68) for o-o-c, F_{max}= 1.15

β

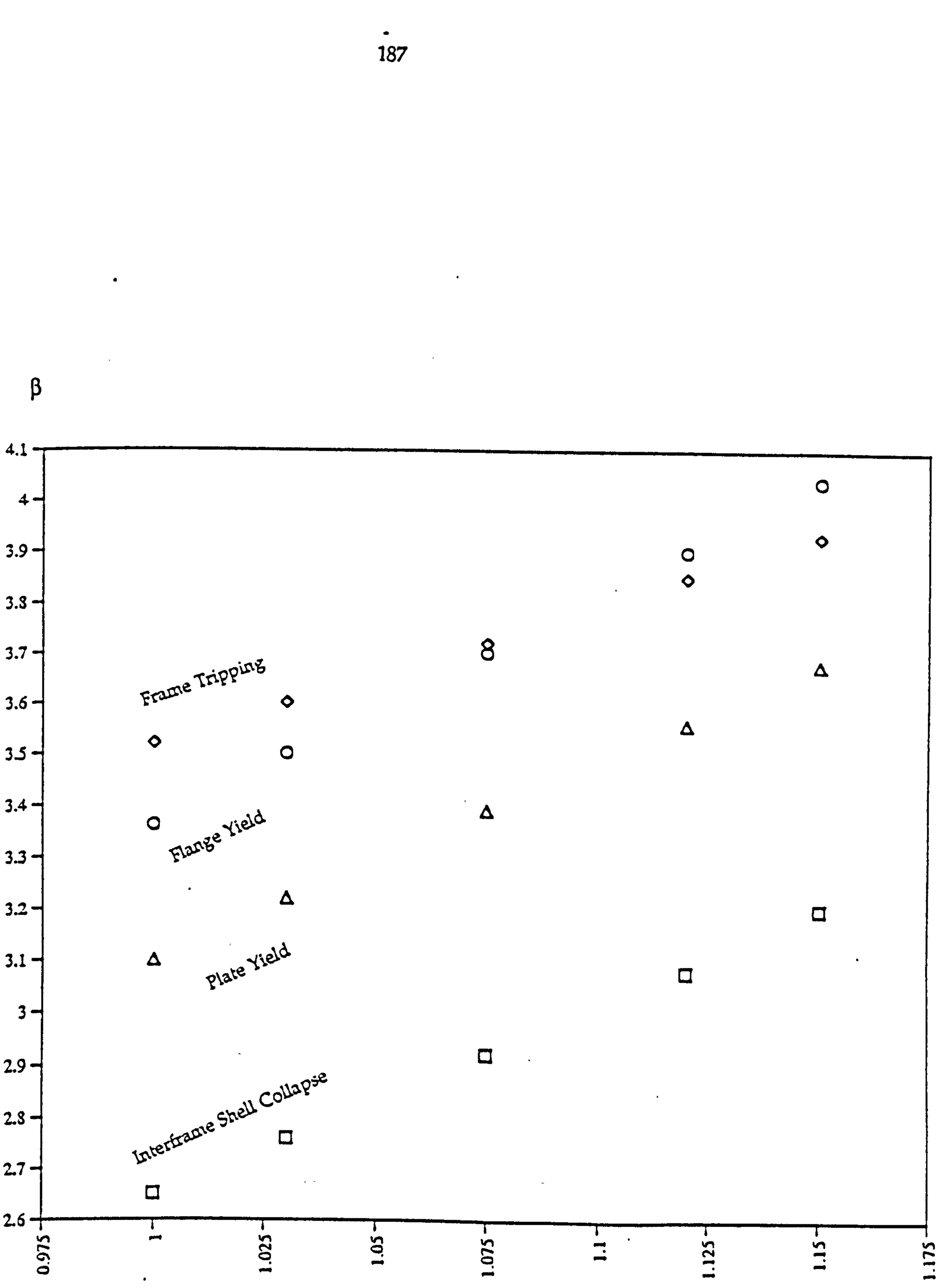

F

Figure 84: Target β vs. F, o-o-c = 0.5% R, F_{max}= 1.15

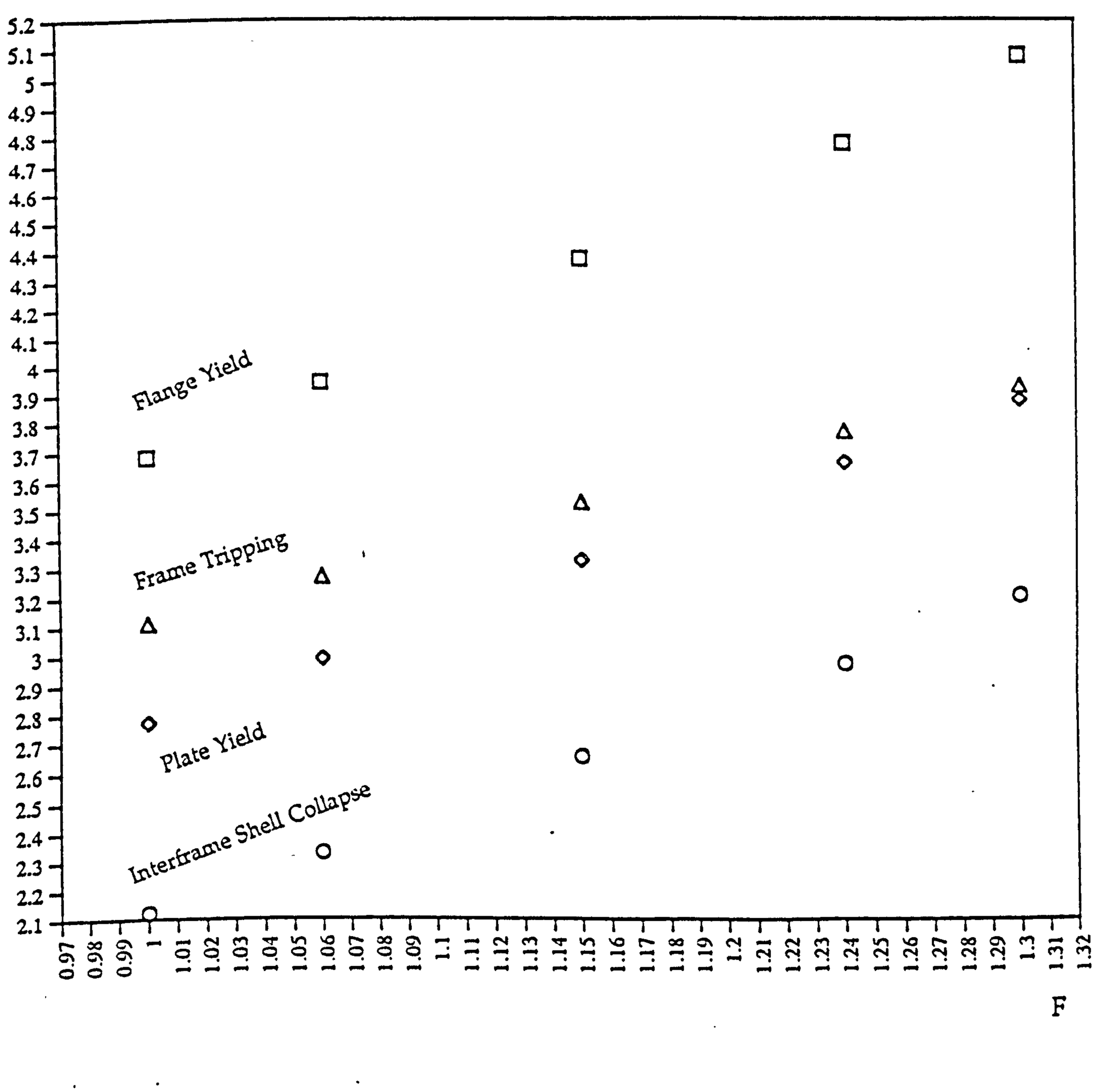

Figure 85: Target β vs. F, Eq. (68) for o-o-c, F_{max}= 1.30

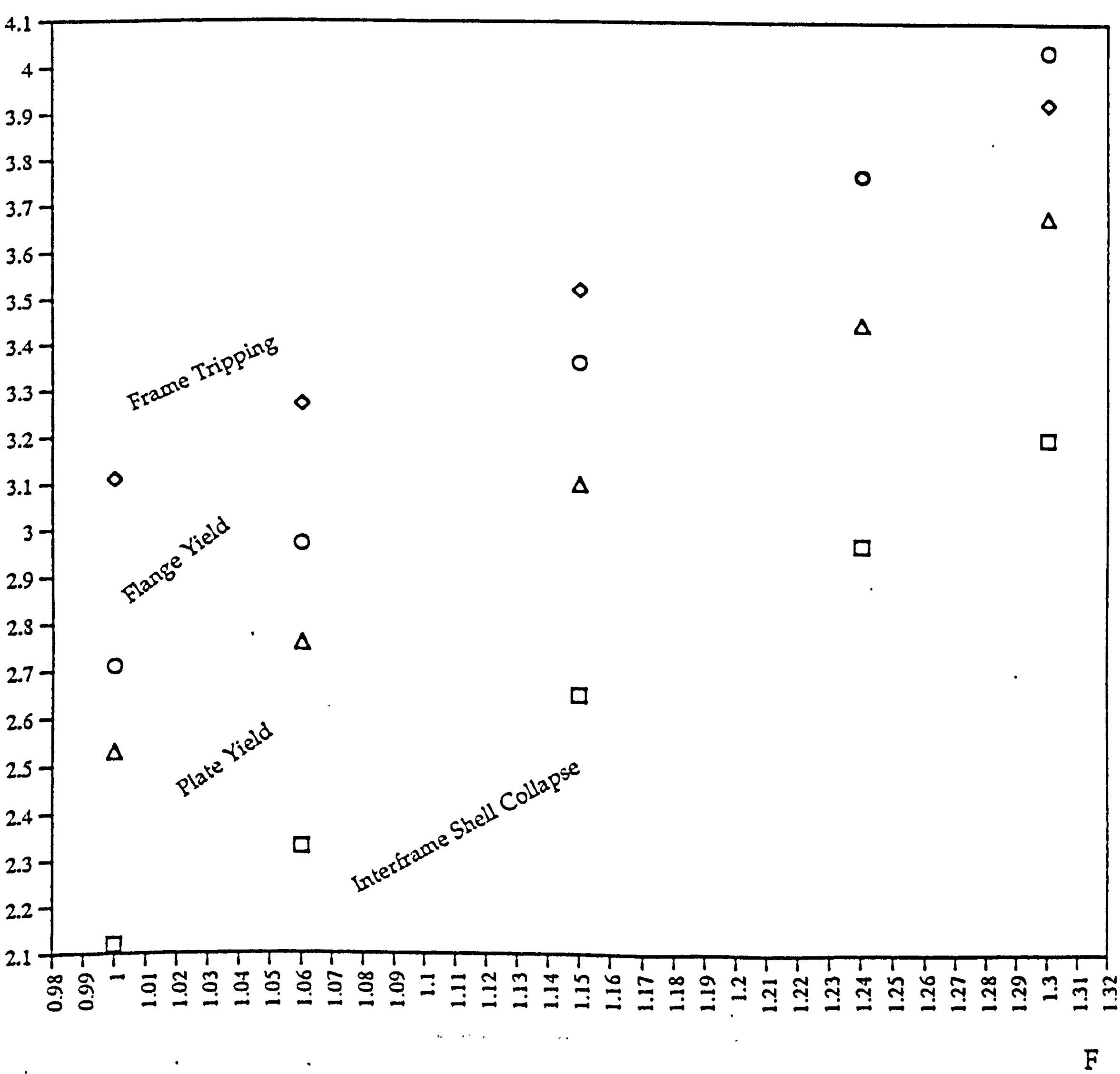

Figure 86: Target β vs. F, o-o-c = 0.5% R, F_{max}= 1.30

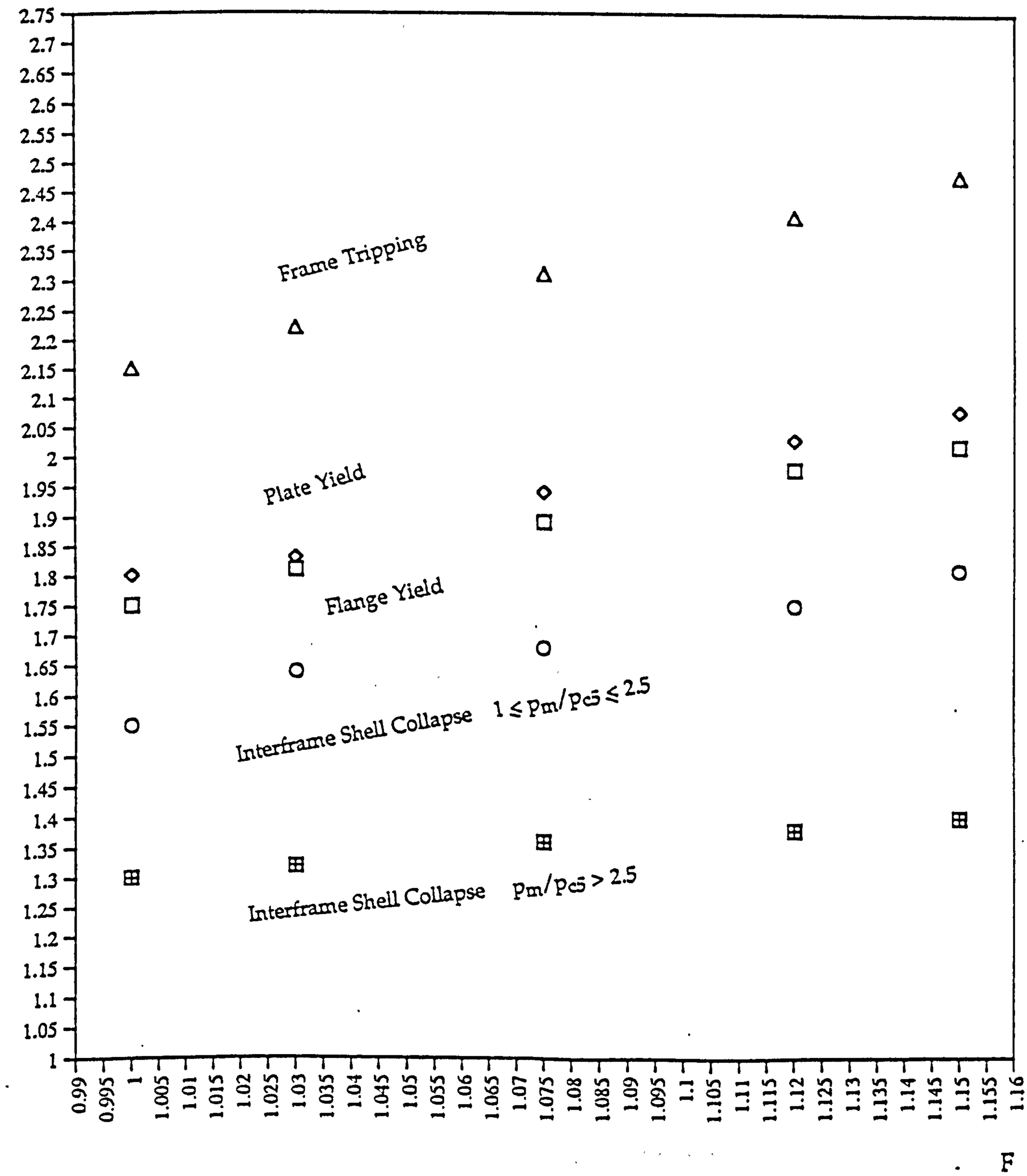

Figure 87: γ_{xm_j} γ_f vs. F, Eq. (68) for o-o-c, F_{max}= 1.15

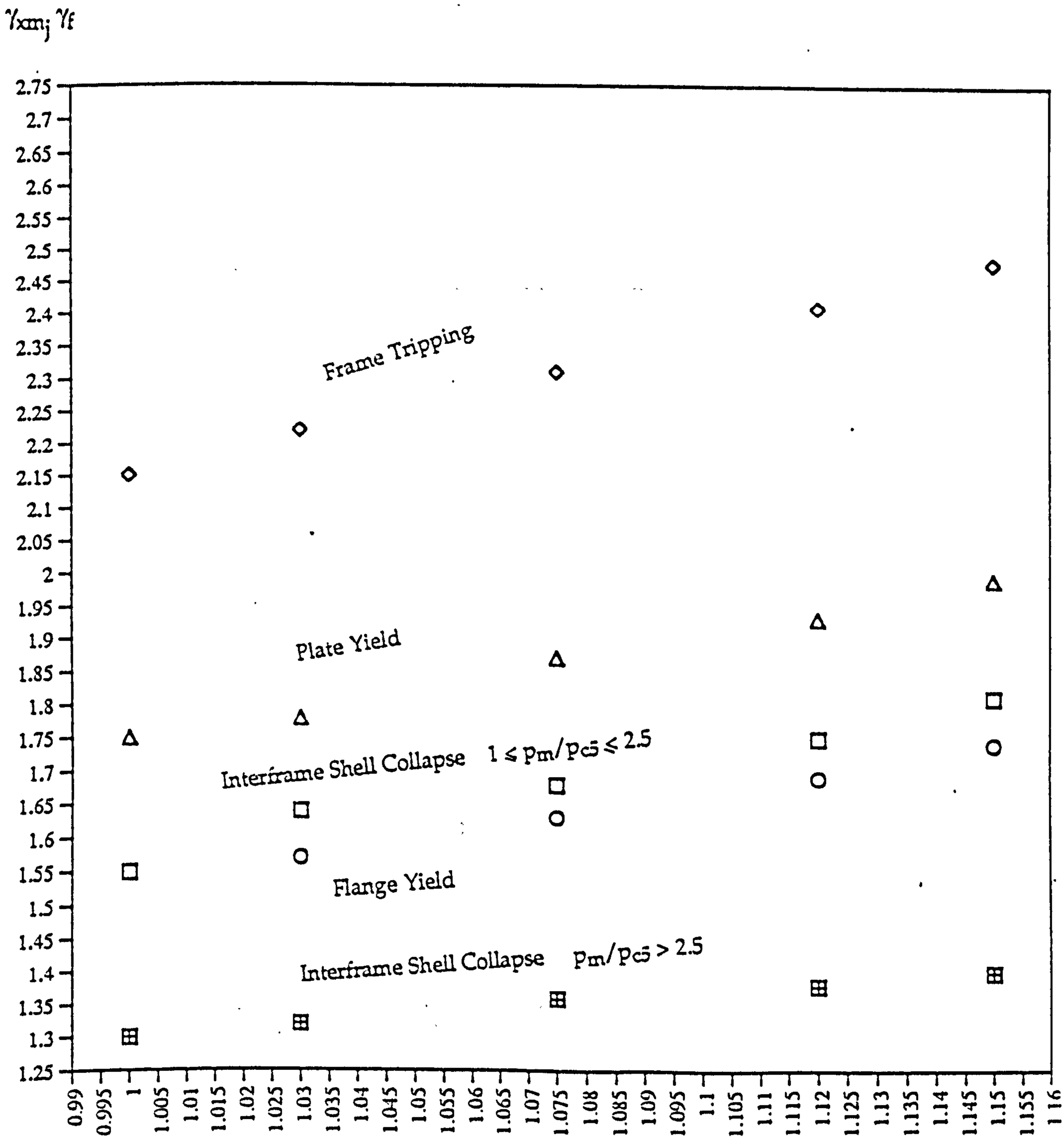

Figure 88: $\gamma_{xm_j}\ \gamma_f$ vs. F, o-o-c = 0.5% R, F_{max}= 1.15

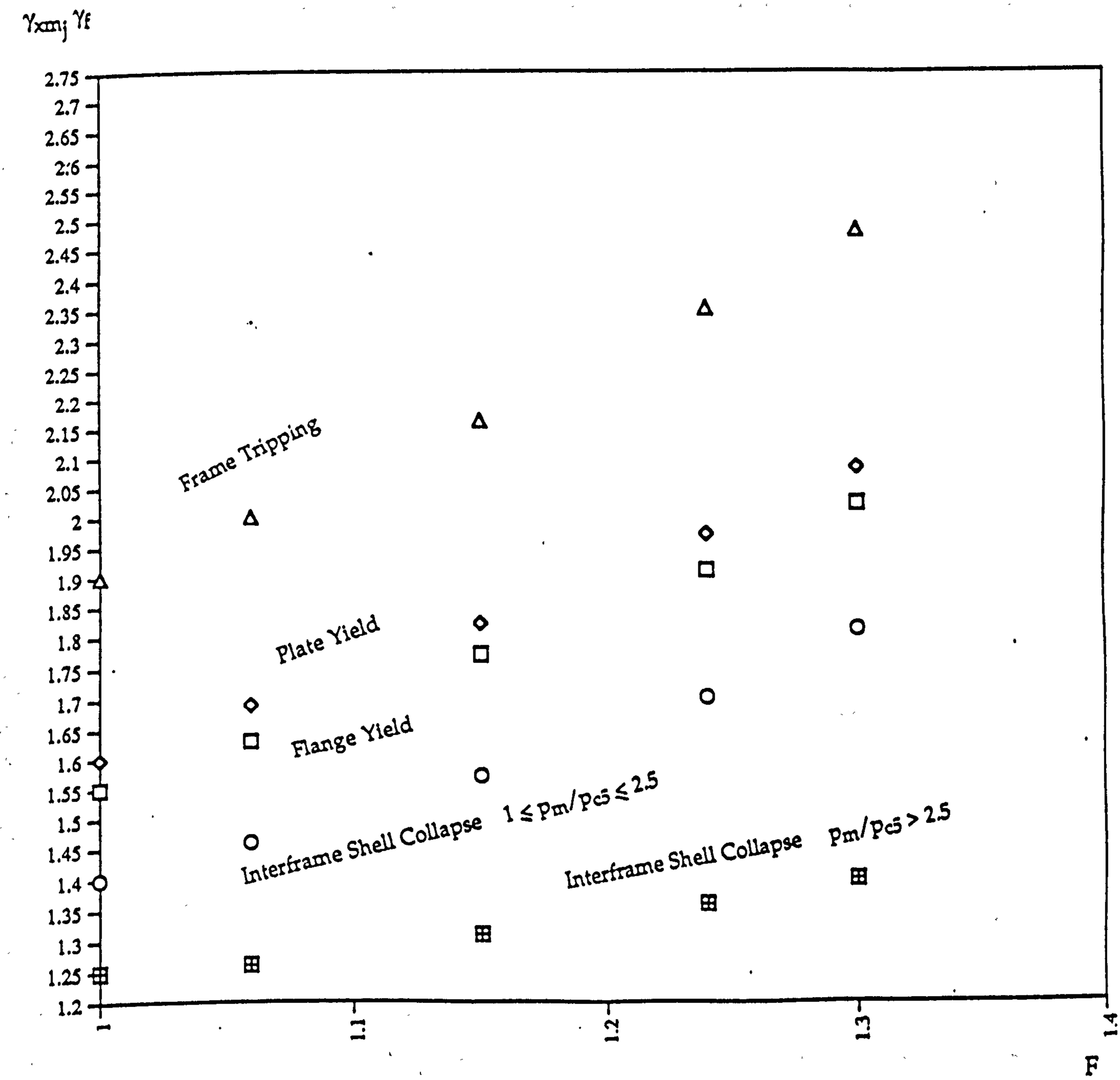

Figure 89: $\gamma_{xm_j}\ \gamma_f$ vs. F, Eq. (68) for o-o-c, F_{max}= 1.30

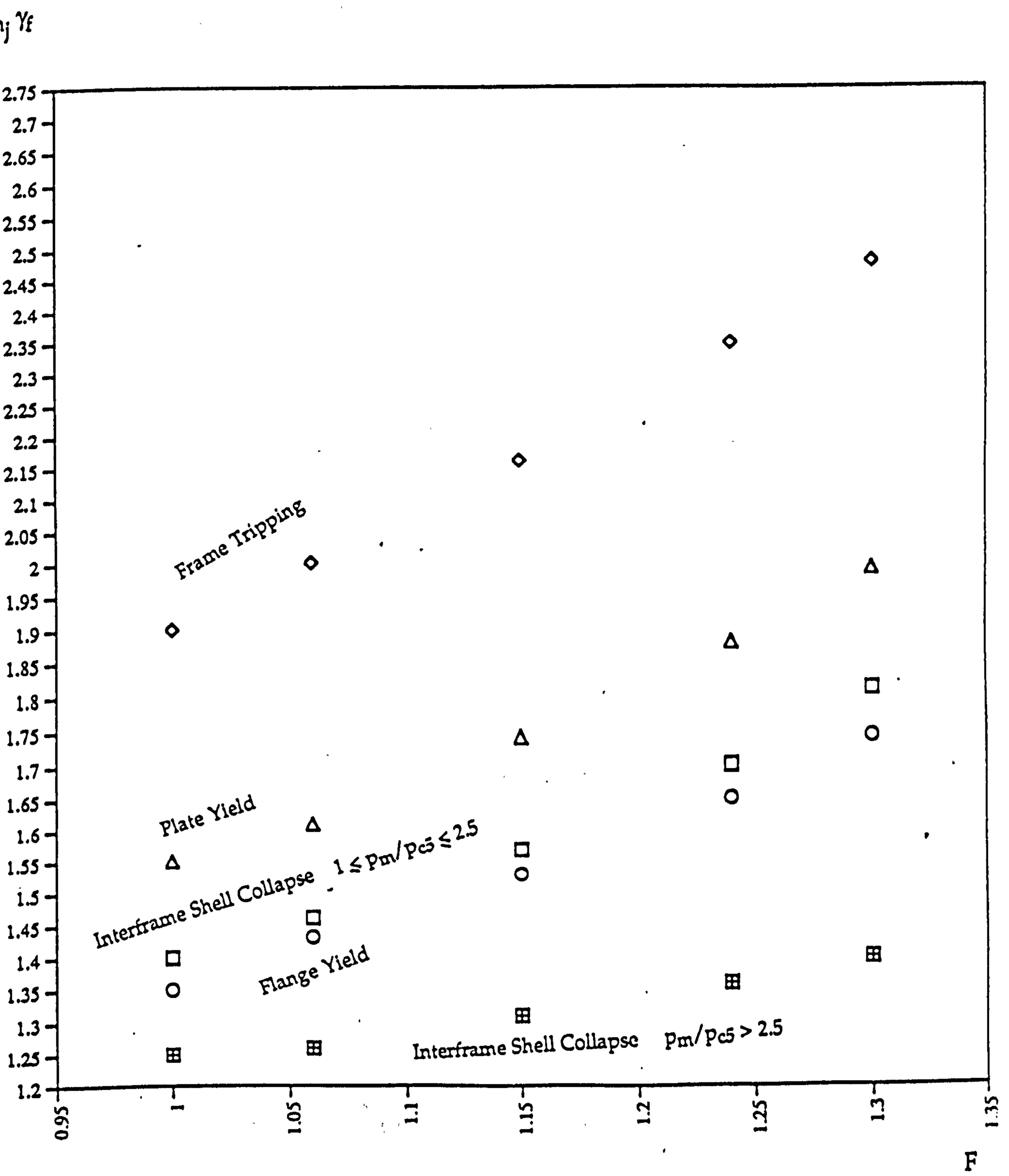

Figure 90: $\gamma_{xm_j}\gamma_f$ vs. F, o-o-c = 0.5% R, F_{max}= 1.30

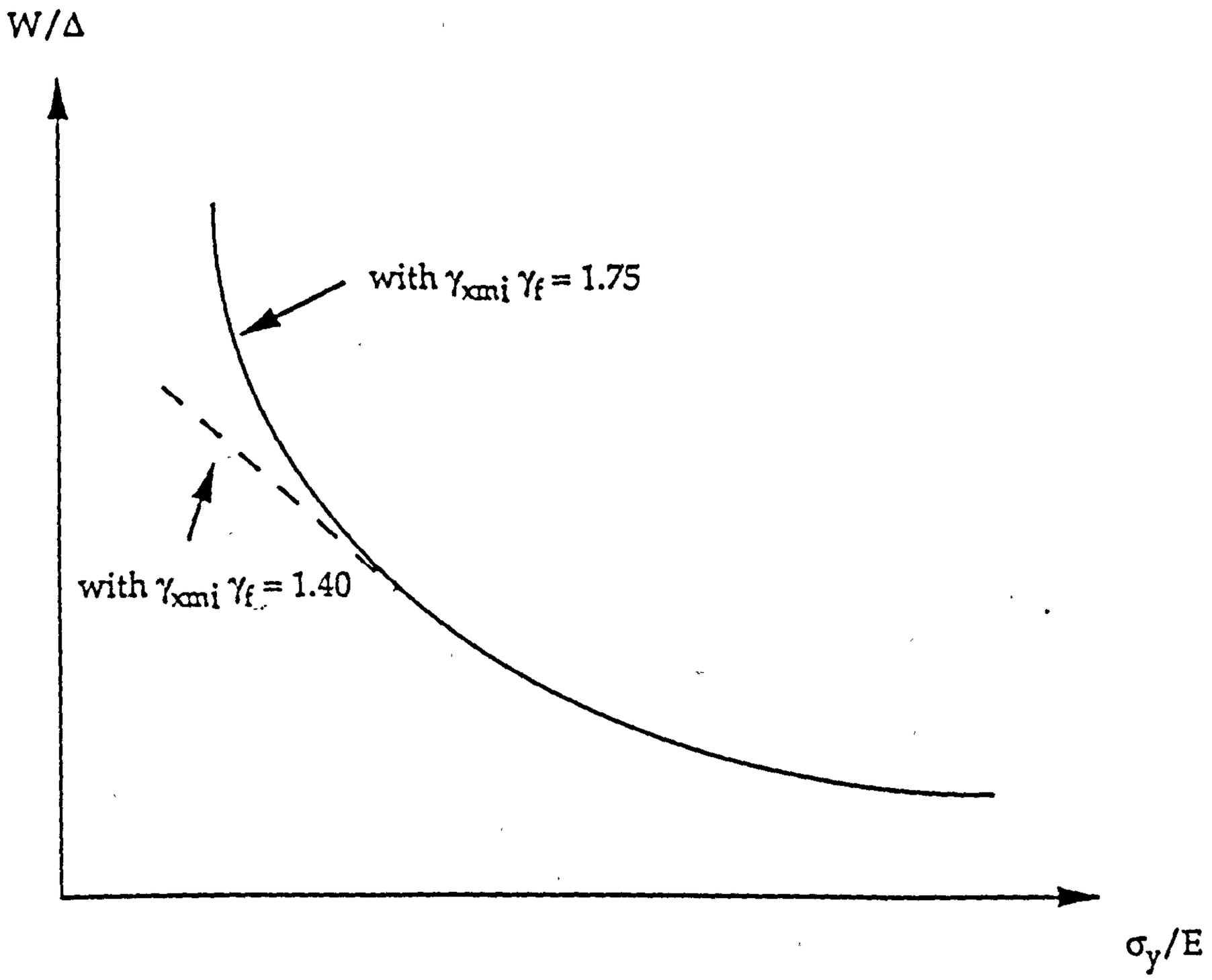

Figure 91: Effect of using $\gamma_{xm_j}\,\gamma_f = 1.4$ for $p_m/p_{c5} > 2.5$

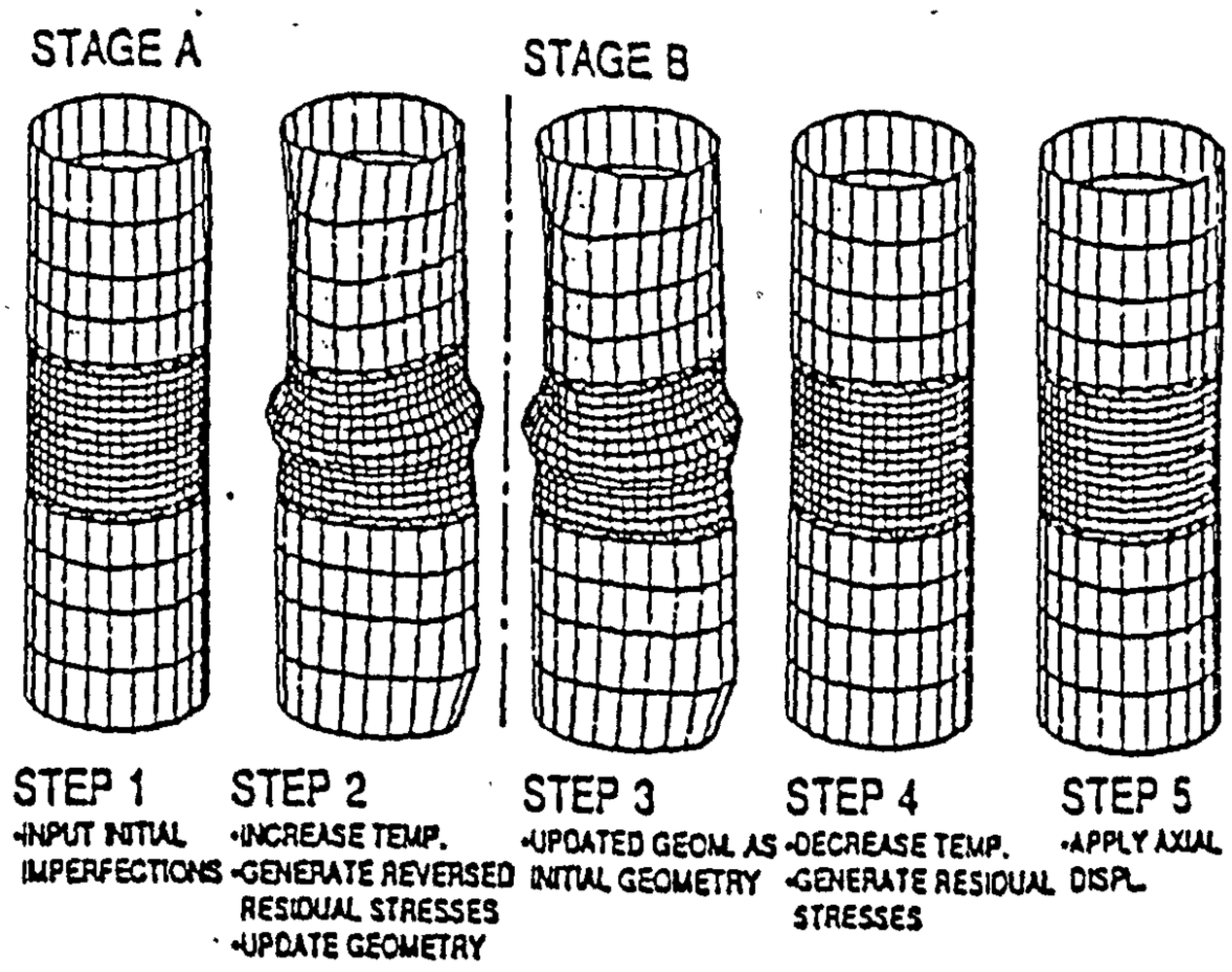

Figure 92: Procedure to Include Imperfections and Residual Stresses in FE Models, [243]

Table 1 - Limiting Slenderness Ratios for Webs and Flanges [38]

Code	BS 5500	API	DnV
$(d_w / t_w)\sqrt{\sigma_{yf} / E}$	1.1	1.0	1.35
$(b_f / t_f)\sqrt{\sigma_{yf} / E}$	0.5	0.375	0.4

Table 2: p_n (N/mm^2), Models 3 and 10 [136]

	Hydrostatic Pressure				Lateral Pressure			
	n=2		n=3		n=2		n=3	
Frames	Int.	Ext.	Int.	Ext.	Int.	Ext.	Int.	Ext.
Case I	2.33	1.73	3.65	2.42	2.45	1.81	3.74	2.52
Case II	2.35	1.75	3.65	2.43	2.46	1.83	3.74	2.53
Case III	4.31	3.93	3.84	2.66	4.41	4.04	3.90	2.72
Case IV	4.32	3.95	3.84	2.66	4.44	4.06	3.90	2.72
Case V	4.32	3.95	3.84	2.66	4.44	4.06	3.90	2.72
Eq.(28)	2.06	2.01	3.29	3.13	2.09	2.03	3.33	3.17
Kendrick	2.43	1.97	4.06	3.35	-	-	-	-
Model 3 (Exper.)								2.96
Model 10 (Exper.)								3.17

Obs. Boundary conditions according to Figure 20

Table 3: Mesh Study for the Frames, Models 3 and 10 [136]
Case III Bound. Cond., Ext. Frames, Lateral Pressure

Type of Element	Numb of Elts. in Web in the Radial Direction	p_n (N/mm^2)
S4R	1	2.06
S4R	2	2.71
S4R	3	2.83
S4R	4	2.86
S8R	1	2.92
S8R	2	2.91
Model 3	(Experimental)	2.96
Model 10	(Experimental)	3.17

Table 4: Comparison Experiments vs. FE Eigenvalue Analysis

Model	Exp. Pressure (N/mm^2)	ABAQUS (N/mm^2)	Exper./ABAQUS	n
3 [136]	2.963	2.914	1.017	3
10 [136]	3.171	2.914	1.088	3
1 [136]	3.031	2.766	1.096	3
5 [136]	3.275	3.100	1.057	3
8 [136]	3.583	3.152	1.137	3
6 [110]	1.296	1.403	0.924	4

(Case III Boundary Conditions)

Table 5: Brief Description of the Experimental Data

Refer.	Number of models	Material	Int./Ext. Frames	Bound. Condit.	Hyd/Lat Pressure	Geometry Range
[85]	24	Steel	Ext.	Various	Hydr.	$Z=8.9$ $3.8<L_c/R_i<10.3$
[74]	10	Steel	Ext.	Discs	Hydr.	$Z=8.9$ $4.8<L_c/R_i<9.3$
[136]	5	Alum.	Ext.	End Rings	Lateral	$8.9<Z<29.2$ $L_c/R_i=7.0$
[109]	4	Alum.	3 Ext. 1 Int.	"	Hydr.	$0.3<Z<0.6$ $L_c/R_i=1.0$
[94]	3	Alum.	Ext.	"	Hydr.	$1.5<Z<4.1$ $1.2<L_c/R_i<1.9$
[110]	3	Alum.	Ext.	"	Hydr.	$Z=9.3$ $L_c/R_i=3.9$
[113]	8	Alum.	Int.	"	Hydr.	$4.0<Z<5.5$ $L_c/R_i=2.3$
[142]	1	Steel	Ext.	"	Hydr.	$Z=3.9$ $L_c/R_i=3.9$
[147]	2	Steel	Ext.	"	Hydr.	$Z=3.9$ $L_c/R_i=3.9$
[148]	4	Steel	Ext.	"	Hydr.	$Z=7.0$ $2.0<L_c/R_i<4.0$
[80]	5	Alum.	Ext.	Deep Fram.	Hydr.	$Z=2.0$ $1.5<L_c/R_i<2.5$
[79]	7	Steel	Ext.	"	Hydr.	$Z=9.4$ $L_c/R_i=3.5$

Obs. More Details in Appendix 1
Z corresponds to $l = L_s$

Table 6 - Sample Design Cases

Cases	1	2	3	4	4b	4c	5	6
Reference	[29]	[26]	[17]	[57]	[57]	[32]	[25]	[58]
R_i (m)	4	2	4	2	2	2	2.7	2.7
t (mm)	34	20	34	17.9	17.9	17.9	25	25
L_s (mm)	560	300	679	600	600	600	750	730
Web	190x16	125x10	276x18	181x9.1	181x9.1	181x9.1	173x9	190x8
Flange	150x51	100x25	225x26	90.5x15.1	60x22.8	40x34.2	100x27	100x16
Ext./Int. Frame	Int.	Int.	Int.	Int.	Int.	Int.	Int.	Ext.
Tee/Flat Frame	Tee	Tee	Tee	Tee	Tee	Tee	Tee	Tee
σ_{yf} (N/mm^2)	550	615	540	390	390	390	390	450
σ_{yp} (N/mm^2)	550	595	540	390	390	390	390	450
E (KN/mm^2)	207	207	207	207	207	207	207	207
p_d (N/mm^2)	3.47	4.67	3.02	1.7	1.7	1.7	2.01	2.01

6b	7	8	9	10
[48]	[23]	[12], HY130	[12], Alum.	[12], Titan.
2.7	1.8	4	2.5	2.5
25	16	31	36	76
730	800	670	600	655
190x8	300x15	236x14	239x16	218x49
100x16		156x21	142x36	193x87
Int.	Int.	Int.	Int.	Int.
Tee	Flat	Tee	Tee	Tee
450	350	890	390	830
450	350	890	390	830
207	207	207	71	110
2.01	1.21	3	3	15

Table 7: p_n (N/mm^2), Case 3 of Table 6
t Increased to 46 mm

	ABAQUS		Analytical		Comparison		
			n=2				
L_c(mm)	Case I	Case III	Eq.(28)	Kendrick	CIII/CI	CI/Eq.(28)	CI/Kendr.
8827	-	-	75.33	69.37	-	-	-
11543	-	-	42.78	40.91	-	-	-
14259	26.85	>34.28	26.62	26.45	>1.28	1.01	1.02
			n=3				
8827	26.92	31.89	29.78	28.56	1.18	0.90	0.94
11543	23.39	26.70	24.56	24.82	1.14	0.95	0.94
14259	21.21	23.16	22.57	23.30	1.09	0.94	0.91
			n=4				
8827	-	-	40.59	40.61	-	-	-
11543	-	-	39.42	40.43	-	-	-
14259	33.14	>37.77	39.02	40.40	>1.14	0.85	0.82

Obs. Boundary conditions according to Figure 20

Table 8: p_n (N/mm^2), Other Cases of Table 6

			ABAQUS		Analytical		Comparison		
					n=2				
	t(mm)	L_c(mm)	Case I	Case III	Eq.(28)	Kend.	CIII/CI	CI/Eq.(28)	CI/Kendr.
Case 2	20	9900	16.68	24.48	15.63	16.69	1.47	1.07	1.0
Case 4	22	11400	12.55	18.67	11.04	11.81	1.49	1.14	1.06
Case 5	25	20250	5.65	8.22	5.05	5.57	1.46	1.12	1.01
Case 6	25	21170	3.35	5.99	4.04	3.82	1.79	0.83	0.88
					n=3				
Case 1	34	12880	15.92	17.78	15.67	16.29	1.12	1.02	0.98

Obs. Boundary conditions according to Figure 20
L_c was adjusted to give an integer number of frames
t was increased to avoid too many Interframe Eigenvalues

Table 9 - Elastic Buckling Pressure (N/mm^2), Case 1 of Table 6

n	FE	Eq. (8)	Eq. (44)	Eq. (45)	Eq. (46)	Eq. (8)/Eq. (46)	Eq. (46)/FE	Mode
2	17.189	18.717	18.797	18.746	18.728	0.999	1.090	Trip.
3	17.188	18.491	18.747	18.534	18.497	1.000	1.076	Trip.
4	17.132	18.197	18.816	18.271	18.216	0.999	1.063	Trip.
5	17.063	17.853	19.096	18.023	17.960	0.994	1.053	Trip.
6	17.025	17.480	19.668	17.845	17.800	0.982	1.046	Trip.
7	17.019	17.097	20.586	17.748	17.795	0.961	1.046	Trip.
8	17.038	16.723	21.887	17.705	17.981	0.930	1.055	Mixed
9	17.060	16.374	23.591	17.663	18.379	0.891	1.077	Mixed
10	17.076	16.062	25.703	17.588	18.994	0.846	1.112	Interf.
11	17.089	15.798	28.223	17.471	19.820	0.797	1.160	Interf.
12	17.126	15.588	31.150	17.328	20.845	0.748	1.217	Interf.
13	17.179	15.435	34.479	17.181	22.054	0.700	1.284	Interf.
14	17.286	15.342		17.053	23.428	0.655	1.355	Interf.
15	17.439	15.308		16.960	24.591	0.623	1.410	Interf.

Table 10 - Elastic Buckling Pressure (N/mm^2), Case 2 of Table 6

n	FE	Eq. (8)	Eq. (44)	Eq. (45)	Eq. (46)	Eq. (8)/Eq. (46)	Eq. (46)/FE	Mode
2	23.445	26.146	25.875	25.841	25.819	1.013	1.101	Trip.
3	23.515	25.808	25.515	25.358	25.322	1.019	1.077	Trip.
4	23.611	25.371	25.516	25.067	24.985	1.015	1.058	Trip.
5	23.761	24.869	26.172	25.078	24.973	0.996	1.051	Trip.
6	23.942	24.332	27.699	25.305	25.380	0.959	1.060	Mixed
7	24.086	23.794	30.224	25.535	26.238	0.907	1.089	Mixed
8	24.170	23.284	33.807	25.602	27.533	0.846	1.139	Interf.
9	24.207	22.824	38.459	25.477	29.220	0.781	1.207	Interf.
10	24.230	22.433	44.170	25.223	31.239	0.718	1.289	Interf.
11	24.269	22.123		24.918				Interf.
12	24.383	21.901		24.620				Interf.
13	24.535	21.773		24.371				Interf.
14	24.814	21.738		24.196				Interf.
15	25.150	21.795		24.106				Interf.

Table 11 - Elastic Buckling Pressure (N/mm^2), Case 3 of Table 6

n	FE	Eq. (8)	Eq. (44)	Eq. (45)	Eq. (46)	Eq. (8)/Eq. (46)	Eq. (46)/FE	Mode
2	16.281	17.633	17.181	17.146	17.160	1.028	1.054	Trip.
3	16.069	17.154	16.516	16.451	16.481	1.041	1.026	Trip.
4	15.826	16.543	16.163	16.127	16.094	1.028	1.017	Trip.
5	15.508	15.851	16.402	16.194	16.156	0.981	1.042	Mixed
6	15.115	15.124	17.395	16.277	16.602	0.911	1.098	Mixed
7	14.667	14.407	19.202	16.083	17.237	0.836	1.175	Interf.
8	14.212	13.735	21.815	15.627	17.861	0.769	1.257	Interf.
9	13.792	13.132	25.202	15.046	18.357	0.715	1.331	Interf.
10	13.430	12.616		14.453	18.695	0.675	1.392	Interf.
11	13.416	12.194		13.911	18.907	0.645	1.409	Interf.
12	12.943	11.870		13.454	19.406	0.612	1.499	Interf.
13	12.829	11.641		13.095	19.159	0.608	1.493	Interf.
14	12.823	11.502		12.833	19.284	0.596	1.504	Interf.
15	12.880	11.448		12.668	19.443	0.589	1.510	Interf.

Table 12 - Elastic Buckling Pressure (N/mm^2), Case 4 of Table 6

n	FE	Eq. (8)*	Eq. (44)*	Eq. (45)*	Eq. (46)*	BOSOR 4	N9E	Eq(8)/Eq(46)	Eq. (46)/FE	Mode
2	17.710	19.700	18.221	17.920	18.143	20.290	22.500	1.086	1.024	Trip.
3	17.474	19.200	16.926	16.220	16.817	19.820	22.000	1:142	0.962	Trip.
4	17.336	18.700	16.317	15.600	16.212	19.060	21.000	1.153	0.935	Trip.
5	15.375	18.000	16.409	16.020	16.227	17.290	18.200	1.109	1.055	Trip.
6	12.788	14.816	15.553	15.003	14.916	15.180	14.800	0.993	1.166	Mixed
7	10.600	11.946	15.020	12.885	13.440	12.470	12.000	0.889	1.268	Mixed
8	8.929	9.808	14.875	10.752	12.031	10.370	9.910	0.815	1.347	Interf.
9	7.729	8.288	15.026	9.070	10.972	8.850	8.400	0.755	1.420	Interf.
10	6.924	7.258		7.880	9.815	7.810	7.370	0.739	1.418	Interf.
11	6.416	6.603		7.100		7.150	6.720			Interf.
12	6.161	6.232		6.635		6.780	6.350			Interf.
13	6.082	6.072		6.408		6.630	6.190			Interf.
14	6.176	6.073		6.358						Interf.
15	6.349	6.196		6.443						Interf.

* For n=2-4, p_m was corrected to account for more than one axial half-wave between frames, see [23]

Table 13 - Elastic Buckling Pressure (N/mm^2), Case 4b of Table 6

n	Eq. (8) *	Eq. (44) *	Eq. (45) *	Eq. (46) *	BOSOR 4	N9E	Eq(8)/Eq(46)	Eq(46)/BOS4	Mode
2	19.990	19.370	19.350	19.287	17.400	19.300	1.036	1.108	Trip.
3	19.610	18.520	18.450	18.354	16.800	18.600	1.068	1.093	Trip.
4	19.120	17.770	16.509	17.482	16.200	17.800	1.094	1.079	Trip.
5	18.567	15.800	14.372	15.503	15.700	16.600	1.198	0.987	Trip.
6	14.900	13.930	13.013	13.319	14.400	14.300	1.119	0.925	Trip.
7	11.999	12.670	11.697	11.617	12.200	11.800	1.033	0.952	Trip.
8	9.844	11.830	10.210	10.290	10.300	9.820	0.957	0.999	Mixed
9	8.316	11.130	8.835	9.290	8.790	8.350	0.895	1.057	Interf.
10	7.284	11.208	7.778	8.600	7.780	7.350	0.847	1.105	Interf.
11	6.630	6.630	7.060	8.170	7.140	6.710	0.812	1.144	Interf.
12	6.262	6.262	6.628		6.780	6.350			Interf.
13	6.107	6.107	6.420		6.640	6.190			Interf.

* For n=2-4, p_m was corrected to account for more than one axial half-wave between frames, see [23]

Table 14 - Elastic Buckling Pressure (N/mm^2), Case 5 of Table 6

n	FE	Eq. (8) *	Eq. (44) *	Eq. (45) *	Eq. (46) *	Eq. (8)/Eq. (46)	Eq. (46)/FE	Mode
2	**	20.870	20.480	20.416	20.464	1.020		
3	**	20.260	19.600	19.352	19.553	1.036		
4	16.363	19.480	18.730	18.281	18.621	1.046	1.138	Trip.
5	15.947	18.609	18.080	17.455	17.810	1.045	1.117	Trip.
6	14.166	15.762	16.122	15.435	15.410	1.023	1.088	Trip.
7	12.042	13.125	14.645	13.401	13.450	0.976	1.117	Trip.
8	10.378	11.091	13.644	11.529	11.910	0.931	1.148	Mixed
9	9.139	9.597	13.041	10.024	10.760	0.892	1.177	Interf.
10	8.701	8.553	12.787	8.923	9.960	0.859	1.145	Interf.
11	7.728	7.869		8.181				Interf.
12	7.435	7.468		7.730				Interf.
13	7.331	7.285		7.550				Interf.
14	7.396	7.273		7.496				Interf.
15	7.588	7.393		7.561				Interf.

* For n=2-4, p_m was corrected to account for more than one axial half-wave between frames, see [23]

** Too many eigenvalues needed

Table 15 - Elastic Buckling Pressure (N/mm^2), Case 6 of Table 6

n	FE	Eq. (8) *	Eq. (44) *	Eq. (45) *	Eq. (46) *	Eq. (8)/Eq. (46)	Eq. (46)/FE	Mode
2	**	20.875	20.450	20.290	20.420	1.022		
3	**	20.255	19.480	18.750	19.410	1.044		
4	19.575	19.472	18.450	17.000	18.360	1.061	0.938	Trip.
5	17.401	18.594	17.472	15.826	17.396	1.069	1.000	Trip.
6	14.820	15.820	15.211	14.877	15.155	1.044	1.023	Trip.
7	12.465	13.300	13.547	13.330	13.301	1.000	1.067	Trip.
8	10.845	11.331	12.383	11.585	11.765	0.963	1.085	Trip.
9	9.576	9.867	11.635	10.136	10.544	0.936	1.101	Mixed
10	8.922	8.831	11.241	9.069	9.631	0.917	1.079	Interf.
11	8.068	8.143	11.155	8.345	9.003	0.904	1.116	Interf.
12	7.731	7.731	11.341	7.902	8.622	0.897	1.115	Interf.
13	7.586	7.536	11.769	7.682	8.444	0.892	1.113	Interf.
14	7.618	7.511	12.413	7.637	8.433	0.891	1.107	Interf.
15	7.775	7.621	13.250	7.731				Interf.

* For n=2-4, p_m was corrected to account for more than one axial half-wave between frames, see [23]

** Too many eigenvalues needed

Table 16 - Elastic Buckling Pressure (N/mm^2), Case 7 of Table 6

n	FE	Eq. (8)	Eq. (44)	Eq. (45)	Eq. (46)	Eq. (8)/Eq. (46)	Eq. (46)/FE	Mode
2	**	19.400	15.700	15.370	15.590	1.244		
3	**	18.900	13.650	12.870	13.320	1.420		
4	12.262	19.100	12.850	11.510	12.180	1.568	0.993	Trip.
5	10.508	17.100	12.000	10.320	10.970	1.559	1.044	Trip.
6	8.829	12.173	10.203	8.808	9.093	1.339	1.030	Trip.
7	6.822	8.379	8.545	7.344	7.375	1.136	1.081	Trip.
8	5.338	6.123	7.292	6.088	6.084	1.006	1.140	Trip.
9	4.437	4.834	6.452	5.130	5.202	0.929	1.172	Mixed
10	3.948	4.145	6.000	4.525	4.679	0.886	1.185	Interf.
11	3.744	3.831	5.874	4.232	4.441	0.863	1.186	Interf.
12	3.746	3.757	6.003	4.144	4.414	0.851	1.178	Interf.
13	3.872	3.843	6.328	4.149	4.538	0.847	1.172	Interf.
14	4.097	4.038	6.804	4.293	4.772	0.846	1.165	Interf.
15	4.398	4.313	7.398	4.517	5.086	0.848	1.156	Interf.

** Too many eigenvalues needed

Table 17 - Bending Stresses due to Initial Tilt for the Geometry of Fig. 42 [18]

Table 17a BENDING STRESS DUE TO AXISYMMETRIC ($n = 0$) INITIAL TILT (APPLIED PRESSURE 568 PSI)

Distance along web (in.)	Initial web tilt (in.)	Web deformation under pressure (in.)	Mean stresses (psi)		Bending stresses (psi)	
			Radial	Circumferential	Radial	Circumferential
0	0	0	−6229	−41,343	62,892	18,868
1·84	0·184	0·018	−5603	−41,968	41,162	11,508
3·68	0·368	0·062	−4943	−42,628	18,973	4338
5·52	0·552	0·119	−4247	−43,325	−1,668	−1027
7·36	0·736	0·176	−3511	−44,060	−19,291	−7168

Table 17b BENDING STRESS DUE TO SINUSOIDAL ($n = 3$) INITIAL TILT (APPLIED PRESSURE 568 PSI)

Distance along web (in.)	Initial web tilt (in.)	Web deformation under pressure (in.)	Mean stresses (psi)		Bending stresses (psi)	
			Radial	Circumferential	Radial	Circumferential
0	0	0	−6229	−41,343	78,408	23,522
1·84	0·184	0·022	−5603	−41,968	47,558	13,162
3·68	0·368	0·075	−4943	−42,628	16,314	3020
5·52	0·552	0·138	−4247	−43,325	−12,273	−5908
7·36	0·736	0·195	−3511	−44,060	−35,852	−12,881

Table 18 - Summary of Khaw's Results [241]

Table 18a. $R/t = 133$, $L_s/R = 0.675$, $E/\sigma_y = 841$, $\sigma_{rc}/\sigma_y = 0.110$, $n = 4.5$

δ_n/R %	SIMPLE SUPPORTED			CLAMPED		
	IR = 0*	IR= 3*	% LOSS	IR = 0	IR = 3	% LOSS
0.00	1369.4	1287.6	6.0	1687.9	1561.5	7.5
0.05	1273.0	1191.8	6.4	1569.2	1443.8	8.0
0.10	1189.3	1108.6	6.8	1466.1	1341.5	8.5
0.20	1051.0	971.2	7.6	1295.8	1172.7	9.5
0.30	941.5	862.4	8.4	1160.9	1038.9	10.5
0.40	852.7	774.2	9.2	1051.5	930.4	11.5
0.50	779.2	701.1	10.0	960.9	840.6	12.5
0.60	717.4	639.7	10.8	884.7	765.1	13.5

Pressures in kN/m^2

* IR = 0 - without welding residual stresses

* IR = 3 - with welding residual stresses

Table 18b $R/t = 133$, $L_s/R = 0.675$, $E/\sigma_y = 841$, $\sigma_{rc}/\sigma_y = 0.125$, $n = 5.0$

δ_n/R %	SIMPLE SUPPORTED			CLAMPED		
	IR = 0	IR = 3	% LOSS	IR = 0	IR = 3	% LOSS
0.00	1369.4	1277.7	6.7	1687.9	1546.6	8.4
0.05	1273.0	1182.0	7.1	1569.2	1429.0	8.9
0.10	1189.3	1098.8	7.6	1466.1	1326.8	9.5
0.20	1051.0	961.6	8.5	1295.8	1158.1	10.6
0.30	941.5	852.9	9.4	1160.9	1024.6	11.7
0.40	852.7	764.7	10.3	1051.5	916.2	12.8
0.50	779.2	691.7	11.2	960.9	826.4	14.0
0.60	717.4	630.4	12.1	884.7	750.9	15.1

Table 18c $R/t = 133$, $L_s/R = 0.675$, $E/\sigma_y = 841$, $\sigma_{rc}/\sigma_y = 0.154$, $n = 6.0$

δ_n/R %	SIMPLE SUPPORTED			CLAMPED		
	IR = 0	IR = 3	% LOSS	IR = 0	IR = 3	% LOSS
0.00	1369.4	1257.6	8.2	1687.9	1516.5	10.1
0.05	1273.0	1162.0	8.7	1569.2	1399.2	10.8
0.10	1189.0	1079.0	9.2	1466.1	1297.2	11.5
0.20	1051.0	941.9	10.3	1295.8	1128.9	12.9
0.30	941.5	833.4	11.5	1160.9	995.5	14.2
0.40	852.7	745.4	12.6	1051.5	887.4	15.6
0.50	779.2	672.6	13.7	960.9	797.8	16.9
0.60	717.4	611.3	14.8	884.7	722.5	18.3

Table 18 Cont'd

Table 18d. $R/t = 133$, $L_s/R = 0.338$, $E/\sigma_y = 841$, $\sigma_{rc}/\sigma_y = 0.154$, $n = 3.0$

δ_n/R %	SIMPLE SUPPORTED			CLAMPED		
	IR = 0	IR = 3	% LOSS	IR = 0	IR = 0	% LOSS
0.00	2839.7	2745.6	3.3	4077.2	3930.7	3.6
0.05	2650.8	2557.2	3.5	3807.7	3661.7	3.8
0.10	2485.5	2392.2	3.7	3571.6	3426.0	4.1
0.20	2209.9	2117.2	4.2	3177.5	3032.5	4.6
0.30	1989.3	1897.0	4.6	2861.7	2717.3	5.0
0.40	1808.8	1716.0	5.2	2603.0	2459.0	5.5
0.50	1658.3	1566.6	5.5	2387.2	2243.6	6.0
0.60	1530.9	1439.5	6.0	2204.5	2061.1	6.5

Table 18e $R/t = 133$, $L_s/R = 0.338$, $E/\sigma_y = 841$, $\sigma_{rc}/\sigma_y = 0.250$, $n = 4.$

δ_n/R %	SIMPLE SUPPORTED			CLAMPED		
	IR = 0	IR = 3	% LOSS	IR = 0	IR = 3	% LOSS
0.00	2839.7	2692.5	5.2	4077.2	3852.9	5.5
0.05	2650.8	2504.3	5.5	3807.7	3584.0	5.8
0.10	2485.5	2339.5	5.9	3571.6	3348.5	6.2
0.20	2209.9	2064.7	6.6	3177.5	2955.5	7.0
0.30	1989.3	1844.8	7.3	2861.7	2640.5	7.7
0.40	1808.8	1664.8	8.0	2603.0	2382.5	8.5
0.50	1658.3	1514.8	8.5	2387.2	2167.2	9.2
0.60	1530.9	1387.8	9.3	2204.5	1984.9	10.0

Table 19 - Collapse Pressure (N/mm²), ABAQUS vs. Refs. [23,140,142,149]

Model	ABAQUS	Other FE	Experimental	Element	Mesh: ni,nw,nf,nc
Mod. 2,[149]	6.16	6.58, ADINA	6.24	S8R	6,2,-,24
Mod. 3,[149]	6.47	6.85, ADINA	6.49	S8R	6,2,-,24
W1, [142]	4.52	5.17*	4.50	S8R	4,2,-,14
W3, [142]	6.68	6.39*	6.22	S8R	4,2,-,14
Geom A, [23]:					
o-o-c 0.25%R	4.26	4.00*		S4R	4,2,2,20
o-o-c 0.5%R	4.01	3.73*		S4R	4,2,2,20
D92a, [140]	1.134	1.135*		S8R	16,8,-,20
D92i, [140]	1.15	1.138*		S8R	16,8,-,20

Table 20 - Collapse Pressure (N/mm²), ABAQUS vs. Smith & Kirkwood [72]
No Residual Stresses

Calculation	o-o-c(%R)	n	Ref. [72]	ABAQUS
1	0.5	2	4.97	5.55
2	0.1	2	6.42	6.38,*
3	0.02	2	7.04	6.37,*
13	0.5	3	5.94	6.23
14	0.1	3	6.96	6.36,*
15	0.02	3	7.22	6.36,*

* $p_{c5} = 6.23$ N/mm²

Table 21 - Collapse Pressure (N/mm²), ABAQUS vs. Smith & Kirkwood [72]
Welding Residual Stresses

Calculation	η	o-o-c(%R)	n	Ref. [72]	ABAQUS *	ABAQUS **
4	2	0.02	2	5.85	5.72	6.1
5	4	0.02	2	4.05	4.36	4.74
16	2	0.02	3	5.92	5.69	6.05
17	4	0.02	3	4.05	4.42	5.46
new	4	0.5	2		3.56	3.61.
new	4	0.1	2		4.19	4.5
new	4	0.5	3		4.05	4.33
new	4	0.1	3		4.42	5.05

* Residual Stresses Modelled by a Corrected Material Curve

** Residual Stresses Modelled as Initial Stresses

Table 22 - Interframe Collapse - Empirical Design Curve

P_c/P_{c5}	P_m/P_{c5}
0.0	0.0
0.200	0.25
0.400	0.50
0.600	0.75
0.734	1.00
0.790	1.25
0.831	1.50
0.865	1.75
0.894	2.00
0.919	2.25
0.941	2.50
0.960	2.75
0.977	3.00
0.992	3.25
1.004	3.50
1.017	3.75
1.028	4.00
1.038	4.25
1.047	4.50
1.055	4.75
1.063	5.00
1.070	5.25
1.077	5.50
1.084	5.75
1.091	6.00
1.098	6.25
1.105	6.50
1.112	6.75
1.119	7.00

Table 23 - ABAQUS Collapse Pressures (N/mm^2) for Sample Cases, General Instability
No Residual Stresses and Shell Cold Bending Residual Stresses

Case	1	2	3	4	5	6	7
n	3	3	2	2	2	3	2
p_{c5} (N/mm^2)	6.63	9.05	6.05	3.64	3.84	4.35	3
p_y (N/mm^2)	5.56	8.17	6.07	3.5	2.76	2.73	3.54
L_c (mm)	10640	7500	16975	12600	18750	13870	18400
Mesh: ni,nw,nf,nc	4,3,2,20	4,2,2,20	4,2,2,20	4,2,2,20	4,2,2,20	4,2,2,20	6,3,-,20
zero o-o-c	7.43	9.96	6.54	4.23	4.53	5.16	3.51
0.25%R o-o-c	6.94	9.63	6.54	4.09	3.76	3.59	3.49
0.5%R o-o-c	6.35	8.93	6.32	3.98	3.21	2.94	3.25
zero o-o-c +cold bend.	7.32	9.81	6.51	4.16	4.47	5.08	3.39
0.25%R o-o-c+cold bend.	6.49	9.13	6.31	4.03	3.51	3.5	3.25
0.5%R o-o-c+cold bend.	5.88	8.35	5.78	3.74	3.07	2.87	3.03
Reduction due to cold bend.:							
zero o-o-c	0.985	0.985	0.995	0.983	0.987	0.984	0.966
0.25%R o-o-c	0.935	0.948	0.965	0.985	0.934	0.975	0.931
0.5%R o-o-c	0.926	0.935	0.915	0.94	0.956	0.976	0.932

Table 24 - ABAQUS Collapse Pressures (N/mm^2) for Sample Cases, General Instability Welding Residual Stresses

* L_c chosen so that $p_y < p_{c5}$

Case	1	2	3	4	5	6	7	8	9	10
n	3	3	2	2	2	3	2	3	2	2
p_{c5} (N/mm^2)	6.63	9.05	6.05	3.64	3.84	4.35	3	8.38	7.14	36.46
σ_{rf} (N/mm^2)	-234	-300	-177	-16	-23	-47	15	—	—	—
σ_{rc} (N/mm^2)	-345	-431	-289	-133	-144	-168	-101	—	—	—
ABAQUS,0.5%R:										
Finite Compartment:										
Comp. Length *	10640	7500	16975	12600	18750	13870	18400	11390	15000	15065
Mesh: ni,nw,nf,nc	4,3,2,20	4,2,2,20	4,2,2,20	4,2,2,20	4,2,2,20	4,2,2,20	6,3,-,20	4,2,2,20	4,2,2,20	4,2,2,20
p_y, 0.5%R, eq. (36)	5.56	8.17	6.07	3.5	2.76	2.73	3.54	5.56	5.55	27.085
p_y, 0.5%R, eq. (46)	3.47	4.39	4.26	3.39	2.92	2.53	3.67	—	—	—
Without Res. Stresses	6.35	8.93	6.32	3.98	3.21	2.94	3.25	6.06	6.89	31.54
With Res. Stresses:										
As Initial Stresses	3.61	4.61	4.15	3.15	3.01	2.45	2.6	—	—	—
Model. by Mat. Curve	3.3	3.89	3.63	3.1	2.84	2.69	2.522	—	—	—
Infinite Comp.:										
Mesh: ni,nw,nf,nc	8,6,4,80	8,8,4,80	8,8,4,80	16,10,4,66	16,8,4,66	16,8,4,66	24,10,-,56	8,4,4,60	8,4,4,60	8,4,4,60
p_y, 0.5%R, eq. (36)	3.6	6.33	4.06	2.99	2.19	1.88	3.49	2.67	4.94	25.088
p_y, 0.5%R, eq. (46)	2.64	3.93	3.11	3.63	2.11	1.78	3.61	—	—	—
Without Res. Stresses	3.96	6.91	4.36	3.36	2.38	1.814	3.4	2.85	5.33	28.84
With Res. Stresses:										
As Initial Stresses	2.86	4.106	3.32	3.02	2.3	1.72	2.66	—	—	—
Model. by Mat. Curve	2.73	3.77	3.16	2.92	2.32	1.77	2.46	—	—	—

Table 25 - ABAQUS Collapse Pressures (N/mm^2) for Sample Cases, Tripping
No Residual Stresses

Case	n	p_{c5} (N/mm^2)	p_{ti} (N/mm^2)	Mesh: ni,nw,nf,nc	0 deg. tilt	2 deg. tilt	4 deg. tilt
1	7	6.63	7.84	20,8,4,36	7.18	6.96	6.83
2	5	9.05	10.69	20,10,4,44	9.75	9.43	9.21
3	4	6.05	7.3	12,10,4,56	6.64	6.37	6.27
4	5	3.64	5.76	20,14,4,50	4.19	4.19	4.19
4b	7	3.64	5.61	20,14,4,40	4.19	4.19	3.96
4c	11	3.64	5.46	20,14,4,30	4.19	4.19	4.19
5	7	3.84	5.27	20,14,4,42	4.5	4.49	4.34
6	8	4.35	5.84	16,16,4,40	5.12	5	4.96
6b	8	4.4	5.35	16,16,4,40	5.09	4.95	4.9
7	8	3	5.76	32,12,-,28	3.5	3.23	3.22
Titanium -1*	7	11.48	10.18	20,8,4,26	11.02	—	8.38
Titanium - 2**	10	14.03	10.15	40,8,4,26	15.16	—	8.81

* R=1.0m p_d= 3 N/mm^2, t=17mm, L_s=485mm, Web 60x11mm, Flange 34x22mm

** R=2.5m p_d= 3 N/mm^2, t=28mm, L_s=550mm, Web 186x15mm, Flange 112x 28mm

Table 26 - Statistical Properties of the Basic Variables

Variable	Distribution	c.o.v. (%)
σ_{yp}	Log-Normal	4.32
σ_{yf}	Log-Normal	4.61
E	Normal	2
R	Normal	3
t	Normal	3
L_s	Normal	3
d_w	Normal	3
t_w	Normal	3
b_f	Normal	3
t_f	Normal	3
L_c *	Normal	3
o-o-c	Normal	eq. (68)
X_m	Normal	see text

* L_c adjusted to just meet the BS5500 criteria for frame yield

Table 27 - Sensitivity Studies, Flange Yield

variable	Case 1	Case 2b	Case 3	Case 4	Case 5
X_m	0.92	0.94	0.91	0.78	0.94
σ_{yf}	0.21	0.20	0.20	0.16	0.18
δ_n (n=2)	-0.07	-0.22	-0.06	-0.37	-0.02
δ_n (n=3)	-0.18	-0.07	-0.14	-0.09	-0.13
X_{m1} (n=2)	0.02	0.14	0.02	0.36	0.01
R	-0.13	-0.15	-0.12	-0.19	-0.11
		Values of α_i			
	Case 1	Case 2b	Case 3	Case 4	Case 5
X_m	1.1/0.6	1.1/0.53	1.1/0.59	1.1/0.68	1.1/0.49
σ_{yf} (N/mm^2)	550/524	615/586	540/513	390/376	390/371
δ_n (n=2)(mm)	7.88/9.27	3.94/6.24	7.88/9.26	3.94/7.62	5.32/5.71
δ_n (n=3) (mm)	3.56/5.22	1.78/2.13	3.56/5	1.78/2.2	2.4/3.33
X_{m1} (n=2)	1.1/1.09	1.1/1.01	1.1/1.09	1.1/0.88	1.1/1.1
R (mm)	4000/4079	2000/2047	4000/4079	2000/2056	2700/2751
		Values of x, x*			
	Case 1	Case 2b	Case 3	Case 4	Case 5
X_m	0.54	0.48	0.53	0.61	0.44
σ_{yf}	0.95	0.95	0.95	0.96	0.95
δ_n (n=2)	1.18	1.58	1.18	1.94	1.07
δ_n (n=3)	1.47	1.2	1.4	1.24	1.39
X_{m1}(n=2)	0.99	0.92	0.99	0.80	1.00
R	1.02	1.02	1.02	1.03	1.02
		Values of PSF			
β	4.942	5.108	5.476	4.932	5.903

Table 28 - Sensitivity Studies, Plate Yield

	Case 1	Case 2b	Case 3	Case 4	Case 5
X_m	0.97	0.97	0.98	0.96	0.98
σ_{yp}	0.16	0.17	0.15	0.13	0.14
δ_n (n=2)	-0.03	-0.10	-0.02	-0.14	-0.01
		Values of α_i:			
	Case 1	Case 2b	Case 3	Case 4	Case 5
Xm	1/0.53	1/0.55	1/0.48	1/0.46	1/0.42
σ_{yp} (N/mm^2)	550/535	595/579	540/525	390/381	390/379
δ_n (n=2)(mm)	7.88/8.32	3.94/4.64	7.88/8.23	3.94/5.17	5.32/5.40
		Values of x, x*			
	Case 1	Case 2b	Case 3	Case 4	Case 5
X_m	0.53	0.55	0.48	0.46	0.42
σ_{yp}	0.97	0.97	0.97	0.98	0.97
δ_n (n=2)	1.06	1.18	1.05	1.31	1.02
		Values of PSF			
β	3.745	5.108	5.476	4.932	5.903

Table 29 - Sensitivity Studies, Interframe Shell Collapse

	Case 1	Case 2	Case 3	Case 4	Case 5
X_m	0.97	0.97	0.97	0.97	0.97
σ_{yp}	0.12	0.12	0.12	0.12	0.11
t	0.14	0.14	0.15	0.17	0.16
		Values of α_i			
	Case 1	Case 2	Case 3	Case 4	Case 5
X_m	1.06/0.59	1.06/0.61	1.06/0.59	1.06/0.58	1.06/0.56
σ_{yp} (N/mm^2)	550/540	595/585	540/531	390/383	390/383
t (mm)	34/33.6	18/17.8	34/33.5	17.9/17.6	25/24.6
		Values of x, x*			
	Case 1	Case 2	Case 3	Case 4	Case 5
X_m	0.56	0.57	0.56	0.54	0.53
σ_{yp}	0.98	0.98	0.98	0.98	0.98
t	0.99	0.99	0.99	0.98	0.98
		Values of PSF			
β	3.123	3.012	3.124	3.243	3.343

Table 30 - Sensitivity Studies, Tripping

	Case 1	Case 2	Case 3	Case 4	Case 5
X_m	0.98	0.98	0.99	0.99	0.99
σ_{yf}	0.13	0.12	0.12	0.09	0.10
		Values of α_i			
	Case 1	Case 2	Case 3	Case 4	Case 5
X_m	1.0/0.45	1.0/0.45	1.0/0.42	1.0/0.31	1.0/0.31
$\sigma_{yf}(N/mm^2)$	550/538	615/602	540/528	390/382	390/382
		Values of x, x*			
	Case 1	Case 2	Case 3	Case 4	Case 5
X_m	0.45	0.45	0.42	0.31	0.31
σ_{yf}	0.98	0.98	0.98	0.98	0.98
		Values of PSF			
β	3.71	3.735	3.921	4.647	4.367
Upper Ditl. (%)	0.109	0.157	0.095	0.06	0.042

Table 31 - Material Properties

Material	ρ (ton/m^3)	σ_y (N/mm^2)	E (KN/mm^2)
HTS (EH-36)	7.8	355	207
HY80 (Q1N)	7.8	550	207
HY100 (Q2N)	7.8	690	207
HY 130 (Q3N)	7.8	890	207
Aluminium L65	2.8	390	70
Titanium 6-4	4.5	830	110

Table 32 - Risk of Death [172]

Exposure	Risk of Death per Hour per 10^3 Persons Exposed	Hours of Exposure per Person Exposed per Year	Risk of Death per 10^4 Exposed Person per Year	Ratio of Wounded to Number of Deaths
Mountain climbing (international)	2700	100	27	
Trawl fishing (deep sea, 1958-1972)	59	2900	17	
Flying (crew)	120	1000	12	<< 1
Coal mining	21	1600	3.3	
Automobile travel	56	400	2.2	20
Construction	7.7	2200	1.7	450
Flying (passengers)	120	100	1.2	<< 1
Home accidents	2.1	5500	1.1	
Factory work	2	2000	0.4	
Building fires	0.15	5500	0.08	5
Structural failure	0.002	5500	0.001	6

Table 33 - Average Reliability, No Overdiving

	Average Pf	Average β	β min	β max
Flange Yield - MoD	2.01E-07	5.08	4.89	5.90
Flange Yield - 0.05%	2.67E-05	4.04	3.60	4.77
Plate Yield - MoD	5.15E-05	3.88	3.56	5.01
Plate yield - 0.05%	1.15E-04	3.68	3.34	4.91
Tripping	4.23E-05	3.93	3.71	4.99
Interf., $1<P_m/P_{c5}<2.5$	6.90E-04	3.20	3.01	3.74
Interf., $P_m/P_{c5}>2.5$	2.10E-07	5.07	4.73	7.34

Table 34 - Average Reliability, 15% Overdiving

	Average Pf	Average β	β min	β max
Flange Yield - MoD	6.42E-06	4.37	4.14	5.42
Flange Yield - 0.05%	3.87E-04	3.36	2.94	4.01
Plate Yield - MoD	4.48E-04	3.32	2.95	4.60
Plate yield - 0.05%	9.69E-04	3.10	2.70	4.49
Tripping	2.18E-04	3.52	3.26	4.74
Interf., $1<P_m/P_{c5}<2.5$	3.98E-03	2.65	2.44	3.27
Interf., $P_m/P_{c5}>2.5$	2.03E-05	4.11	3.72	6.62

Table 35 - Average Reliability, 30% Overdiving

	Average Pf	Average β	β min	β max
Flange Yield - MoD	1.17E-04	3.68	3.42	4.67
Flange Yield - 0.05%	3.40E-03	2.71	2.20	3.30
Plate Yield - MoD	2.78E-03	2.77	2.35	4.19
Plate yield - 0.05%	5.87E-03	2.53	2.07	4.06
Tripping	9.48E-04	3.11	2.82	4.49
Interf., $1<P_m/P_{c5}<2.5$	1.69E-02	2.12	1.88	2.81
Interf., $P_m/P_{c5}>2.5$	6.77E-04	3.20	2.75	5.92

Table 36 - f for Format I, No Overdiving

	f	β min	β max
Flange Yield - MoD	2.02	4.66	5.30
Flange Yield - 0.05%	1.74	3.57	4.43
Plate Yield - MoD	2.08	3.84	3.93
Plate yield - 0.05%	2.00	3.61	3.73
Tripping	2.48	3.94	3.96
Interf., $1<P_m/P_{c5}<2.5$	1.81	3.15	3.26
Interf., $P_m/P_{c5}>2.5$	1.40	3.15	3.26

Table 37 - f for Format I, 15% Overdiving

	f	β min	β max
Flange Yield - MoD	1.75	3.85	4.50
Flange Yield - 0.05%	1.55	2.99	3.74
Plate Yield - MoD	1.80	3.21	3.30
Plate yield - 0.05%	1.75	3.05	3.17
Tripping	2.15	3.50	3.51
Interf., $1<P_m/P_{c5}<2.5$	1.55	2.57	2.65
Interf., $P_m/P_{c5}>2.5$	1.30	2.57	2.65

Table 38 - f for Format I, 30% Overdiving

	f	β min	β max
Flange Yield - MoD	1.55	3.19	3.82
Flange Yield - 0.05%	1.35	2.26	2.89
Plate Yield - MoD	1.60	2.68	2.76
Plate yield - 0.05%	1.55	2.48	2.59
Tripping	1.90	3.08	3.10
Interf., $1<P_m/P_{c5}<2.5$	1.40	2.12	2.31
Interf., $P_m/P_{c5}>2.5$	1.25	2.12	2.31

Table 39 - Comparison with Present Practice

	γ_{xmj}	γ_{xmj}	γ_{xmj} γ_f (max)	Present
Flange Yield - MoD	1.55	1.75	2.02	—
Flange Yield - 0.05%	1.35	1.55	1.75	1.8
Plate Yield - MoD	1.6	1.80	2.10	—
Plate yield - 0.05%	1.55	1.75	2.00	—
Tripping	1.9	2.15	2.50	—
Interf., $1<p_m/P_{c5}<2.5$	1.4	1.55	1.80	1.75
Interf., $P_m/P_{c5}>2.5$	1.25	1.3	1.40	1.75
	F_{max}=1.30	F_{max}=1.15		

APPENDIX 1

Experimental Results, Machined Models failing by Elastic General Instability

TEXT BOUND INTO THE SPINE

Reference	R_i	L_c	L_s	t	d_w	t_w	b_f	t_f	E	σ_y	p_{exp}	Exper. *n*
	mm	mm	mm	mm	mm	mm	mm	mm	(N/mm^2)	(N/mm^2)	(N/mm^2)	
[80] 10-10	25.400	64.008	6.350	0.762	0.889	0.508	0.000	0.000	71000.0	560.00	7.274	4
[80] 11-11	25.400	64.008	6.350	0.762	0.889	0.508	0.000	0.000	71000.0	560.00	7.033	4
[80] 15-6	25.400	64.008	6.350	0.762	0.889	0.508	0.000	0.000	71000.0	560.00	7.226	4
[80] 20-5	25.400	63.500	6.350	0.762	0.889	0.508	0.000	0.000	71000.0	560.00	7.412	4
[80] 24-10	25.400	38.608	6.350	0.762	0.889	0.508	0.000	0.000	71000.0	560.00	11.749	5
[136] M1	127.000	889.000	49.276	2.032	7.366	3.556	0.000	0.000	71000.0	241.33	3.031	3
[136] M3	127.000	889.000	63.500	2.032	8.382	4.064	0.000	0.000	71000.0	241.33	2.963	3
[136] M5	127.000	889.000	74.168	2.032	9.144	4.572	0.000	0.000	71000.0	241.33	3.275	3
[136] M8	127.000	889.000	88.900	2.032	9.906	5.080	0.000	0.000	71000.0	241.33	3.583	3
[136] M10	127.000	889.000	63.500	2.032	8.382	4.064	0.000	0.000	71000.0	241.33	3.171	3
[94] 25-22F	25.400	48.514	7.569	0.521	1.524	0.483	0.000	0.000	72401.0	563.30	9.791	4
[94] 20-22F	25.400	39.065	6.121	0.500	1.372	0.457	0.000	0.000	72401.0	554.40	10.480	5
[94] 15-22F	25.400	29.794	4.648	0.516	1.245	0.406	0.000	0.000	72401.0	568.10	11.859	5
[110] 4	130.175	505.968	50.800	2.032	2.032	2.032	0.000	0.000	71019.0	155.83	0.827	4
[110] 5	130.175	505.968	50.800	2.032	3.048	2.032	0.000	0.000	71019.0	155.83	1.020	4
[110] 6	130.175	505.968	50.800	2.032	4.064	2.032	0.000	0.000	71019.0	155.83	1.296	4
[74,85] 6, I	103.099	399.847	29.261	0.889	4.293	2.184	0.000	0.000	207000.0	689.50	3.475	3
[74,85] 6, II	103.099	399.847	29.261	0.889	4.293	2.184	0.000	0.000	207000.0	689.50	3.972	3
[74,85] 6, III	103.099	399.847	29.261	0.889	4.293	2.184	0.000	0.000	207000.0	689.50	3.972	3
[74,85] 6, V	103.099	399.847	29.261	0.889	4.293	2.184	0.000	0.000	207000.0	689.50	4.827	3
[74,85] 2A, I	103.099	721.720	29.261	0.889	4.293	2.184	0.000	0.000	207000.0	689.50	2.337	2
[74,85] 2A, II	103.099	721.720	29.261	0.889	4.293	2.184	0.000	0.000	207000.0	689.50	2.517	2
[74,85] 2A, III	103.099	721.720	29.261	0.889	4.293	2.184	0.000	0.000	207000.0	689.50	2.717	3

Eq. (28) with R_s (N/mm^2)	Theor. n Eq. (28)	X_{m1} Eq. (28) with R_s	Eq. (28) with R_c (N/mm^2)	X_{m1} Eq. (28) with R_c	Kendr. (N/mm^2)	Theor. n Kendr.	X_{m1} Kendr.	R_i / t	z $l = L_s$	L_c / R_i	p_{yf} (N/mm^2)
5.394	4	1.349	5.771	1.260	6.694	4	1.087	33.333	1.987	2.520	22.560
5.394	4	1.304	5.771	1.219	6.694	4	1.051	33.333	1.987	2.520	22.560
5.394	4	1.340	5.771	1.252	6.694	4	1.079	33.333	1.987	2.520	22.560
5.425	4	1.366	5.802	1.278	6.728	4	1.102	33.333	1.987	2.500	22.560
8.439	5	1.392	9.016	1.303	11.146	5	1.054	33.333	1.987	1.520	22.560
1.863	2	1.627	1.936	1.566	1.809	2	1.676	62.500	8.975	7.000	6.762
1.983	2	1.494	2.064	1.436	2.002	2	1.480	62.500	14.905	7.000	7.446
2.118	2	1.546	2.206	1.485	2.208	2	1.483	62.500	20.333	7.000	8.048
2.206	2	1.624	2.298	1.559	2.393	2	1.497	62.500	29.213	7.000	8.657
1.983	2	1.599	2.064	1.536	2.002	2	1.584	62.500	14.905	7.000	7.446
8.100	4	1.209	8.696	1.126	8.432	4	1.161	48.780	4.132	1.910	17.526
9.127	4	1.148	9.612	1.090	9.410	4	1.114	50.761	2.812	1.538	16.503
10.956	5	1.082	11.634	1.019	11.763	5	1.008	49.261	1.574	1.173	17.305
0.422	4	1.961	0.435	1.902	0.648	4	1.277	64.063	9.306	3.887	3.139
0.622	4	1.641	0.649	1.572	0.850	4	1.201	64.063	9.306	3.887	3.260
0.937	4	1.383	0.987	1.313	1.159	3	1.118	64.063	9.306	3.887	3.381
3.549	3	0.979	3.621	0.960	3.407	3	1.020	115.972	8.911	3.878	11.293
3.549	3	1.119	3.621	1.097	3.407	3	1.166	115.972	8.911	3.878	11.293
3.549	3	0.979	3.621	1.097	3.407	3	1.166	115.972	8.911	3.878	11.293
3.549	3	1.119	3.621	1.333	3.407	3	1.417	115.972	8.911	3.878	11.293
2.478	2	0.943	2.325	1.005	2.162	2	1.081	115.972	8.911	7.000	11.293
2.478	2	1.016	2.325	1.083	2.162	2	1.164	115.972	8.911	7.000	11.293
2.478	2	0.943	2.325	1.169	2.162	2	1.257	115.972	8.911	7.000	11.293

P_{exp} / P_{yf}	χ	k_l Kendr.	k_l Eq. (28)	$1/\chi$	X_{m1} P_{yf}/χ	FE- B.C. Case I Theor. n (N/mm^2)	FE- B.C. Case I Exp. n (if diff.) (N/mm^2)	FE- B.C. Case III Theor. n (N/mm^2)	FE- B.C. Case III Exp. n (if diff.) (N/mm^2)	Chosen FE (N/mm^2)
0.322	3.555	0.890	0.780	0.281	1.145	6.473		8.118		6.473
0.312	3.555	0.890	0.780	0.281	1.109	6.473		8.118		6.473
0.320	3.555	0.890	0.780	0.281	1.138	6.473		8.118		6.473
0.329	3.525	0.880	0.770	0.284	1.160	6.473		8.118		6.473
0.521	2.145	0.930	0.750	0.466	1.118	9.981		10.494		9.981
0.448	2.785	0.780	0.800	0.359	1.248	1.785	2.562	4.019	2.766	2.766
0.398	2.541	0.800	0.830	0.394	1.011	1.897	2.735	4.098	2.915	2.915
0.407	2.342	0.800	0.820	0.427	0.953	2.018	2.934	4.203	3.100	3.100
0.414	2.214	0.780	0.790	0.452	0.917	2.095	2.993	4.193	3.152	3.152
0.426	2.541	0.780	0.810	0.394	1.082	2.018	2.934	4.203	3.100	3.100
0.559	1.639	0.850	0.860	0.610	0.916	7.612	9.405	10.804	10.886	10.804
0.635	1.405	0.920	0.920	0.712	0.892	8.407	8.667	12.697	11.017	11.017
0.685	1.177	0.990	0.970	0.850	0.806	9.841	10.374	12.440	13.987	12.440
0.264	6.675	0.780	0.530	0.150	1.762	0.904	0.643	2.216	0.960	0.960
0.313	4.609	0.780	0.610	0.217	1.443	0.994	0.817	2.320	1.143	1.143
0.383	3.235	0.850	0.750	0.309	1.239	1.136	1.104	2.480	1.434	1.434
0.308	2.370	1.000	1.050	0.422	0.730	3.061		5.323		3.061
0.352	2.370	0.880	0.880	0.422	0.834	3.061		5.323		3.061
0.352	2.370	1.000	1.050	0.422	0.834	3.061		5.323		3.061
0.427	2.370	0.880	0.880	0.422	1.012	3.061		5.323		5.323
0.207	4.168	1.000	1.040	0.240	0.863	2.082	2.399	5.468	2.758	2.082
0.223	4.168	0.970	0.990	0.240	0.929	2.082	2.399	5.468	2.758	2.758
0.241	4.168	1.000	1.040	0.240	1.004	2.082	2.399	5.468	2.758	2.758

Chosen n	Min Case I	Min Case III	$1000\ \sigma_y / E$	X_{m1}	Case I/Eq. (28)	Case III/Eq. (28)	Eq. (28)/Kendr	C III/C I	C III/C I
	(N / mm^2)	(N / mm^2)		FE				Theor. n	Exp. n (if diff.)
4	6.473	8.118	7.887	1.124	1.122	1.407	0.862	1.254	
4	6.473	8.118	7.887	1.086	1.122	1.407	0.862	1.254	
4	6.473	8.118	7.887	1.116	1.122	1.407	0.862	1.254	
4	6.473	8.118	7.887	1.145	1.116	1.399	0.862	1.254	
5	9.981	10.494	7.887	1.177	1.107	1.164	0.809	1.051	
3	1.785	2.766	3.399	1.096	0.922	1.429	1.070	2.252	1.080
3	1.897	2.915	3.399	1.016	0.919	1.412	1.031	2.160	1.066
3	2.018	3.100	3.399	1.056	0.915	1.405	0.999	2.083	1.057
3	2.095	3.152	3.399	1.137	0.912	1.372	0.960	2.001	1.053
3	2.018	3.100	3.399	1.023	0.978	1.502	1.031	2.083	1.057
4	7.612	10.804	7.780	0.906	0.875	1.242	1.031	1.419	1.157
5	8.407	11.017	7.657	0.951	0.875	1.146	1.021	1.510	1.271
4	9.841	12.440	7.847	0.953	0.846	1.069	0.989	1.264	1.348
4	0.643	0.960	2.194	0.862	1.478	2.207	0.671	2.451	1.493
4	0.817	1.143	2.194	0.893	1.259	1.761	0.764	2.334	1.399
4	1.104	1.434	2.194	0.904	1.119	1.453	0.852	2.183	1.299
3	3.061	5.323	3.330	1.135	0.845	1.470	1.063	1.739	
3	3.061	5.323	3.330	1.298	0.845	1.470	1.063	1.739	
3	3.061	5.323	3.330	1.298	0.845	1.470	1.063	1.739	
3	3.061	5.323	3.330	0.907	0.845	1.470	1.063	1.739	
2	2.082	2.758	3.330	1.122	0.895	1.186	1.075	2.626	1.150
2	2.082	2.758	3.330	0.913	0.895	1.186	1.075	2.626	1.150
3	2.082	2.758	3.330	0.985	0.895	1.186	1.075	2.626	1.150

[74,85] 2A, IV	103.099	721.720	29.261	0.889	4.293	2.184	0.000	0.000	207000.0	689.50	2.744	3
[74,85] 2A, V	103.099	721.720	29.261	0.889	4.293	2.184	0.000	0.000	207000.0	689.50	2.820	3
[74,85] 3A, I	103.099	897.280	29.261	0.889	4.293	2.184	0.000	0.000	207000.0	689.50	1.579	2
[74,85] 3A, II	103.099	897.280	29.261	0.889	4.293	2.184	0.000	0.000	207000.0	689.50	1.696	2
[74,85] 3A, III	103.099	897.280	29.261	0.889	4.293	2.184	0.000	0.000	207000.0	689.50	2.055	2
[74,85] 3A, IV	103.099	897.280	29.261	0.889	4.293	2.184	0.000	0.000	207000.0	689.50	2.172	2
[74,85] 3A, V	103.099	897.280	29.261	0.889	4.293	2.184	0.000	0.000	207000.0	689.50	2.606	2
[74,85] 4A, I	103.099	1072.850	29.261	0.889	4.293	2.184	0.000	0.000	207000.0	689.50	1.227	2
[74,85] 4A, II	103.099	1072.850	29.261	0.889	4.293	2.184	0.000	0.000	207000.0	689.50	1.303	2
[74,85] 4A, III	103.099	1072.850	29.261	0.889	4.293	2.184	0.000	0.000	207000.0	689.50	1.593	2
[74,85] 4A, IV	103.099	1072.850	29.261	0.889	4.293	2.184	0.000	0.000	207000.0	689.50	1.572	2
[74,85] 4A, V	103.099	1072.850	29.261	0.889	4.293	2.184	0.000	0.000	207000.0	689.50	1.993	2
[74,85] 4A -1	103.099	497.007	29.261	0.889	4.293	2.184	0.000	0.000	207000.0	689.50	3.261	3
[74,85] 4A -2	103.099	612.975	29.261	0.889	4.293	2.184	0.000	0.000	207000.0	689.50	2.910	3
[74,85] 4A -3	103.099	673.030	29.261	0.889	4.293	2.184	0.000	0.000	207000.0	689.50	2.841	3
[74,85] 4A -4	103.099	731.014	29.261	0.889	4.293	2.184	0.000	0.000	207000.0	689.50	2.765	3
[74,85] 4A -5	103.099	760.006	29.261	0.889	4.293	2.184	0.000	0.000	207000.0	689.50	2.744	3
[74,85] 4A -6	103.099	788.998	29.261	0.889	4.293	2.184	0.000	0.000	207000.0	689.50	2.717	3
[74,85] 4A -7	103.099	820.061	29.261	0.889	4.293	2.184	0.000	0.000	207000.0	689.50	2.696	3
[74,85] 4A -8	103.099	849.053	29.261	0.889	4.293	2.184	0.000	0.000	207000.0	689.50	2.641	2
[74,85] 4A -9	103.099	907.038	29.261	0.889	4.293	2.184	0.000	0.000	207000.0	689.50	2.269	2
[74,85] 4A -10	103.099	965.022	29.261	0.889	4.293	2.184	0.000	0.000	207000.0	689.50	1.938	2
[79] 1	103.099	357.124	34.773	1.194	2.946	2.184	0.000	0.000	207000.0	689.50	2.841	4
[79] 2	103.099	357.124	34.773	1.194	2.946	2.184	0.000	0.000	207000.0	689.50	2.820	4
[79] 3	103.099	357.124	34.773	1.194	2.946	2.184	0.000	0.000	207000.0	689.50	2.786	4
[79] 4	103.099	357.124	34.773	1.194	2.946	2.184	0.000	0.000	207000.0	689.50	2.751	4

2.478	2	0.943	2.325	1.180	2.162	2	1.269	115.972	8.911	7.000	11.293
2.478	2	1.016	2.325	1.213	2.162	2	1.304	115.972	8.911	7.000	11.293
1.542	2	1.024	1.573	1.004	1.484	2	1.064	115.972	8.911	8.703	11.293
1.542	2	1.100	1.573	1.078	1.484	2	1.143	115.972	8.911	8.703	11.293
1.542	2	1.024	1.573	1.306	1.484	2	1.385	115.972	8.911	8.703	11.293
1.542	2	1.024	1.573	1.381	1.484	2	1.464	115.972	8.911	8.703	11.293
1.542	2	1.100	1.573	1.657	1.484	2	1.756	115.972	8.911	8.703	11.293
1.243	2	0.987	1.281	0.958	1.240	2	0.990	115.972	8.911	10.406	11.293
1.243	2	1.048	1.281	1.017	1.240	2	1.051	115.972	8.911	10.406	11.293
1.243	2	0.987	1.281	1.244	1.240	2	1.285	115.972	8.911	10.406	11.293
1.243	2	1.048	1.281	1.227	1.240	2	1.268	115.972	8.911	10.406	11.293
1.243	2	1.048	1.281	1.556	1.240	2	1.607	115.972	8.911	10.406	11.293
2.954	3	1.104	3.067	1.063	2.956	3	1.103	115.972	8.911	4.821	11.293
2.708	3	1.074	2.821	1.031	2.793	3	1.042	115.972	8.911	5.945	11.293
2.647	3	1.073	2.723	1.043	2.533	2	1.122	115.972	8.911	6.528	11.293
2.200	2	1.257	2.263	1.222	2.105	2	1.313	115.972	8.911	7.090	11.293
2.050	2	1.339	2.089	1.314	1.945	2	1.411	115.972	8.911	7.372	11.293
1.901	2	1.429	1.944	1.397	1.813	2	1.498	115.972	8.911	7.653	11.293
1.771	2	1.522	1.814	1.486	1.696	2	1.590	115.972	8.911	7.954	11.293
1.668	2	1.583	1.711	1.543	1.605	2	1.645	115.972	8.911	8.235	11.293
1.507	2	1.505	1.549	1.464	1.464	2	1.550	115.972	8.911	8.798	11.293
1.387	2	1.397	1.430	1.355	1.362	2	1.423	115.972	8.911	9.360	11.293
2.508	4	1.133	2.606	1.090	2.734	4	1.039	86.348	9.370	3.464	12.080
2.508	4	1.124	2.606	1.082	2.734	4	1.031	86.348	9.370	3.464	12.080
2.508	4	1.111	2.606	1.069	2.734	4	1.019	86.348	9.370	3.464	12.080
2.508	4	1.097	2.606	1.056	2.734	4	1.006	86.348	9.370	3.464	12.080

0.243	4.168	1.000	1.040	0.240	1.013	2.082	2.399	5.468	2.758	2.758
0.250	4.168	0.970	0.990	0.240	1.042	2.082	2.399	5.468	2.758	2.758
0.140	5.348	0.960	1.000	0.187	0.749	1.400	2.289	3.151	2.455	1.400
0.150	5.348	0.920	0.950	0.187	0.802	1.400	2.289	3.151	2.455	1.400
0.182	5.348	0.960	1.000	0.187	0.973	1.400	2.289	3.151	2.455	2.455
0.192	5.348	0.960	1.000	0.187	1.027	1.400	2.289	3.151	2.455	2.455
0.231	5.348	0.920	0.950	0.187	1.235	1.400	2.289	3.151	2.455	2.455
0.109	6.400	1.020	1.060	0.156	0.698	1.131	2.282	2.137	2.358	1.131
0.115	6.400	0.950	0.980	0.156	0.736	1.131	2.282	2.137	2.358	1.131
0.141	6.400	1.020	1.060	0.156	0.902	1.131	2.282	2.137	2.358	2.137
0.139	6.400	0.950	0.980	0.156	0.890	1.131	2.282	2.137	2.358	2.137
0.176	6.400	0.950	0.980	0.156	1.126	1.131	2.282	2.137	2.358	2.137
0.289	2.978	0.850	0.910	0.336	0.861	5.624	2.615	6.452	3.850	3.850
0.258	3.672	0.850	0.910	0.272	0.947	3.099	2.447	6.452	3.081	3.081
0.252	4.032	0.830	0.890	0.248	1.016	2.453	2.415	6.452	2.880	2.880
0.245	4.380	0.900	0.900	0.228	1.073	2.022	2.398	5.283	2.744	2.744
0.243	4.553	0.860	0.880	0.220	1.106	1.861	2.392	4.775	2.693	2.693
0.241	4.727	0.830	0.850	0.212	1.139	1.727	2.389	4.334	2.651	2.651
0.239	4.913	0.800	0.820	0.204	1.174	1.616	2.386	3.952	2.615	2.615
0.234	5.087	0.770	0.800	0.197	1.190	1.522	2.385	3.619	2.585	2.585
0.201	5.434	0.780	0.810	0.184	1.092	1.377	2.384	3.075	2.539	2.539
0.172	5.782	0.790	0.820	0.173	0.995	1.272	2.384	2.657	2.505	2.384
0.235	4.125	0.920	0.880	0.242	0.969	3.252	2.472	7.397	3.498	2.472
0.233	4.125	0.940	0.900	0.242	0.961	3.252	2.472	7.397	3.498	2.472
0.231	4.125	0.970	0.900	0.242	0.953	3.252	2.472	7.397	3.498	2.472
0.228	4.125	0.970	0.910	0.242	0.941	3.252	2.472	7.397	3.498	2.472

3	2.082	2.758	3.330	0.995	0.895	1.186	1.075	2.626	1.150
3	2.082	2.758	3.330	1.022	0.895	1.186	1.075	2.626	1.150
2	1.400	2.455	3.330	1.128	0.890	1.561	1.060	2.251	1.073
2	1.400	2.455	3.330	1.212	0.890	1.561	1.060	2.251	1.073
3	1.400	2.455	3.330	0.837	0.890	1.561	1.060	2.251	1.073
3	1.400	2.455	3.330	0.885	0.890	1.561	1.060	2.251	1.073
3	1.400	2.455	3.330	1.062	0.890	1.561	1.060	2.251	1.073
2	1.131	2.137	3.330	1.085	0.883	1.668	1.033	1.889	1.033
2	1.131	2.137	3.330	1.152	0.883	1.668	1.033	1.889	1.033
2	1.131	2.137	3.330	0.745	0.883	1.668	1.033	1.889	1.033
2	1.131	2.137	3.330	0.736	0.883	1.668	1.033	1.889	1.033
2	1.131	2.137	3.330	0.933	0.883	1.668	1.033	1.889	1.033
3	2.615	3.850	3.330	0.847	0.853	1.255	1.038	1.147	1.472
3	2.447	3.081	3.330	0.944	0.867	1.092	1.010	2.082	1.259
3	2.415	2.880	3.330	0.986	0.887	1.058	1.075	2.630	1.193
2	2.022	2.744	3.330	1.008	0.894	1.213	1.075	2.613	1.144
2	1.861	2.693	3.330	1.019	0.891	1.289	1.074	2.566	1.126
2	1.727	2.651	3.330	1.025	0.888	1.364	1.072	2.510	1.110
2	1.616	2.615	3.330	1.031	0.891	1.442	1.070	2.446	1.096
2	1.522	2.585	3.330	1.022	0.890	1.511	1.066	2.378	1.084
2	1.377	2.539	3.330	0.893	0.889	1.639	1.058	2.233	1.065
2	1.272	2.505	3.330	0.813	0.890	1.752	1.050	2.089	1.051
4	2.472	3.498	3.331	1.149	0.949	1.342	0.953	2.275	1.415
4	2.472	3.498	3.331	1.141	0.949	1.342	0.953	2.275	1.415
4	2.472	3.498	3.331	1.127	0.949	1.342	0.953	2.275	1.415
4	2.472	3.498	3.331	1.113	0.949	1.342	0.953	2.275	1.415

[79] 5	103.099	357.124	34.773	1.194	2.946	2.184	0.000	0.000	207000.0	689.50	2.751	4
[79] 6	103.099	357.124	34.773	1.194	2.946	2.184	0.000	0.000	207000.0	689.50	2.799	4
[79] 7	103.099	357.124	34.773	1.194	2.946	2.184	0.000	0.000	207000.0	689.50	2.730	4
[148] 1	147.700	300.000	50.000	2.300	8.500	2.500	0.000	0.000	199000.0	1400.00	19.964	4
[148] 2	147.700	450.000	50.000	2.300	10.500	2.500	0.000	0.000	199000.0	1400.00	18.676	4
[148] 3	147.700	450.000	50.000	2.300	11.500	2.500	0.000	0.000	199000.0	1400.00	21.681	4
[148] 4	147.700	600.000	50.000	2.300	13.500	2.500	0.000	0.000	199000.0	1400.00	21.252	3
[147] 1	247.500	960.500	50.000	2.500	9.000	2.500	0.000	0.000	215600.0	588.00	3.822	4
[147] 2	247.500	960.500	50.000	2.500	12.000	2.500	0.000	0.000	215600.0	588.00	5.145	4
[142]	247.500	960.500	50.000	2.500	14.500	2.500	0.000	0.000	210000.0	561.50	7.840	4
[113] A1	201.676	480.314	25.400	0.762	5.207	2.667	0.000	0.000	71000.0	241.33	0.894	not given
[113] A2	201.676	480.314	25.400	0.813	5.207	2.667	0.000	0.000	71000.0	241.33	0.894	"
[113] A3	201.676	480.314	25.400	0.838	5.207	2.667	0.000	0.000	71000.0	241.33	0.819	"
[113] D1	201.676	459.990	33.020	1.041	5.969	2.667	0.000	0.000	71000.0	241.33	1.179	"
[113] D2	201.676	459.990	33.020	1.118	5.969	2.667	0.000	0.000	71000.0	241.33	1.220	"
[113] D3	201.676	459.990	33.020	1.016	5.969	2.667	0.000	0.000	71000.0	241.33	1.145	"
[113] F1	201.676	459.990	33.020	0.940	3.429	2.667	0.000	0.000	71000.0	241.33	0.448	"
[113] F2	201.676	459.990	33.020	0.965	3.429	2.667	0.000	0.000	71000.0	241.33	0.469	"
[74,85] 1	103.099	546.151	29.261	0.889	4.293	2.184	0.000	0.000	207000.0	689.50	3.389	3
[74,85] 2	103.099	721.720	29.261	0.889	4.293	2.184	0.000	0.000	207000.0	689.50	2.810	3
[74,85] 3	103.099	897.280	29.261	0.889	4.293	2.184	0.000	0.000	207000.0	689.50	2.211	2
[74,85] 4	103.099	1072.850	29.261	0.889	4.293	2.184	0.000	0.000	207000.0	689.50	1.639	2
[74,85] 5	103.099	1423.975	29.261	0.889	4.293	2.184	0.000	0.000	207000.0	689.50	1.192	2

2.508	4	1.097	2.606	1.056	2.734	4	1.006	86.348	9.370	3.464	12.080
2.508	4	1.116	2.606	1.074	2.734	4	1.024	86.348	9.370	3.464	12.080
2.508	4	1.089	2.606	1.048	2.734	4	0.999	86.348	9.370	3.464	12.080
13.509	4	1.478	14.369	1.389	13.604	4	1.468	64.217	7.020	2.031	33.990
13.077	3	1.428	13.929	1.341	13.061	3	1.430	64.217	7.020	3.047	35.952
15.206	3	1.426	16.317	1.329	15.171	3	1.429	64.217	7.020	3.047	36.930
17.674	3	1.202	19.437	1.093	18.250	3	1.164	64.217	7.020	4.062	38.888
2.911	3	1.313	3.007	1.271	2.832	3	1.350	99.000	3.854	3.881	8.700
4.546	3	1.132	4.772	1.078	4.456	3	1.155	99.000	3.854	3.881	9.269
6.313	3	1.242	6.702	1.170	6.263	3	1.252	99.000	3.854	3.881	9.305
	4		0.650	1.376	0.701	4	1.275	264.667	4.005	2.382	1.940
	4		0.679	1.317	0.734	4	1.217	248.064	3.753	2.382	1.998
	4		0.694	1.180	0.751	4	1.091	240.663	3.641	2.382	2.027
	4		0.916	1.287	0.980	4	1.204	193.659	4.952	2.281	2.277
	4		0.965	1.265	1.031	4	1.183	180.455	4.614	2.281	2.362
	4		0.900	1.272	0.962	4	1.190	198.500	5.076	2.281	2.249
	5		0.322	1.391	0.358	5	1.254	214.595	5.487	2.281	1.813
	5		0.329	1.425	0.365	5	1.285	208.947	5.343	2.281	1.843
	3		2.933	1.155	2.859	3	1.185	115.972	8.911	5.297	11.293
	2		2.325	1.209	2.162	2	1.300	115.972	8.911	7.000	11.293
	2		1.573	1.406	1.484	2	1.490	115.972	8.911	8.703	11.293
	2		1.281	1.279	1.240	2	1.322	115.972	8.911	10.406	11.293
	2		1.098	1.086	1.084	2	1.100	115.972	8.911	13.812	11.293
				mean=1.253			mean=1.250				
				st.dev.=0.190			st.dev.=0.194				
				cov=0.152			cov=0.155				

0.228	4.125	0.970	0.910	0.242	0.941	3.252	2.472	7.397	3.498	2.472
0.232	4.125	0.940	0.900	0.242	0.957	3.252	2.472	7.397	3.498	2.472
0.226	4.125	0.980	0.910	0.242	0.932	3.252	2.472	7.397	3.498	2.472
0.587	1.887	0.640	0.730	0.530	1.108	19.092	12.888	23.170	18.816	18.816
0.519	2.006	0.740	0.800	0.499	1.041	11.555	14.260	19.020	16.443	16.443
0.587	1.727	0.750	0.790	0.579	1.014	13.084	16.679	20.631	18.867	18.867
0.546	1.768	0.700	0.810	0.566	0.965	14.714	21.807	18.551	22.607	18.551
0.439	2.660	0.750	0.810	0.376	1.168	2.748	3.266	5.522	3.956	3.956
0.555	1.660	0.870	0.930	0.602	0.921	4.194	6.001	7.091	6.732	6.001
0.843	1.187	0.770	0.830	0.842	1.001	5.735	8.847	8.663	9.584	8.663
0.461	2.674	0.772	0.762	0.374	1.233	0.693	0.876	0.897	0.921	0.897
0.447	2.658	0.810	0.788	0.376	1.188	0.736	0.933	0.950	0.986	0.950
0.404	2.651	0.910	0.857	0.377	1.071	0.753	0.958	0.978	1.008	0.753
0.518	2.206	0.828	0.812	0.453	1.143	0.975	1.175	1.342	1.281	1.281
0.517	2.203	0.834	0.757	0.454	1.139	1.028	1.241	1.352	1.354	1.352
0.509	2.208	0.834	0.820	0.453	1.124	0.957	1.131	1.231	1.197	1.197
0.247	5.185	0.795	0.715	0.193	1.281	0.355	0.423	0.740	0.466	0.466
0.254	5.179	0.765	0.690	0.193	1.315	0.432	0.362	0.759	0.477	0.477
0.300	3.271	0.780	0.800	0.306	0.981					
0.249	4.168	1.000	1.040	0.240	1.038					
0.196	5.348	0.960	1.000	0.187	1.048					
0.145	6.400	0.950	0.980	0.156	0.928					
0.106	8.529	0.930	0.950	0.117	0.904					
					mean = 1.03					
					stdev =0.17					
					cov=0.165					

4	2.472	3.498	3.331	1.113	0.949	1.342	0.953	2.275	1.415
4	2.472	3.498	3.331	1.132	0.949	1.342	0.953	2.275	1.415
4	2.472	3.498	3.331	1.105	0.949	1.342	0.953	2.275	1.415
4	12.888	18.816	7.035	1.061	0.897	1.309	1.056	1.214	1.460
4	11.555	16.443	7.035	1.136	0.830	1.180	1.066	1.646	1.153
4	13.084	18.867	7.035	1.149	0.802	1.156	1.076	1.577	1.131
4	14.714	18.551	7.035	1.146	0.757	0.954	1.065	1.261	1.037
4	2.748	3.956	2.727	0.966	0.914	1.316	1.062	2.009	1.211
3	4.194	6.732	2.727	0.857	0.879	1.411	1.071	1.691	1.122
3	5.735	8.663	2.674	0.905	0.856	1.293	1.070	1.511	1.083
4	0.693	0.897	3.399	0.996	1.067	1.381	0.927	1.294	1.051
4	0.736	0.950	3.399	0.941	1.084	1.399	0.925	1.291	1.057
4	0.753	0.978	3.399	1.088	1.085	1.409	0.924	1.299	1.052
5	0.975	1.281	3.330	0.920	1.065	1.399	0.935	1.376	1.090
4	1.028	1.352	3.330	0.903	1.066	1.402	0.935	1.315	1.091
4	0.957	1.197	3.330	0.956	1.064	1.331	0.935	1.286	1.058
5	0.355	0.466	3.330	0.962	1.102	1.447	0.901	2.085	1.102
5	0.362	0.477	3.330	0.983	1.100	1.449	0.902	1.757	1.318
				mean=1.020	mean=0.947	mean=1.397			
				st.dev.=0.121	st. dev.=0.119	st.dev.=0.200			
				cov=0.118	cov=0.126	cov=0.143			

[109] 48	96.520	97.282	2.819	0.287	0.109	1.295	0.000	0.000	69640.0	271.00	0.064	
[109] 50	96.520	95.758	2.819	0.267	0.198	1.422	0.000	0.000	69640.0	271.00	0.083	
[109] 54 (int.)	96.520	97.282	2.819	0.249	0.211	1.346	0.000	0.000	69640.0	271.00	0.095	
[109] 55	96.520	96.774	2.819	0.137	0.302	1.372	0.000	0.000	69640.0	271.00	0.063	

0.032		2.000	1.008		0.045			336.307	0.274	1.008	
0.046		1.820	0.992		0.058			361.498	0.294	0.992	
0.043		2.204	1.008		0.061			387.631	0.315	1.008	
0.034		1.853	1.003		0.038			704.526	0.573	1.003	

APPENDIX 2

Analytical Solution for the Elastic Tripping Pressure

A) FLANGED FRAME

The main assumptions are:

The frame remains circular along its curve of attachment to the shell plating

The rotational constraint provided by the shell is first calculated assuming the shell is stable; it is then assumed to decrease linearly with the ratio p_t/p_m valid for p_t up to $2p_m$ to allow for destabilising actions arising from Von Mises buckling of the shell

The mode number n for the complete left and right tripping waves of the ring frames coincides with the Von Mises mode n and wave length. This has been verified in F.E. eigenvalue buckling analyses

Web deformation is allowed for. A deformation function is assumed for the web and any point on the web centerline is described in terms of u_s and β_s of the shear centre of the section, assumed in the centre of the flange, Fig. A2.1

The relation between external tripping pressure p_t and the tripping stress σ_t is that arising from the axisymmetric hoop stress at the frame centroid making allowance for normal axisymmetric stable deformations of the pressure hull shell and framing: $p_t = \sigma_t / \xi$. Variation in this stress is then ignored throughout the frame cross section. Radial stresses acting at the frame are also neglected

Adamchack [104] assumed the deformation function of a beam cantilevered at the flange and loaded by a force and a moment at the other end:

$$u_w = 0.5\left\{\left[\frac{z}{d_c}\left(3-\frac{z^2}{d_c^2}\right)-3C'\frac{z}{d_c}\left(1-\frac{z}{d_c}\right)^2\right]u_s+\left[\frac{z}{d_c}\left(\frac{z^2}{d_c^2}-1\right)+C'\frac{z}{d_c}\left(1-\frac{z}{d_c}\right)^2\right]d_c\beta_s\right\} \qquad \text{(a2.1)}$$

u_s, β_s - Displacement and rotation of the shear centre
u,w - Displacements in the x,z directions of a point in the cross section
u_w - Displacement in the x direction of a point in the web

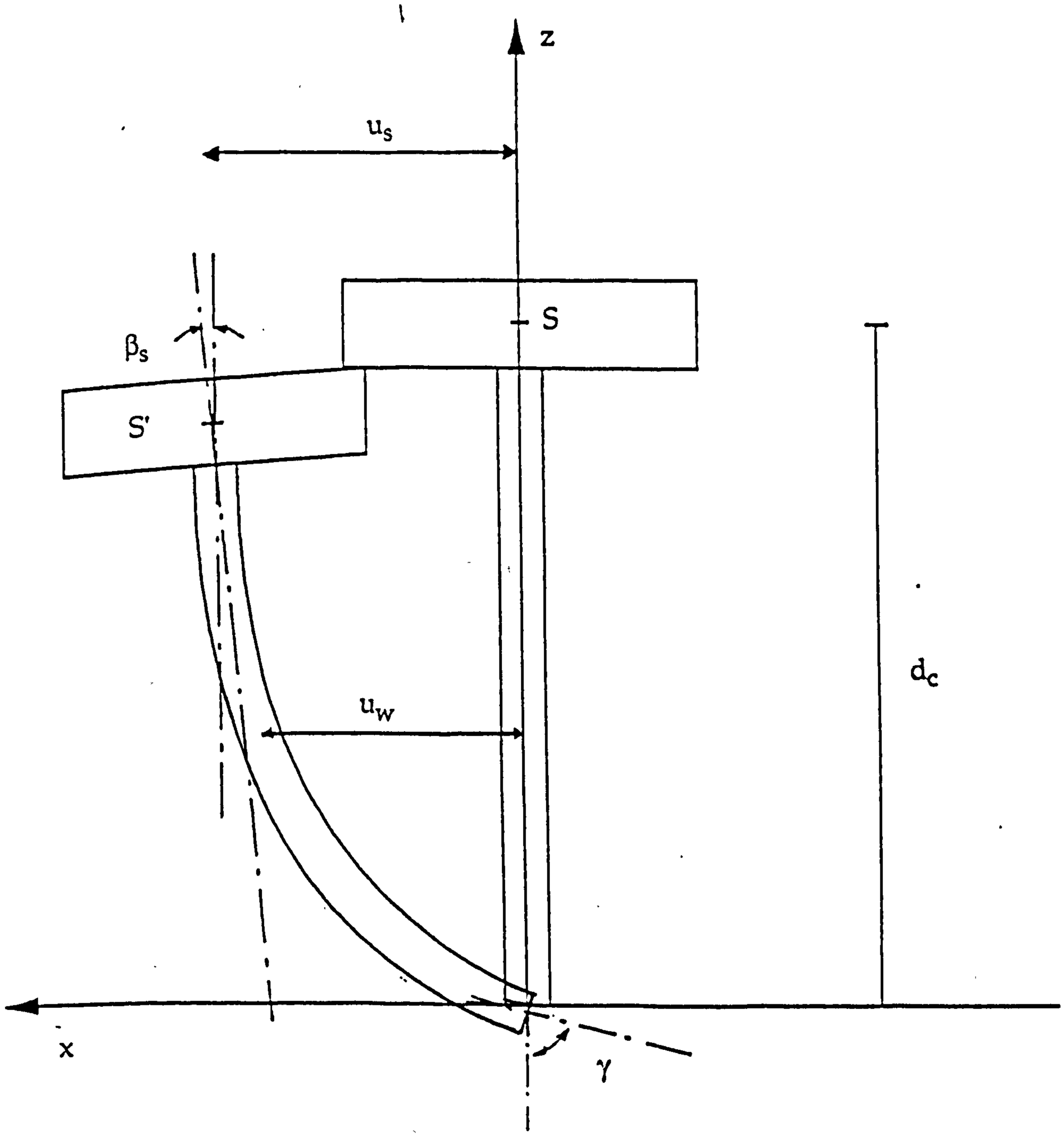

Figure A2.1 - Geometry and Notation (Appendix 2)

$$\text{where: } C' = \frac{\frac{Cd_c}{4D_w}}{1+\frac{Cd_c}{4D_w}} \tag{a2.2}$$

$$\text{and } C = C_{0n}\left(1 - p_t / p_m\right), \tag{a2.3}$$

The factor C′ in the deformation function leads to a solution in the form of a polynomial of the 6th. degree. So in this derivation a deformation function corresponding to a beam cantilevered at the flange and loaded only by a simply supported force at the other end was assumed:

$$u_w = u_s - \beta_s(d_c - z) - 0.5(u_s - \beta_s d_c)\left(\frac{d_c - z}{d_c}\right)^2\left[3 - \left(\frac{d_c - z}{d_c}\right)\right] \tag{a2.4}$$

The rotation of the toe of the web is then:

$$\gamma = 1.5\,(u_s - \beta_s d_c)/\,d_c \tag{a2.5}$$

The strain energy stored in an element of the web with thickness t_w and length dy is:

$$dV = \frac{EI}{2}\int_0^{d_c}\left(\frac{du_w}{dz}\right)^2 dz = \frac{1}{2}\frac{Et_w^3}{4d_c^3}(u_s - \beta_s d_c)^2 \tag{a2.6}$$

The total strain energy is given by:

$$V = \frac{1}{2}\int_0^l \left\{EI_z u_s''^2 + E\Gamma_2 \beta_s''^2 + G'J\beta_s'^2 + C\left[\beta_s + 1.5(u_s - \beta_s d_c)/\,d_c\right]^2 + \frac{Et_w^3}{4d_c^3}(u_s - \beta_s d_c)^2\right\} dy \tag{a2.7}$$

where primes indicate derivatives in relation to y.

The potential energy of the load is given by:

$$U_w = -\frac{1}{2}\iiint \sigma_t\left(u^2 + w^2\right) dx\,dz\,dy \tag{a2.8}$$

For the flange: $u = u_s$, $w = -x\beta_s$. For the web: $u = u_w$, eq. (a2.4), $w=0$ (a2.9)

Substituting (a2.9) into (a2.8) and doing the proper integrations:

$$U_w = -\frac{1}{2}\int_0^1 \sigma_t \left[u_s'^2 \left(A_s - \frac{18}{35} t_w d_c \right) + \beta_s'^2 \left(I_s - \frac{11}{35} d_c^3 t_w \right) - 2u_s'\beta_s' \frac{3}{35} d_c^2 t_w \right] dy \quad \text{(a2.10)}$$

The total potential is $U = V + U_w = \frac{1}{2}\int_0^1 \Phi \, dy$, eq. (a2.7) + eq. (a2.10)

The theorem of stationary potential energy requires the above integral to be a minimum and leads to the following two Eulerian equations:

$$\frac{\partial \Phi}{\partial u_s} - \frac{d\left(\frac{\partial \Phi}{\partial u_s'}\right)}{dy} + \frac{d^2\left(\frac{\partial \Phi}{\partial u_s''}\right)}{dy^2} = 0 \quad \text{(a2.11)}$$

$$\frac{\partial \Phi}{\partial \beta_s} - \frac{d\left(\frac{\partial \Phi}{\partial \beta_s'}\right)}{dy} + \frac{d^2\left(\frac{\partial \Phi}{\partial \beta_s''}\right)}{dy^2} = 0 \quad \text{(a2.12)}$$

doing the proper differentiations we obtain:

$$\left(\frac{Et_w^3}{4d_c^3} + \frac{9C}{4d_c^2} \right) u_s + \sigma_t \left(A_s - \frac{18}{35} t_w d_c \right) u_s'' + EI_z u_s^{iv} - \left(\frac{Et_w^3}{4d_c^3} + \frac{1}{3}\frac{9C}{4d_c^2} \right) \beta_s d_c - \sigma_t \frac{3}{35} d_c^2 t_w \beta_s'' = 0 \quad \text{(a2.13)}$$

$$\left(\frac{Et_w^3}{4d_c^3} + \frac{1}{3}\frac{9C}{4d_c^2} \right) u_s d_c + \sigma_t \frac{3}{35} d_c^2 t_w u_s'' - \left(\frac{Et_w^3}{4d_c^3} + \frac{1}{9}\frac{9C}{4d_c^2} \right) \beta_s d_c^2 + \left[G'J - \sigma_t \left(I_s - \frac{11}{35} d_c^3 t_w \right) \right] \beta_s'' - E\Gamma_2 \beta_s^{iv} = 0 \quad \text{(a2.14)}$$

by assuming $u_s = u_o \sin(n\theta)$, $\beta_s = \beta_o \sin(n\theta)$, $\theta = y/R_m$, and regrouping, we obtain a set of two homogeneous equations:

$$D_1 u_o \sin(n\theta) + D_2 \beta_o \sin(n\theta) = 0 \quad \text{(a2.15)}$$

$$E_1 u_o \sin(n\theta) + E_2 \beta_o \sin(n\theta) = 0 \quad \text{(a2.16)}$$

Nonvanishing solutions for u_o and β_o can only exist if the determinant of the coefficients of these equations is zero: $D_1E_2 - D_2E_1=0$ (a2.17)

Eq. (a2.17), using C given by (a2.3), will lead to a quadratic equation in σ_t and consequently a solution in the form:

$\sigma_t = \frac{b-\sqrt{b^2-4ac}}{2a}$, Eq. (46) of the main text, repeated

where:

$$a=\left(\frac{n}{R_m}\right)^2\left(c_5c_3-c_4^2\right)+\frac{c_2c_6}{\xi p_m}$$

$$b=c_2c_6+c_1c_7+\left[G'J+E\Gamma_2\left(\frac{n}{R_m}\right)^2\right]\left[c_3\left(\frac{n}{R_m}\right)^2+\frac{c_2}{\xi p_m}\right]+E\Gamma_1\left(\frac{n}{R_m}\right)^2\left[\frac{c_5}{d_c^2}\left(\frac{n}{R_m}\right)^2+\frac{c_2}{9\xi p_m}\right]$$
$$+\frac{4c_1c_2d_c^2}{9\xi p_m}\left(\frac{R_m}{n}\right)^2$$

$$c=\frac{4}{9}c_1c_2d_c^2\left(\frac{n}{R_m}\right)^2+\left[G'J+E\Gamma_2\left(\frac{n}{R_m}\right)^2\right]\left[c_1+c_2+EI_z\left(\frac{n}{R_m}\right)^4\right]+E\Gamma_1\left(\frac{n}{R_m}\right)^2\left[c_1+\frac{c_2}{9}\right]$$

$$c_1=\frac{Et_w^3}{4d_c^3} \qquad c_2=\frac{9C_{0n}}{4d_c^2} \qquad c_3=A_s-\frac{18}{35}t_wd_c \qquad c_4=\frac{3}{35}d_c^2t_w \qquad c_5=I_s-\frac{11}{35}d_c^3t_w$$

$$c_6=I_s+\frac{A_sd_c^2}{9}-\frac{3}{7}d_c^3t_w \qquad c_7=I_s+b_ft_fd_c^2$$

B) FLAT BAR FRAME

The same procedure is followed, but with u_s and β_s representing the displacements of the flat bar extremity and the strain energy given by:

$$V=\frac{1}{2}D_w\int_0^1\int_0^{d_w}\left[\left(v_{yy}+v_{zz}\right)^2-2(1-\nu)\left(v_{yy}v_{zz}-v_{yz}^2\right)\right]dzdy+\frac{1}{2}\int_0^1 C\gamma^2\,dy \qquad \text{(a2.18)}$$

The subscripts now indicate differentiation. The elastic tripping stress has again a quadratic form:

$$\sigma_t=\frac{E}{12\left(1-\nu^2\right)}\left(\frac{t_w}{d_w}\right)^2\frac{b-\sqrt{b^2-4ac}}{2a} \qquad \text{(a2.19)}$$

and is a function of 3 parameters:

$$a_1=\left(\frac{n\,d_w}{R_m}\right)^2 \quad a_2=\frac{C_{0n}d_w}{Et_w^3} \quad a_3=\frac{C_{0n}}{\xi p_m d_w t_w}$$

since:

$$a=a_1^2+\frac{75}{4}a_3a_1$$

$$b=225\left(1-\nu^2\right)a_1a_2+2a_1^3+90(1-\nu)a_1^2+525a_1+\frac{75}{4}a_3\left[84+\frac{42}{5}a_1(3-5\nu)+a_1^2\right]$$

$$c=a_1^4+90(1-\nu)a_1^3+\left[1029-21(2+5\nu)^2\right]a_1^2+3150(1-\nu)a_1$$
$$+225\left(1-\nu^2\right)a_2\left[84+\frac{42}{5}a_1(3-5\nu)+a_1^2\right]$$

C) COEFFICIENTS OF EQ. (45) OF THE MAIN TEXT

If the deformation function of Eq. (a2.1) is used, a solution in the form:

$\sigma_t^2\left(k_2k_4-k_6^2\right)+\sigma_t\left(k_1k_4+k_2k_3-2k_5k_6\right)+\left(k_1k_3-k_5^2\right)=0$, Eq. (45) repeated

The coefficients k_1-k_6 are given by:

For tee frames:

$$k_1 = EI_z\left(\frac{n}{R_m}\right)^2 + 3\frac{D_w}{d_c^3}\left(\frac{R_m}{n}\right)^2(1+3C')$$

$$k_2 = -A_s + d_c t_w\left(\frac{18}{35}+\frac{19C'}{140}-\frac{3C'^2}{140}\right)$$

$$k_3 = G'J + E\Gamma_2\left(\frac{n}{R_m}\right)^2 + 3\frac{D_w}{d_c}\left(\frac{R_m}{n}\right)^2\left(1+\frac{C'}{3}\right)$$

$$k_4 = -I_s + d_c^3 t_w\left(\frac{11}{35}+\frac{C'}{84}-\frac{C'^2}{420}\right)$$

$$k_5 = -3\frac{D_w}{d_c^2}\left(\frac{R_m}{n}\right)^2(1+C')$$

$$k_6 = d_c^2 t_w\left(\frac{3}{35}-\frac{17C'}{420}+\frac{C'^2}{140}\right)$$

For flat bars:

$$k_1 = \frac{D_w}{d_w}\left(\frac{R_m}{n\ d_w}\right)^2\left[3(1+3C')+\frac{3}{5}\left(\frac{n\ d_w}{R_m}\right)^2(4-C'+C'^2)+\left(\frac{n\ d_w}{R_m}\right)^4\left(\frac{17}{35}-\frac{19C'}{140}+\frac{3C'^2}{140}\right)\right]$$

$$k_2 = -d_w t_w\left[\frac{17}{35}-\frac{19C'}{140}+\frac{3C'^2}{140}+\frac{4-C'+C'^2}{40}\left(\frac{t_w}{d_w}\right)^2\right]$$

$$k_3 = D_w d_w\left(\frac{R_m}{n\ d_w}\right)^2\left[3+C'+\left(\frac{n\ d_w}{R_m}\right)^2\frac{6-3C'+C'^2}{15}+\left(\frac{n\ d_w}{R_m}\right)^4\left(\frac{2}{105}-\frac{C'}{84}+\frac{C'^2}{420}\right)\right]$$

$$k_4 = -d_w^3 t_w\left[\frac{2}{105}-\frac{C'}{84}+\frac{C'^2}{420}+\frac{6-3C'+C'^2}{360}\left(\frac{t_w}{d_w}\right)^2\right]$$

$$k_5 = -D_w\left(\frac{R_m}{n\ d_w}\right)^2\left[3(1+3C')+\left(\frac{n\ d_w}{R_m}\right)^2\left(\frac{2}{5}+\nu-\frac{2C'}{5}+\frac{C'^2}{5}\right)\right.$$
$$\left.+\left(\frac{n\ d_w}{R_m}\right)^4\left(\frac{3}{35}-\frac{17C'}{420}+\frac{C'^2}{140}\right)\right]$$

$$k_6 = d_c^2 t_w\left[\frac{3}{35}-\frac{17C'}{420}+\frac{C'^2}{140}+\frac{2-2C'+C'^2}{120}\left(\frac{t_w}{d_w}\right)^2\right]$$

APPENDIX 3

Experimental Results, Welded Models failing by General Instability

Reference	$\|R_1\|$	$\|L_c\|$	$\|L_s\|$	t	$\|d_w\|$
	mm	mm	mm	mm	mm
[143]-1	56.60	95.0	24.00	0.370	1.670
[143]-2	56.60	83.1	21.02	0.420	1.820
[143]-3	56.60	83.0	21.11	0.440	2.010
[143]-4	56.60	83.0	21.11	0.540	2.210
[143]-5	56.60	83.1	21.00	0.540	2.420
[143]-6	56.50	84.2	21.31	0.630	2.010
[143]-7	56.60	94.8	24.01	0.620	2.480
[143]-8	56.60	84.2	21.40	0.720	2.290
[143]-9	56.60	84.2	21.40	0.820	2.700
[143]-10	56.60	114.0	23.00	0.380	1.590
[143]-11	56.60	104.0	21.01	0.440	1.820
[143]-12	56.60	104.2	21.01	0.440	2.010
[143]-13	56.60	104.1	21.00	0.520	2.200
[143]-14	56.60	104.0	21.02	0.520	2.400
[143]-15	56.60	105.6	21.39	0.610	2.270
[143]-16	56.60	105.6	21.39	0.670	2.690
[143]-17	56.60	95.1	15.98	0.320	1.380
[143]-18	56.60	95.0	15.99	0.620	1.980
[126]-7	159.61	120.0	24.00	0.600	5.000
[126]-8	159.64	120.0	24.00	0.600	5.000
[149]-1	110.00	480.0	40.00	2.700	8.000
[149]-2	110.00	480.0	40.00	2.700	8.000
[149]-3	110.00	480.0	40.00	2.700	8.000
[124]-R1	160.00	200.0	40.00	0.600	4.800
[124]-R2	160.00	200.0	40.00	0.600	4.800
[147]	495.00	1920.0	100.00	5.000	24.000
[142]	495.00	1920.0	100.00	5.000	40.000
[148]-1	482.50	1470.0	163.00	7.500	38.000
[148]-2	482.50	1960.0	163.00	7.500	44.000
[139]-15	189.74	4876.8	1209.93	12.573	42.672
[139]-16	194.54	4876.8	811.91	7.899	35.560
[139]-17	196.47	4876.8	805.05	6.604	33.020
[139]-18	196.19	4876.8	1236.27	6.629	36.830
[139]-19	299.06	4876.8	1215.59	4.978	33.528
[139]-20(int)	299.57	4876.8	1224.41	4.978	33.020

$\lvert t_w \rvert$	$\lvert b_f \rvert$	$\lvert t_f \rvert$	E	$\lvert \sigma_v \rvert$	$\lvert p_{exp} \rvert$
mm	mm	mm	(N / mm^2)	(N / mm^2)	(N / mm^2)
1.000	0	0	196000	282.20	0.949
1.020	0	0	196000	279.30	1.291
1.010	0	0	205800	257.70	1.330
1.010	0	0	205800	257.70	1.779
0.990	0	0	205800	257.70	1.981
1.310	0	0	205800	257.70	2.084
1.210	0	0	196000	282.20	2.248
1.400	0	0	205800	257.70	2.565
1.400	0	0	196000	282.20	3.320
1.000	0	0	196000	282.20	0.654
1.010	0	0	205800	257.70	0.944
1.010	0	0	205800	257.70	0.937
1.000	0	0	205800	257.70	1.750
1.020	0	0	205800	257.70	1.843
1.390	0	0	196000	282.20	1.991
1.390	0	0	196000	282.20	2.820
0.780	0	0	196000	282.20	0.838
0.990	0	0	196000	282.20	2.171
0.600	6	0.6	205000	376.00	1.860
0.600	0	0	205000	376.00	1.560
5.500	0	0	71000	250.00	7.140
5.500	0	0	71000	250.00	6.240
5.500	0	0	71000	250.00	6.490
0.600	0	0	208000	387.00	0.500
0.600	0	0	208000	387.00	0.550
5.000	0	0	215600	561.54	4.498
5.000	0	0	205800	561.54	6.223
8.200	0	0	199000	1420.00	18.320
8.200	0	0	199000	1420.00	18.099
12.830	0	0	204092	301.30	11.377
6.990	0	0	198576	315.10	5.378
9.780	0	0	194439	312.30	3.758
6.910	0	0	199955	307.50	2.772
5.030	0	0	189612.5	310.96	0.683
5.210	0	0	189612.5	310.96	0.621

n	p_{cs}	p_{yf}	Eq. (28)	p_y	p_y / p_{cs}
experim.	(N / mm^2)	(N / mm^2)	(N / mm^2)	(N / mm^2)	
6	1.793	3.434	2.290	0.473	0.264
7	2.034	3.752	3.730	0.660	0.324
5	1.969	3.661	4.730	0.689	0.350
6	2.453	4.211	6.560	0.876	0.357
6	2.455	4.312	7.640	0.976	0.398
6	2.907	4.773	7.200	0.958	0.330
7	3.054	5.443	7.820	1.152	0.377
6	3.363	5.435	10.420	1.265	0.376
6	4.254	6.747	15.010	1.750	0.411
6	1.844	3.420	1.860	0.443	0.240
6	1.972	3.537	3.280	0.568	0.288
6	1.970	3.660	3.960	0.681	0.345
6	2.357	4.107	5.380	0.807	0.342
6	2.357	4.250	6.340	0.932	0.396
6	3.075	5.404	7.070	1.223	0.398
5	3.416	6.010	9.830	1.585	0.464
7	1.600	2.752	1.760	0.376	0.235
6	3.310	4.790	6.450	1.026	0.310
9	1.677	2.678	8.650	2.119	1.264
10	1.552	2.087	3.380	1.186	0.764
3	7.315	11.500	10.970	4.360	0.596
3	7.315	11.500	10.970	3.631	0.496
3	7.315	11.500	10.970	3.922	0.536
	1.435	2.164	2.090	0.085	0.059
	1.435	2.164	1.410	0.093	0.065
3	6.463	8.852	4.770	2.570	0.398
4	6.894	10.302	13.230	5.171	0.750
3	23.843	37.580	16.700	13.500	0.566
3	24.064	39.409	19.400	15.125	0.629
2	19.325	38.962	20.460	1.809	0.094
2	12.540	24.275	8.850	0.939	0.075
2	10.324	23.114	7.750	1.051	0.102
2	10.217	21.536	5.420	0.472	0.046
2	5.133	9.858	0.980	0.170	0.033
2	5.125	8.512	1.030	0.260	0.051

The, App.3

p_y / Eq.(28)	p_{exp} / p_y	e / R (%)	Statistical. Prop. of p_{exp} / p_y
0.207	2.006	1.00	
0.177	1.956	1.00	all models:
0.146	1.929	1.00	mean=2.48
0.134	2.031	1.00	st.dev.=1.545
0.128	2.030	1.00	cov=0.62
0.133	2.174	1.00	
0.147	1.951	1.00	models with
0.121	2.027	1.00	$0.3 \le e / R \le 1.0$:
0.117	1.897	1.00	mean=1.797
0.238	1.478	1.00	st.dev.=0.301
0.173	1.663	1.00	cov=0.167
0.172	1.377	1.00	
0.150	2.169	1.00	
0.147	1.977	1.00	
0.173	1.628	1.00	
0.161	1.779	1.00	
0.214	2.229	1.00	
0.159	2.116	1.00	
0.245	0.878	0.13	
0.351	1.316	0.11	
0.397	1.638	0.75	
0.331	1.719	1.04	
0.358	1.655	0.88	
0.041	5.882	3.00	
0.066	5.914	3.00	
0.539	1.750	0.60	
0.391	1.203	0.60	
0.808	1.357	0.30	
0.780	1.197	0.30	
0.088	6.285	2.54	
0.106	5.727	2.72	
0.136	3.577	2.46	
0.087	5.867	3.42	
0.173	4.020	2.70	
0.252	2.392	1.67	

APPENDIX 4

ABAQUS Post-Processing Results

o-o-c = 0.1%R, Load Increment 5

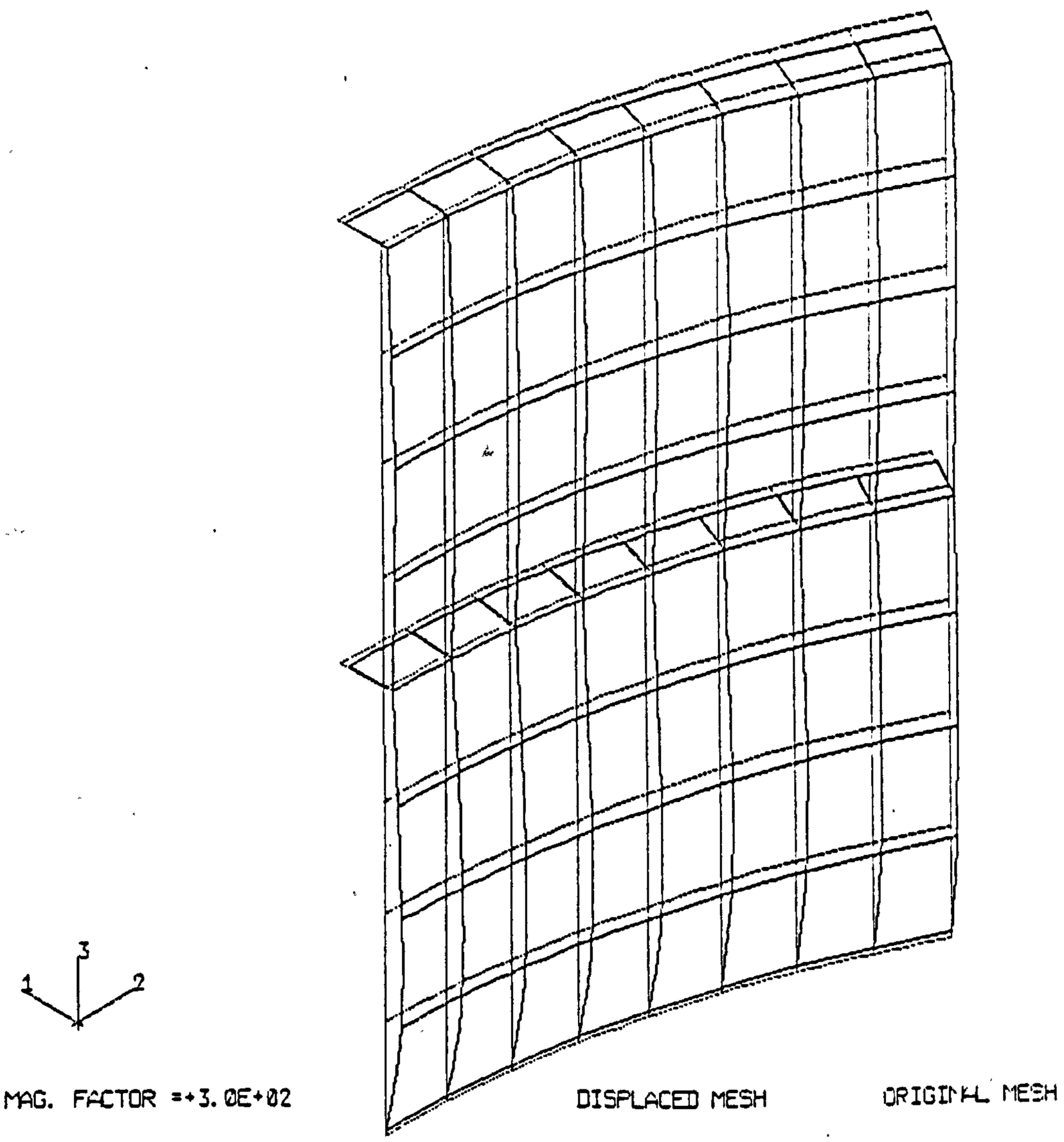

o-o-c = 0.1%R, Load Increment 5

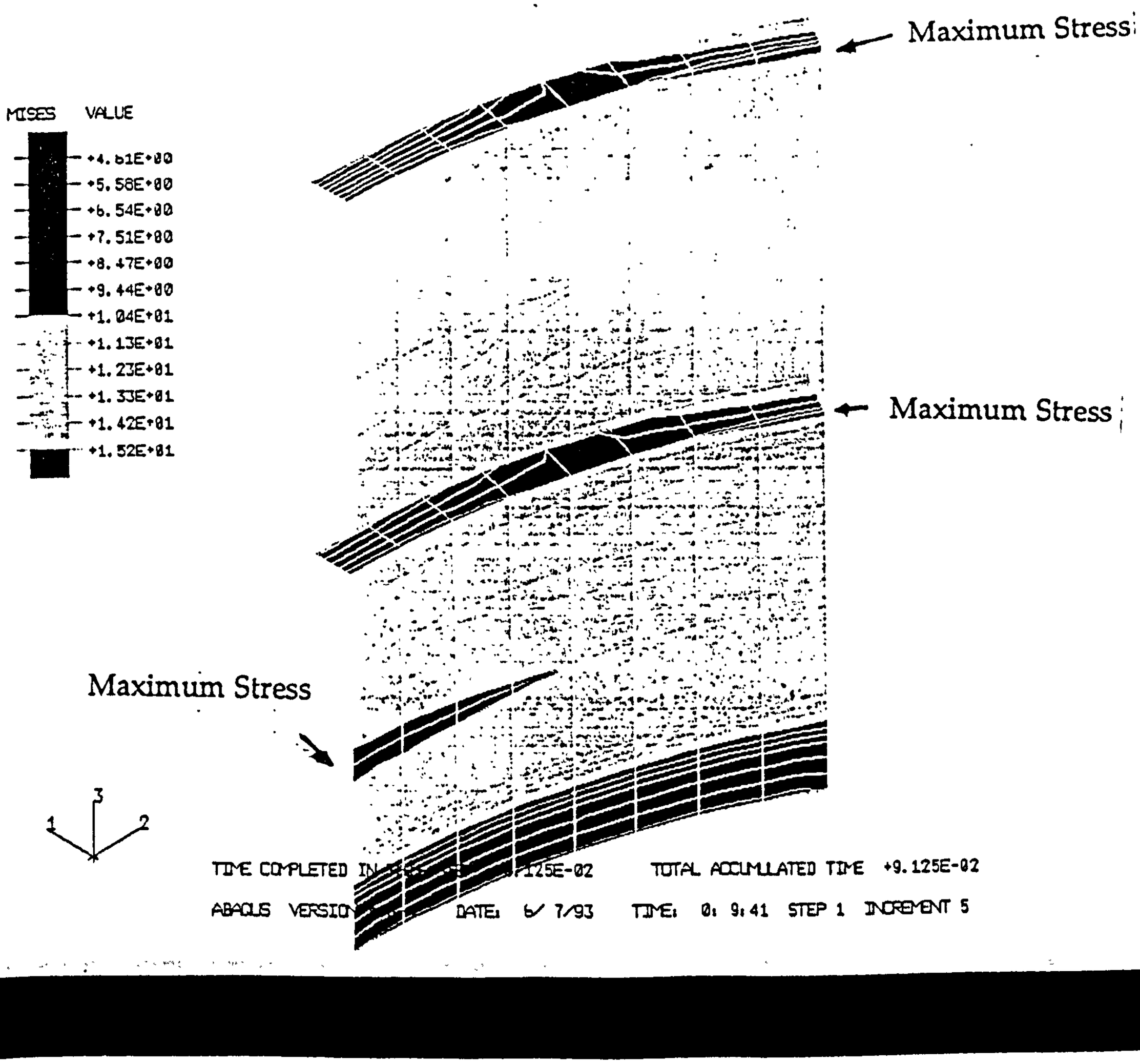

o-o-c = 0.1%R, Load Increment 10

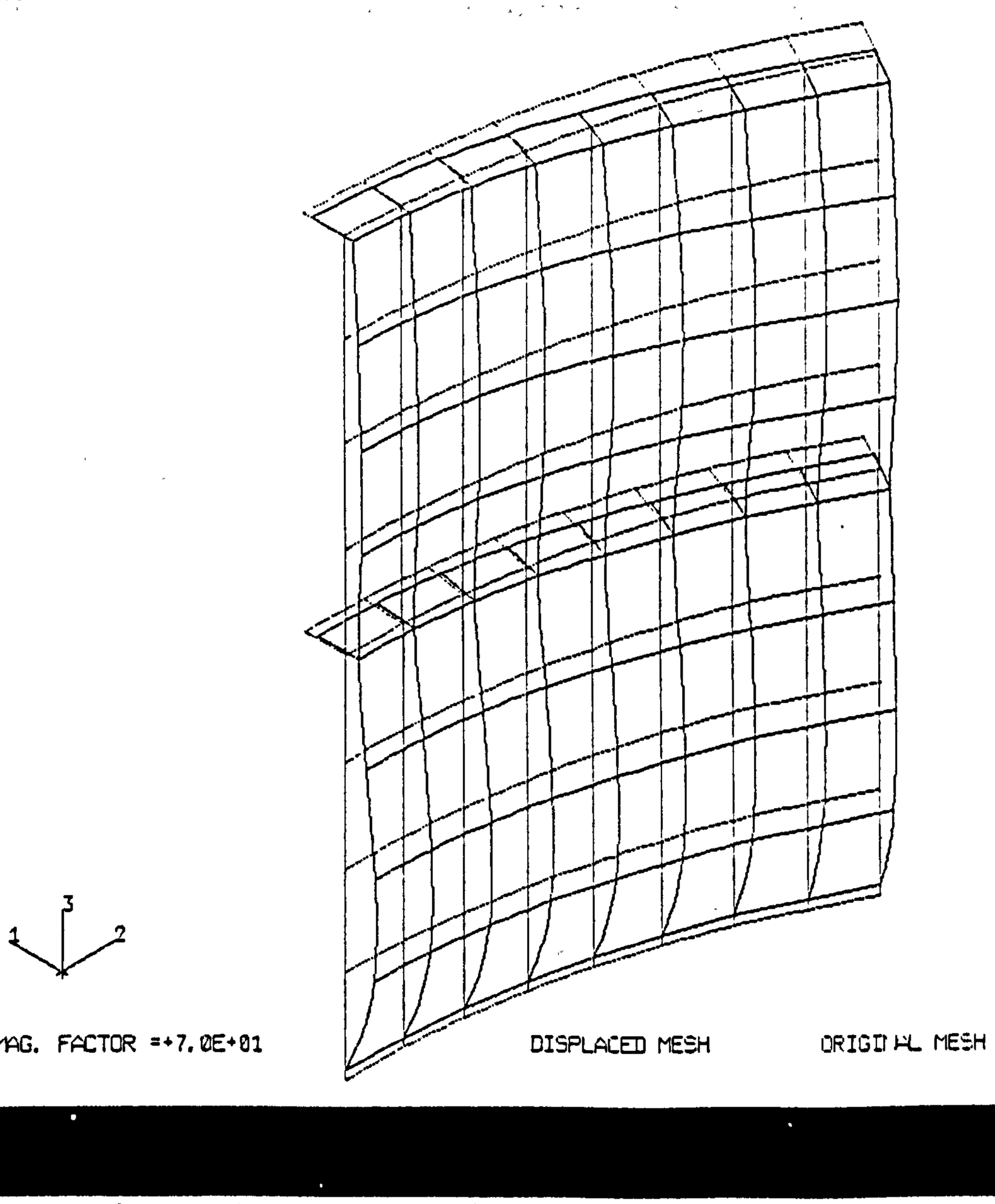

o-o-c = 0.1%R, Load Increment 10

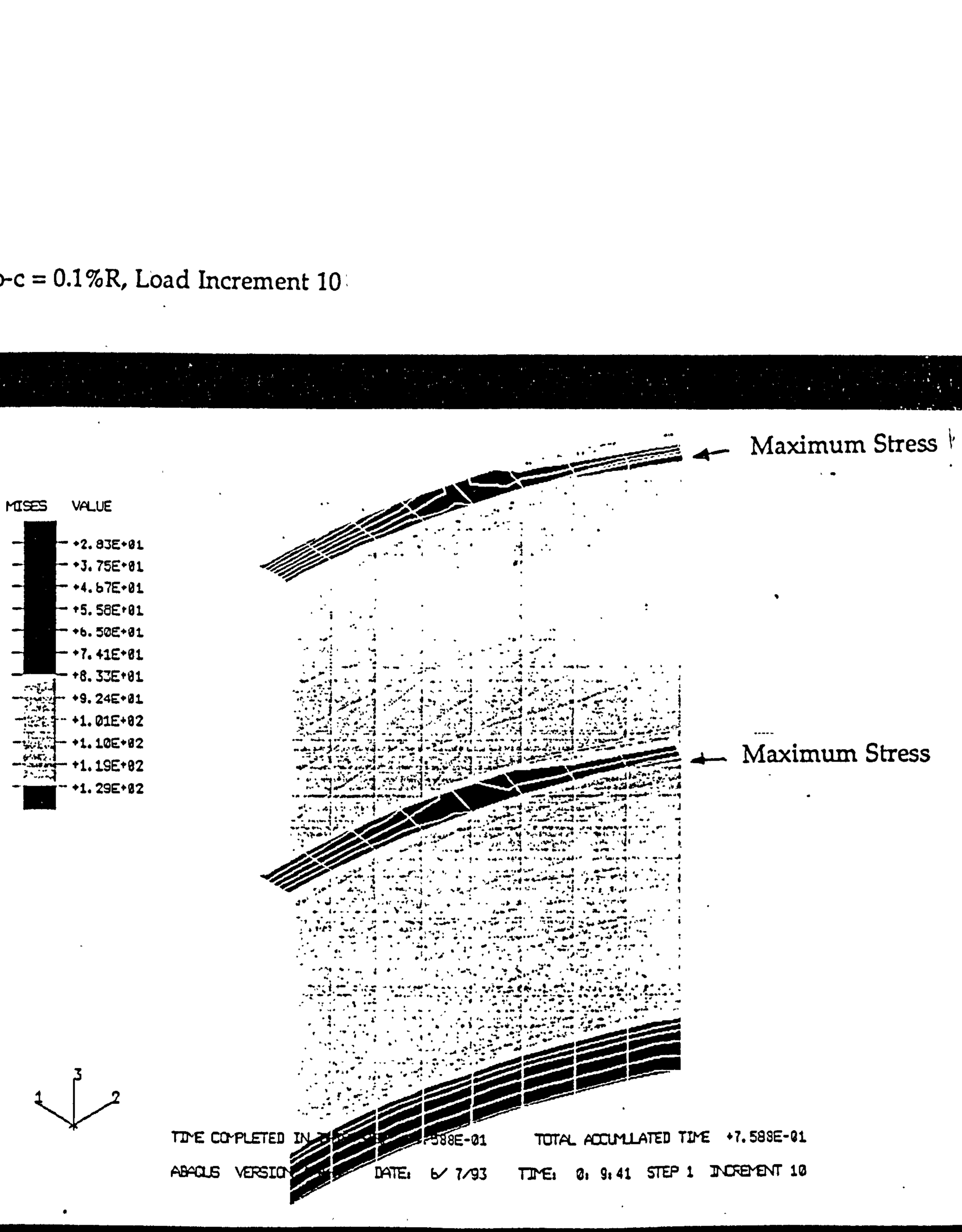

o-o-c = 0.1%R, Load Increment 15

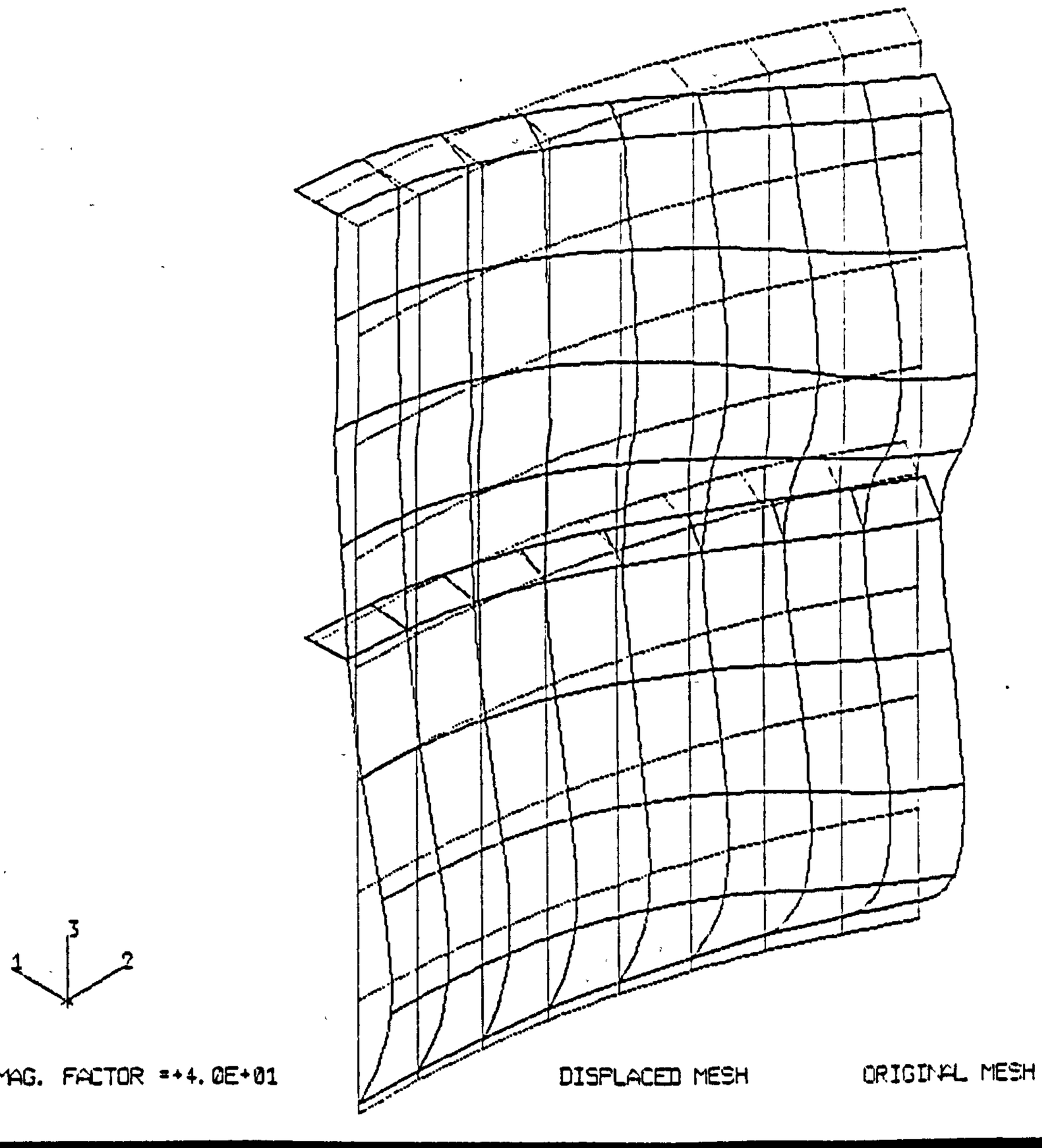

o-o-c = 0.1%R, Load Increment 15

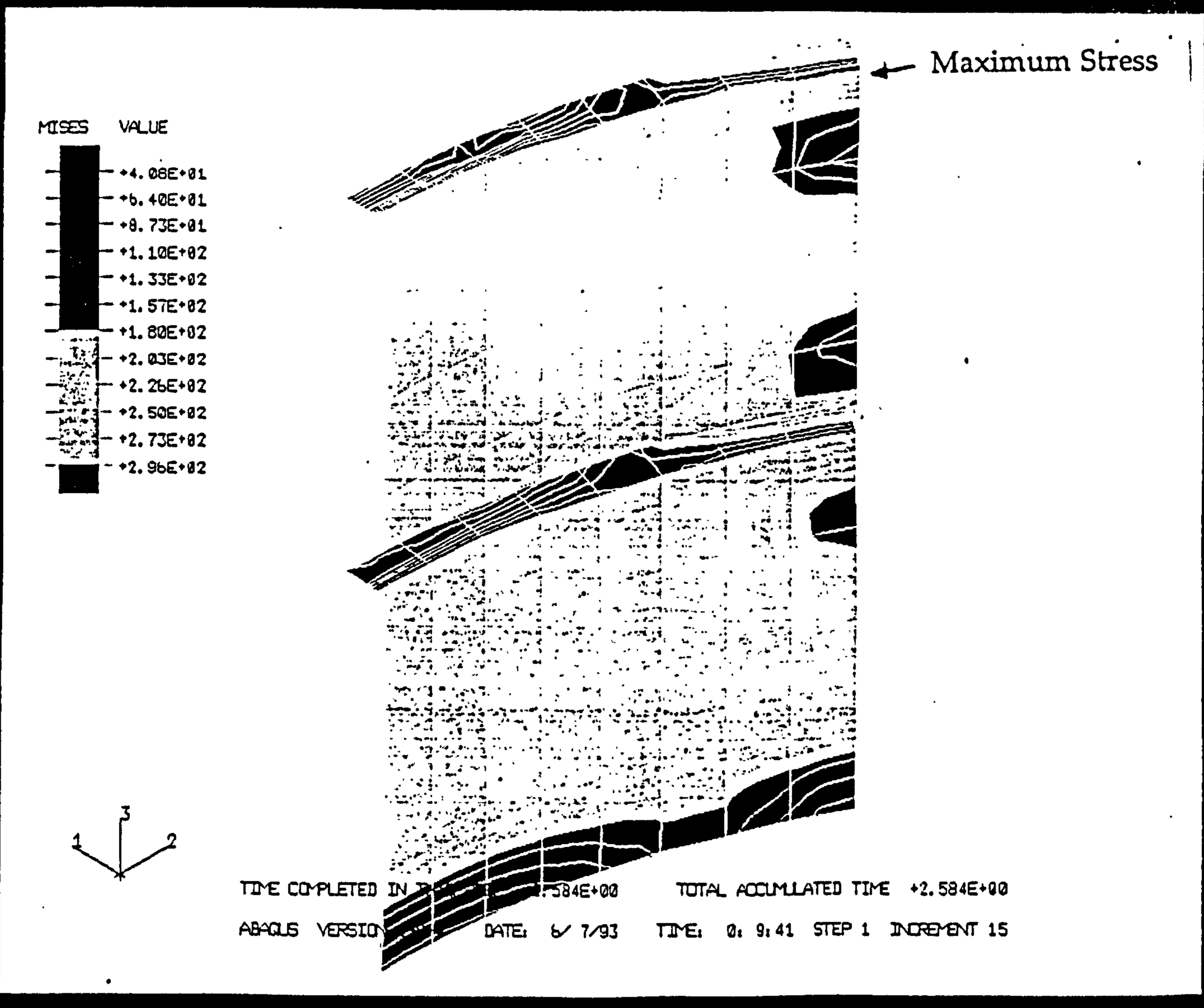

o-o-c = 0.1%R, Shell Radial Deflection at Mid-Compartment

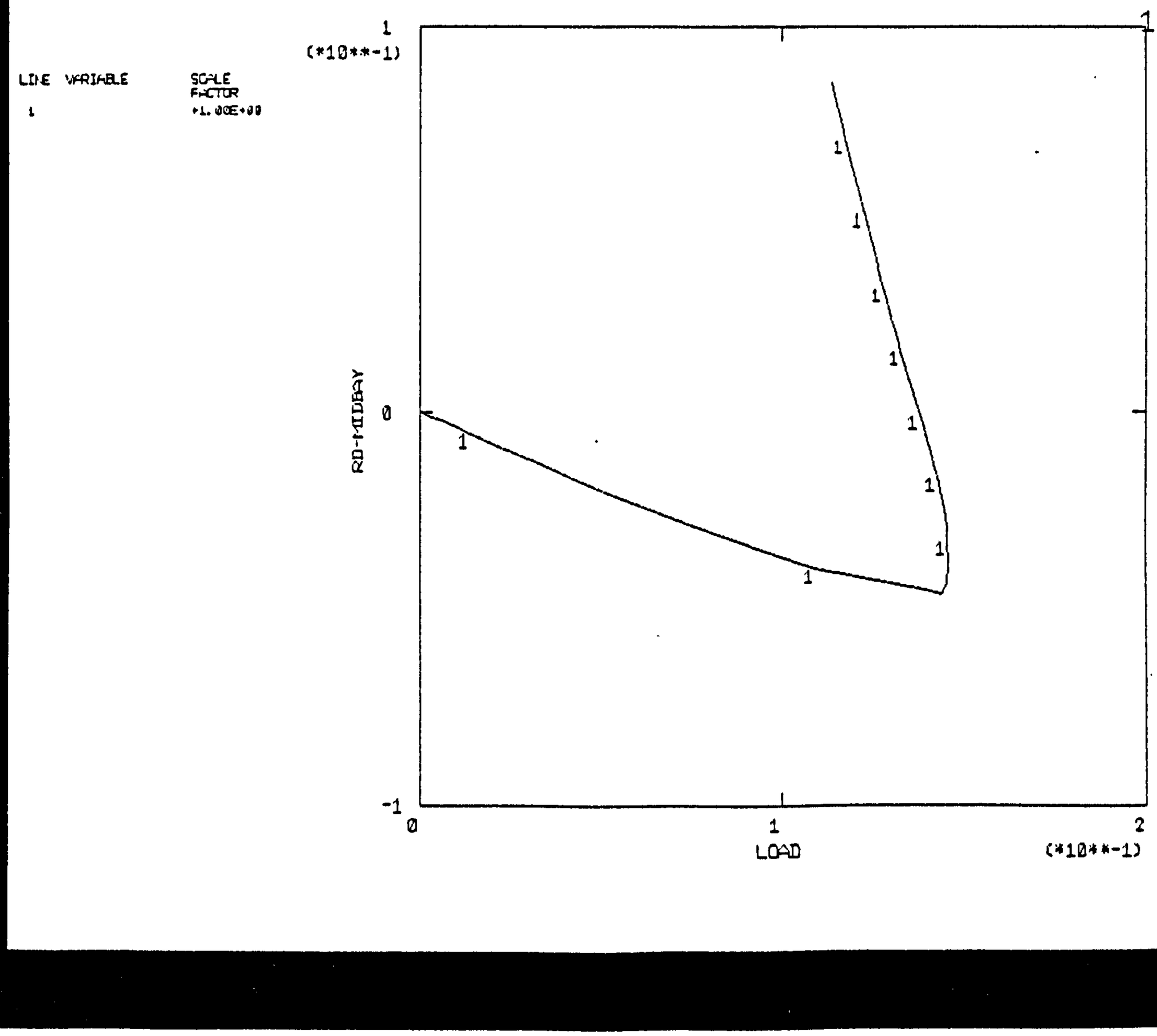

o-o-c = 0.1%R,Frame Radial Deflection at Mid-Compartment

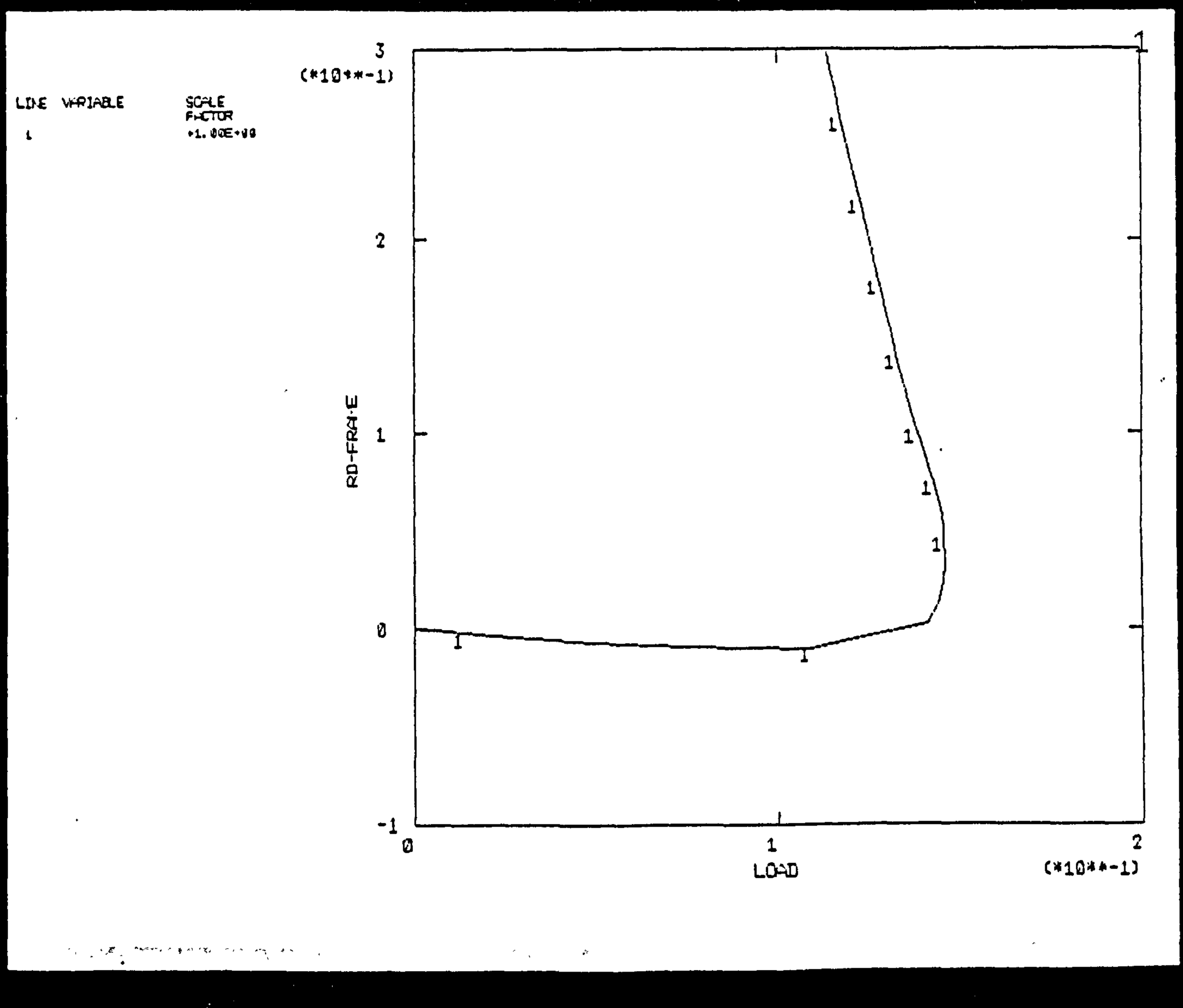

o-o-c = 0.5%R, Load Increment 5

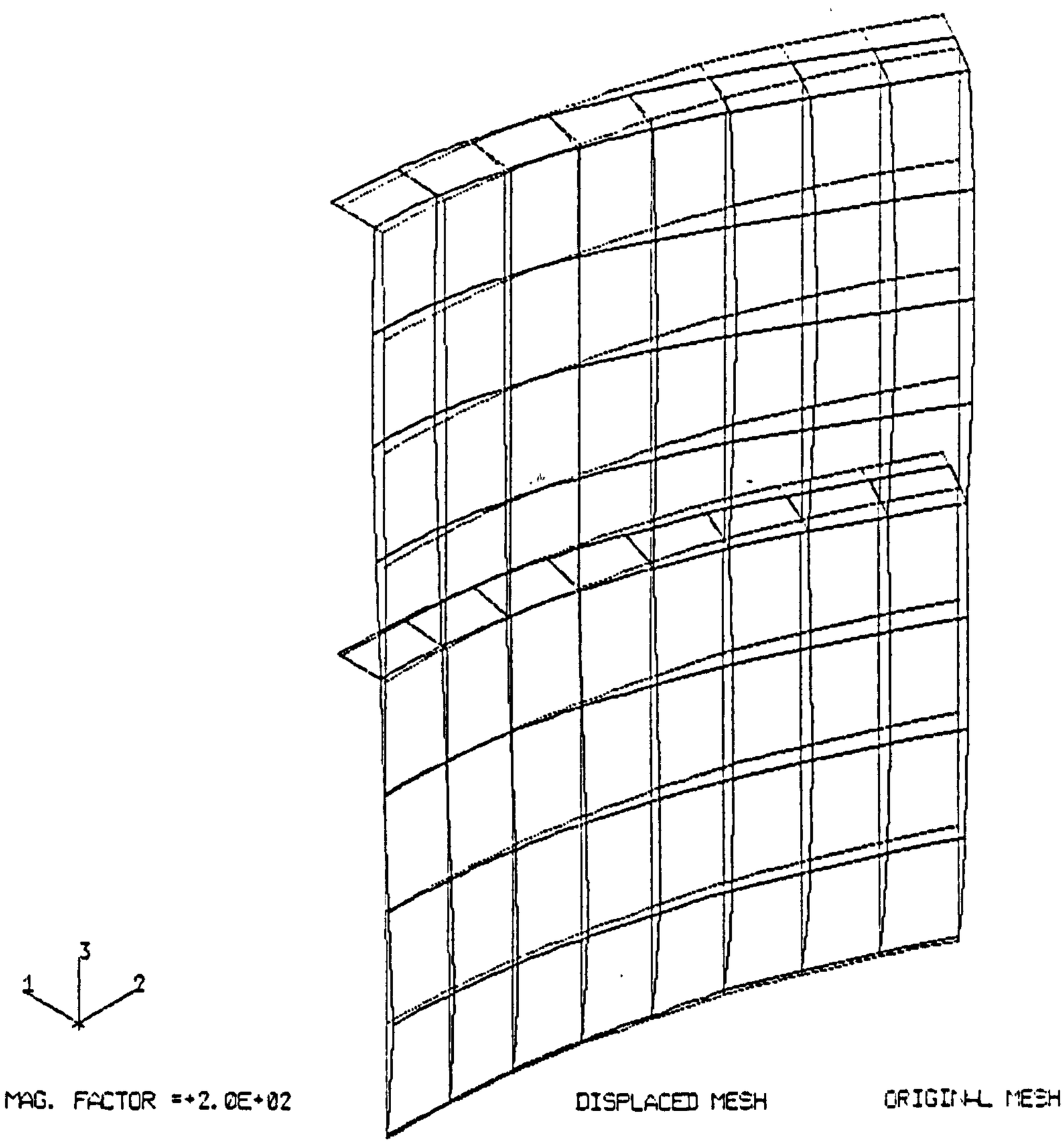

o-o-c = 0.5%R, Load Increment 5

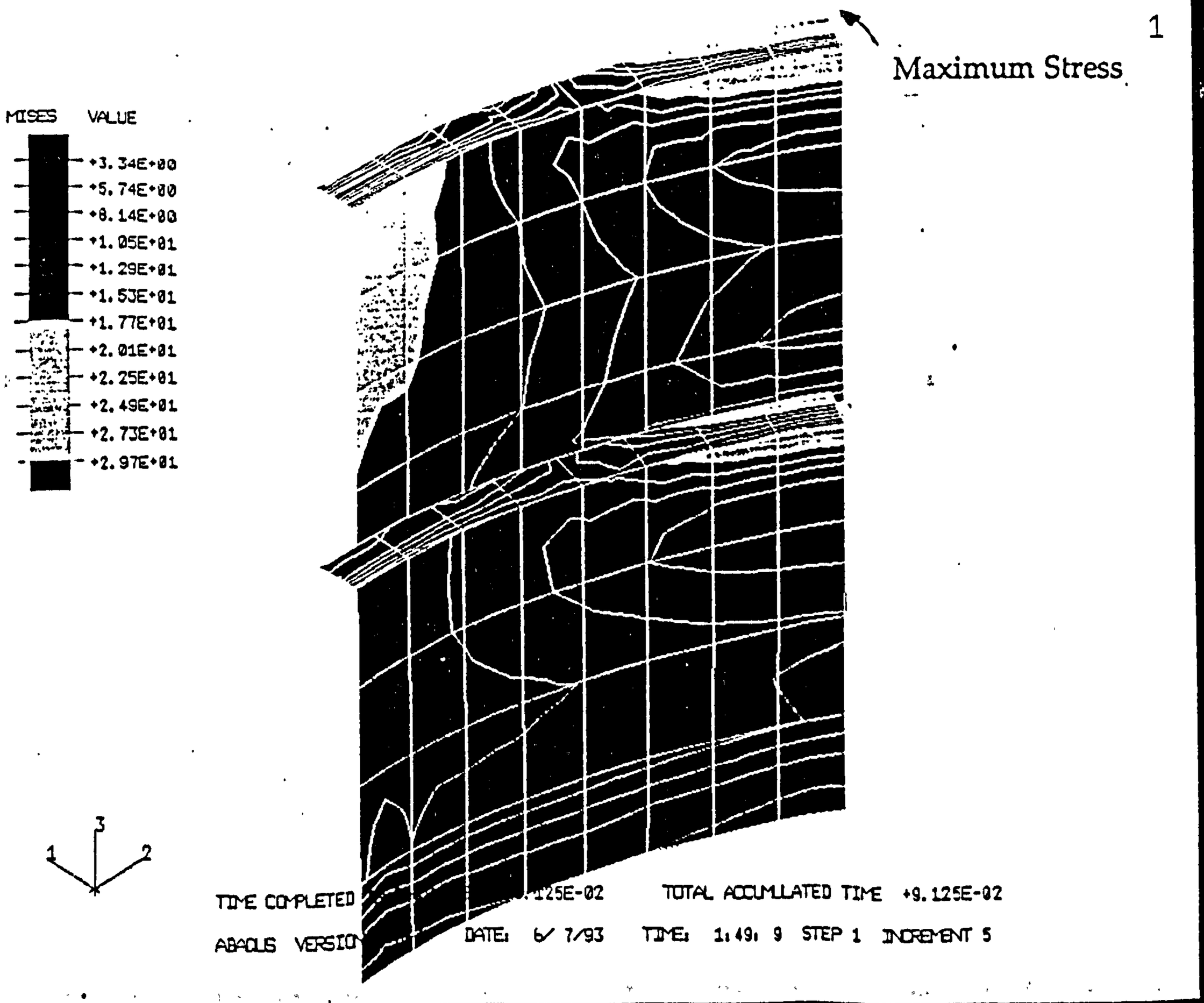

o-o-c = 0.5%R, Load Increment 10

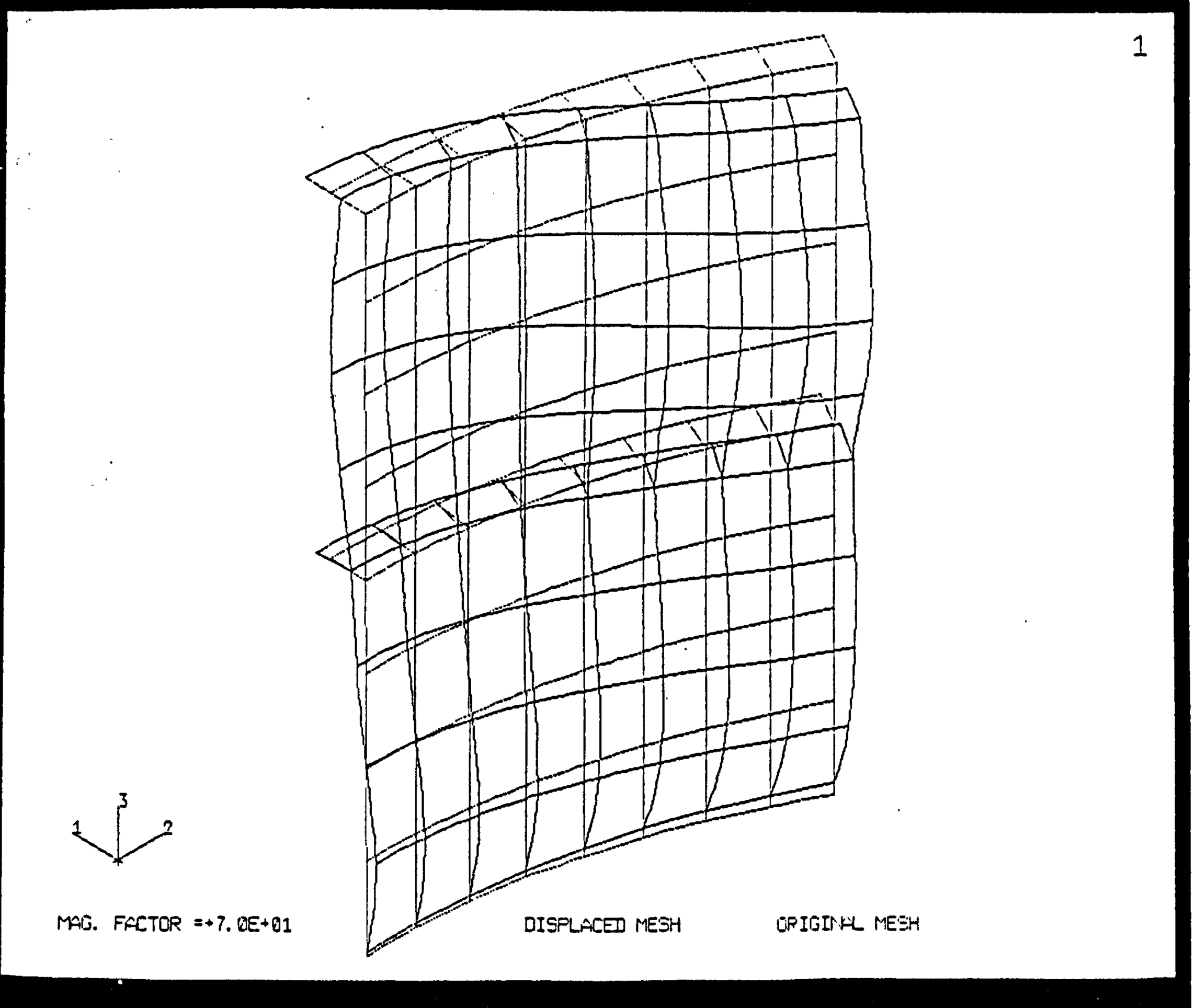

o-o-c = 0.5%R, Load Increment 10

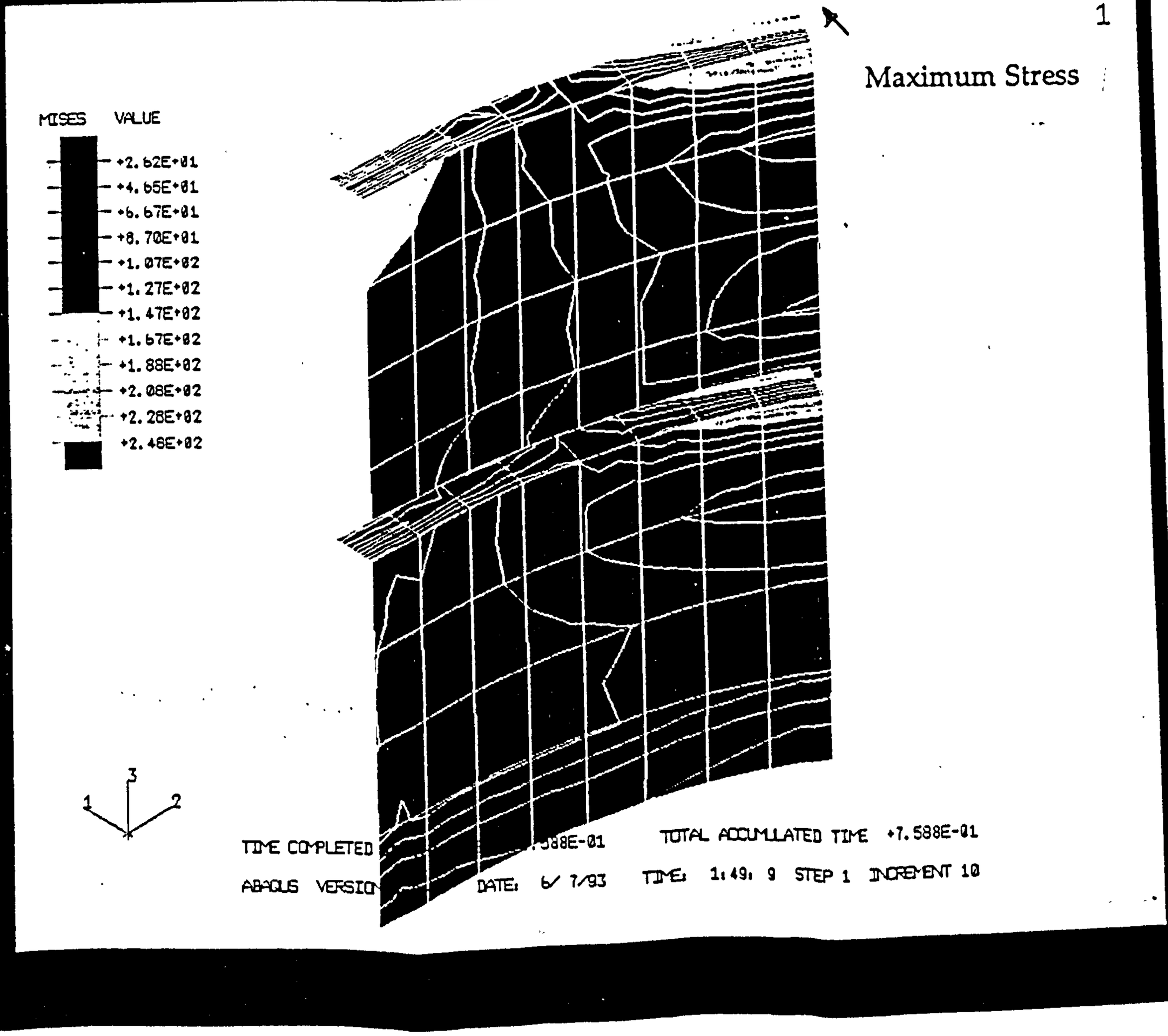

o-o-c = 0.5%R, Load Increment 15

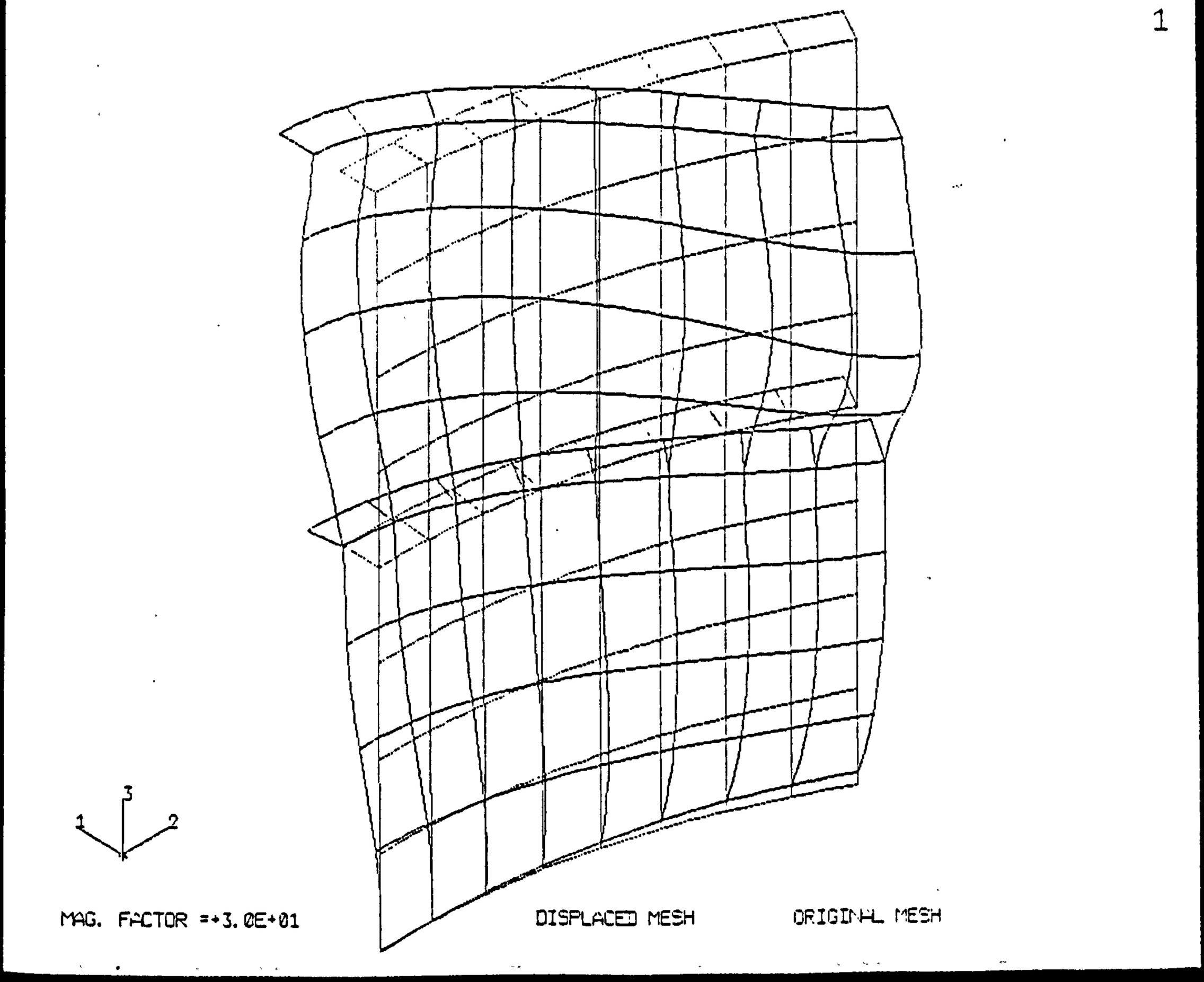

o-o-c = 0.5%R, Load Increment 15

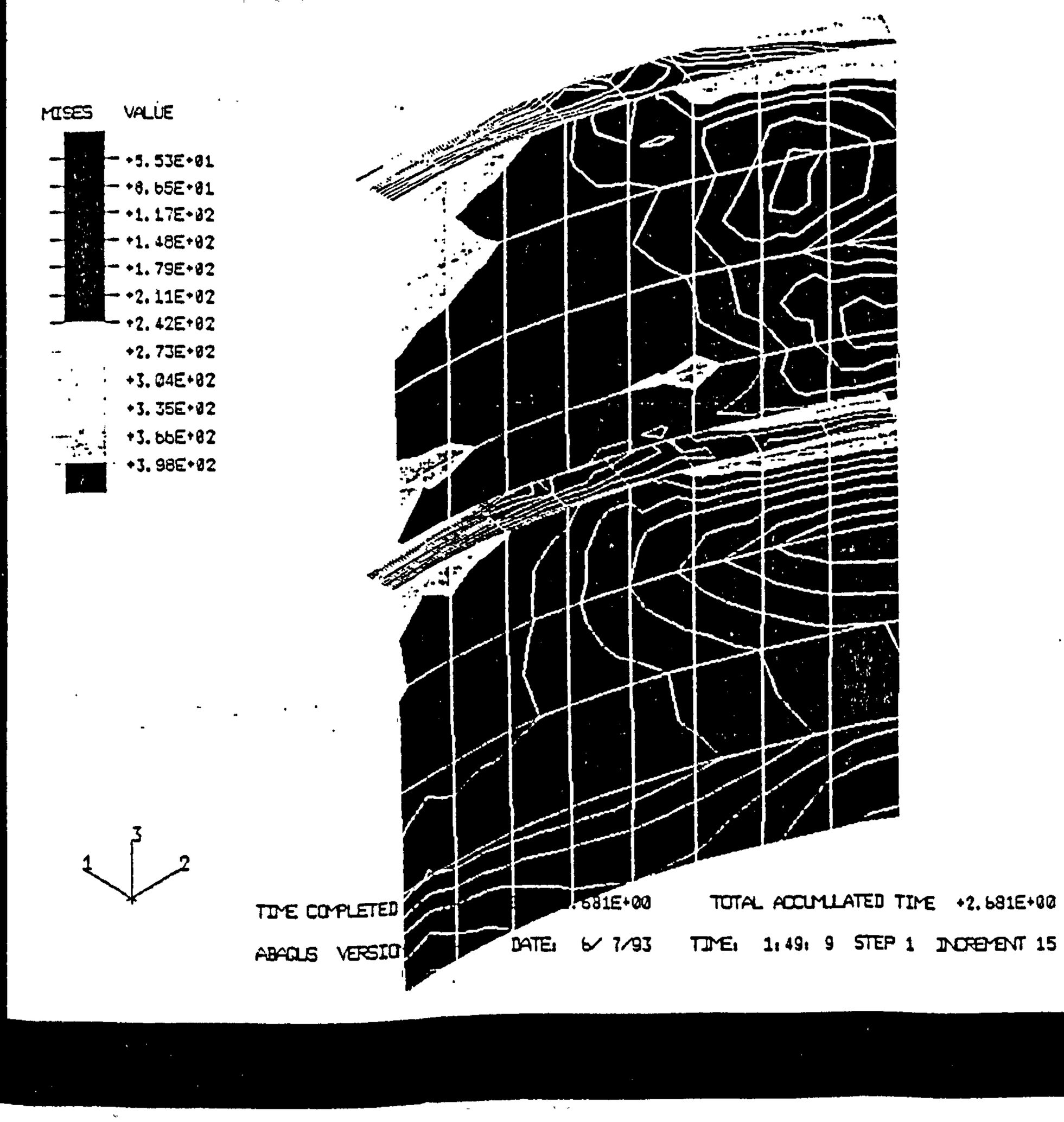

o-o-c =2%R, Load Increment 5

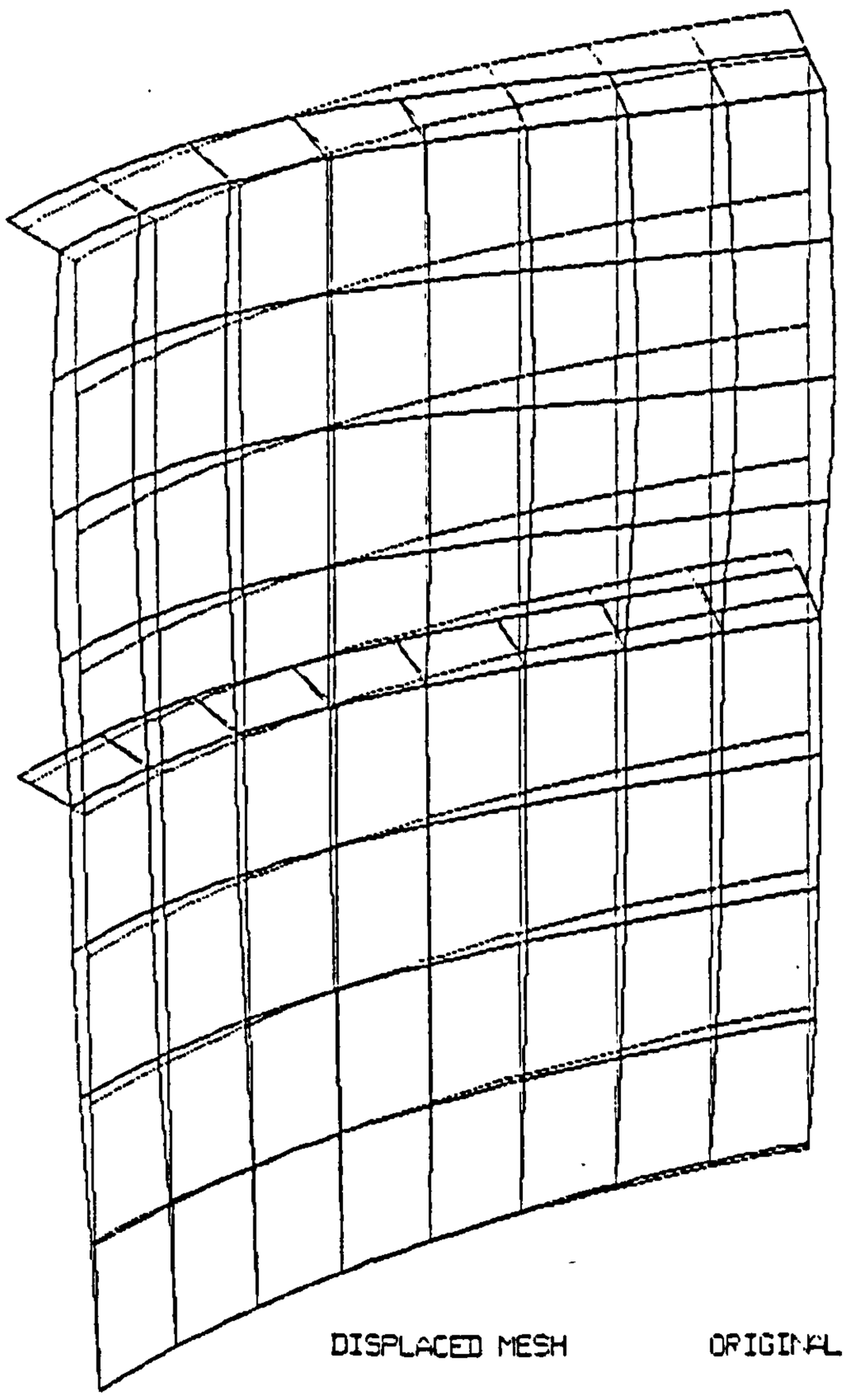

START

o-o-c = 2%R, Load Increment 5

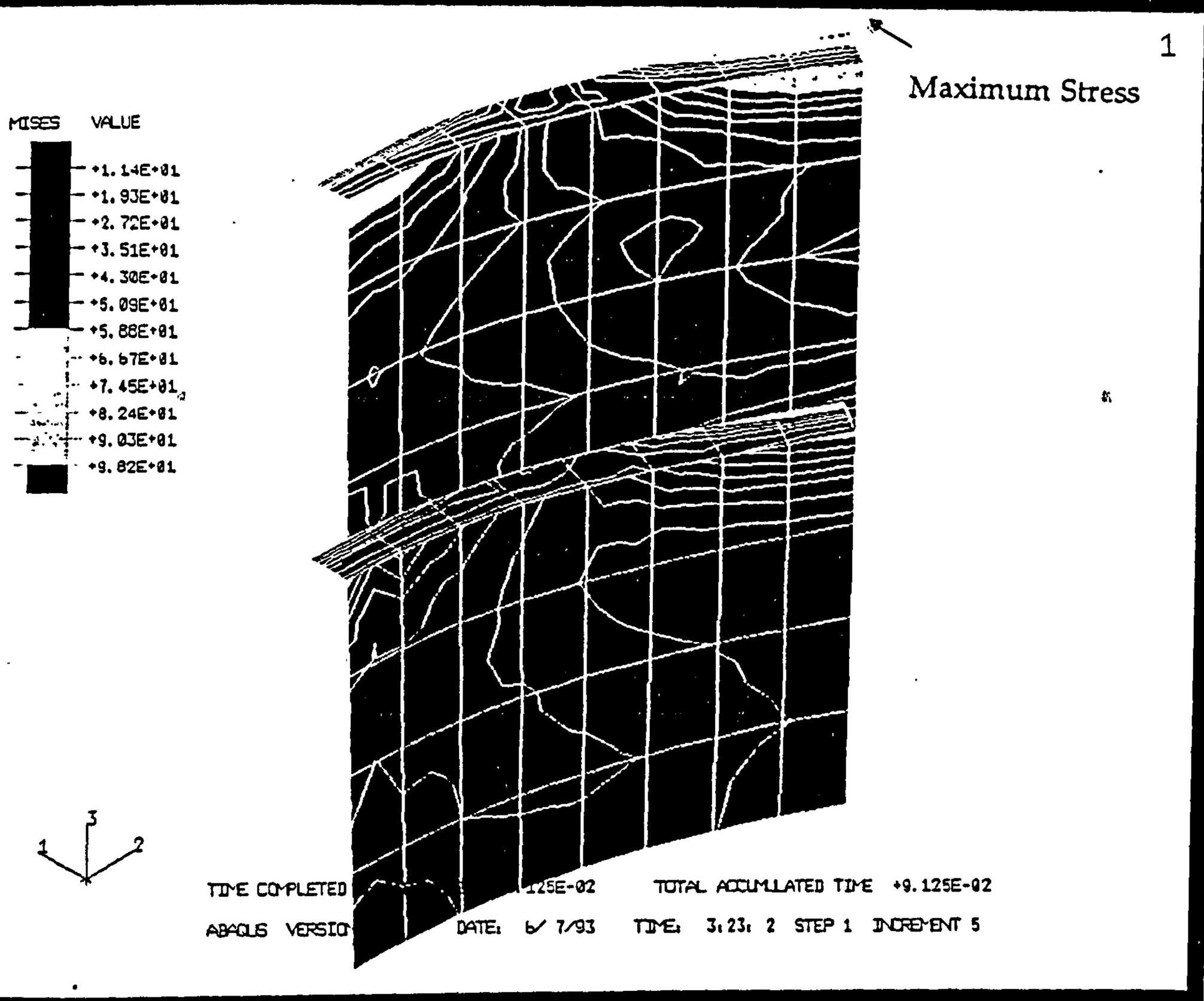

o-o-c = 2%R, Load Increment 10

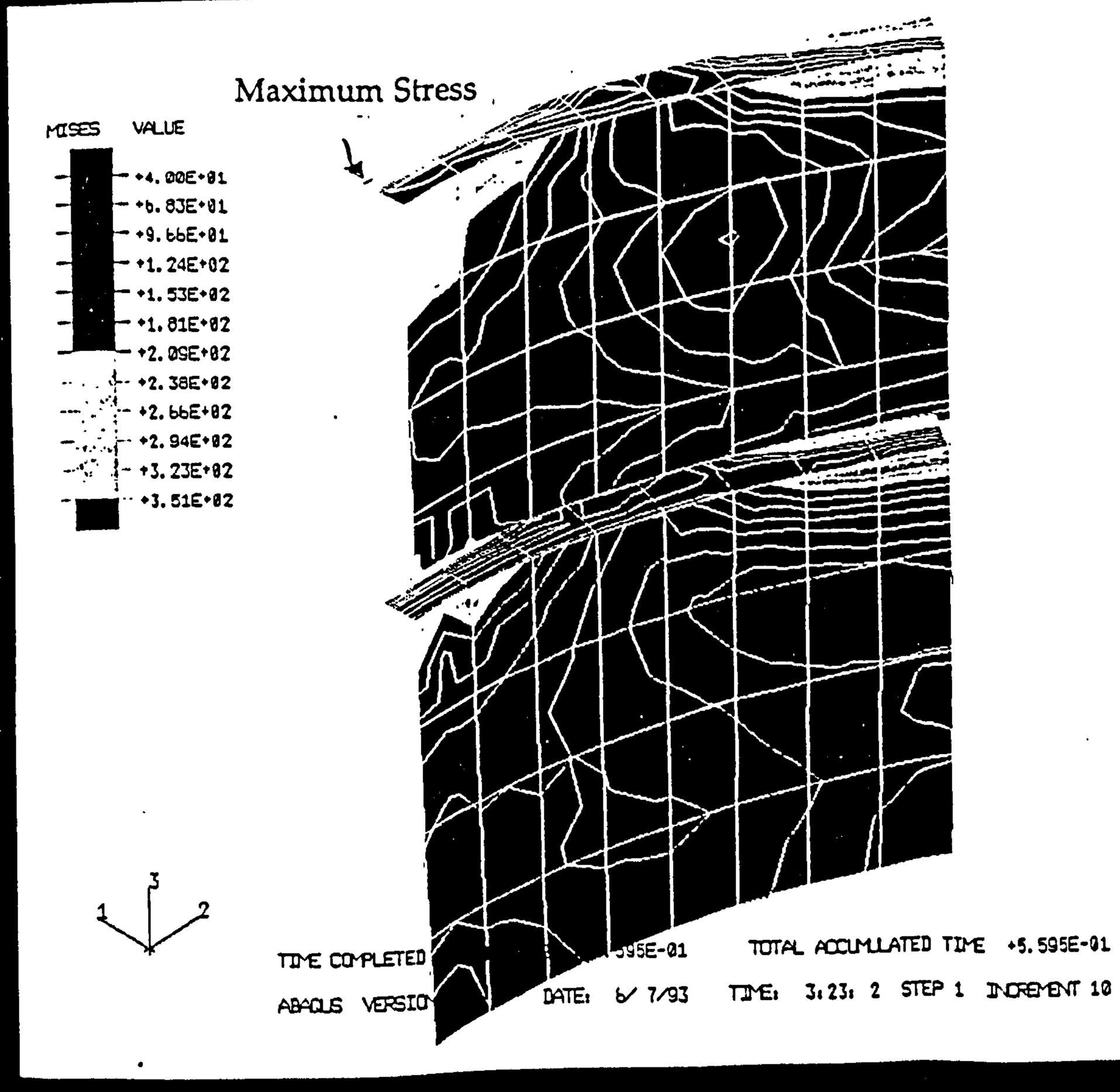

o-o-c = 2%R, Load Increment 15

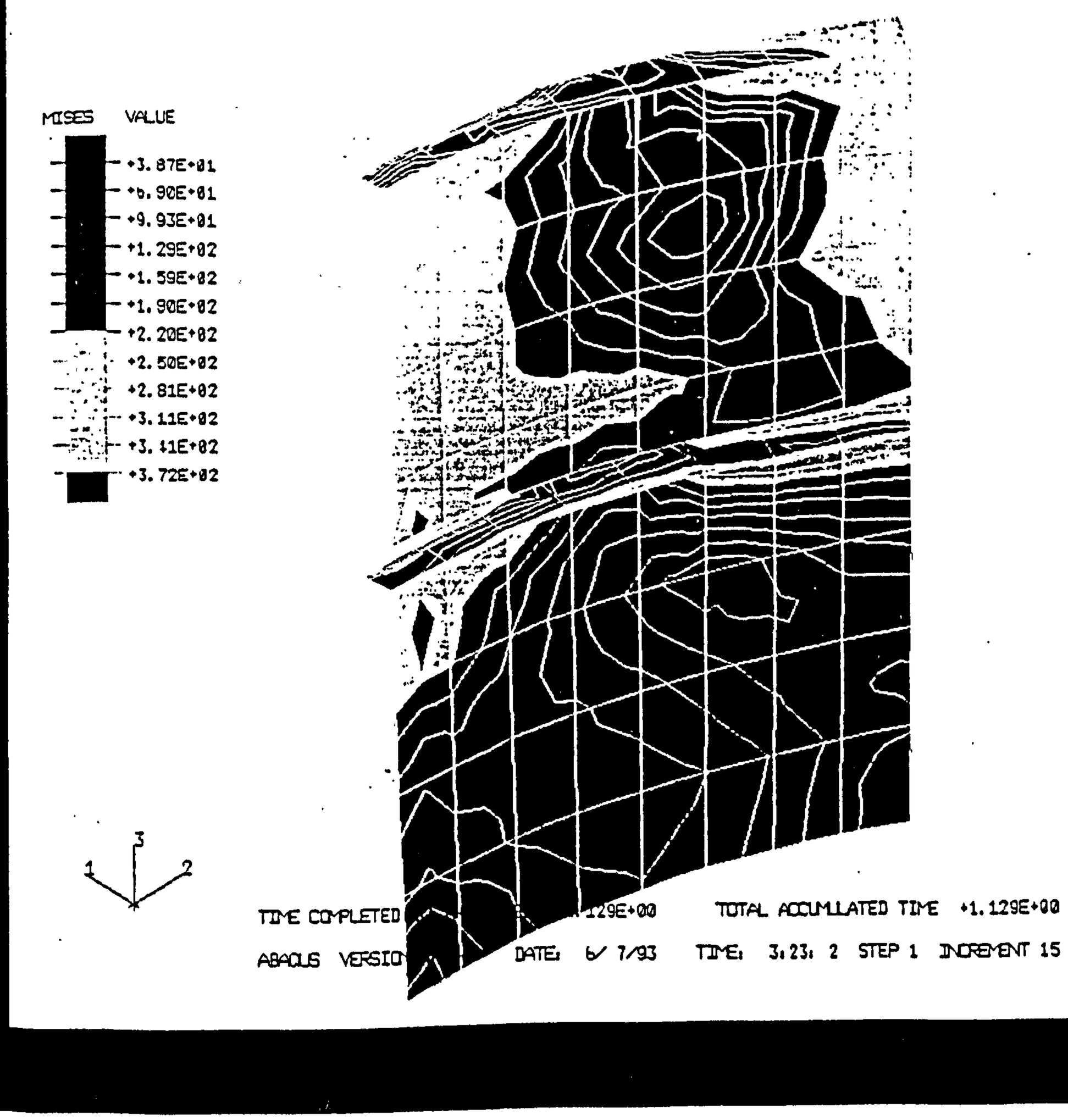

APPENDIX 5

Design Solutions for Partial Safety Factor Optimisation

The, app. 5

	R_1	p_d	t	L_s	d_w
	m	(N / mm^2)	mm	mm	mm
HTS	4.0	300	42	704	237
HY80	4.0	300	34	672	268
HY100	4.0	300	32	669	283
HY130	4.0	300	31	670	236
HTS	4.0	600	94	673	163
HY80	4.0	600	61	676	226
HY100	4.0	600	52	633	238
HY130	4.0	600	42	670	226
HY100	4.0	1500	149	668	152
HY130	4.0	1500	119	669	187
HTS	2.5	300	32	703	272
HY80	2.5	300	25	589	201
HY100	2.5	300	23	559	205
HTS	2.5	600	53	625	204
HY80	2.5	600	39	652	259
HY100	2.5	600	35	627	265
HY130	2.5	600	32	622	250
HTS	2.5	1500	169	682	133
HY80	2.5	1500	91	639	166
HY100	2.5	1500	70	685	195
HY130	2.5	1500	58	780	218
HTS	1.0	300	16	532	84
HY80	1.0	300	14	509	77
HY100	1.0	300	13	490	87
HTS	1.0	600	27	516	171
HY80	1.0	600	21	519	123
HY100	1.0	600	19	502	92
HY130	1.0	600	18	508	100
HTS	1.0	1500	66	638	135
HY80	1.0	1500	41	557	155
HY100	1.0	1500	34	520	160
HY130	1.0	1500	30	515	131

The, app. 5

t_w	b_f	t_f	W	W / Δ	P_y
mm	mm	mm	ton		(N / mm^2)
27	200	67	161.650	0.261	5.42
14	184	34	111.870	0.181	5.42
15	167	22	100.600	0.163	5.45
14	156	21	94.100	0.152	5.42
56	212	140	346.670	0.572	10.85
31	216	78	219.710	0.362	10.87
25	185	63	181.850	0.300	10.86
27	155	66	150.970	0.249	10.93
61	212	151	487.970	0.805	27.14
48	205	118	388.970	0.642	27.19
13	141	30	77.424	0.262	5.49
12	96	28	60.790	0.205	5.48
11	100	19	54.890	0.185	5.51
32	175	77	151.990	0.514	10.87
23	183	33	103.290	0.349	10.97
14	150	30	85.940	0.290	10.88
15	148	22	78.240	0.264	10.90
69	210	172	428.870	1.449	27.14
56	181	139	259.830	0.878	27.14
44	193	110	200.830	0.679	27.92
35	204	86	161.400	0.545	27.22
8	60	18	4.670	0.296	5.42
8	51	13	3.980	0.252	5.59
8	39	9	3.730	0.236	5.69
12	59	29	8.150	0.516	11.41
9	61	16	6.030	0.382	10.93
10	48	20	5.470	0.346	10.90
10	51	12	5.110	0.323	11.42
27	141	63	20.410	1.292	27.51
17	96	43	12.540	0.794	27.14
21	68	31	10.600	0.671	29.76
12	70	28	8.850	0.560	27.31

The, app. 5

p_{yp}	p_c	σ_t / ξ	σ_t from Eq.(33)
(N / mm^2)	(N / mm^2)	(N / mm^2)	
5.42	4.68	10.97	
6.21	4.48	5.81	
6.87	4.49	3.37	
7.26	4.52	3.44	
11.18	12.16	32.26	
11.64	10.97	17.75	
12.32	10.82	10.22	
12.43	9.12	6.22	
30.15	33.95	45.04	
31.68	34.29	30.18	
5.81	4.45	7.15	
6.53	4.58	3.43	
6.85	4.54	3.03	
10.85	10.08	29.52	
11.82	9.17	15.56	
12.51	9.09	8.93	
13.21	9.05	7.61	
28.65	32.06	125.30	
28.01	28.65	54.60	
27.84	25.31	45.65	
28.39	22.61	39.53	
5.75	4.45	14.17	
7.07	4.75	8.73	
7.79	4.45	3.24	
11.56	9.12	8.90	
12.54	9.22	10.20	
13.51	9.36	8.26	
15.21	9.47	6.85	
31.94	22.93	19.98	
27.19	22.71	50.40	
36.35	22.61	16.16	
30.57	22.77	18.72	

APPENDIX 6

BS5500 [24] Method for Effective Breadth Calculation

The following method is used to calculate the effective breadth of plating associated with a frame using the method given in BS 5500 [24]. The variables, a,b,c are arbitrary variables used in this appendix. Tables A6.1 to A6.4 give values of L_e/L_s, and Table A6.5 is used to provide correction factors in cases outside the range of the other Tables.

Initially, the following values are calculated:

$$a = \frac{L_s}{2\pi R_m} \quad \text{and} \quad b = \frac{t^2}{12R_m^2}$$

If $b < 10^{-7}$, L_e is set to L_s.

Using the values of b, one or two of Tables A6.1 to A6.4 are selected for use:

$b \geq 10^{-4}$: Table A6.1

$10^{-4} > b \geq 10^{-5}$: Tables A6.1 and A6.2

$10^{-5} > b \geq 10^{-6}$: Tables A6.2 and A6.3

$10^{-6} > b \geq 10^{-7}$: Tables A6.3 and A6.4

Then for each table selected a value for L_e/L_s is calculated. If $0 > a \geq 0.1$ then given mode number n, linearly interpolate in the table for a to obtain the value of L_e/L_s. Then using the row of Table A6.5 which corresponds to the current table, retrieve a value for the correction factor Z. Then set:

$$\frac{L_e}{L_s} = \frac{c}{100a^2} + \frac{(a-0.1)}{6.28a^2}Z$$

Finally, if two tables were selected, logarithmic interpolation for b is used to obtain the final value of L_e/L_s and thus L_e. If $n > 20$, $n = 20$ is used in accessing all the tables.

Table A6.1

Values of L_e/L_s for $b = \frac{t^2}{12R_m^2} \geq 10^{-4}$

$a = \frac{L_s}{2\pi R_m}$	mode n 2	3	4	5	6
0	1.0980	1.0980	1.0980	1.0980	1.0980
0.01	1.0823	1.0823	1.0663	1.0663	1.0504
0.02	1.0663	1.0504	1.0265	0.9948	0.9629
0.03	1.0504	1.0027	0.9549	0.9019	0.8435
0.04	0.9907	0.9231	0.8515	0.7838	0.7082
0.05	0.8976	0.8276	0.7512	0.6716	0.5952
0.06	0.7921	0.7298	0.6609	0.5871	0.5143
0.07	0.6866	0.6321	0.5707	0.5025	0.4343
0.08	0.6111	0.5630	0.5088	0.4480	0.3877
0.09	0.5355	0.4940	0.4470	0.3935	0.3410
0.10	0.4600	0.4249	0.3852	0.3390	0.2944

Table A6.2

Values of L_e/L_s for $b = \frac{t^2}{12R_m^2} = 10^{-5}$

$a = \frac{L_s}{2\pi R_m}$	mode n 2	3	4	5	6
0	1.0980	1.0980	1.0980	1.0980	1.0980
0.01	1.0323	1.0823	1.0663	1.0663	1.0504
0.02	1.0345	1.0186	0.9947	0.9629	0.9311
0.03	0.9019	0.8807	0.8541	0.8117	0.7639
0.04	0.7242	0.7003	0.6724	0.6326	0.5929
0.05	0.5602	0.5411	0.5200	0.4934	0.4647
0.06	0.4483	0.4350	0.4218	0.4005	0.3793
0.07	0.3752	0.3661	0.3547	0.3388	0.3206
0.08	0.3263	0.3163	0.3084	0.2964	0.2805
0.09	0.2920	0.2847	0.2775	0.2660	0.2525
0.10	0.2531	0.2531	0.2467	0.2355	0.2244

Table A6.3

Values of L_e/L_s for $b = \frac{t^2}{12R_m^2} = 10^{-6}$

$a = \frac{L_s}{2\pi R_m}$	mode n 2	3	4	5	6
0	1.0980	1.0980	1.0980	1.0980	1.0980
0.01	1.0663	1.0504	1.0504	1.0504	1.0345
0.02	0.8276	0.8196	0.8037	0.7878	0.7719
0.03	0.5252	0.5199	0.5146	0.5040	0.4934
0.04	0.3740	0.3700	0.3661	0.3621	0.3541
0.05	0.2960	0.2928	0.2897	0.2865	0.2801
0.06	0.2661	0.2632	0.2604	0.2575	0.2521
0.07	0.2362	0.2336	0.2311	0.2285	0.2241
0.08	0.2063	0.2040	0.2018	0.1996	0.1961
0.09	0.1763	0.1744	0.1725	0.1706	0.1681
0.10	0.1464	0.1448	0.1432	0.1416	0.1401

Table A6.4

Values of L_e/L_s for $b = \frac{t^2}{12R_m^2} = 10^{-7}$

$a = \frac{L_s}{2\pi R_m}$	mode n 2	3	4	5	6
0	1.0980	1.0980	1.0980	1.0980	1.0980
0.01	0.9072	0.9072	0.8913	0.8913	0.8913
0.02	0.4297	0.4297	0.4218	0.4218	0.4218
0.03	0.2759	0.2759	0.2759	0.2759	0.2759
0.04	0.2207	0.2207	0.2207	0.2191	0.2191
0.05	0.1655	0.1655	0.1655	0.1623	0.1623
0.06	0.1487	0.1487	0.1487	0.1461	0.1461
0.07	0.1324	0.1318	0.1318	0.1299	0.1299
0.08	0.1159	0.1149	0.1149	0.1136	0.1136
0.09	0.0993	0.0980	0.0980	0.0974	0.0974
0.10	0.0828	0.0812	0.0182	0.0812	0.0812

Table A6.5

Values of correction factor Z

$b = \frac{t^2}{12R_m^2}$	mode n	2	3	4	5	6
>	10^{-4}	0.273	0.257	0.235	0.207	0.180
	10^{-5}	0.159	0.159	0.154	0.147	0.140
	10^{-6}	0.091	0.090	0.090	0.089	0.087
	10^{-7}	0.051	0.051	0.051	0.051	0.051